

AD-A039 286

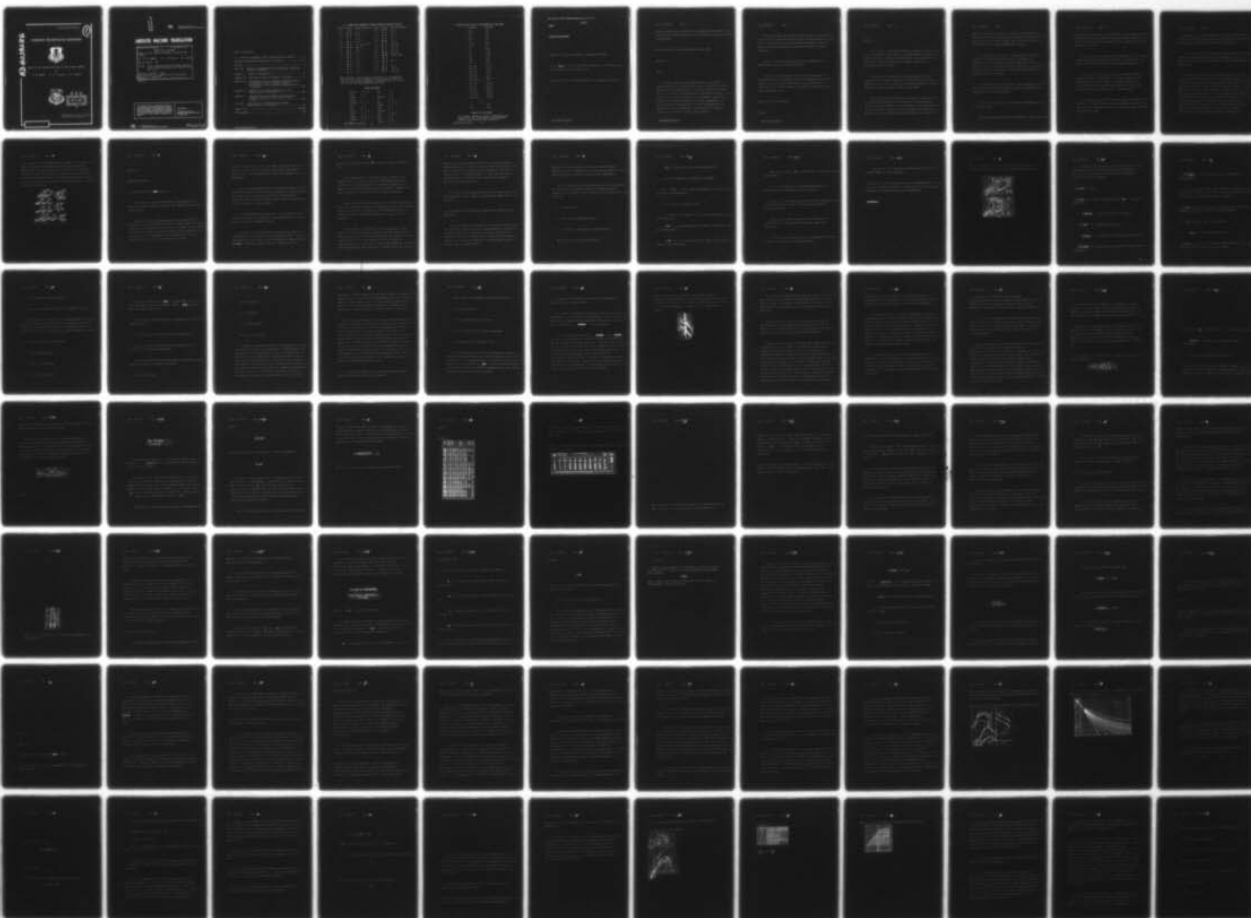
FOREIGN TECHNOLOGY DIV WRIGHT-PATTERSON AFB OHIO
ATLAS OF THE CASCADE PROFILES OF AXIAL-FLOWS TURBINE, (U)
DEC 76 M Y DEYCH, G A PHILIPP, L Y LAZAREV
FTD-ID(RS)T-1693-76

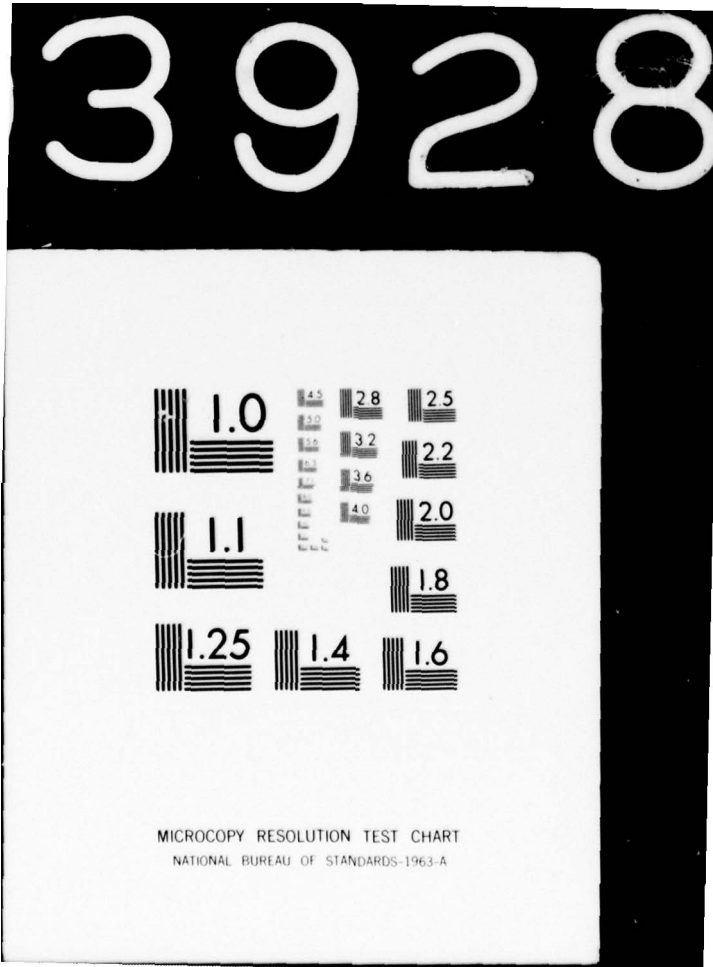
F/G 21/5

UNCLASSIFIED

NL

1 OF 5
AD
A039286





FTD-ID(RS)T-1693-76

①
NW

AD-A039286

FOREIGN TECHNOLOGY DIVISION



ATLAS OF THE CASCADE PROFILES OF AXIAL-FLOWS TURBINE

by

M. Ye. Deych, G. A. Philipp, L. Ya. Lazarev



DDC
RECEIVED
MAY 12 1977
D

Approved for public release;
distribution unlimited.

FTD-

ID(RS)T-1693-76

UNEDITED MACHINE TRANSLATION

FTD-ID(RS)T-1693-76

15 December 1976

FD-76-C-001314

ATLAS OF THE CASCADE PROFILES OF AXIAL-FLOWS
TURBINE

By: M. Ye. Deych, G. A. Philipp, L. Ya. Lazarev

English pages: 384

Source: Atlas Profiley Reshetok Osevykh Turbin,
Izd-vo "Mashinostroyeniye," Moscow, 1965,
PP. 1-96.

Country of origin: USSR

This document is a machine aided translation.

Requester: AFAPL/TBC

Approved for public release; distribution un-
limited.

THIS TRANSLATION IS A RENDITION OF THE ORIGINAL FOREIGN TEXT WITHOUT ANY ANALYTICAL OR EDITORIAL COMMENT. STATEMENTS OR THEORIES ADVOCATED OR IMPLIED ARE THOSE OF THE SOURCE AND DO NOT NECESSARILY REFLECT THE POSITION OR OPINION OF THE FOREIGN TECHNOLOGY DIVISION.

PREPARED BY:

TRANSLATION DIVISION
FOREIGN TECHNOLOGY DIVISION
WP-AFB, OHIO.

FTD-

ID(RS)T-1693-76

Date 15 Dec 19 76

Table of Contents

U. S. Board on Geographic Names Transliteration System.....	ii
Russian and English Trigonometric Functions.....	iii
Preface.....	4
Part One. Methods of Shaping and the Aerodynamic Characteristics of Cascades.....	9
Chapter I. General Information.....	11
Chapter II. Calculation and the Shaping of Cascades.....	66
Chapter III. Calculation of the Aerodynamic Characteristics of Cascades, Effect of Some Geometric Parameters on the Aerodynamic Characteristics of Cascades.....	199
Chapter IV. Effect of the Regime Parameters on the Effectiveness of Cascades.....	293
Chapter V. Calculation of the Stages of Steam and Gas Turbines According to the Data of Static Studies.....	321
Part Two. Airfoils, the Aerodynamic and Strength Characteristics of Cascades.....	331
Pages 1-52.....	332-383
Bibliography.....	384

U. S. BOARD ON GEOGRAPHIC NAMES transliteration SYSTEM

Block	Italic	Transliteration	Block	Italic	Transliteration
А а	<i>А а</i>	A, a	Р р	<i>Р р</i>	R, r
Б б	<i>Б б</i>	B, b	С с	<i>С с</i>	S, s
В в	<i>В в</i>	V, v	Т т	<i>Т т</i>	T, t
Г г	<i>Г г</i>	G, g	У у	<i>У у</i>	U, u
Д д	<i>Д д</i>	D, d	Ф ф	<i>Ф ф</i>	F, f
Е е	<i>Е е</i>	Ye, ye; E, e*	Х х	<i>Х х</i>	Kh, kh
Ж ж	<i>Ж ж</i>	Zh, zh	Ц ц	<i>Ц ц</i>	Ts, ts
З з	<i>З з</i>	Z, z	Ч ч	<i>Ч ч</i>	Ch, ch
И и	<i>И и</i>	I, i	Ш ш	<i>Ш ш</i>	Sh, sh
Й й	<i>Й й</i>	Y, y	Щ щ	<i>Щ щ</i>	Shch, shch
К к	<i>К к</i>	K, k	Ъ ъ	<i>Ъ ъ</i>	"
Л л	<i>Л л</i>	L, l	Ы ы	<i>Ы ы</i>	Y, y
М м	<i>М м</i>	M, m	Ь ь	<i>Ь ь</i>	'
Н н	<i>Н н</i>	N, n	Э э	<i>Э э</i>	E, e
О о	<i>О о</i>	O, o	Ю ю	<i>Ю ю</i>	Yu, yu
П п	<i>П п</i>	P, p	Я я	<i>Я я</i>	Ya, ya

*ye initially, after vowels, and after ъ, ь; e elsewhere.
 When written as ë in Russian, transliterate as yë or ë.
 The use of diacritical marks is preferred, but such marks
 may be omitted when expediency dictates.

GREEK ALPHABET

Alpha	Α α	α	Nu	Ν ν
Beta	Β β		Xi	Ξ ξ
Gamma	Γ γ		Omicron	Ο ο
Delta	Δ δ		Pi	Π π
Epsilon	Ε ε	ε	Rho	Ρ ρ ϱ
Zeta	Ζ ζ		Sigma	Σ σ ς
Eta	Η η		Tau	Τ τ
Theta	Θ θ	θ	Upsilon	Υ υ
Iota	Ι ι		Phi	Φ φ ϕ
Kappa	Κ κ	κ χ	Chi	Χ χ
Lambda	Λ λ		Psi	Ψ ψ
Mu	Μ μ		Omega	Ω ω

RUSSIAN AND ENGLISH TRIGONOMETRIC FUNCTIONS

Russian	English
---------	---------

sin	sin
-----	-----

cos	cos
-----	-----

tg	tan
----	-----

ctg	cot
-----	-----

sec	sec
-----	-----

cosec	csc
-------	-----

sh	sinh
----	------

ch	cosh
----	------

th	tanh
----	------

cth	coth
-----	------

sch	sech
-----	------

csch	csch
------	------

arc sin	\sin^{-1}
---------	-------------

arc cos	\cos^{-1}
---------	-------------

arc tg	\tan^{-1}
--------	-------------

arc ctg	\cot^{-1}
---------	-------------

arc sec	\sec^{-1}
---------	-------------

arc cosec	\csc^{-1}
-----------	-------------

arc sh	\sinh^{-1}
--------	--------------

arc ch	\cosh^{-1}
--------	--------------

arc th	\tanh^{-1}
--------	--------------

arc cth	\coth^{-1}
---------	--------------

arc sch	sech^{-1}
---------	----------------------------

arc csch	csch^{-1}
----------	----------------------------

rot	curl
-----	------

lg	log
----	-----

GRAPHICS DISCLAIMER

All figures, graphics, tables, equations, etc. merged into this translation were extracted from the best quality copy available.

~~see NACCEP ABLE APE P A3 3 I 3~~

Page 1

~~1561~~

~~SUBJECT CODE 41570~~

ATLAS OF THE CASCADE PROFILES OF AXIAL-FLOWS TURBINE.

M. Ye. Deych, doctor of technical sciences, G. A. Philipp, Cand.
tech. sciences, L. Ya. Lazarev, Eng.

Is allowed by the Ministry/department of the higher and special

secondary education of the RSFSR as textbook for the students of the higher academic institutions, which are trained on specialty "turbine construction".

Publishing house "machine-building", Moscow, 1965.

Pages 1-96.

Page 2.

The atlas contains the airfoil/profiles of the nozzle and running cascades of the axial-flows turbine, designed for subsonic, transonic and supersonic speeds. In atlas are given the special shapes of the blades of low altitudes, characteristic cross sections of step/stages with long blades, etc. Furthermore, examined the effect of the different geometric and regime parameters on the characteristics of grid/cascades is given the analysis of the possibility of the calculation of the step/stages of turbines according to the given in atlas characteristics.

Atlas is intended as textbook for the students of VTUZ [99sp04 - higher technical educational institution] of energy specialties, and also it can be useful to the technical-engineering and scientific workers of turbine-constructing plants and scientific research institutes.

Atlas is released to the sixty-year-old anniversary of the Moscow Order of Lenin of energy institute.

Reviewers: the department for the turbine construction of Leningrad polytechnic institute (doctor of technical sciences Prof. Cantor, the s. a., and the Cand. of the tech. sciences of the instructor of the native lands k. g.); doctor of technical sciences Prof. Kazandzhan, p. k.

Page 3. Tables of Contents.

Page 4.

Preface.

For the latter decades Soviet turbine construction passed to the new, aerodynamically more advanced airfoil/profiles of nozzle and running cascades, developed and investigated in the laboratories of the leading scientific research and academic institutes and turbine-constructing plants.

The proposed by laboratories airfoil/profiles of turbine grid/cascades for subsonic speeds lay as the basis of the atlas of airfoil/profiles, and then also the standards, published by central boiler and turbine institute (TsKTI) in 1960-1961.

After having emerged into the world/light of these materials, the works on investigation and improvement of cascade profiles successfully were developed. In the laboratory of the turbomachines of the Moscow Power Engineering Institute (MPI) were developed the airfoil/profiles of nozzle and running cascades for transonic and

supersonic speeds, were created the groups of grid/cascades for step/stages with short blades, for the step/stages, designed for the low relations of the speeds of $\frac{u}{a}$, and also for the last/latter step/stages of the powerful condensation turbines.

As the basis of the shaping of grid/cascades, were placed analytical and semi-empirical methods of calculation. All grid/cascades underwent detailed investigation under the static conditions and in experimental turbines, which made it possible to obtain the reliable aerodynamic characteristics, necessary for the thermal design of step/stages.

The accumulated in the laboratory of the turbomachines of the MPI materials on shaping and study of turbine grid/cascades were systematized and were generalized.

The results of the made work found their reflection, also, in the present atlas.

During training/preparation and compilation of atlas, were used

the materials, obtained in the laboratories of the leading scientific research institutes and turbine-constructing plants. However, into atlas entered only that the airfoil/profiles, which were developed directly in the MPI.

The atlas contains the sufficiently broad class of the various airfoil/profiles, which have the low losses of energy with those which were assigned: velocity triangle, Reynolds numbers and m .

In accordance with this in atlas, are included nozzle and working (active) of grid/cascade for subsonic, transonic and supersonic speeds, to the different reentrance angles and output/yield (with the assigned mach number), and also special grid/cascades for step/stages with the twisted blades.

In atlas are placed also the special shapes of grid/cascades for low relative height/altitudes, nozzle cascades for control stages with revolving diaphragms and for the step/stages, which work with low relations of $\frac{h}{c}$.

The presented in atlas cascade profiles can be used during the design of the control stages of high and low pressure, intermediate and last/latter step/stages of steam and gas turbines.

In the first part of the atlas, are briefly presented the design concepts and calculation of turbine grid/cascades and are given practical procedures of the construction of some airfoil/profiles of special type.

The need for bringing the materials, presented in the first part, is caused by the fact that in many instances during the design of turbines are necessary the grid/cascades, coming out from their parameters beyond the limits of the nomenclature of atlas. Chapter of II-IV make it possible to the reader to estimate effect the groups of the supplementary parameters on the aerodynamic characteristics of grid/cascades. The number of such parameters includes the space and the span of the blade, the angle of setting and the form of airfoil/profile, Re number, M, the reentrance angle of flow, the value of fan-shape and form of the enclosures of circular grid/cascades, overlap/ceiling, roughness, turbulence etc.

In conclusion is set forth the procedure for calculation of step/stages according to the data of the static studies of the isolated/insulated grid/cascades and is given the comparison of the calculated and experimental efficiency (on tests in experimental turbine).

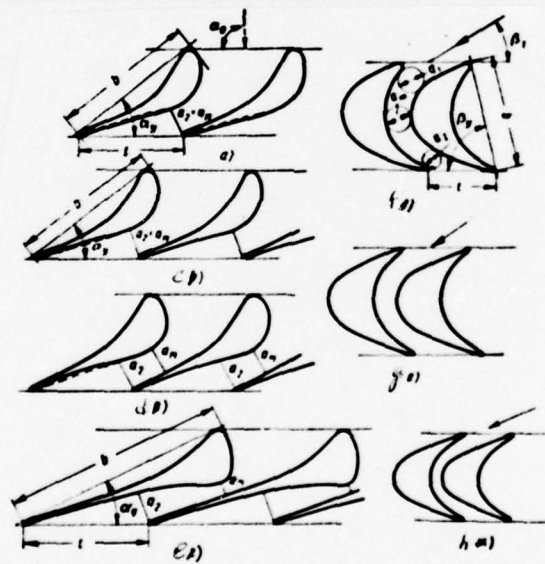
The placed in atlas cascade profiles passed testing in full-scale and model turbines and widely they are utilized in industry.

In the calculations, design and the experimental study of grid/cascades, took part the large group of the colleagues of the laboratory of the turbomachines of the MPI: Candidates of Technical Science V. V. Frolov, V. A. Baranov, A. Ye. Zaryankin, M. P. Zatsepin and A. V. Gubarev; the engineers Ye. V. Mayorskiy, A. G. Sheynkman et al.

Part One

Methods of shaping and the aerodynamic characteristics of
/cascades.

Fig. 1. Forms of airfoil/profiles and channels of jet/reactive and impulse cascades for different mach numbers: a) jet/reactive grid/cascade for subsonic and transonic speeds; b) jet/reactive grid/cascade with constrictions and concave back in skew shear; c, d) jet/reactive grid/cascades with constricting by expanding ducts for supersonic speeds; e, f, g) impulse cascades for subsonic, transonic and supersonic speeds.



Chapter I.

GENERAL INFORMATION.

§ 1. Classification of ~~grid~~/cascades.

All the used in turbine construction grid/cascades can be divided on several groups, by classing them according to different sign/criteria.

According to the designation/purpose of the grid/cascade of turbines, are subdivided into jet/reactive nozzle (fixed) and workers (rotating), and also into active workers and rotary. The latter in turn, can be divided on several groups in terms of Mach numbers ¹ at entry or at the output/yield: A are subsonic ($M < M^*$); b - transonic ($M^* < M < 1.2$); C - supersonic ($M > 1.2$).

FOOTNOTE 1. Mach number = c/a - the ratio of rate of flow c to the speed of sound a ; M^* - the critical Mach number with which at certain point on airfoil/profile is reached the aaaaaaaa (see 2).
ENDFOOTNOTE.

For jet/reactive grid/cascades the characteristically clearly expressed convergent flow in intervane channels. In impulse cascades the medium static pressures at entry and at output/yield are approximately identical and usually differ only by the magnitude of losses of pressure in vane channels.

The classification of grid/cascades can be produced also on geometric parameters - to relative height/altitude and the fanning whose effect must be examined together.

In flow area of the steam and gas turbines, are applied the grid/cascades of low relative height/altitude ($\bar{h} = h/b < 1.0$) and of low fanning ($\theta = d/l > 20$), of the grid/cascade of medium altitude ($\bar{h} = 1.0-3.0$) and of the medium fanning ($\theta = 10-20$) and of the

grid/cascade of high altitude ($\bar{\lambda} > 3.0$) and of large fanning ($\theta < 10$).

In the grid/cascades of the first group, in spite of low fanning, flow it has clearly expressed three-dimensional/space structure in connection with the low altitude which leads to the joining of the secondary flows. Low fanning makes it possible with large reliability to utilize the test results of lattices.

During the simplified investigation of the second group cascade flow can be examined by plane, by eliminating the root and peripheral cross sections where the motion has three-dimensional nature as a result of secondary currents, overflows and a series of other reasons.

The flow about the long blades of large fanning one should relate to the group of spatial problems. The mean sections of such grid/cascades in the first approximation, can be calculated from the characteristics of the foil lattices of the corresponding airfoil/profiles. The blades of the third group usually are fulfilled alternating/variable airfoil/profile by height, and in this case very

important task is the connecting/fitting of the cross sections between themselves. By height of blades should to be provided for a smooth change in the isobars of static pressure on back and the concave surface of airfoil/profiles. In this case, the forms of airfoil/profiles in different cross sections must answer the appropriate Mach numbers and Re.

The forms of the basic airfoil/profiles and grid/cascades with the designation of some geometric parameters are given in Fig. 1 and in Table 1.

§ 2. Designations of basic values, geometric and regime lattice parameters.

The grid/cascades are determined by the form of airfoil/profile and interblade channel. The form of airfoil/profile is assigned by coordinate method 1 in rectangular coordinate system (x, y) , whereupon X-axis it is combined with the chord of airfoil/profile (Fig. 2); the origin of coordinates is arranged/located near the entering edge of airfoil/profile.

FOOTNOTE 1. In the practice of some plants and NII [99sp03 - Scientific Research Institute], it is accepted to assign the form of airfoil/profile and channel by circular arcs. ENDFOOTNOTE.

With the assigned form of airfoil/profile, the size/dimensions and the form of vane channels depend on the basic geometric parameters grid/cascade to number of which they are related (see Fig. 1 and 2):

b - airfoil chord;

t - blade pitch (airfoil/profiles);

B - the width of grid/cascade (airfoil/profile);

l - span of the blade (grid/cascade);

α_i, β_i - the angles of setting airfoil/profiles;

d - the mean diameter of grid/cascade (circular);

the a_1, a_m, a_2 of the width of channel at the entry, in mean section and at output/yield;

δ is a thickness of trailing edge;

R - a radius of the rounding of the intake and trailing edges of airfoil/profile;

$\alpha_{sk}(\beta_{sk})$ are skeletal/skeleton α angles of the entering edges of airfoil/profiles;

$\alpha_{sk}(\beta_{sk})$ are the skeletal/skeleton α angles of the trailing edges of airfoil/profiles;

$\alpha_{1,2} = \arcsin a_2/t_1, \quad \beta_{1,2} = \arcsin a_2/t_2$ - effective carbon of grid/cascades;

x, y - the coordinates of airfoil/profile, which are simultaneously the coordinates of canal surface;

$\Delta B_1; \Delta B_2$ - the difference between the width of grid/cascade and band/shroud/tires entry also at output/yield (hanging of band/shroud/tires);

$\Delta y_1; \Delta y_2$ - the normal distances between the front of grid/cascade and measuring cross sections at entry and at output/yield;

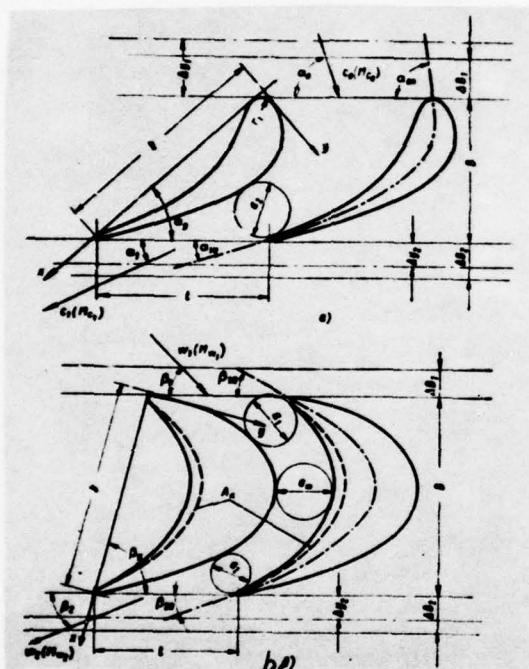
s - distance from entering edge to the assigned cross section throughout the enclosure of airfoil/profile;

s_{tot} are the total length of airfoil/profile of back and the concave surface of airfoil/profile.

FCCTNOTE 2. The skeletal/skeleton angles of airfoil/profile these are the angles between the tangent to camber line on the trailing edges (illegible) of grid/cascade (Fig. 2). ENDFCCTNOTE.

~~End Section.~~

Fig. 2. Designations of the basic geometric and regime parameters of the turbine grid/cascades: a) nozzle cascade; b) running cascade.



In accordance with the rules of the theory of similitude and simulation, and also the taken procedure for calculation and construction of grid/cascades, are introduced dimensionless (relative) geometric parameters;

$\gamma = \frac{h}{b}$ are space;

$l = \frac{h}{b}$ are a relative height/altitude; $\theta = \frac{\alpha}{\gamma}$ - the fanning of grid/cascade;

$\delta_1 = \frac{h_1}{b_1}; \delta_2 = \frac{h_2}{b_2}$ are relative widths of channels;

$\delta = \frac{t}{b}$ - the thickness ratio of edge;

$\bar{x} = \frac{x}{b}; \bar{y} = \frac{y}{b}$ are relative coordinates of airfoil/profile;

$\bar{z} = \frac{z}{b}$ - the relative surface roughness of airfoil/profile (channel);

$\frac{z}{L}$ are a relative distance on the enclosure of airfoil/profile.

In the examination of the joint operation of two grid/cascades (by nozzle and worker), i.e., during the design of step/stage, are introduced the supplementary geometric parameters:

Δ_1 are the upper (peripheral) overlap/ceiling, which shows an increase in altitude of running cascade of periphery;

Δ_2 - lower (is root) overlap/ceiling;

$\Delta_1 + \Delta_2$ - complete overlap/ceiling;

Δ_3 are end play - the distance between trailing edges nozzle and by the entering edges of running cascade.

Flow conditions of the gas through the grid/cascades of turbines are determined by the joint value of the group of the parameters, establish/installed also in accordance with theory of similitude and the rules of simulation. To the group of regime lattice parameters they are related:

α, β - the reentrance angles of flow into grid/cascade;

$M = c/a$; $\lambda = \frac{c}{a}$; $\xi = \frac{w}{a}$ are dimensionless inlet velocities into grid/cascade or after grid/cascade; c ; w is an inlet velocity or at output/yield from nozzle and with respect running cascades;

a - the velocity of propagation of slight disturbances (speed of sound);

c^* are critical speed;

c_{∞} - the maximum escape velocity;

$Re = \frac{c_{\infty} d}{\nu}$ - Reynolds number;

ν are kinematic viscosity;

$\lambda = \frac{u}{c_{\infty}}$ are relative peripheral speed;

u - peripheral speed;

ΔT are the fictitious speed, equivalent to the available heat drop in step/stage;

the $\lambda = \frac{1}{\sqrt{2}} \sqrt{\frac{\Delta T}{c_p T_0}}$ of the degree of flow turbulence before the grid/cascade (initial turbulence level);

c' - fluctuating velocity component;

Δt - the interval of the time of the averaging of speeds.

The dimensionless speeds M ; λ ; ϵ Reynolds numbers are calculated from flow parameters at entry or after grid/cascade. The indicated values can be determined by absolute or relative velocities. In accordance with this, is utilized the following indexing of values:

1 - at the entry into grid/cascade;

2 - after grid/cascade;

c - for an absolute flow;

w - for a relative flow.

Thus, for instance, the M_∞ of Mach number and Re at the entry into running cascade in absolute motion; M_∞, Re_∞ are the same, in relative motion etc.

The aerodynamic characteristics of grid/cascades are called the following values:

ζ - the coefficient of energy losses in grid/cascade;

$\alpha_1; \beta_2$ - the flow exit angles from grid/cascade; μ is a coefficient of expenditure/consumption.

For the designation of the coefficients of constituting energy losses, is accepted the following indexing:

ζ_r - profile losses;

kcn - tip losses;

kr - edge losses;

tr - friction losses;

sum - the total losses.

To turbine-constructing plants and in laboratories are accepted the different methods of the designation of airfoil/profiles and grid/cascades. When selecting the notation of grid/cascades in present atlas were considered the fundamental geometric and the performance characteristics, the convergence of the channels of grid/cascade, the optimum reentrance angles and flow discharge and the calculated dimensionless velocities. Earlier was accepted the notation, in which the first letter T indicated the group of grid/cascade (turbine), the second letter C or F - the type of

grid/cascade (nozzle, working jet/reactive or worker is active). By numeral 0, 1, 2, 3, ... etc. are conditionally shown the reentrance angles and flow discharge (0 - the lowest angles of departure). The last/latter letter in designation indicates the calculated Mach number; A are subsonic speeds, b - transonic and C - supersonic.

For the target/purpose of an increase in the clarity during the development of atlas, the notation was changed. In new designations the first letter indicates the type of grid/cascade (C - nozzle or worker jet/reactive; P - is worker active). The first pair of numerals designates the optimum reentrance angle, and the is second optimum angle of departure (for airfoil/profiles with reentrance angles more than 100° the first three numerals designate reentrance angle). One should emphasize, that each grid/cascade can work in certain, sufficiently the wide, range of the reentrance angles and output/yield; in the designation of airfoil/profile, are indicated the average values of the angles of the optimum zone, given in the table of airfoil/profiles (see Table 1).

The last/latter letter, as in old designations, determines design conditions according to Mach number.

Indices after the last/latter letters they designate:

m - meridian shaping;

k - the grid/cascade of low altitude;

p - the grid/cascade of revolving diaphragms;

r - grid/cascade with expanding ducts.

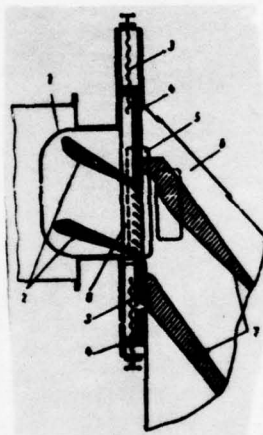
Thus, for instance, grid/cascade of aaaaaaaa is jet/reactive (nozzle or worker), designed for reentrance angle $\alpha_0 = 90^\circ$, angle of departure $\alpha_1 = 15^\circ$, subsonic speeds and carried out with meridian shaping; the grid/cascades of ~~aaaaa~~ - active, worker, calculated are reentrance angles $\beta_1 = 30^\circ$ and output/yield $\beta_2 = 21^\circ$, subsonic speeds and carried out for a low altitude.

3. Procedure for experimental determining the aerodynamic characteristics of grid/cascades.

The primary aerodynamic characteristics, given in atlas, are the coefficients of energy losses in grid/cascades ζ and to the flow exit angles α_1 , β_2 depending on the different regime (M , Re ; α_0 ; β_1 ; E_0 , etc.) and geometric ~~parameters~~ etc.) parameters.

All the characteristics, except ~~some~~ and ~~some~~ are obtained experimental by the way: the tests of direct/straight and tip grid/cascades in wind tunnels by the method of the traversing of flow by probes. The large part of the experimental data is related to grid/cascade tests in air. Some characteristics are obtained in the steam wind tunnels, which work on water vapor. The application/use water pair made it possible to considerably expand the ranges of a change in Re numbers and M , to reliably measure the coefficients of the expenditure of grid/cascades and to carry out the study of grid/cascades of the presence of humidity.

Fig. 3. Diagram of large steam-air wind tunnel the MPI: 1 - converging nozzle section; 2 - the directing nozzle; 3 - the drives of slides; 4 - slides; 5 - the hatch of coordinate spacer apparatus; 6 - the exhaust chamber; 7 - diffuser; 8 - the band plates of package.



The preliminary investigations showed that tests of grid for air and overheated to pair give the satisfactory agreement of results; profile pressure distribution, the coefficients of losses and flow rate, obtained by air and steam tests, they will agree well between themselves.

Design concepts of the used wind tunnels for the study of grid/cascades are very diverse. Very frequently in the MPI are utilized air and vapour pipes with the rotary walls of distributing nozzle, closed (or opened) by test section and diffuser.

Principle diagram of one of the tubes with closed test section is shown in Fig. 3. The study of grid/cascades in this tube is realize/accomplished on vapor and air. In test section are establish/installed the packages of blades by height/altitude to 100 mm by length along front to 350 mm. The reentrance angle of flow into grid/cascade is changed from 15 to 165°. The flow exit angle can oscillate within limits from 8 to 50°. At output/yield into test section, is placed converging nozzle section 1. The pressure chamber of test section provides the uniform field of the speeds of flow at the entry into distributing nozzle 2, arrange/located before the grid/cascade. In pressure chamber is arranged the vent system for

determining the static pressures and pressures of braking. The construction of test section makes it possible to conduct the point measurements of flow direction at the entry into grid/cascade.

The reentrance angle of flow into grid/cascade is assigned by distributing nozzle 2, which specially shaped to the assigned range of the reentrance angles and Mach numbers. Rotary nozzle liners are fastened motionlessly to the band plates of 8 package of blades and together with it are established/installed in test section. In test section the package is clamped by sliders 4, which have helical drives 3. At output/yield from grid/cascade, is established/installed diffuser 7, which makes it possible substantially to increase Mach number at output/yield from grid/cascade.

The exhaust chamber has the branched vent system for the measurement of static pressures. Here are placed probes for the study of flow after grid/cascade. Probes are moved in the special hatch of coordinate spacer apparatus 5, where it is fixed on the condensed stock/rod of the coordinate spacer apparatus, which has four degrees of freedom.

Control of the coordinate spacer apparatus, established/installed on test section, complete automatic. There are several protective systems, which duplicate one another and eliminating a breakage in the probe in the process of experiment.

By the direct continuation of test section serves the diffuser, carried out with the relation of the yield cross sections and entry, equal to 2.0-2.5. The corresponding pressure ratio in diffuser is 2-2.5. Diffuser is connected with the exhaust duct, derived into condenser/capacitor.

During determining the total characteristics of grid/cascades, the inlet boundary layer into grid/cascade was not intercept/detached, and the thickness of it comprised $\delta = 1.5-2.5$ mm depending on mode/conditions (Re numbers and M). Thus, the field of inlet velocities by height of grid/cascade during tests was nonuniform. The open end play (clearance between the distributing nozzle and the band/shroud/tires of grid/cascade) he was accepted zero. Overlap/ceiling in experiments was accepted different: nozzle cascades were experience/tested without overlap/ceiling, and workers - with overlap/ceiling from 1.5 to 3 mm to side. The number of blades in package composed $z = 6-12$.

The measurement flow parameters was conducted at a distance (0.1-0.2) b (b is an airfoil chord) by the pneumatic probes of complete and static pressure and by azimuth scale protractor. The outer diameter of the picture tubes of probes is accepted 0.5-0.8 mm.

Processing the experimental data was conducted by conventional procedure [6]. For determining the local coefficients of the losses of aaaa, was measured constant stagnation pressure before grid/cascade p_0 , change of the stagnation pressure in each point after the grid/cascade of aaaa and static pressure after grid/cascade p_1 .

The coefficient of energy losses at point was determined from known formula [6]

$$\zeta = 1 - \frac{M_1^2}{M_0^2} = \frac{k-1}{k} \frac{1 - \left[1 - \frac{\Delta p_0}{p_0} (1-\epsilon)\right]^{\frac{k-1}{k}}}{\left(1 - \epsilon^{\frac{k-1}{k}}\right) \left[1 - \frac{\Delta p_0}{p_0} (1-\epsilon)\right]^{\frac{k-1}{k}}}, \quad (1)$$

where of the $\pi = \frac{p_1}{p_0}$ - ratio of pressure at point after grid/cascade;

$\Delta p_t = (p_{t0} - p_{t1})$ - a change of the stagnation pressure in grid/cascade;

$p_0 = (p_0 - p_1)$ - excess initial pressure.

Before the spout of probe at supersonic speeds, is formed the normal shock wave; the correction, which considers a change of the stagnation pressure in jump, easy to introduce into equation (1).

Let us present

$$\Delta p_i = \Delta p_n - \Delta p_{st}$$

where the Δp_n - reading manometer;

Δp_{st} - the change of the stagnation pressure in normal shock, determined in the formula:

$$\Delta p_{st} = p_0 \left[1 - \frac{\left(\frac{k+1}{k-1} \right)^{\frac{k+1}{k-1}} M_1^2 \frac{2k}{k-1}}{\left(M_1^2 + \frac{2}{k-1} \right)^{\frac{k}{k-1}} \left(\frac{2k}{k-1} M_1^2 - 1 \right)^{\frac{1-k}{k}}} \right] \quad (2)$$

here M_1 is Mach number before the jump;

k - the index of isentropic process.

The averaging of losses after grid/cascade was conducted directly by area by graphical integration not allowing for expenditure velocity component. This averaging gives to somewhat to high loss factors.

Pressure measurements were realized/accomplished by U-shaped water or mercury pressure gauges. With large pressure differentials, which correspond to supersonic speeds after grid/cascade, the measurements were carried out by spring specimen manometers. Temperatures were measured by platinum resistance thermometers and by mercury thermometers with scale value 0.1°C . During the study of grid/cascades on water vapor, all the coupling communications of the meters of pressure were derived/concluded horizontally, in order to exclude the effect being condensed pair on readings of manometers. The flow exit angle was measured by probe by the azimuth scale protractor, picture tubes of which were arranged one above another. This arrangement of tubes made it possible to considerably decrease

an error of measurement of the flow exit angle in point, which was being strongly changed on lattice spacing.

Systematic investigations and the careful calibration of instruments ensured the high accuracy/precision of experiment. The accuracy/precision of the determination of the coefficient of losses ζ in airfoil cascade during static investigations it is possible to estimate, by utilizing the common/general/total expression for the calculation of the maximum relative error:

$$\delta_{\zeta} = \frac{\Delta \zeta}{\zeta} = \pm \frac{k-1}{k} \times$$

$$\times \left[\frac{ds}{s} + \frac{de}{e^{\frac{1}{k}+1}} + \frac{d \left(\frac{\Delta p_t}{\rho_0} \right) (1-e) - \frac{\Delta p_t}{\rho_0} de}{\left[1 - \frac{\Delta p_t}{\rho_0} (1-e) \right] - \left[1 - \frac{\Delta p_t}{\rho_0} (1-e) \right]^{\frac{2k-1}{k}}} \right], \quad (3)$$

where

$$d\left(\frac{\Delta p_i}{\rho_0}\right) = \pm \left(\frac{d\Delta p_i}{\Delta p_i} + \frac{d\rho_0}{\rho_0}\right) \frac{\Delta p_i}{\rho_0};$$

$$\frac{d\Delta p_i}{\Delta p_i} = \pm \left(\frac{d\rho_1}{\rho_1} + \frac{d\rho_0}{\rho_0}\right).$$

the accuracy of reading of the entering the formula values it comprises: $\Delta \Delta p_i = \Delta p_i = \Delta p_i = 0.5$ mm mercury column (in experiments on mercury pressure gauges).

Let us examine the concrete/specific/actual case in practice minimum the pressure differential in grid/cascade when using the mercury pressure gauges: $p'_0 = 250$ mm mercury column; the remaining parameters of measurements the following: $p_1 = 750$ mm Hg. column; $\Delta p_i = 11$ mm Hg. column. The ratio of pressure on cascade composes $\mu = 0.75$, and the coefficient of losses $\zeta = 40\%$.

Calculation for this mode/conditions gives the maximum relative

error:

$$\Delta \mu = \frac{\Delta \zeta}{\zeta} = \pm 0.04.$$

the absolute error of determination ζ in this case comprises

$$\Delta \zeta = \pm 0.16\%.$$

necessary to note that the basic experimental error during the static studies of grid/cascades is connected with a relative error in value determination of $\Delta \mu$. The root-mean-square error of experiments, which characterizes the value of random errors during determination ζ , comprised $\pm (0.3-0.6)$ c/c. The accuracy/precision of the angle measurement of flow discharge from grid/cascades comprised in experiments 0.3-0.5°.

During the determination of the coefficients of the flow rate μ

in nozzle and running cascades, the real consumption of air was determined from metering orifice with accuracy/precision $\pm 1.50\%$, while during the studies of grid/cascades on water vapor with the aid of measuring tanks - with accuracy/precision $\pm 0.50\%$. Theoretical flow rate was calculated from the formula:

$$G = F_1 \sqrt{\frac{2}{\gamma-1} \cdot \frac{p_0}{\rho_0}} \sqrt{\frac{\gamma}{\gamma-1} \left(1 - \frac{p}{p_0} \right)^{\frac{\gamma-1}{\gamma}}}. \quad (4)$$

where F_1 is an area of the minimum cross section of nozzle.

Page 10.

Table 1.

1	2	3	4	5	6	7	8	9	10	11	12	13	14	15	16	17	18	19	20	21	22	23	24	25	26	27	28	29	30	31	32	33	34	35	36	37	38	39	40	41	42	43	44	45	46	47	48	49	50	51	52	53	54	55	56	57	58	59	60	61	62	63	64	65	66	67	68	69	70	71	72	73	74	75	76	77	78	79	80	81	82	83	84	85	86	87	88	89	90	91	92	93	94	95	96	97	98	99	100	101	102	103	104	105	106	107	108	109	110	111	112	113	114	115	116	117	118	119	120	121	122	123	124	125	126	127	128	129	130	131	132	133	134	135	136	137	138	139	140	141	142	143	144	145	146	147	148	149	150	151	152	153	154	155	156	157	158	159	160	161	162	163	164	165	166	167	168	169	170	171	172	173	174	175	176	177	178	179	180	181	182	183	184	185	186	187	188	189	190	191	192	193	194	195	196	197	198	199	200	201	202	203	204	205	206	207	208	209	210	211	212	213	214	215	216	217	218	219	220	221	222	223	224	225	226	227	228	229	230	231	232	233	234	235	236	237	238	239	240	241	242	243	244	245	246	247	248	249	250	251	252	253	254	255	256	257	258	259	260	261	262	263	264	265	266	267	268	269	270	271	272	273	274	275	276	277	278	279	280	281	282	283	284	285	286	287	288	289	290	291	292	293	294	295	296	297	298	299	300	301	302	303	304	305	306	307	308	309	310	311	312	313	314	315	316	317	318	319	320	321	322	323	324	325	326	327	328	329	330	331	332	333	334	335	336	337	338	339	340	341	342	343	344	345	346	347	348	349	350	351	352	353	354	355	356	357	358	359	360	361	362	363	364	365	366	367	368	369	370	371	372	373	374	375	376	377	378	379	380	381	382	383	384	385	386	387	388	389	390	391	392	393	394	395	396	397	398	399	400	401	402	403	404	405	406	407	408	409	410	411	412	413	414	415	416	417	418	419	420	421	422	423	424	425	426	427	428	429	430	431	432	433	434	435	436	437	438	439	440	441	442	443	444	445	446	447	448	449	450	451	452	453	454	455	456	457	458	459	460	461	462	463	464	465	466	467	468	469	470	471	472	473	474	475	476	477	478	479	480	481	482	483	484	485	486	487	488	489	490	491	492	493	494	495	496	497	498	499	500	501	502	503	504	505	506	507	508	509	510	511	512	513	514	515	516	517	518	519	520	521	522	523	524	525	526	527	528	529	530	531	532	533	534	535	536	537	538	539	540	541	542	543	544	545	546	547	548	549	550	551	552	553	554	555	556	557	558	559	560	561	562	563	564	565	566	567	568	569	570	571	572	573	574	575	576	577	578	579	580	581	582	583	584	585	586	587	588	589	590	591	592	593	594	595	596	597	598	599	600	601	602	603	604	605	606	607	608	609	610	611	612	613	614	615	616	617	618	619	620	621	622	623	624	625	626	627	628	629	630	631	632	633	634	635	636	637	638	639	640	641	642	643	644	645	646	647	648	649	650	651	652	653	654	655	656	657	658	659	660	661	662	663	664	665	666	667	668	669	670	671	672	673	674	675	676	677	678	679	680	681	682	683	684	685	686	687	688	689	690	691	692	693	694	695	696	697	698	699	700	701	702	703	704	705	706	707	708	709	710	711	712	713	714	715	716	717	718	719	720	721	722	723	724	725	726	727	728	729	730	731	732	733	734	735	736	737	738	739	740	741	742	743	744	745	746	747	748	749	750	751	752	753	754	755	756	757	758	759	760	761	762	763	764	765	766	767	768	769	770	771	772	773	774	775	776	777	778	779	780	781	782	783	784	785	786	787	788	789	790	791	792	793	794	795	796	797	798	799	800	801	802	803	804	805	806	807	808	809	810	811	812	813	814	815	816	817	818	819	820	821	822	823	824	825	826	827	828	829	830	831	832	833	834	835	836	837	838	839	840	841	842	843	844	845	846	847	848	849	850	851	852	853	854	855	856	857	858	859	860	861	862	863	864	865	866	867	868	869	870	871	872	873	874	875	876	877	878	879	880	881	882	883	884	885	886	887	888	889	890	891	892	893	894	895	896	897	898	899	900	901	902	903	904	905	906	907	908	909	910	911	912	913	914	915	916	917	918	919	920	921	922	923	924	925	926	927	928	929	930	931	932	933	934	935	936	937	938	939	940	941	942	943	944	945	946	947	948	949	950	951	952	953	954	955	956	957	958	959	960	961	962	963	964	965	966	967	968	969	970	971	972	973	974	975	976	977	978	979	980	981	982	983	984	985	986	987	988	989	990	991	992	993	994	995	996	997	998	999	1000
C 8000A	7-11	70-120	0.72-0.85	27-31	0.65-0.95	TC-0A	1																																																																																																																																																																																																																																																																																																																																																																																																																																																																																																																																																																																																																																																																																																																																																																																																																																																																																																																																																																																																																																
C 8012A	10-14	70-120	0.72-0.87	31-35	0.60-0.85	TC-1A	2-3																																																																																																																																																																																																																																																																																																																																																																																																																																																																																																																																																																																																																																																																																																																																																																																																																																																																																																																																																																																																																																
C 8015A	13-17	70-120	0.70-0.85	35-40	0.50-0.75	TC-2A	4-5																																																																																																																																																																																																																																																																																																																																																																																																																																																																																																																																																																																																																																																																																																																																																																																																																																																																																																																																																																																																																																
C 8018A	16-20	70-120	0.70-0.80	40-44	0.40-0.85	TC-3A	5																																																																																																																																																																																																																																																																																																																																																																																																																																																																																																																																																																																																																																																																																																																																																																																																																																																																																																																																																																																																																																
C 8022A	20-24	70-120	0.70-0.80	43-46	0.60-0.95	—	6																																																																																																																																																																																																																																																																																																																																																																																																																																																																																																																																																																																																																																																																																																																																																																																																																																																																																																																																																																																																																																
C 8027A	24-30	70-120	0.65-0.75	46-50	0.60-0.90	—	7																																																																																																																																																																																																																																																																																																																																																																																																																																																																																																																																																																																																																																																																																																																																																																																																																																																																																																																																																																																																																																
C 8030A	30-36	70-120	0.62-0.75	51-59	0.65-0.95	—	7																																																																																																																																																																																																																																																																																																																																																																																																																																																																																																																																																																																																																																																																																																																																																																																																																																																																																																																																																																																																																																
C 8038A	36-42	70-120	0.60-0.75	60-67	0.65-0.95	—	8																																																																																																																																																																																																																																																																																																																																																																																																																																																																																																																																																																																																																																																																																																																																																																																																																																																																																																																																																																																																																																
C 8045A	42-48	70-120	0.72-0.87	51-57	0.70-0.95	TC-1A-1	9																																																																																																																																																																																																																																																																																																																																																																																																																																																																																																																																																																																																																																																																																																																																																																																																																																																																																																																																																																																																																																
C 8050A	48-54	70-120	0.70-0.85	61-67	0.70-0.95	—	10																																																																																																																																																																																																																																																																																																																																																																																																																																																																																																																																																																																																																																																																																																																																																																																																																																																																																																																																																																																																																																
C 1525A	21-28	35-65	0.60-0.75	63-69	0.65-0.95	—	11																																																																																																																																																																																																																																																																																																																																																																																																																																																																																																																																																																																																																																																																																																																																																																																																																																																																																																																																																																																																																																
C 6030A	27-34	45-85	0.52-0.70	68-73	0.65-0.95	—	12																																																																																																																																																																																																																																																																																																																																																																																																																																																																																																																																																																																																																																																																																																																																																																																																																																																																																																																																																																																																																																
C 6035A	32-38	45-85	0.42-0.65	70-75	0.70-0.95	—	13																																																																																																																																																																																																																																																																																																																																																																																																																																																																																																																																																																																																																																																																																																																																																																																																																																																																																																																																																																																																																																
C 6020A	17-23	50-85	0.60-0.70	50-56	0.70-0.95	—	14																																																																																																																																																																																																																																																																																																																																																																																																																																																																																																																																																																																																																																																																																																																																																																																																																																																																																																																																																																																																																																
C 7025A	22-28	55-90	0.50-0.67	57-63	0.70-0.95	—	15																																																																																																																																																																																																																																																																																																																																																																																																																																																																																																																																																																																																																																																																																																																																																																																																																																																																																																																																																																																																																																
P 2314A	12-16	20-30	0.60-0.75	75-80	0.75-0.95	TP-0A	16-17																																																																																																																																																																																																																																																																																																																																																																																																																																																																																																																																																																																																																																																																																																																																																																																																																																																																																																																																																																																																																																
P 2617A	15-19	23-35	0.60-0.70	75-80	0.75-0.95	TP-1A	17-18																																																																																																																																																																																																																																																																																																																																																																																																																																																																																																																																																																																																																																																																																																																																																																																																																																																																																																																																																																																																																																
P 3021A	19-24	25-40	0.58-0.68	77-81	0.70-0.90	TP-2A	19-20																																																																																																																																																																																																																																																																																																																																																																																																																																																																																																																																																																																																																																																																																																																																																																																																																																																																																																																																																																																																																																
P 3525A	22-28	30-50	0.55-0.65	78-82	0.60-0.85	TP-3A	21-22																																																																																																																																																																																																																																																																																																																																																																																																																																																																																																																																																																																																																																																																																																																																																																																																																																																																																																																																																																																																																																
P 4629A	25-32	44-60	0.45-0.58	78-80	0.55-0.85	TP-4A	22																																																																																																																																																																																																																																																																																																																																																																																																																																																																																																																																																																																																																																																																																																																																																																																																																																																																																																																																																																																																																																
P 5033A	30-36	47-65	0.43-0.55	76-80	0.55-0.85	TP-5A	23																																																																																																																																																																																																																																																																																																																																																																																																																																																																																																																																																																																																																																																																																																																																																																																																																																																																																																																																																																																																																																
P 5535A	32-38	50-70	0.42-0.52	77-81	0.55-0.85	TP-6A	24																																																																																																																																																																																																																																																																																																																																																																																																																																																																																																																																																																																																																																																																																																																																																																																																																																																																																																																																																																																																																																
P 6038A	35-42	55-75	0.41-0.51	75-80	0.55-0.85	TP-7A	24																																																																																																																																																																																																																																																																																																																																																																																																																																																																																																																																																																																																																																																																																																																																																																																																																																																																																																																																																																																																																																
P 2314A _u	12-16	20-30	0.60-0.75	75-80	0.70-0.95	TP-0A _u	25-26																																																																																																																																																																																																																																																																																																																																																																																																																																																																																																																																																																																																																																																																																																																																																																																																																																																																																																																																																																																																																																
P 2617A _u	15-19	23-35	0.60-0.70	77-81	0.70-0.95	TP-1A _u	26-27																																																																																																																																																																																																																																																																																																																																																																																																																																																																																																																																																																																																																																																																																																																																																																																																																																																																																																																																																																																																																																
P 3021A _u	19-24	25-40	0.58-0.68	78-82	0.70-0.90	TP-2A _u	28-29																																																																																																																																																																																																																																																																																																																																																																																																																																																																																																																																																																																																																																																																																																																																																																																																																																																																																																																																																																																																																																
P 3525A _u	22-28	30-50	0.55-0.65	78-82	0.60-0.85	TP-3A _u	29-30																																																																																																																																																																																																																																																																																																																																																																																																																																																																																																																																																																																																																																																																																																																																																																																																																																																																																																																																																																																																																																
C 8012B	10-14	70-120	0.72-0.87	31-35	0.65-1.10	TC-1B	31																																																																																																																																																																																																																																																																																																																																																																																																																																																																																																																																																																																																																																																																																																																																																																																																																																																																																																																																																																																																																																
C 8015B	13-17	70-120	0.70-0.85	35-40	0.65-1.10	TC-2B	32																																																																																																																																																																																																																																																																																																																																																																																																																																																																																																																																																																																																																																																																																																																																																																																																																																																																																																																																																																																																																																
C 8018B	16-20	70-120	0.70-0.80	40-44	0.65-1.10	TC-3B	31																																																																																																																																																																																																																																																																																																																																																																																																																																																																																																																																																																																																																																																																																																																																																																																																																																																																																																																																																																																																																																
P 2717B	15-19	23-35	0.57-0.65	76-81	0.80-1.10	TP-1B	33-34																																																																																																																																																																																																																																																																																																																																																																																																																																																																																																																																																																																																																																																																																																																																																																																																																																																																																																																																																																																																																																
P 2717B _u	15-19	23-35	0.57-0.68	76-81	0.85-1.10	—	34-35																																																																																																																																																																																																																																																																																																																																																																																																																																																																																																																																																																																																																																																																																																																																																																																																																																																																																																																																																																																																																																
P 3021B	19-24	25-40	0.55-0.65	77-81	0.85-1.10	TP-2B	36																																																																																																																																																																																																																																																																																																																																																																																																																																																																																																																																																																																																																																																																																																																																																																																																																																																																																																																																																																																																																																
P 3525B	22-28	30-50	0.55-0.65	77-81	0.85-1.10	TP-3B	37																																																																																																																																																																																																																																																																																																																																																																																																																																																																																																																																																																																																																																																																																																																																																																																																																																																																																																																																																																																																																																
P 4629B	25-32	44-60	0.53-0.68	77-81	0.85-1.10	TP-4B	37																																																																																																																																																																																																																																																																																																																																																																																																																																																																																																																																																																																																																																																																																																																																																																																																																																																																																																																																																																																																																																
C 8000B	7-10	70-120	0.60-0.70	27-31	1.4-1.60	—	38																																																																																																																																																																																																																																																																																																																																																																																																																																																																																																																																																																																																																																																																																																																																																																																																																																																																																																																																																																																																																																
C 8012B	10-14	70-120	0.58-0.68	36-43	1.4-1.70	—	38																																																																																																																																																																																																																																																																																																																																																																																																																																																																																																																																																																																																																																																																																																																																																																																																																																																																																																																																																																																																																																
C 8015B	13-17	70-120	0.55-0.65	38-42	1.4-1.70	—	40																																																																																																																																																																																																																																																																																																																																																																																																																																																																																																																																																																																																																																																																																																																																																																																																																																																																																																																																																																																																																																
C 8018B	16-20	70-120	0.55-0.65	47-52	1.4-1.70	—	41																																																																																																																																																																																																																																																																																																																																																																																																																																																																																																																																																																																																																																																																																																																																																																																																																																																																																																																																																																																																																																
P 2116B	16-20	19-24	0.60-0.70	66-69	1.3-1.60	TP-1B	42																																																																																																																																																																																																																																																																																																																																																																																																																																																																																																																																																																																																																																																																																																																																																																																																																																																																																																																																																																																																																																
P 3522B	20-24	23-27	0.54-0.65	87-90	1.35-1.60	TP-2B	43																																																																																																																																																																																																																																																																																																																																																																																																																																																																																																																																																																																																																																																																																																																																																																																																																																																																																																																																																																																																																																
P 3522B _u	23-27	26-32	0.53-0.63	87-90	1.35-1.60	TP-2B _u	44																																																																																																																																																																																																																																																																																																																																																																																																																																																																																																																																																																																																																																																																																																																																																																																																																																																																																																																																																																																																																																
P 3522B _u	26-32	30-36	0.51-0.61	87-90	1.35-1.60	TP-4B	46																																																																																																																																																																																																																																																																																																																																																																																																																																																																																																																																																																																																																																																																																																																																																																																																																																																																																																																																																																																																																																
P 3522B _u	23-27	26-32	0.48-0.58	87-90	1.35-1.75	—	45																																																																																																																																																																																																																																																																																																																																																																																																																																																																																																																																																																																																																																																																																																																																																																																																																																																																																																																																																																																																																																
C 8013B	10-16	70-120	0.41-0.50	43-47	—	—	46																																																																																																																																																																																																																																																																																																																																																																																																																																																																																																																																																																																																																																																																																																																																																																																																																																																																																																																																																																																																																																
C 8013B _u	10-16	70-120	0.55-0.67	41-49	—	—	47																																																																																																																																																																																																																																																																																																																																																																																																																																																																																																																																																																																																																																																																																																																																																																																																																																																																																																																																																																																																																																
P 2726B	26-32	30-35	0.																																																																																																																																																																																																																																																																																																																																																																																																																																																																																																																																																																																																																																																																																																																																																																																																																																																																																																																																																																																																																																				

Key: (1). Designation. (2). opt. α_1 opt. β_2 in deg. (3). opt. α_0 opt. β_1 in deg. (4) opt. are aaaa opt. aaaa in deg. (5). Old designation. (6). plate.

Table 2. Airfoil/profiles of nozzle (directing) and running cascades, connected in standard.

1	2 Диапазон углов в град.		3	Прочностные характеристики *				4	5	6	7
	назад α_1 ; β_1	вперед α_2 ; β_2		$\sigma_{\text{ср}}$	$\sigma_{\text{сн}}$	$\sigma_{\text{г ст. ср}}$	$\sigma_{\text{г ст. ср}}$				
H-1	9-15	70-110	2,403	0,313	0,385	1,676	0,905	0,1976	2,127	C-1	8 ЦНДН
H-2	12-20	70-110	1,46	0,135	0,184	0,770	0,455	0,0916	1,000	TH-2	8 м. Крылья
H-3	9-15	70-110	2,43	0,230	0,300	1,000	0,550	0,3165	2,401	TH-3	ЦНДН
H-4	10-17	70-110	2,185	0,222	0,300	1,000	0,700			TC-1A	8 м. Крылья
IP-1	17	30	7,105	1,531	2,305	5,005	3,023	2,94	12,61	A-30	9 ЦНДН
3P-1	24	35	7,001	1,005	2,110	5,100	3,002	2,007	11,00	A-34	м. Крылья
4P-1	31	45	6,155	1,205	1,817	4,001	2,105	1,204	10,05	A-35	ЦНДН
IP-2	17	30	7,457	2,000	2,605	5,315	4,177	3,002	11,00	T-1	8 м. Крылья
3P-2	24	35	7,131	1,027	2,312	5,007	3,740	2,000	11,00	T-2A	ЦНДН
3P-2	24	35	5,004	1,310	1,807	3,907	3,013	1,777	8,704		
3P-4	20	30	7,300	1,007	2,400	5,300	3,700	2,307	11,10	TP-2A	
4P-4	31	45	4,850	0,800	1,100	3,207	2,600	1,600	7,300	TP-4A	8 м. Крылья
5P-4	24	30	4,113	0,6007	0,8005	2,970	2,100	0,7014	6,400	TP-5A	

* Даны для стандартных режимов работы: $B=15$ мм и для режимов работы: $B=10$ мм; $\sigma_{\text{ср}}$, $\sigma_{\text{сн}}$, $\sigma_{\text{г ст. ср}}$ — статические характеристики профилей стандартных серий 1-1 и 2-2 (см. 4); $\sigma_{\text{г ст. ср}}$ — статическая нагрузка стандартных серий 1-1 и 2-2 (см. 4); $\sigma_{\text{г ст. ср}}$ — статическая нагрузка стандартных серий 1-1 и 2-2 (см. 4).

DOC = 76021693

PAGE

~~25~~
44

Key: (1). Adopted in normal designations of airfoil/profiles. (2).
Range of angles in deg. (3). Strength characteristics ¹.

FOOTNOTE 1. Are given for nozzle cascades by width $B = 25$ mm and for running cascades by width $B = 50$ mm; $\omega_x, \omega_y (cm^3)$ - torque/moments of resistance of airfoil/profiles relative to axle/axes of x-x and y-y (Fig. 4); J_x, J_y - the torque/moments of inertia relative to axle/axes of x-x and y-y (cm^3); F - sectional area blade (cm^2).
ENDFOOTNOTE.

(4). Old designation of airfoil/profile. (5) the organizations, which developed airfoil/profile. (6). output/yield. (7). entry. (8). named after Krylov. (9). named after Krylov.

§ 4. General table of the airfoil/profiles of turbine grid/cascades.

The given in the present atlas jet/reactive and impulse cascades are subdivided into 3 groups: 1 - subsonic $M_{\infty} = 0.4-0.9$ (group A), 2 - transonic $M_{\infty} = 0.9-1.2$ (group B) and 3 - supersonic $M > 1.2$ (group C).

The airfoil/profiles of group A have enclosures vary smoothly curvature, whereupon intake and trailing edge are rounded off. Vane channels are carried out being smoothly constricted to output/yield. The maximum convergence corresponds to the channels of nozzle and jet/reactive running cascades, and minimum - to the channels of active running cascades.

For low relative height/altitudes impulse cascades should be performed with divergent-convergent channels (group of A₁) while for nozzle cascades is applied three-dimensional/space, meridional shaping (group of A₂).

The airfoil/profiles of nozzle cascades for transonic speeds (group b) are carried out with straight portions on back in skew shear. The active running cascades of group b have rectilinear enclosures also on the intake of back. Channels of the grid/cascades of this group being smoothly constricted. A radius of the rounding of entering edges is decreased.

Nozzle cascades for supersonic speeds (group c) are carried out with concave surface on the output section of back in skew shear. For high supersonic speeds vane channels constrict-being expanded. Impulse cascades with $M > 1.5$ are fulfilled also with the contracting-expanding channels.

In atlas are given the airfoil/profiles of the characteristic cross sections of the step/stages of large fanning. Root cross sections are intended for a work at the reentrance angles of flow β_1 , equal or less than angle of departure β , from grid/cascade. Peripheral cross sections are designed at angles of entry β_1 , which considerably exceed 90° .

Are separately examined the airfoil/profiles of the nozzle cascades, intended for the intermediate step/stages, which work in the low relations of $\frac{1}{4}$: jet/reactive grid/cascades with low reentrance angle $\alpha_0 < 90^\circ$.

All the given in atlas airfoil/profiles and their basic geometric and regime parameters are brought in Table 1.

§ 5. Standards to cascade profiles.

The used at the point of at present turbine-constructing plants airfoil/profiles of turbine grid/cascades have low profile and tip losses. The nomenclature of these airfoil/profiles is very great.

For the target/purpose of the limitation of the number of airfoil/profiles and their typical dimensions, part of the airfoil/profiles of nozzle and running cascades is normalized. In

standard are included the airfoil/profiles only for subsonic speeds (group A). Table 2 gives the basic parameters of the normalized grid/cascades.

Standard includes four airfoil/profile of nozzle blades and nine airfoil/profiles of active type rotor blades. The airfoil/profiles of the nozzle (guides) grid/cascades H-1, H-2 and H-4 have approximately the identical range of the flow exit angles $\alpha_1 = 9-15^\circ$ (20°), but different mechanical characteristics. The airfoil/profiles of running cascades cover the range of angles of departure $\beta_2 = 17-34^\circ$. The optimum reentrance angles are changed in interval $\beta_1 = 20-50^\circ$.

Table 2 gives the new designations of airfoil/profiles. Complete designations let us examine in an example of airfoil/profiles H-12-B and 4P-42-B. Here letter H and with respect to P indicates the type of grid/cascade (directing, i.e., nozzle and worker). Numeral after letters H and P (1, 2, 3, 4, ...) indicates the organization, which developed airfoil/profile.

For running cascades the numerals before letter P indicate the angle of rotation of flow, i.e., the geometry of airfoil/profile on

velocity triangle. With an increase in the number, the angles of departure and entry grow/rise, but the angle of rotation of flow with respect decreases. The second numeral in designation of nozzle (guides) and the third in the designation of running cascades characterizes the thickness of trailing edge.

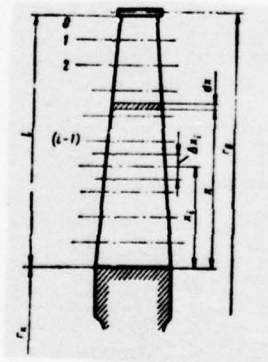


Fig. 5. On the calculation of the strength characteristics of grid/cascades.

Letter V gives the width of airfoil/profile in millimeters. All airfoil/profiles of the nozzle and running cascades of the development of group depending on the thickness ratio of trailing edge δ .

Aerodynamic characteristics include the dependences of the coefficients of the profile and tip energy losses and flow exit angles from the basic geometric and regime lattice parameters. Characteristics are obtained experimentally, the tests of lattices in wind tunnels by the method of traversing, with the cut-off of the boundary layer of the distributing nozzles of test sections.

Aerodynamic characteristics can be reliably used when selecting the optimum version of grid/cascades for the design/projected step/stage, and also to evaluate the effect of the marked out changes in the geometric and regime parameters.

§ 6. Strength air foil data.

For structural/design molding and strength calculation of blade

machinery of turbine, it is necessary to have the dimensional characteristics of airfoil/profiles.

The dimensional characteristics of flat/plane profile cross section (Fig. 4) can be determined by the different methods, known in the literature [18].

The coordinates of the center of gravity x_0 and y_0 are obtained from the condition of equality to zero of static moments relative to central axle/axes.

The area of airfoil/profile F was determined by the measuring with planimeter of the cross section, traced to scale 10:1, and it was checked analytically, by the indicated method.

The moments of inertia of J_{x_0} and J_{y_0} are calculated relative to axle/axes x_1 and y_1 , parallel to x and y axes and passing through the center of gravity of airfoil/profile (Fig. 4).

In the majority of cases for turbine blades, the principal axes of inertia ξ and η compose with axle/axes x_1 and y_1 sufficiently small angle; however, if necessary the principal moments of inertia of J_{ξ} and J_{η} and angle of rotation β the principal axis of inertia relative to x -axis can be determined by formulas

$$J_{\xi} = J_x - \frac{1}{2}(J_{xx} + J_{yy} - \sqrt{(J_{xx} - J_{yy})^2 + 4J_{xy}^2});$$

$$J_{\eta} = J_y + \frac{1}{2}(J_{xx} + J_{yy} + \sqrt{(J_{xx} - J_{yy})^2 + 4J_{xy}^2});$$

$$\tan 2\beta = \frac{2J_{xy}}{J_{xx} - J_{yy}}.$$

where the J_{xy} is product of inertia.

By having geometric parameters of airfoil/profile and moments of inertia, it is possible to determine the modulus of section, relative to the appropriate axle/axis: $W = \frac{J}{r_{\max}}$. Here J is the moment of inertia relative to which interests us axle/axis;

r_{\max} - the maximum distance from this axle/axis to the point

of airfoil/profile.

Give in the tables of the atlas of value w are related:

J_{x_1} - the moment of resistance for a back relative to axle/axis x_1 ;

$J_{x_1}^{\text{edges}}$ - moment of resistance for edges relative to axle/axis x_1 ;

J_{y_1} - moment of resistance for an entering edge relative to axle/axis y_1 ;

$J_{y_1}^{\text{trailing}}$ - moment of resistance for a trailing edge relative to axle/axis y_1 .

For the calculation of the vibration characteristics of blade, it is necessary to know the radius of inertia, which can be found on

formula

$$\sigma = \sqrt{\frac{J}{F}}$$

where ρ and J - radius of inertia and the moment of inertia for the appropriate axle/axis;

F - the sectional area of airfoil/profile.

Some dimensional characteristics of airfoil/profiles are given in atlas for one airfoil chord, designated on drawings. In the case of a difference of the chord from drawing size/dimensions, the conversion of dimensional characteristics for another chord is conducted by the multiplication of the tabulated data by the appropriate factor $k_1 = b_1/b$ - for coordinates; $k_2 = (b_1/b)^2$ - for an area; $k_3 = (b_1/b)^3$ - for a moment of resistance; $k_4 = (b_1/b)^4$ - for the moment of inertia (b is a drawing airfoil chord; b_1 - the assigned airfoil chord).

Page 15.

When the chord changes, it is advisable to select the radius of curvature not in terms of a linear dependence, but according to the formula

$$r = r_0 \sqrt{\frac{r}{r_0}}$$

where r and r_0 are the radii of curvature of the exit edge of a newly designed and initial profile.

During the design of the blades of steam and gas turbines, must be satisfied the requirements for cost-effectiveness/efficiency, strength and manufacturability. First are performed thermal and gas-dynamic calculations, is constructed blade, and then is fulfilled verifying stress analysis, i.e., are determined the acting in blade voltage/stresses and are compared with permissible. Safety factor must correspond to the taken norms. In work with the high temperatures propellants, it is necessary to carry out the calculations for creep, and also to consider thermal stresses. Furthermore, is checked dynamic strength of blades, connected with their oscillation/vibrations. All these questions minutely are examined in special courses [18]; here will be only given the basic formulas for the stress analysis of blades, which are located under the action of centrifugal forces and gas force.

In the general case of the blade of variable profile, given in Fig. 5, the breaking stress in cross section at a distance x from the bearing edge of blade into disk will be written as

$$G_r = \frac{c + G}{r} \left[\frac{r}{r_0} \right], \quad (5)$$

where the $c = \omega^2 \int_{r_0}^r F(r_0 + x) dx$ are the centrifugal force of part of the blade, arranged/located between radii of $(r_0 + x)$ and $(r_0 + 0)$;

$G_r = \omega^2 V_r \rho_r$ are the centrifugal force of band/shroud/tire;

$F [m^2]$ - the cross-sectional area of blade on an arbitrary radius of $(r_0 + x)$;

$\rho [kg/m^3]$ are a density of metal;

$\omega [1/sec]$ - angular velocity;

$V [m^3]$ - the volume of the band/shroud/tire, which is necessary to one blade.

If blade is divided into a series of sections and in each of them area F is considered constant, then the stress in the i cross section of the blade through the stress in that preceding/previous from top will be written in the form [19]

$$\sigma_i = \sigma_{i-1} \frac{F_{i-1}}{F_i} + \frac{1}{4} \rho \omega^2 \left(1 + \frac{F_{i-1}}{F_i} \right). \quad (6)$$

the reading of cross sections it is conducted from periphery to the root of blade, and coordinate x is counted off from root cross section.

For the approximate computations of stress the in tip cross sections of blades it is possible to use the following formulas:

1. For the blade of constant airfoil/profile

$$\sigma = 20 \frac{\pi}{9} \left[\frac{n}{\omega^2} \right] \quad (7)$$

2. For the blade of the alternating/variable cross section when the areas of airfoil/profile are changed according to linear law,

$$\sigma = 10 \frac{\pi}{9} \frac{1 + F_2}{F_1} \left[\frac{n}{\omega^2} \right] \quad (8)$$

in these formula: u (m/s) are peripheral speed at the mean diameter of blades;

$$\sigma = \frac{F_2}{F_1}; \quad F_1, \quad \frac{F_2}{F_1}$$

for the calculation of blades for bending we will use Fig. 5, only number of cross sections now we will relate to sections, beginning with the first.

Page 12.

Through the Δx_i to the let us designate the length of the i section, while through the x_i - distance from blade root to the middle of the i section.

Let us find the bending moments of the forces of pressure of gases relative to axle/axes $u-o$ and $a-o$ (see Fig. 4) in the lower section of the n section:

$$\left. \begin{aligned} M_u(x_n) &= \sum_{i=1}^n P_{ui}(x_i - x_n); \\ M_a(x_n) &= \sum_{i=1}^n P_{ai}(x_i - x_n). \end{aligned} \right\} \quad (9)$$

here:

$$\begin{aligned} P_{ui} &= G_i (c_{1u} - c_{2u}); \\ P_{ai} &= -G_i (c_{1a} - c_{2a}) + (p_1 - p_2)_i l_{zi} \Delta x_i. \end{aligned}$$

the bending moments with respect to of the principal central inertia axes are determined from the formulas:

$$\left. \begin{aligned} M_{\eta}(x_a) &= M_a \sin \gamma - M_a \cos \gamma, \\ M_{\xi}(x_a) &= M_a \cos \gamma + M_a \sin \gamma. \end{aligned} \right\} \quad (10)$$

then the stress on the trailing edge of blade, caused by bending from the forces of pressure of gases,

$$\sigma_a(x_a) = \frac{M_{\eta} y_a}{J_{\eta, x_1}} + \frac{M_{\xi}(1-x_a)}{J_{\xi, y_1}}. \quad (11)$$

analogously are determined the stresses on entering edge and on of blade back.

DCC = 76031693

PAGE

66

Page 13.

Chapter II.

CALCULATION AND THE SHAPEING OF ~~GRID~~/CASCADES.

§ 7. Selection of the type of grid/cascade and its fundamental characteristics.

Selection and detailed calculation of grid/cascades for the design/projected step/stage is realized/accomplished on the basis of the data of preliminary thermal design. According to these data are established/installed the tentative values of velocities at entrance and exit from grid/cascade c_1 , w_1 , w_2 (and, correspondingly, M_1, M_2, M_3) angles α_1 ; β_1 ; β_2 ; α_2 in absolute and relative motion and also the distribution of the parameters and reaction by height of blade.

For the step/stages of low correctness (with large relation diameter to span of the blade $\theta > 20$) a change in the parameters in a radius is small for the selection of grid/cascades sufficient to examine velocity triangles at the mean diameter.

In the step/stages of large fanning, it is necessary to select cascade profiles for several cross sections on a radius, constructing then of blade taking into account the special feature/peculiarities of spatial flow, strength and technology of manufacture.

In flow area of multistaged turbine, the specific volumes, Mach numbers and Re in absolute motion are changed within very wide limits. Consequently, height/altitudes, and also the optimum forms of the airfoil/profiles of nozzle and running cascades will be different for different step/stages.

§ 8. Calculation of potential flow and the methods of the shaping of grid/cascades at subsonic speeds.

In the theory of airfoil cascades, are examined two basic task (is straight line and reverse/inverse). Direct/straight the problem is that on the assigned form of airfoil/profile and its arrangement in grid/cascade (angle of setting and the space), velocity and its direction to grid/cascade are determined: the distribution of speed according to the enclosures of airfoil/profile and flow direction after grid/cascade, and also the forces, which act on airfoil/profile in grid/cascade. The obtained as a result of the solution to direct problem distribution of speeds makes it possible to estimate the degree of the aerodynamic cleanness of the form of airfoil/profile and channel, to determine the sections whose flow about can turn out

to be unsatisfactory.

Another task, reverse/inverse, entails the determination of the form of airfoil/profile and its arrangement in grid/cascade from the specified distribution of speeds along the enclosures of airfoil/profile, and also from some geometric parameters of the airfoil/profile: the thickness and the form of trailing edge, the area of airfoil/profile and so forth. The solution of the reverse problem makes it possible to construct the highly efficient airfoil/profile, which satisfies the predetermined rational distribution of speeds according to the enclosures of airfoil/profile.

It is known many methods of the solution of the indicated problems basic from which, depending on the used methods and the hydrodynamic diagrams of flow, can be broken into the following groups ¹.

FOOTNOTE ¹. Within the framework of atlas, is impossible the consecutive presentation of the methods of calculation of potential cascade flow. Here is given only short list of methods with references to appropriate literature. Is in more detail possible

entire zone of flow, which requires the high expenditures of time and is not justified by the necessities of practice.

For the more effective solution of direct problem of the theory of hydrodynamic grids/cascades (calculation of speed distribution according to the duct of airfoil/profile) are utilized the integral equations of the relatively unknown functions, connected with flow around the assigned airfoil/profile. Methods of calculation according to integral equations are more convenient for a programming and therefore they can be recommended for the machine solution of problem [23]. This method is based on the solution to the integral equation, unknown function in which is the velocity potential.

The solution to this equation can be found by successive approximation. For solving such an equation in the calculator of EVM-20 in TSKT1, is comprised the program, which provides for the calculation of the airfoil/profiles, assigned both circular arcs and by the cuts of straight lines and assigned by the coordinates of back and concave surface; in this case the coordinates must be assigned/prescribed with even pitch. The calculations show that with the sufficiently large number of intervals of the laying out of the duct of the airfoil/profile ($n = 120$) of the diagram/curve of speeds,

before it was developed the simple engineering method of calculation, based on the theory of channel. ENDFOOTNOTE.

1. Methods, based on the solution to the integral or differential equations of flow of liquid in grid/cascade [28, 37; 7].

The initial differential equations, which describe the potential flow of flow about the grid/cascade of the incompressible ideal fluid, are the equations of Laplace for unknown velocity potential $\phi(x, y)$ and the function of the current of $\psi(x, y)$, which are equivalent to the equations of continuity and absence of eddy/vortices. These equations under the assigned boundary conditions (form of airfoil/profile, the arrangement in grid/cascade and the condition of inleakage) are solved by numerical methods, by successive approximation.

Indicated calculation of the flow through the grid/cascade is connected with the determination of the unknown functions in an

obtained in calculator, coincides well with experimental. The machine time, necessary for one calculation in machine, is 5-6 min, while by manual calculations 50-60 h.

2. Methods of the solution of straight line and of the inverse problem of the cascade theories, which are characterized by the application/use of a method of conformal mapping [7; 37; 21].

If is known the flow about certain simple grid/cascade (plates or circles), i.e., is known the grid orthogonal to each other of the flow lines and equipotential lines, then, after reflecting this region to certain other, it is possible to obtain the flow pattern of the arbitrary, preassigned grid/cascade. By these methods can be solved inverse problem. The difficulties, which appear when using a method of conformal mapping, consist in the fact that is unknown the mapping function; it is necessary to search for by successive approximation.

3. For solution reverse/inverse is applied also the hodograph analysis which was for the first time proposed to N. Ye. Joukowski (1890).

The practical value of this method they consist in the fact that during the assignment of the hodograph of speed it is possible to ensure the rational distribution of speeds, and namely: to restrict the maximum velocity and to obtain a monotonic change in the speed on the larger part of the enclosure of airfoil/profile. The expenditures of time during the calculation by hodograph analysis are great (by manual calculations 30-50 h).

4. Very frequently for determining flow around grid/cascade with the airfoil/profiles of arbitrary form are applied the analog methods or simulation [36; 37].

In two-dimensional problems of the flow of ideal fluid, is most common the method of electrohydrodynamic analogy (EHDA), which is based on the analogy between the differential equations of the flow of electric current in conductor and of the flow of ideal fluid. Field measurements of electric potentials on model give the picture of the potential distribution of the speed in the foil lattice of airfoil/profiles.

Besides electrohydrodynamic analogy, frequently is applied the membrane/diaphragm analogy, based on what the function of the sagging/deflection of diaphragm/membrane and the function of the current of flat/plane eddy of the ideal incompressible fluid is described one and the same differential equation (equation of Poisson); the lines of the equal sagging/deflections of diaphragm/membrane depict flow lines, and the angles of the slope of its surface are proportional to the speed of liquid.

5. The approximate computation of the distribution of the speeds according to airfoil/profile in dense grid/cascade can be carried out by using solution of the problem of the flow of gas in channel. Since in the case of dense grid/cascades flow in skew shear in practice does not depend on the conditions of flow on the intake of airfoil/profile, can be approximately flow in the middle part of the vane channel considered as flow in unit channel, by disregarding the mutual effect of airfoil/profiles. Considerations about the calculation of irrotational flow to in channel have at G. Fluegel and A. Stodola. Late this method was developed, by G. Yu. Stepanov, by A. N. Sherstyuk and G. S. Samoylovichem [7; 37; 45; 35].

Fig. 6. Comparison of the calculated (according to the method of channel) and experimental distribution of pressures according to the enclosure of airfoil/profile.

Key: (1). Calculated. (2). Experimental. (3). Back. (4). Concave.

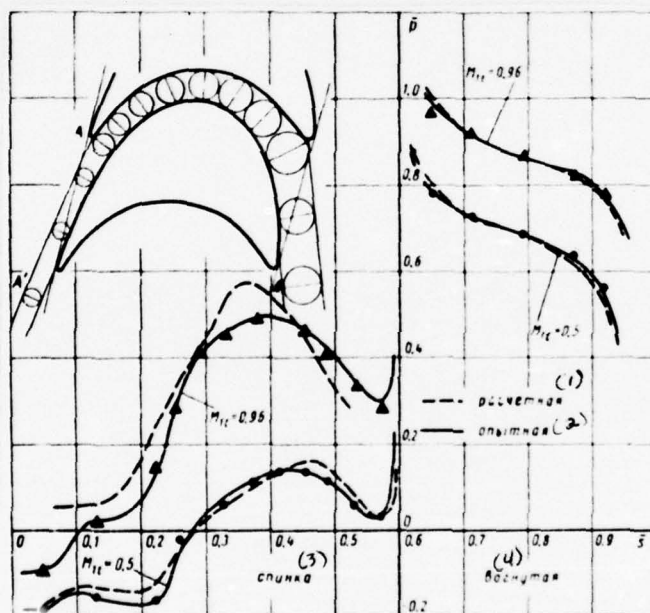
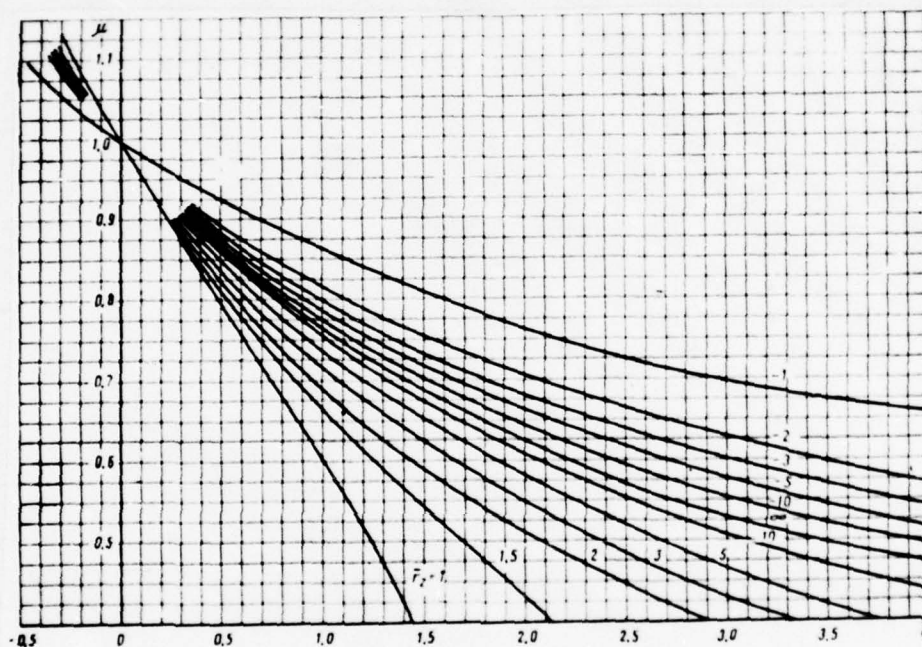


Fig. 7. Dependence of the coefficient of consumption on the geometric parameters of grid/cascade.



For conducting the calculation of grid/cascade, it is necessary to continue channel on intake and in skew shear at output/yield [7]. On the output section of channel profile can be continued on straight line AA' (Fig. 6), which is carried out tangentially to concave surface at an angle of $\beta_{2, \text{opt}}$. On duct inlet can be approximately continued on straight line, carried out at an angle of the entry of flow β_1 .

The integral determination of consumption must be produced on equipotential, since speed is normal to it. However, the form of equipotential is previously unknown. Calculations show that the error is small, if we equipotential replace with the curve which is normal to the walls of channel (for example by circular arc).

Speed distribution along equipotential is subordinated to hyperbolic law and is selected in the form [7]

$$C = \frac{a}{1 + b\eta + c\eta^2}, \quad (12)$$

where c - the gas velocity in the arbitrary point of channel;

η - coordinate along equipotential;

a ; b ; e are the coefficients which are determined from the boundary conditions:

with

1) η (on the back of airfoil/profile) $c = c_1$ and $a = c_1$;

$$2) \begin{matrix} \eta \\ \eta \end{matrix} \begin{matrix} 0 \\ \delta \end{matrix} \left(1 + \frac{1}{c} \frac{dc}{d\eta} \right) = b \quad \text{and} \quad \begin{cases} b \frac{1}{c_1} = K_1 \\ b \frac{1}{c_2} = K_2 \end{cases} \quad (13)$$

then coefficient

$$c = \frac{K_2 + K_1 K_2 \delta - K_1}{2\delta - K_2 \delta^2},$$

where δ is width of channel along equipotential.

Let us introduce the coefficient of the consumption μ , which considers the nonuniformity of consumption along equipotential and it depends only on the geometry of the channel:

$$\mu = \frac{2/\delta}{\sqrt{4e-1}} \operatorname{arctg} \frac{\sqrt{4e-1}}{2/\delta-1}, \quad (14)$$

when $(4e - 1 > 0)$ and

$$\mu = \frac{2/\delta}{V_{1-4e}} \operatorname{arcth} \frac{V_{1-4e}}{2/\delta - 1}, \quad (15)$$

when $(4e - 1 < 0)$.

here: $\delta = \delta/r_1$ - the dimensionless width of channel;

$$c = er_1^2 \frac{1 + \delta - i_2}{(2i_2 - \delta)\delta}, \quad (16)$$

let us note the special cases which can meet in the calculation:

a) $r_2 \rightarrow \infty$ and $r_1 \rightarrow \infty$; then $\bar{e} = 1/2\delta$;

b) $r_1 \rightarrow \infty$, then $\mu = 1$;

c) $r_1 < 0$ - airfoil/profile has reverse/inverse curvature; from (14) and (15) we have: $\mu > 1$.

From formulas (14) and (15) it is obvious that the coefficient of consumption μ depends only on two geometric parameters $\bar{\delta}$ and \bar{r}_2 (see Fig. 7).

For the calculation of the flow of compressible liquid in curvilinear channel ($M > 0.4$) it is necessary to consider density change. Over a wide range of subsonic speeds (to $M = 0.8-0.9$) the channel design taking into account compressibility can be produced by the introduction of the average density in this cross section. Is briefly presented the order of calculation of given channel:

a) after in the calculated channel are inscribed circumferences and are carried out the equipotential through the points of contact of the tangency of these circumferences with walls, is determined the length of equipotential (circular arcs) δ and the radii of curvature of the line of demarcation of channel r_1 and r_2 in all calculated cross-sections:

b) further for each equipotential are calculated dimensionless geometric parameters $\bar{\delta}$; \bar{r}_2 ; \bar{e} ; μ according to formulas (14, 15 and 16);

c) are determined the parameters of gas at the entry into the grid/cascade: dimensionless speed $\lambda_1 = \frac{c_1}{a_1}$, the given consumption $q_1 = q_1(\lambda_1)$ (on the tables of gas-dynamic functions);

d) average given consumption along channel is calculated from the given consumption at the entry into grid/cascade

$$q_{cp} = \frac{G_1}{G_{1*}} = \frac{q_{1*} l \sin \beta_1}{\lambda_{1*} \sigma_*} = q_1 \frac{l}{\lambda_1} \sin \beta_1 \quad (17)$$

on q_{cp} the dimensionless speed of λ_{cp} (on tables);

d) we find dimensionless speed λ_1 on the back of airfoil/profile

$$\lambda_1 = \frac{\lambda_{cp}}{\mu}$$

and dimensionless speed λ_2 on concave canal surface

$$\lambda_2 = \frac{\lambda_1}{1 + \delta + \epsilon \delta^2} \quad (18)$$

about the accuracy/precision of the determination of the speeds in grid/cascade by the method of channel it is possible to judge by Fig. 6, where is given the comparison of calculation and experimental data for one of the grid/cascades. The approximate computation of grid/cascade according to the method of channel is fulfilled during 5-6 manhour.

§ 9. The approximation methods of the construction of subsonic grid/cascades. Lemniscate method ¹.

FOOTNOTE ¹. Lemniscate method is developed together with lower by V. Nauman. Lemniscate curves for airfoil/profiles were applied by

Zhuravlev S. I. and by Kopelev S. Z., and also by G. I. Khrushchev.
ENDFOOTNOTE.

The methods of the solution of the reverse problem (construction of airfoil cascades enumerated above according to the specified distribution of speeds) have the essential deficiency/lacks, basic from which they are: 1) large labor expense; 2) arbitrariness in selection the diagram/curve of the speeds even 3) the difficulty of the construction of skew shear of grid/cascade according to the specified distribution of speeds.

Fig. 8. The principal notations of lemniscate airfoil/profiles.

Key: (1). $0.625 a$. (2). Evolute.

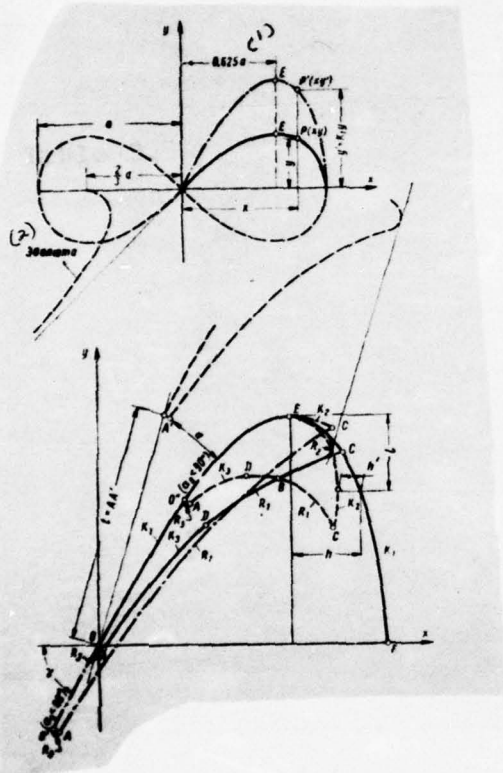
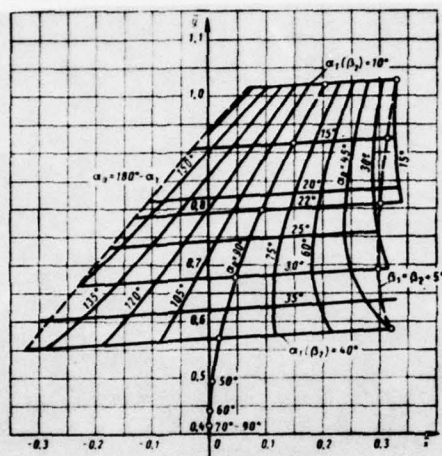


Tabelle 3.

α_0 (°), γ (°), β (°)	10	15	20	25	30	35	40	50	60	75	90
K_1	3,2	2,75	2,38	2,05	1,75	1,48	1,25	0,98	0,6	0,275	0,05
$n' 10^6$	7,5	6,8	6,25	5,75	5,0	4,0	3,0	—	—	—	—
$n'' 10^6$	21	19	15,8	10,3	0	—	—	—	—	—	—
\bar{x}_B	0,525	0,56	0,585	0,605	0,63	0,65	0,655	—	—	—	—
\bar{y}_B	0,735	0,685	0,605	0,53	0,46	0,385	0,34	—	—	—	—
$\alpha_0 = 90^\circ$	$\bar{x}_{A'}$	0,204	0,148	0,104	0,071	0,045	0,027	0,014	0,005	0,001	0
	$\bar{y}_{A'}$	1,02	0,914	0,822	0,743	0,677	0,618	0,566	0,494	0,44	0,415
$\beta_1 = \beta_2 + \beta_3$	$\bar{x}_{A'}$	0,332	0,315	0,305	0,298	0,290	0,282	—	—	—	—
	$\bar{y}_{A'}$	1,026	0,922	0,833	0,755	0,69	0,635	0,584	—	—	—

Key: (1) deg.

Fig. 9. To the construction of lemniscate airfoil/profiles.



In practice are widely common the approximate geometric methods of the construction of the airfoil/profiles which are based on numerous experimental data. One of such methods is the curvature of the initial axisymmetric airfoil/profile on center line (center line is the locus of the centers of the circumferences, inscribed in airfoil/profile) [44; 33]. As center line is accepted usually the parabola, tangent to which at entry composes with the front of grid/cascade angle β_1 , and at output/yield β_2 .

The constructed according to the described method grid/cascades possess sufficiently low losses.

To M. I. Joukowskis [22] is proposed the method of the construction of airfoil/profiles, based on the use of a series of the well experimentally waste grid/cascades. During the construction of new airfoil/profile, produce themselves small changes in the form of the intake or output sections of two adjacent airfoil/profiles of this series. Since the form of new airfoil/profile is close to the form of the initial effective airfoil/profiles, then their characteristics turn out to be close.

Are utilized also the methods of the construction of the enclosures of airfoil/profiles along curves, with smoothly-changing curvature, in particular on parabola [37].

Is here briefly presented method of the construction of nozzle and running cascades on lemniscate curves. As the basis of method, is placed the experimental material, accumulated by many scientific-research organizations. Lemniscate [equation $(x^2 + y^2)^2 = a^2 (x^2 - y^2)$] it turns out to be the most favorable curved for the construction of subsonic airfoil/profiles, since it makes it possible to select in any cross section of channel the point of the maximum curvature and to ensure a smooth change of the curvature along the enclosures of airfoil/profile (Fig. 8). Scale of ordinate K_1 ($y' = K_1 y$), it is possible to displace point E in any direction in direct/straight $x = 0.625 a$ and thereby to ensure the desired form of the back of airfoil/profile for the different reentrance angles and flow discharge.

The flow about the concave surface of airfoil/profile occurs, as a rule, with accelerating pressure gradients, and therefore here possibly less careful shaping. Therefore in some parts of the concave surface of lemniscate, they are replaced by circular arcs.

Each of airfoil/profile consists of the following parts (Fig. 8):

A. Back of the airfoil/profile:

1. OO' - is straight line (there exists only at $\alpha_0 > 90^\circ$).

2. OE ($O'E$) - lemniscate K_1 .

3. EC is lemniscate K_2 , formed from EF (K_1) according to the determined law.

B. The concave surface:

4. AD is lemniscate K_3 .

AD-A039 286

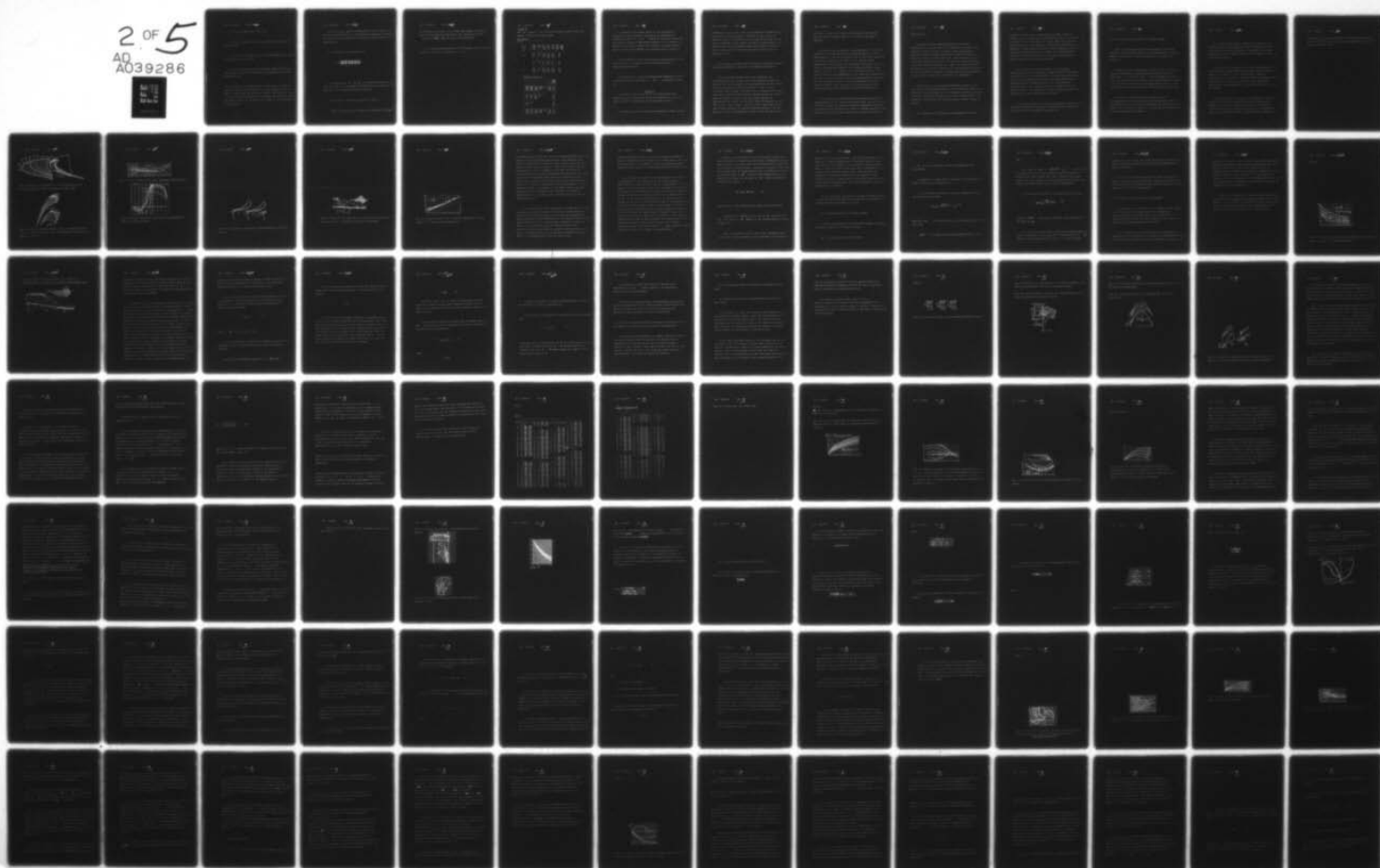
FOREIGN TECHNOLOGY DIV WRIGHT-PATTERSON AFB OHIO
ATLAS OF THE CASCADE PROFILES OF AXIAL-FLOWS TURBINE, (U)
DEC 76 M Y DEYCH, G A PHILIPP, L Y LAZAREV
FTD-ID(RS)T-1693-76

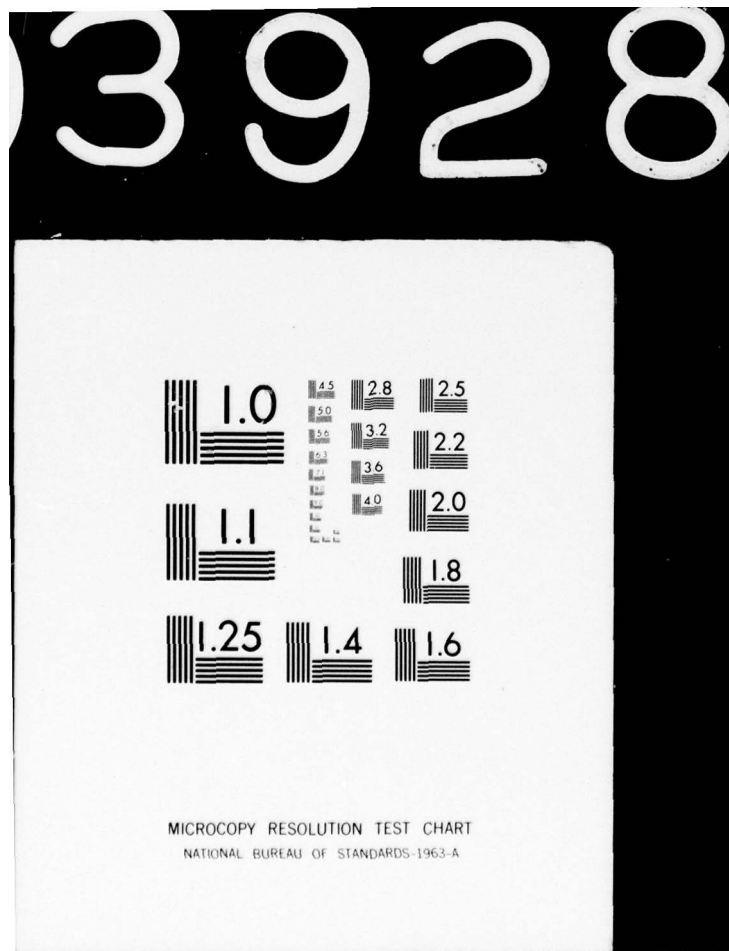
F/G 21/5

UNCLASSIFIED

NL

2 OF 5
AD A039286





5. DC is a circular arc of radius R_1 .

6. At $\alpha_0 > 90^\circ$ there is no part AD, and there is only arc of circle AC (R_1).

C. The intake and output part of the airfoil/profile are formed from circular arcs R_2 and R_3 .

For airfoil/profiles with the reentrance angles of flow $\alpha_0 < 100^\circ$ tangent to camber line at entry was selected to 5° less than calculated angle.

the constructions of airfoil/profile assigned are the reentrance angles and output/yield α_0 (β_1) and α_1 (β_2), airfoil chord (or the width of grid/cascade B). Speeds are subsonic. Plotting scale (a) is selected freely. Subsequently all curve/graphs and tables are given in relative values. Let us examine the methods of the construction of airfoil/profile.

1. On the preset angle of output/yield α_1 or β_2 on Table 3 is selected coefficient K_1 and is constructed the lemniscate according to formula $y' = K_1 y$ (Fig. 8) (at intermediate angles one should use interpolation).

2. Is determined the coefficient K_2 :

$$\text{when } \begin{cases} \alpha_1 < 90^\circ & K_2 = K_1 - \alpha_1(\alpha_1 - 90^\circ) \\ \alpha_1 > 90^\circ & K_2 = K_1 - \alpha_1(90^\circ - \alpha_1) \end{cases}$$

The coefficient of α_1 and α_2 is determined depending on α_1 (β_2) from Table 3. On the basis of lemniscate K_1 , is constructed the curve K_2 on the following dependences (Fig. 8):

$$\text{at } \alpha_0 \leq 90^\circ \quad h' = K'_2 h_1; \quad \text{at } \alpha_0 \geq 90^\circ \quad h'' = K''_2 1.$$

3. Point C lie/rests on the curve K_2 . Its coordinates of L_2

are determined from Table 4. For a more fine reading at angles α_0 (β_1) $\geq 90^\circ$ is given the coordinate of \bar{x}_0 with α_0 (β_1) $\leq 90^\circ$ coordinate of $\bar{x} - \frac{K}{2}$ (but the scale of construction).

4. The direct/straight section $00'$ (for angles α_0 (β_1) $> 90^\circ$) is constructed according to equation $\text{tg } \gamma = K_1$.

Table 4.

Key: (1). Parameters. (2). Reentrance angles α_0 (β_1) in deg. (3).Angles of departure α_1 (β_2) in deg.

(1) Параметры	(2) Углы входа α_0 (β_1) в град	β_1	β_2 в град	30	45	60	75	90
$\bar{x}_c = \frac{x_c}{a}$ ($\alpha_0 > 90^\circ$)	0.585 0.495 0.415 0.325 0.235	0.65 0.535 0.425 — —	0.71 0.59 0.475 0.355 0.235	0.775 0.65 0.525 0.4 0.275	0.84 0.71 0.575 0.44 0.31	0.905 0.77 0.625 0.485 0.35	0.855 0.855 0.855 0.855 0.855	
$\bar{y}_c = \frac{y_c}{a}$ ($\alpha_0 < 90^\circ$)	0.27 0.32 0.37 0.43 0.5	0.312 0.35 0.38 — —	0.37 0.405 0.445 0.475 0.5	0.44 0.483 0.525 0.56 0.595	0.535 0.59 0.64 0.682 0.725	0.69 0.76 0.835 0.91 1.0		
K_3	1.2 1.2 1.23 1.3 1.4	1.6 1.42 1.28 — —	2.0 1.74 1.55 1.45 1.4	2.4 2.07 1.82 1.67 1.6	2.8 2.4 2.08 1.9 1.8	3.2 2.72 2.35 2.12 2.0		
$R_2 = \frac{R_2}{a}$	0.021 0.021 0.02 0.016 0.012	0.03 0.027 0.021 — —	0.04 0.036 0.029 0.021 0.012	0.05 0.045 0.038 0.028 0.018	0.059 0.054 0.046 0.036 0.025	0.065 0.06 0.052 0.043 0.03		

Table continued.

105	120	135	150	165	$\alpha_0 = 180^\circ - \alpha_1$	(3) Углы выхода α_1 (β_2) в град
0.858 0.852 0.845 0.82 0.75	0.825 0.81 0.788 0.728 0.62	0.77 0.74 0.695 0.587 0.425	0.685 0.62 0.525 0.34 —	0.5 0.36 — — —	0.365 0.36 0.35 0.34 0.325	10 15 22 30 40
1.0 1.15 1.35 1.6 1.9	1.8 2.15 2.65 3.3 4.3	4.0 4.7 6.0 8.25 12.5	8.75 11 20 — —	24 — — — —	— — — — —	10 15 22 30 40
3.6 3.05 2.61 2.34	4.0 3.37 — —	— — — —	— — — —	— — — —	— — — —	10 15 22 30 40
0.068 0.062 0.054 0.045 0.03	0.066 0.06 0.05 0.04 0.024	0.06 0.052 0.041 0.028 0.014	0.047 0.038 0.026 0.012 —	0.025 0.015 — — —	0.015 0.015 0.014 0.012 0.01	10 15 22 30 40

5. Depending on reentrance angles α_0 (β_1) and angles of departure α_1 (β_2) from Table 3 and Fig. 9, is determined the coordinate of point A' (x_A, y_A). Thereby in essence are determined the angle of setting and the lattice spacing. If it is necessary to change lattice spacing (within small limits), one should change the angle of setting for providing the calculated angle of departure.

6. The thickness of the trailing edge of airfoil/profile OA (O'A or O''A) (Fig. 8) is selected from structural/design and technological conditions.

7. Depending on α_1 (β_2) are determined the coordinates of point B (coordinates of the point of B_{x_B} and y_B are brought in Table 3).

or A and C

8. Through points B and C (if is not assigned/prescribed coefficient K_3) is carried out circle with radius of $R_1 - R_{1a}$. The value of radii is determined from by the datum of Table 4.

9. Through point A, is carried out lemniscate K_3 , which concerns

circumference R_1 at point D. For the construction of lemniscate K_3 , is utilized the right branch of lemniscate K_1 (Fe, of Fig. 8), whereupon point F is transferred and is combined with point A. The scale of lemniscate K_3 is selected on Table 4. Extrapolation is not allowed/assumed. For the remaining cases (for example α_0 , 120° , $\alpha_1 = 30^\circ$) the concave part of the airfoil/profile consists only of circular arc R_1 .

10. A radius of entering edge \overline{R}_2 depends on reentrance angles α_0 (β_1) and output/yield α_1 (β_2) and is determined from Table 4.

By the procedure examined above were constructed the airfoil/profiles for the broad band of the reentrance angles and output/yield. Fig. 10, depicts the airfoil/profiles and the channels of grid/cascades for an angle of departure α_1 (β_2) = 15° and reentrance angles α_0 (β_1) = 20° - 165° , i.e., is enveloped the range of all possible active and jet/reactive airfoil/profiles with constant angle of departure α_1 (β_2) = 15° . The similar drawings of grid/cascades are carried out for other angles of departure α_1 (β_2) = 10° ; α_1 (β_2) = 22° ; α_1 (β_2) = 30° and α_1 (β_2) = 40° . Change in the form of airfoil/profile at constant reentrance angle $\alpha_0 = 90^\circ$ and alternate angles of output/yield is given in Fig. 11a while in Fig.

11b shown a change in the form of airfoil/profile for impulse cascades whose reentrance angle to 5° is greater than angle of departure.

The test results of lemniscate airfoil/profiles. To tests were subjected four airfoil/profile for reentrance angle $\alpha_0 = 90^\circ$ and output/yield $\alpha_1 = 10, 15, 20$ and 40° . Fig. 12, gives the curve/graphs of the loss factors from the number of M_u for all tested grid/cascades. For grid/cascades with angles of departure $15, 20$ and 40° , are experimentally obtained sufficiently low profile losses (with $M = 0.6-0.9$ $\zeta_{pr} = 20/o$). For a grid/cascade with $\alpha_1 = 10^\circ$ profile losses they are approximately $30/o$, which also corresponds to the level of losses for the better/best grid/cascades of such type. Not less important is the fact that the dependence of the loss factors on number M (Re) turns out to be flatter than of other airfoil/profiles, which were being experience/tested earlier.

Is of interest pressure distribution according to enclosures airfoil/profile for the tested grid/cascades (Fig. 13). First of all it should be noted that pressure distribution pronounces favorable: the evacuation/rarefaction and the extent of diffuser section in skew shear on back is small. This explains the low level of losses in

grid/cascades.

The second special feature/peculiarity of the tested grid/cascades is the fact that in the throat (in the minimum cross section) of channel on back at subsonic speeds considerably is changed the static pressure with change of angle of departure α_1 . Thus, for instance, at small angles ($\alpha_1 = 10^\circ$) pressure on back in the minimum cross section is more than pressure after grid/cascade, and at wide angles of departure ($\alpha_1 = 40^\circ$) - it is less than after grid/cascade. At subsonic speeds this can substantially be reflected in rate of discharge through the grid/cascade, and, correspondingly, on the computed values of the coefficients of consumption.

Besides testing the specially manufactured according to the procedure presented airfoil/profiles, was conducted the comparison of lemniscate airfoil/profiles with the better/best, developed according to precise methods and the tested in the MFI airfoil/profiles. This comparison was conducted with airfoil/profiles F-2314A, P-3021A and F-4629A.

The enclosures of the compared airfoil/profiles virtually

coincide. Profile losses in grid/cascades P-2314A, P-3021A and P-4629A with $M = 0.6-0.9$ they are approximately 40/o; it is possible to assume that the same will be the losses, also, for lemniscate airfoil/profiles. A good agreement of dimensional characteristics of lemniscate airfoil/profiles is obtained during comparison with other better/best airfoil/profiles, for example with airfoil/profiles C-9015A and C-5515A, which have in the optimum mode/conditions profile losses 1.8 and 2.20/o respectively.

Thus, according to the test results of the lemniscate airfoil/profiles and the comparison conducted with the better/best previously developed airfoil/profiles one should expect low losses, also, in other parameters (reentrance angles and output/yield) of grid/cascades. The lemniscate method of the construction of airfoil/profiles can be used, also, for the shaping of the long twisted blades of the step/stages of large fanning, calculated for subcritical or small supercritical heat drops.

The airfoil/profiles of the nozzle (jet/reactive) grid/cascades, constructed according to lemniscate method, and their aerodynamic characteristics are represented on plates 6-8.

§ 10. Shaping of nozzle cascades for transonic speeds.

Nozzle cascades for transonic speeds (group b) in geometric parameters insignificantly differ from the grid/cascades of group A. However, flow pattern in these grid/cascades is essentially different.

Actually, for the grid/cascades of group A of the speed in any point of the enclosure of airfoil/profile less than the speed of sound ($M_{loc} < 1$, where the M_{loc} — are the maximum Mach number at the point of the enclosure of back); in the nozzle cascades of group b is a determined section of the airfoil/profile on back, in limits of which the speed supersonic; this section is closed by shock wave.

The numerous experimental results showed that the airfoil/profiles of nozzle cascades for transonic speeds must have rectilinear back in skew shear. Consequently, the nozzle cascades of group b can be obtained by means of the strain of the output section of the airfoil/profile of group A.

As a result of this strain, decreases the curvature of the concave surface of airfoil/profile. Back is fulfilled rectilinear up to minimum cross section, whereupon is recommended the somewhat involve/tightening of straight portion into the depth of channel for narrow cross section.

A decrease in the curvature of the back of road profile of the rectification of output section in skew shear makes it possible to tighten the beginning of the crisis increase of losses in grid/cascade to Mach numbers = 1.0-1.25. Thus, the application/use of nozzle cascades of group b is expedient at the speeds after grid/cascade, which correspond to a change of Mach number in limits of 0.9-1.25.

With jump/drops in the pressure to grid/cascade, that exceed critical, by skew shear is formed the wave spectrum, minutely examined in [6]. In the narrow cross section of grid/cascade, is establish/install the critical speed. Since after grid/cascade pressure is lower than critical, on trailing edge is formed and is

propagated in oblique section/shear the rarefaction wave, which, after achieving the back of adjacent airfoil/profile, is reflected also by rarefaction wave.

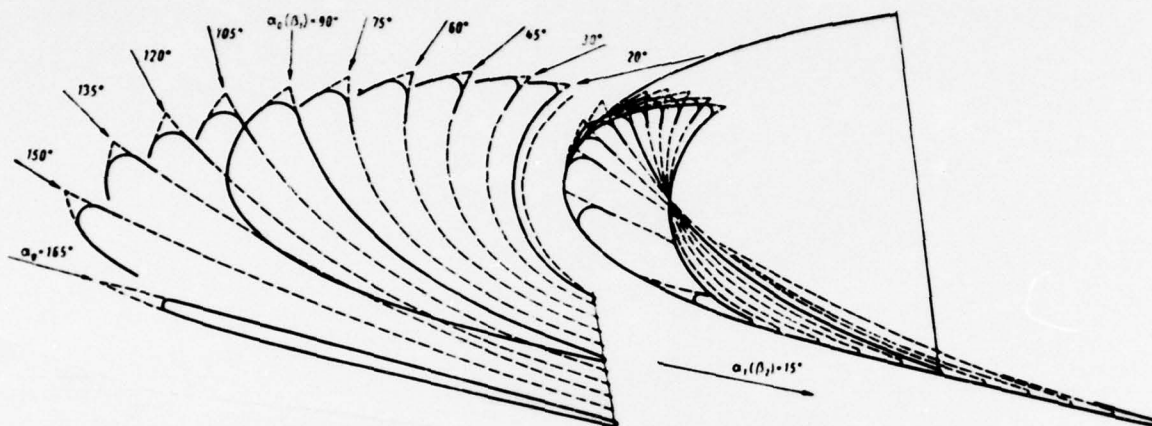


Fig. 10. Lemniscate airfoil/profile for the broad band of the reentrance angles and angle of departure $\alpha_1(\beta_2) = 15^\circ$.

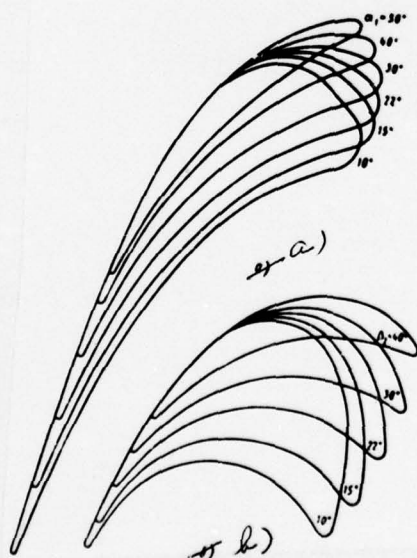


Fig. 11. Lemniscate airfoil/profiles: a) for a constant reentrance angle $\alpha_0 = 90^\circ$ and different angles of departure; b) for a reentrance angle $\beta_1 = \beta_2 + 5^\circ$.

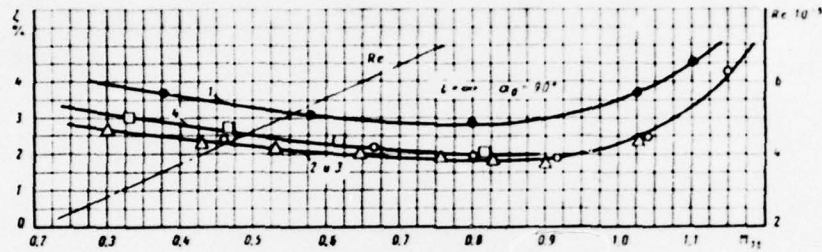


Fig. 12. The test result of the nozzle lemniscate airfoil/profiles:

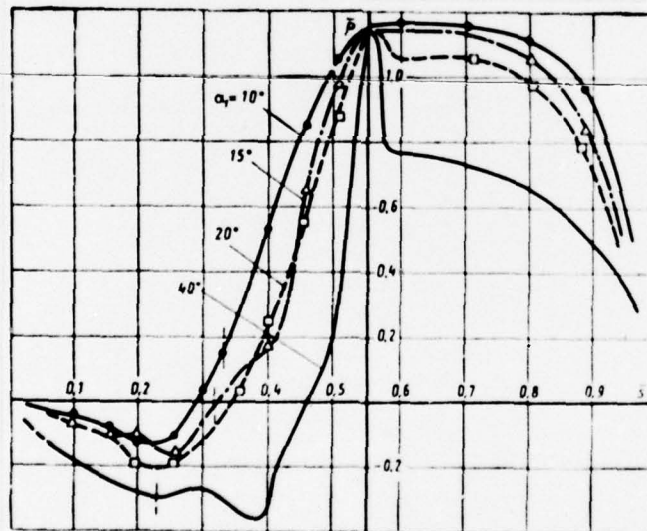


Fig. 13. Pressure distribution according to the enclosures of lemniscate airfoil/profiles.

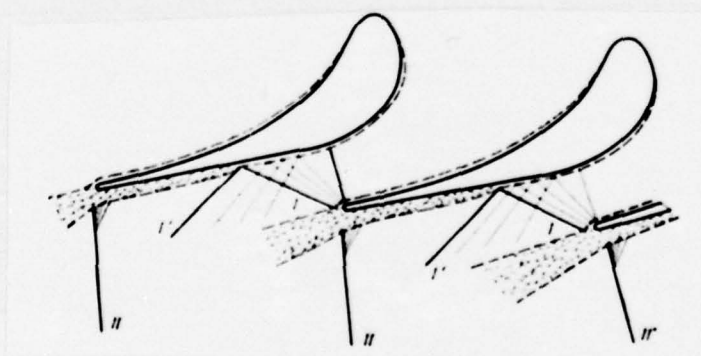


Fig. 14. Flow pattern at cutput/yield frogrid/cascade at supersonic speeds.

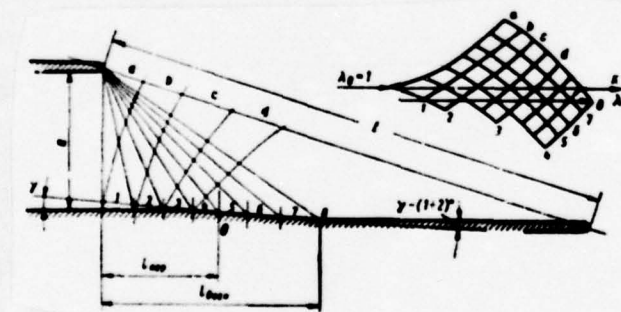


Fig. 15. Diagram of the construction of the back of airfoil/profile for transonic and to supersonic speeds with constriction.

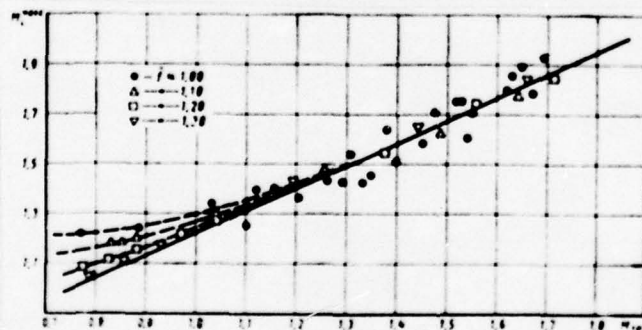


Fig. 16. Maximum numbers of M_{max} on back in skew shear of nozzle cascades as a function of the number of M_u

At certain distance after edge, occurs the merging/coalescence of two streams of flow, which wash airfoil/profile from different sides. With merging/coalescence occurs the sharp rotation of streams, as a result of which occurs the system of jumps I and II (Fig. 14). The overexpansion of flow in primary and that which was reflected rarefaction waves partially is compensated for primary and that which was reflected rarefaction waves partially is compensated for by primary jump I, which, after achieving the back of airfoil/profile, in turn, is reflected by shock wave I'. The overexpansion of flow in rarefaction waves, the intensity of edge jumps I and II, and also their position are determined by the curvature of the back of airfoil/profile in skew shear, with a thickness and by the form of trailing edge, etc.

In $M > 1.2-1.25$, one should apply nozzle cascades with the being constricted intervane channels, but the back of airfoil/profiles in skew shear is fulfilled concave. Theoretically most advantageous, from the viewpoint of the distribution of the speeds in cross section after grid/cascade, is the concave back, constructed as flow line during the flow about the point of inflection (edge of the preceding/previous airfoil/profile). However, with this form of the back of airfoil/profile, it is not possible to construct the foil lattice of airfoil/profiles, since the angle of the

formation/education of edge is obtained negatively (trimming of edge). Consequently, with the shaping of blade back in skew shear of grid/cascade it is necessary to ensure the sufficiently wide structural/design angle of the formation/education of trailing edge.

Fig. 15, shows an example of the construction of the back of airfoil/profile in skew shear with the aid of the diagram of characteristics. Calculated Mach number for grid/cascade $M = 1.4$. The diagram of the construction of flow the is following: 1) sonic line is straight line in narrow cross section; 2) at point of inflection appears the rarefaction wave in which flow it is expanded from $M = 1$ to M_{inf} ; 3) the back of airfoil/profile on the initial section is convex, and then part of the rarefaction waves it is extinguished by the corresponding rotation of wall. The angle among the tangent to back at point of inflection and the tangent to back on trailing edge to 1-2 is less than the angle between the tangent to back in the narrow cross section of channel and the tangent to back at point of inflection (Fig. 15). By this is reached the positive angle of the formation/education of edge. In the same Fig. 15, is shown a consecutive change in the given speed of λ upon transition through rarefaction waves in the diagram of characteristics.

However, the real picture of flow in skew shear differs from that constructed by method of characteristics. Overexpansion on back does not reach those values which were obtained from the calculation by the method of characteristics. Processing the results of the study of the large number of nozzle cascades made it possible to determine the maximum number of M_{tr}^{max} on back in skew shear depending on the number of M_{tr} (Fig. 16). The value of M_{tr}^{max} can be approximately determined by formula

$$M_{tr}^{max} = 0.9 M_{tr} + (0.25 \div 0.30). \quad (18)$$

where the M_{tr} - the calculated Mach number after grid/cascade.

Formula (18) is suitable in the range of $M_{tr} = 1.2-1.8$. When $M_{tr} < 1.2$ value of M_{tr}^{max} depends on the expansion ratio of channel f (Fig. 16).

After the achievement of the speed, which corresponds the M_{tr} on the back of airfoil/profile appears shock wave. The presence of

concave back in real flow brings as they showed experiments, to the transfer of laminar boundary layer to turbulent, since it occurs a sign change of the curvature of the enclosure of airfoil/profile. Thus, if shock wave falls in back after point of inflection, then it interacts with turbulent boundary layer, which decreases the probability of breakaway. Furthermore, the concavity of back decreases the angle between vectors of speed after jump and tangent to the back of airfoil/profile, which also decreases the danger of boundary-layer separation.

For the approximate computation of the back of airfoil/profile in skew shear of grid/cascade with constrictions it is possible to recommend following procedure [8, 10, 14].

Are assigned/prescribed the following values:

a - the size/dimension of the narrow cross section of channel, determined according to the known gas flow;

α_{eff} are an effective flow exit angle;

M_{1p} - the calculated Mach number at output/yield from grid/cascade.

1. According to formula (18) or from Fig. 16 is determined the value of M_1^{max} for the assigned M_{1p} .

2. Is determined the position of point of inflection (see Fig. 15) with respect to formula

$$l_{inf} = \frac{a \cdot q(M_{1p})}{\operatorname{tg} \left[\arcsin \frac{1}{M_1^{max}} + \frac{\Delta(M_{1p}) - \Delta(M_1^{max})}{2} (1 + 2) \right]}. \quad (19)$$

where the $\Delta(M_{1p})$ - the airflow angle with of expansion from $M = 1$ to M_{1p} [42]:

$\Delta(M_1^{max})$ - the airflow angle during expansion from $M = 1$ to

M_i^{max}

3. We round the value of $\left| \frac{\delta(M_{ip}) - \delta(M_i^{max})}{2} \cdot (1+2) \right|$ to the integer of degrees; from narrow cross section to point of inflection, we construct the correct broken line, which contains γ cuts (angle between cuts 1.0). Through the salient points of the obtained line, we carry out smooth convex line to point of inflection 0.

4. We determine the length of the concave part of the back

$$l_{conc} = \frac{\alpha \cdot q(M_i^{max})}{\lg \left[\frac{1}{M_i^{max}} \cdot \frac{\delta(M_{ip}) - \delta(M_i^{max})}{2} \right]} \quad (20)$$

where the $q(M_i^{max})$ - the given consumption, which corresponds to the number of M_i^{max} .

5. We construct concave correct broken line, beginning from the point of inflection 0 and to point with the coordinate of l_{conc} . The number of cuts of broken line is equal to $\gamma - (1-2)$; the angle

between cuts 1.0° . Through the salient points of the obtained line, we carry out smooth concave line being mated with convex line in point of inflection.

6. At the end of the concave line, we carry out tangent and, after determining by a and u_{∞} lattice spacing t , we construct the trailing edge of airfoil/profile. After concave follows the straight portion of the back of airfoil/profile.

§ 11. Shaping of nozzle supersonic grid/cascades.

In proportion to the increase in the calculated number of $M_{tr} > 1.4$ at output/yield from grid/cascade it is necessary to transfer/convert to application/use of the combined type of the grid/cascades, which have the small expansion of vane channel and concave back of airfoil/profile in skew shear.

It is known that at supersonic speeds the cascade/grid with expanding ducts are sensitive to a change in the mode/conditions and, in particular, Mach number [9, 10]. The character of a change of the

losses in grid/cascade during a change in the mode/conditions (M) depends substantially on the geometric parameters of grid/cascade and, in essence, on the form of vane channel. So, if the grid/cascades with constrictions usually are characterized by low losses at subsonic speeds, and with $M > 1$ loss sharply they grow/rise, then for grid/cascades with expanding ducts losses are low in the narrow range of supersonic speeds, and with transonic and aaaaaa reach high values [14].

Analyzing the behavior of the characteristics of supersonic jet/reactive grid/cascades with expanding channels during varying loads, it is not difficult to establish that the effectiveness of grid/cascades depends on form and shock configuration in the divergent section of the channel and in skew shear [8].

Page 19.

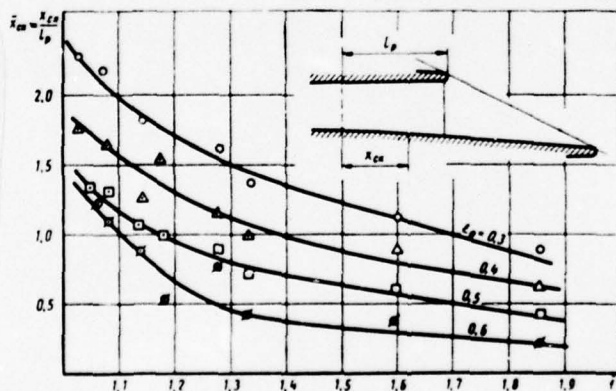
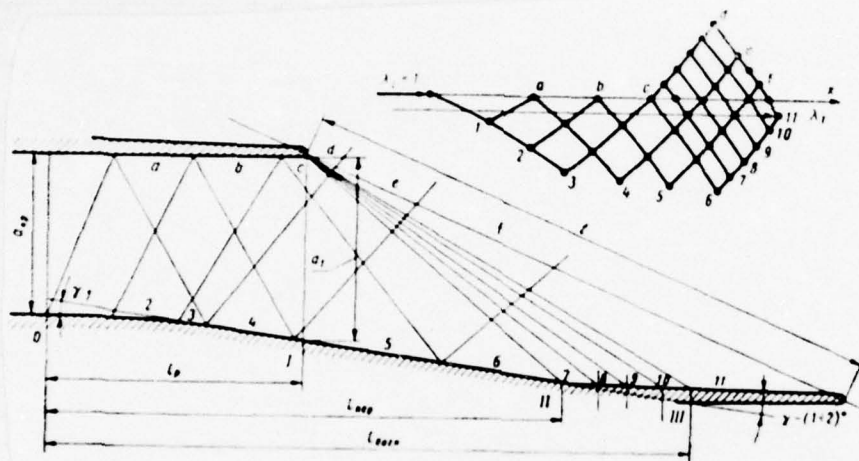


Fig. 17. Change of the shock position depending on the expansion ratio of channel f and of mode/conditions.

Fig. 18. Diagram of the construction of the back of the airfoil/profile of supersonic grid/cascade with expanding ducts.



The results of processing the curve/graphs of pressure distribution according to the back of different airfoil/profiles (Fig. 17) show that the current position of the compression shock $x_{cs} = \frac{x_{cs}}{l_p}$ is changed depending on the relation of pressures on grid/cascade and the expansion ratio of channel $\bar{\Gamma}$.

From curves in Fig. 17, distinctly it follows that with decrease in $\bar{\Gamma}$ the jumps faster leave channel and transfer/convert in oblique section/shear, i.e., in just one ratio of the pressure of π_0 jumps in intervane channel that are nearer to exit section, than less $\bar{\Gamma}$. This result from physical side explains the detectable experimentally dependence of losses and flow exit angle from the ratio of pressure in off-design conditions. The lesser the geometric parameter $\bar{\Gamma}$, the lesser part of back and concave surface of airfoil/profile it is located under the effect of the system of jumps in off-design conditions. Furthermore, in moving in oblique section/shear they change structure into the intensity of the jumps: curvilinear (close to straight lines) jumps in channel upon transition in oblique section/shear become oblique. Since in grid/cascades with low expansion ratio with a decrease in the π_0 jumps faster are moved in oblique section/shear, oblique section/shear faster enters the work. Consequently, in grid/cascades with low $\bar{\Gamma}$ the flow exit angle is changed more intense during a change in the mode/conditions. The

selection of the rational value of parameter f makes it possible to most expediently distribute the acceleration of the flow between divergent section of the channel and skew shear [14].

For the grid/cascades, which have calculated number $1.4 < M_{1p} < 2$, the expansion ratio of vane channel it is possible to select according to the empirical formula, obtained by processing the numerous experimental data:

$$f = 1 - K \left[\frac{1}{q(M_{1p})} - 1 \right], \quad (21)$$

where $K = aM_{1p} + b$; $a = 0.5$; $b = 0.4$.

For the construction of skew shear and divergent section of the intervane channel of nozzle cascade, can be used the following procedure.

Assigned are the values: $a_{xp} (a_{xus})$; M_{1p} ; $\sin \alpha_{1xp}$ $\frac{a_{xp}}{l}$ (Fig. 18).

1. Let us determine the expansion ratio of vane channel through formula (21) we find the size/dimension of the exit section of the channel:

$$a_1 = a_{inf}$$

2. On the tables of gas-dynamic functions, we determine number M_1 in the exit section of expanding duct, corresponding $q(M_1) = 1/\bar{F}$; the back of airfoil/profile within the limits of divergent section is made rectilinear, and the angle between tangents in the exit section of expanding duct and in narrow cross section comprises $\delta(M_1)/2$, where $\delta(M_1)$ is an airflow angle during expansion from $M = 1$ to M_1 . Let us designate the rounded to integer value $\delta(M_1)/2$ by γ_0 . Then the length of the divergent section of the channel

$$l_p = \frac{a_1 - a_{ap}}{\lg \gamma_0} \quad (22)$$

we connect points O and by I (Fig. 18) convex correct broken line, which contains γ_0 cuts (angle between the adjacent cuts of broken line it composes 10°). Then we connect points of inflection by clean-cut line.

3. We determine according to formula (18) the maximum number of M_1^{max} on back and we find the position of the point of inflection of the back of the airfoil/profile:

$$l_{inf} = l_p + \frac{a_1}{\lg \left[\arcsin \frac{1}{M_1} \frac{\gamma_0}{2} (1 - 2) \right]} \quad (23)$$

where

$$\bar{h}_1 = \frac{1}{q(M_1^{max})}$$

we carry out tangent to the back of airfoil/profile in point I
we continue it to point of inflection II.

4. We determine the position of point III the end of the concave part

$$l_{III} = l_p + \frac{u_{II}}{V_s} \lg \left[\frac{1}{\arcsin \frac{1}{M_{II}}} \right] \quad (24)$$

we connect points II and III (Fig. 18) by the correct concave broken line, which consists of γ_1 cuts (γ_1 - the airflow angle with of expansion from M_1 to M_{II}). The angle between the adjacent cuts of broken line it composes 10° .

5. We carry out in point III tangent to back and, after determining by a_1 and lattice spacing t , we construct the trailing edge of airfoil/profile.

The intake of supersonic nozzle airfoil/profiles is calculated and is constructed just as for subsonic speeds. The airfoil/profiles of nozzle cascades for near- and supersonic speeds and their aerodynamic characteristics are given on plates 38-41.

§ 12. Shaping of running cascades for transonic and supersonic speeds the shaping of grid/cascades by the method of "eddy/vortex".

At supersonic inlet velocities into impulse cascades, appear the bow waves, connected with the flow about the entering edges of airfoil/profiles. The form of bow waves and their arrangement relative to edges depends on Mach number at entry, the form of edges and vane channels. The form of the intake and output sections of airfoil/profile and the form of channel must provide:

a) the minimum wave losses in the head and trailing-edge shock waves:

b) nonseparable flow with the minimum losses for friction in vane channel.

In the majority of cases, with supersonic inlet velocities into grid/cascade in intervane channel, appear the flow breakaway and the complex system of the curvilinear jumps, which interact between themselves, with the walls of channel and the boundary of separation zone. Therefore recommendations regarding the shaping of supersonic active cascades are based mainly on experimental data.

At the small supersonic speeds $M_1 < 1.3$ bow waves close in form to straight lines. Since losses in normal shock at such speeds are low, the grid/cascades of group b are shaped according to the method "normal shock". In grid/cascades of such type, the intake and trailing edges of airfoil/profile are made those which were sharpened and rectilinear, but vane channels being smoothly constricted [3,

11]. The curvilinear sections of back and concave surface have alternating/variable curvature, whereupon the form of curvilinear part is calculated from channel method (§ 8).

The shaping of impulse cascades for $M > 1.3$ is realized/accomplished by different methods, distinguished by the organization of flow on entering edges, by the form of channel and by the form of the back of airfoil/profile in skew shear at output/yield from grid/cascade.

Page 20.



Fig. 19. Flow pattern before the grid/cascade at supersonic speeds.

Fig. 20. Picture of the rearrangement of the uniform supersonic flow before the grid/cascade into vortex flow within channel.

Key: (1). Concave transition section. (2). Convex transfer section.
(3). Compression waves. Rarefaction waves.

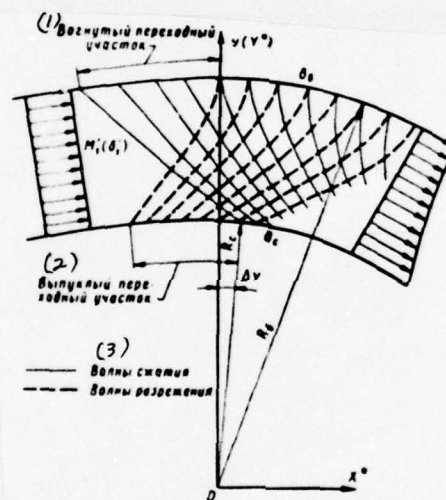
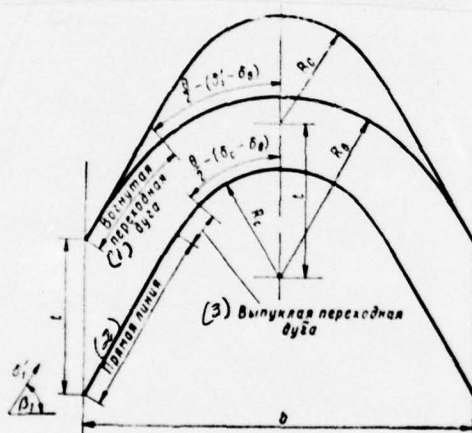


Fig. 21. The principal notations of the grid/cascades, constructed by the method of "eddy/vortex".

Key: (1). Concave transfer arc. (2). Straight line. (3). Convex transfer arc.



The intakes of the back of the airfoil/profile of supersonic grid/cascades can provide: 1) the constancy of velocity after bow wave (rectilinear back at entry) (Fig. 19a); 2) graded braking flow in the system of jumps (broken back at entry) (Fig. 19b); 3) smooth braking along concave wall at the entry into grid/cascade (Fig. 19c).

Vane channel can be contracting-expanding (minimum cross section is arranged within channel) and then flow is braked at first, occurs its rotation at low velocities, and then it is accelerated in the divergent section of the channel and in skew shear. If curvilinear channel has constant section, then braking flow occurs (because of friction) before exit section, and acceleration occurs only in skew shear. The output section of the back of airfoil/profile in skew shear must be made by rectilinear or concave (with subsequent transition to straight section). The concave back of airfoil/profile can be designed by the method of characteristics. With all methods of shaping, intake and trailing edges are design/projected tapered and those which were sharpened.

The flow of gas in supersonic grid/cascades can be that which was mixed or completely supersonic. Only in the latter case the most approximate possible theoretical solution to direct or reverse/inverse problems.

Below is set forth one of the methods of the construction of active supersonic grid/cascades with completely supersonic flow in vane channels.

The method of "eddy/vortex", or the method "completely supersonic flow", was proposed independently to M. F. Zhukov (1950) and by Boxer and Sterret [49] (1952), but late by Oswatitsch [52, 53] (1956). Method is based on the rational combination of circulation irrotational flow ($\lambda R = \text{const}$) and of the corresponding levelling off flows (Fig. 20).

For construction of cascades are given by the even distribution of the speeds of flow at entry. Further is constructed the flow, which transforms uniform velocity diagram into the diagram/curve, which corresponds to the hyperbolic distribution of the speeds in the middle part of the channel. The construction of this flow is provided by the appropriate shaping of transfer arcs. Flow with the hyperbolic distribution of speeds is turned to preset angle in the channel, generatrices of which are the concentric circumferences. Transfer

arcs at output/yield translate/transfer the vortex/eddy distribution of speeds into uniform flow after grid/cascade.

The construction of transfer arcs is conducted by method of characteristics.

/ let us examine the construction of grid/cascade in the case of the infinitely fine/thin intake edges of blade. At the assigned inlet velocity M_1 , on the transfer section of concave surface the flow must be inhibited to the selected velocity of M_2 and on the transfer section of back is accelerated to M_2 . Let us designate: δ is an angle of deflection of the supersonic flow with of its expansion from $M = 1$ to assigned M . Then δ'_1 - angle of deflection during expansion from $M = 1$ to M'_1 (Fig. 20); δ_1 are from $M = 1$ to M_1 and δ_2 from $M = 1$ to M_2 .

In compression zone on the transfer section of concave surface, the angle of deflection decreases by the value of $\delta_2 - \delta_1$; in rarefaction zone on the transfer section of back, the angle of deflection grow/rises by the value of $\delta_1 - \delta_2$. Both transfer sections must turn flow to identical angle. Consequently,

$$\text{and } \left. \begin{aligned} \delta'_1 - \delta_e + \Delta v &= \delta_e - \delta'_1 \\ \Delta v &= \delta_e + \delta_e - 2\delta'_1 \end{aligned} \right\} \quad (25)$$

where the Δv - the angle of shift of the transfer sections of back and concave surface (Fig. 20).

By the authors [49] were designed by the algebraic method of the coordinate of transfer sections for different velocities and the reentrance angles and output/yield (Table 5). The coordinates of transfer sections are given here in the Cartesian system of coordinates (X *; Y *). By utilizing table, possible for the selected values of δ'_1 (M'_1); δ_e and an δ_e to construct arcs in

rectilinear coordinates. Since concave arc begins with $v = 0$, a convex with $v = \Delta v$, after the construction of its convex transfer section must be misaligned to the angle of α clockwise around center O. Radii of the circular arcs of vane channel at the rated values of δ_1 and δ_2 also are contained in Table 5 (R_1, R_2 with of $v = 0$).

The form of airfoil/profile and vane channel is determined by number M_1 at the entry, by the angle of rotation of flow in grid/cascade $\theta = (\beta_1 + \beta_2)$ and by the selected values of $\delta_1(M_1)$ and $\delta_2(M_1)$ on concave surface and back. For a symmetrical airfoil/profile (Fig. 21) θ angle of rotation $2\beta_1$.

FOOTNOTE 1. Here β_1 and β_2 are angles between vectors of velocity w_1 and w_2 and the vector of the axial component of velocities.

ENDFOOTNOTE.

In this case the concave surface and back have a length, determined by angles $\theta = 2(\delta_1 - \delta_2)$ and $\theta = 2(\delta_2 - \delta_1)$ respectively. Transfer sections on back are connected with edges by the line segments, which together with the transitional sections of concave

surface form infinitely fine/thin edges. Virtually such edges turn out to be impracticable. This difficulty it is possible to overcome, if intake and trailing edges are fulfilled tapered with sufficiently low wedge angle then so that the forming on entering edge jump would be that which was connected.

In the case when the axial component of inlet velocity is subsonic (Fig. 22a), wedge form with concave side, and back arrange/locate in parallel to the incident flow.

Page 21.

Table 5.

$-v$	δ_1	$-X^*$	Y^*	$-v$	δ_1	$-X^*$	Y^*	$-v$	δ_1	$-X^*$	Y^*	$-v$	δ_1	$-X^*$	Y^*
(1) Вогнутая сторона				25	26	1.1860	0.6416	24	28	0.9918	0.6163	5	15	0.1399	0.7497
$\Delta_s = 0^\circ$				26	27	1.2288	0.6093	25	29	1.0507	0.5894	6	16	0.1698	0.7468
0.0	0.0	0.0000	1.0000	27	28	1.3241	0.5742					7	17	0.2004	0.7433
1	1	0.0607	0.9992	28	29	1.3970	0.5362	$\Delta_s = 6^\circ$				8	18	0.2316	0.7392
2	2	0.9953	0.9983	$\Delta_s = 2^\circ$				0	6	0.0000	0.8152	9	19	0.2667	0.7344
3	3	0.1302	0.9967	0	2	2.0000	0.9035	1	7	0.0290	0.8150	10	20	0.2972	0.7288
4	4	0.1741	0.9965	1	3	0.0326	0.9032	2	8	0.0587	0.8142	11	21	0.3310	0.7225
5	5	0.2184	0.9930	2	4	0.0667	0.9023	3	9	0.0891	0.8129	12	22	0.3651	0.7156
6	6	0.2632	0.9862	3	5	0.1018	0.9008	4	10	0.1203	0.8110	13	23	0.4007	0.7077
7	7	0.3082	0.9810	4	6	0.1377	0.8986	5	11	0.1522	0.8084	14	24	0.4374	0.6989
8	8	0.3546	0.9750	5	7	0.1743	0.8957	6	12	0.1847	0.8053	15	25	0.4774	0.6885
9	9	0.4015	0.9680	6	8	0.2118	0.8927	7	13	0.2178	0.8015	16	26	0.5165	0.6777
10	10	0.4491	0.9600	7	9	0.2499	0.8878	8	14	0.2518	0.7970	17	27	0.5550	0.6663
11	11	0.4915	0.9522	8	10	0.2888	0.8826	9	15	0.2866	0.7918	18	28	0.5967	0.6531
12	12	0.5409	0.9420	9	11	0.3285	0.8767	10	16	0.3223	0.7859	19	29	0.6399	0.6386
13	13	0.5975	0.9295	10	12	0.3690	0.8699	11	17	0.3588	0.7791	20	30	0.6846	0.6228
14	14	0.6494	0.9171	11	13	0.4104	0.8622	12	18	0.3962	0.7715	21	31	0.7311	0.6054
15	15	0.7025	0.9033	12	14	0.4528	0.8536	13	19	0.4346	0.7630	22	32	0.7794	0.5864
16	16	0.7571	0.8882	13	15	0.4962	0.8440	14	20	0.4740	0.7535	23	33	0.8296	0.5656
17	17	0.8132	0.8716	14	16	0.5407	0.8333	15	21	0.5146	0.7430	24	34	0.8820	0.5428
18	18	0.8707	0.8534	15	17	0.5863	0.8215	16	22	0.5564	0.7314	25	35	0.9365	0.5179
19	19	0.9299	0.8336	16	18	0.6332	0.8085	17	23	0.5994	0.7186	26	36	0.9934	0.4908
20	20	0.9909	0.8120	17	19	0.6814	0.7942	18	24	0.6438	0.7046	27	37	1.0529	0.4611
21	21	1.0540	0.7884	18	20	0.7279	0.7795	19	25	0.6897	0.6893	28	38	1.1152	0.4286
22	22	1.1192	0.7627	19	21	0.7788	0.7624	20	26	0.7371	0.6727	(2) Выпуклая сторона			
23	23	1.1865	0.7348	20	22	0.8344	0.7428	21	27	0.7861	0.6541	$\Delta_s = 40^\circ$			
24	24	1.2560	0.7046	21	23	0.8888	0.7224	22	28	0.8369	0.6341	0	40	0.0000	0.5441
25	25	1.3309	0.6704	22	24	0.9450	0.7003	23	29	0.8866	0.6123	1	39	0.0186	0.5419
26	26	1.4059	0.6346	23	25	1.0031	0.6762	$\Delta_s = 8^\circ$				2	38	0.0370	0.5416
27	27	1.4810	0.5972	24	26	1.0632	0.6501	0	8	0.0000	0.7833	3	37	0.0549	0.5426
28	28	1.5617	0.5562	25	27	1.1256	0.6216	1	9	0.0278	0.7831	4	36	0.0724	0.5416
29	29	1.6457	0.5095	26	28	1.1904	0.5907	2	10	0.0562	0.7823	5	35	0.0894	0.5402
$\Delta_s = 1^\circ$				27	29	1.2576	0.5571	3	11	0.0853	0.7810	6	34	0.1061	0.5386
0	1	0.0000	0.9373	$\Delta_s = 4^\circ$				4	12	0.1150	0.7792	7	33	0.1226	0.5368
1	2	0.0417	0.9370	0	4	0.0000	0.8536	5	13	0.1453	0.7768	8	32	0.1398	0.5346
2	3	0.0709	0.9362	1	5	0.0305	0.8533	6	14	0.1764	0.7739	9	31	0.1546	0.5323
3	4	0.1084	0.9346	2	6	0.0619	0.8525	7	15	0.2081	0.7702	10	30	0.1701	0.5297
4	5	0.1467	0.9322	3	7	0.0941	0.8511	8	16	0.2406	0.7659	11	29	0.1855	0.5268
5	6	0.1857	0.9291	4	8	0.1272	0.8491	9	17	0.2739	0.7610	12	28	0.2007	0.5238
6	7	0.2254	0.9253	5	9	0.1610	0.8464	10	18	0.3080	0.7553	13	27	0.2156	0.5205
7	8	0.2659	0.9207	6	10	0.1954	0.8431	11	19	0.3430	0.7488	14	26	0.2304	0.5169
8	9	0.3070	0.9153	7	11	0.2306	0.8391	12	20	0.3788	0.7415	15	25	0.2450	0.5132
9	10	0.3489	0.9090	8	12	0.2666	0.8344	13	21	0.4157	0.7333	16	24	0.2593	0.5092
10	11	0.3918	0.9019	9	13	0.3033	0.8289	14	22	0.4537	0.7242	17	23	0.2735	0.5050
11	12	0.4355	0.8938	10	14	0.3407	0.8226	15	23	0.4927	0.7141	18	22	0.2876	0.5005
12	13	0.4800	0.8847	11	15	0.3792	0.8154	16	24	0.5331	0.7029	19	21	0.3014	0.4959
13	14	0.5257	0.8746	12	16	0.4188	0.8074	17	25	0.5746	0.6906	20	20	0.3151	0.4911
14	15	0.5725	0.8633	13	17	0.4593	0.7984	18	26	0.6173	0.6771	21	19	0.3286	0.4860
15	16	0.6204	0.8509	14	18	0.5008	0.7884	19	27	0.6617	0.6622	22	18	0.3419	0.4808
16	17	0.6697	0.8373	15	19	0.5434	0.7774	20	28	0.7076	0.6460	23	17	0.3551	0.4753
17	18	0.7203	0.8223	16	20	0.5872	0.7653	21	29	0.7552	0.6282	24	16	0.3689	0.4696
18	19	0.7233	0.8059	17	21	0.6323	0.7519	$\Delta_s = 10^\circ$				25	15	0.3859	0.4616
19	20	0.8259	0.7880	18	22	0.6788	0.7372	0	10	0.0000	0.7559	26	14	0.3959	0.4569
20	21	0.8810	0.7684	19	23	0.7267	0.7212	1	11	0.0269	0.7557	27	13	0.4056	0.4520
21	22	0.9381	0.7471	20	24	0.7761	0.7037	2	12	0.0542	0.7550	28	12	0.4176	0.4458
22	23	0.9969	0.7239	21	25	0.8272	0.6846	3	13	0.0821	0.7537	29	11	0.4293	0.4394
23	24	1.0578	0.6987	22	26	0.8802	0.6637	4	14	0.1106	0.7520	30	10	0.4407	0.4330
24	25	1.1208	0.6713	23	27	0.9350	0.6410					31	9	0.4517	0.4265
												32	8	0.4622	0.4201
												33	7	0.4720	0.4138
												34	6	0.4810	0.4079

Table 5 (Continued.)

λ	δ_1	λ^*	λ^*	λ	δ_1	λ^*	λ^*	λ	δ_1	λ^*	λ^*
$\Delta_c = 38^\circ$				$\Delta_c = 34^\circ$				$\Delta_c = 30^\circ$			
0	38	0.0000	0.5525	23	13	0.3675	0.4903	19	13	0.3239	0.5293
1	37	0.0190	0.5523	24	12	0.3806	0.4816	20	12	0.3382	0.5212
2	36	0.0375	0.5519	25	11	0.3934	0.4788	21	11	0.3522	0.5196
3	35	0.0556	0.5511	26	10	0.4058	0.4729	22	10	0.3658	0.5137
4	34	0.0734	0.5500	27	9	0.4177	0.4669	23	9	0.3789	0.5081
5	33	0.0908	0.5486	28	8	0.4291	0.4610	24	8	0.3915	0.5037
6	32	0.1080	0.5470	29	7	0.4399	0.4551	25	7	0.4035	0.4991
7	31	0.1247	0.5451	30	6	0.4499	0.4495	26	6	0.4146	0.4949
8	30	0.1410	0.5429								
9	29	0.1572	0.5405								
10	28	0.1732	0.5378	0	34	0.0000	0.5707	0	30	0.0000	0.5913
11	27	0.1889	0.5349	1	33	0.0196	0.5705	1	29	0.0203	0.5911
12	26	0.2043	0.5318	2	32	0.0389	0.5700	2	28	0.0403	0.5906
13	25	0.2196	0.5284	3	31	0.0577	0.5692	3	27	0.0598	0.5898
14	24	0.2348	0.5246	4	30	0.0761	0.5681	4	26	0.0792	0.5886
15	23	0.2495	0.5209	5	29	0.0942	0.5667	5	25	0.0980	0.5871
16	22	0.2642	0.5169	6	28	0.1119	0.5650	6	24	0.1163	0.5853
17	21	0.2786	0.5126	7	27	0.1293	0.5630	7	23	0.1344	0.5833
18	20	0.2928	0.5081	8	26	0.1464	0.5607	8	22	0.1522	0.5809
19	19	0.3069	0.5038	9	25	0.1633	0.5582	9	21	0.1697	0.5783
20	18	0.3208	0.4995	10	24	0.1798	0.5555	10	20	0.1869	0.5754
21	17	0.3346	0.4953	11	23	0.1961	0.5524	11	19	0.2039	0.5723
22	16	0.3481	0.4908	12	22	0.2122	0.5492	12	18	0.2207	0.5689
23	15	0.3614	0.4862	13	21	0.2277	0.5457	13	17	0.2371	0.5652
24	14	0.3745	0.4768	14	20	0.2433	0.5420	14	16	0.2533	0.5614
25	13	0.3872	0.4710	15	19	0.2591	0.5379	15	15	0.2692	0.5573
26	12	0.3997	0.4650	16	18	0.2742	0.5337	16	14	0.2848	0.5529
27	11	0.4120	0.4589	17	17	0.2892	0.5293	17	13	0.3001	0.5484
28	10	0.4238	0.4528	18	16	0.3039	0.5246	18	12	0.3150	0.5437
29	9	0.4353	0.4466	19	15	0.3184	0.5198	19	11	0.3297	0.5388
30	8	0.4462	0.4404	20	14	0.3327	0.5147	20	10	0.3443	0.5340
31	7	0.4565	0.4343	21	13	0.3466	0.5095	21	9	0.3570	0.5288
32	6	0.4660	0.4285	22	12	0.3602	0.5042	22	8	0.3710	0.5233
				23	11	0.3736	0.4986	23	7	0.3835	0.5181
				24	10	0.3865	0.4930	24	6	0.3953	0.5131
				25	9	0.3990	0.4873				
				26	8	0.4110	0.4816	$\Delta_c = 28^\circ$			
				27	7	0.4224	0.4759	0	28	0.0000	0.6026
				28	6	0.4328	0.4705	1	27	0.0207	0.6024
$\Delta_c = 36^\circ$								2	26	0.0411	0.6019
0	36	0.0000	0.5614					3	25	0.0611	0.6010
1	35	0.0191	0.5612					4	24	0.0806	0.5998
2	34	0.0380	0.5607					5	23	0.0998	0.5983
3	33	0.0565	0.5599	0	32	0.0000	0.5867	6	22	0.1186	0.5965
4	32	0.0746	0.5588	1	31	0.0199	0.5865	7	21	0.1372	0.5944
5	31	0.0924	0.5574	2	30	0.0395	0.5860	8	20	0.1553	0.5920
6	30	0.1097	0.5558	3	29	0.0587	0.5852	9	19	0.1732	0.5894
7	29	0.1268	0.5538	4	28	0.0775	0.5841	10	18	0.1908	0.5864
8	28	0.1436	0.5516	5	27	0.0959	0.5826	11	17	0.2081	0.5832
9	27	0.1601	0.5491	6	26	0.1140	0.5819	12	16	0.2251	0.5797
10	26	0.1764	0.5464	7	25	0.1318	0.5808	13	15	0.2418	0.5760
11	25	0.1924	0.5435	8	24	0.1492	0.5795	14	14	0.2582	0.5721
12	24	0.2082	0.5403	9	23	0.1664	0.5780	15	13	0.2743	0.5679
13	23	0.2237	0.5368	10	22	0.1833	0.5761	16	12	0.2900	0.5636
14	22	0.2391	0.5331	11	21	0.2000	0.5741	17	11	0.3054	0.5590
15	21	0.2542	0.5292	12	20	0.2163	0.5728	18	10	0.3205	0.5543
16	20	0.2690	0.5251	13	19	0.2325	0.5712	19	9	0.3349	0.5495
17	19	0.2838	0.5207	14	18	0.2483	0.5693	20	8	0.3489	0.5445
18	18	0.2983	0.5162	15	17	0.2640	0.5672	21	7	0.3622	0.5395
19	17	0.3126	0.5114	16	16	0.2795	0.5649	22	6	0.3746	0.5347
20	16	0.3267	0.5064	17	15	0.2945	0.5624				
21	15	0.3406	0.5012	18	14	0.3093	0.5597				
22	14	0.3542	0.4958								

DOC = 76041693

PAGE ~~5~~

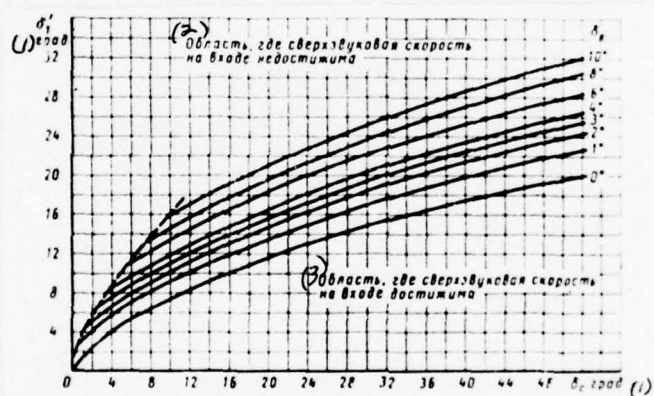
139

Key: (1). Concave side. (2). Convex side.

Page 22.

~~Fig.~~ Fig. 23. To the determination of the supersonic mode/conditions before the grid/cascade.

Key: (1). deg. (2). Region where the supersonic inlet velocity is unattainable. (3). Region where the supersonic inlet velocity is achieved.



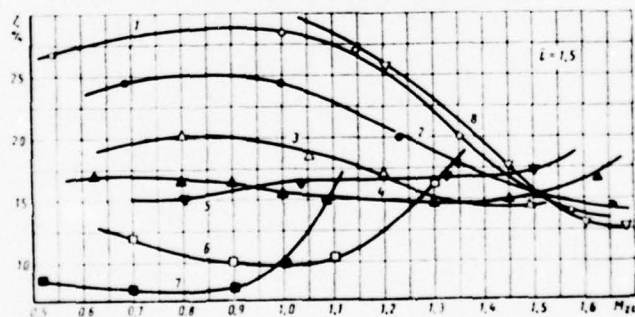


Fig. 24. Comparison of losses in the supersonic grid/cascades: 1. , 2. , 3. , 4. grid/cascade with the contracting-expanding channels; 5 - with the constant section of channel; 6 - R-2617B; 7 R-2617A; 8 - the R-3025V: (M_{21} - the value of Mach number after grid/cascade for a theoretical process).

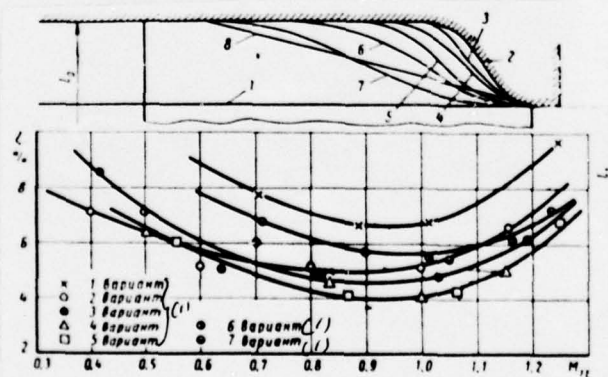


Fig. 25. Effect of the form of band/shroud/tire on losses in nozzle cascade.

Key: (1). Version.

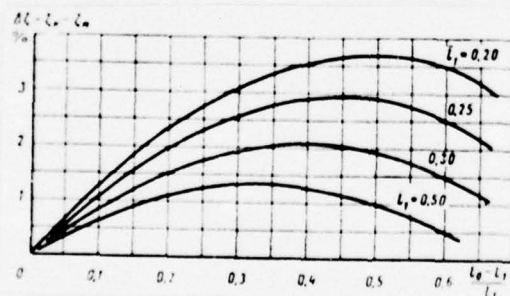


Fig. 26. Effect of the relative compression of aaaa and height/altitude of aaaa on a decrease in the losses in the grid/cascades: aaaaaaaa - the loss factors in that which was not shaped and that which was shaped grid/cascades.

Then the appearing on entering edge from concave side shock wave does not affect the flow outside channel. In order to extinguish this jump, is applied the fracture of the back of airfoil/profile in the point of impact on it in the jump. The velocity after jump M'_1 easily is determined by calculation, since wedge angle γ and M_1 are known. From points A and B, begin transfer sections on concave side and on back. Angle of rotation of flow in channel 2 ($\beta_1 - \gamma$).

When axial component of relative velocity at the entry into grid/cascade is supersonic, then inlet wedge is arrange/located so that shock wave would appear from the side of back, and line AC (Fig. 22b) arrange/locate in parallel to velocity vector M_1 . Shock wave is extinguished at point A, in the forming here rarefaction wave. Angle of rotation of flow in the channel: 2 ($\beta_1 + \gamma$). Vane channel and transfer section in the case of wedge edges ($\gamma \neq 0$) are calculated from velocity M'_1 after shock wave.

During the calculation of grid/cascades by the indicated method it is necessary to be convinced of the fact that with the selected numbers of $M_1(\delta)$ and $M_2(\delta)$ can exist the supersonic flow at the entry into vane channels. This problem is solved by using the equation of continuity. Let us note that the maximum number of M_1

is determined from the condition of the maximum consumption through grid/cascade taking into account losses and the curvatures of flow lines.

Fig. 23, gives the curves of the dependences of the maximum angles of δ_1 on δ_2 for certain interval of the values of δ_2 . Curves in Fig. 23 give the boundary values of numbers M'_1 (δ'_1) at the entry depending on the numbers of $M_2(\delta_2)$ and $M_1(\delta_1)$, whereupon the corresponding lines of $\delta_1 = \text{const}$ divide diagram into two regions: higher than the curves is arranged the region in which the supersonic inlet velocities arise cannot.

The experimental studies showed that the grid/cascades, profiled according to the method of "eddy/vortex", have the moderate profile ($\zeta_{\text{imp}} = 12-13\%$) and total ($\zeta_{\text{tot}} = 20\%$ when $bl = 0.5$) energy losses with $M_{21} = 1.6-1.7$.

The effectiveness of grid/cascade, especially strongly affects the form of channel, which is confirmed by experiments. The comparison of losses in the supersonic grid/cascades, designed by different methods, it is shown in Fig. 24. Are here given the

characteristics of supersonic grid/cascades with the channels of various forms with graded braking at entry and without it. Graded braking gives noticeable advantage with $M_{tr} > 1.5-1.6$. In grid/cascades with the channels of the constant section of loss at transonic and subsonic speeds, it is substantially lower than in grid/cascades with the contracting-expanding channels. However, the latter when $M_{tr} > 1.4-1.5$ are characterized by minimum losses. The optimum degree of the compression of channel at entry and expansion ratio at output/yield (relations of $\frac{a_1}{a_m}$ and $\frac{a_2}{a_m}$ depend on the numbers of M_{tr} and $M_{tr'}$ and angle of rotation in grid/cascade. For the interval of the numbers $M_{tr} = 1.15-2.0$ the relations lie within $a_1/a_m = 1.1-1.2$ and $a_2/a_m = 1.15-1.25$ [3]. The geometric and aerodynamic characteristics of impulse cascades for transonic and supersonic speeds are given on plates 33-37 and 43-45.

§ 13. Shaping of nozzle cascades with low relative spans of the blade.

To a decrease in the tip and total losses in the nozzle cascades of low altitude, gives meridian shape to channels. This method it allows:

1) to decrease the transverse gradients of pressure in the place of the maximum curvature of channel and thereby to decrease the secondary overflowing;

2) because of an increase in the convergence of channel in oblique section/shear to attenuate of boundary layer in exit section on the back of airfoil/profile;

3) to adjust flow to the root cross section of blades and, correspondingly, to decrease the losses of lower cylindrical band/shroud/tire. Furthermore, meridian shaping makes it possible to partially align static pressures by height of blades, i.e., to decrease a change in the degree of reaction for radius [6, 14].

To the effectiveness of grid/cascades with meridian shaping a basic effect has the form of the enclosures of band/shroud/tire. Fig. 25, gives the test results of nozzle cascade with different shaping. Optimum turn out to be versions with small compression in skew shear. Besides the form of the upper enclosure, the cost-effectiveness/efficiency of grid/cascade affects the relative compression, characterized by the value of $M_0 \frac{l_0 - l_1}{l_1}$. The results of

the corresponding experiments are given in Fig. 26. Here it is distinctly shown that the optimum values of α_{opt} depend on the height/altitude of grid/cascades.

The application/use of an unsymmetric compression in intermediate step/stages can lead to a sharp increase in the overlap/ceiling at the entry into the nozzle cascade, intake height/altitude of which h_0 (Fig. 27) it is substantially more output. In these cases the nozzle cascade must have at entry diffuser, as is shown in Fig. 27 by prime. The intake height/altitude of h_0 is selected less than the h_0' whereupon an altitude difference of h_0 and h_0' of the output height/altitude of the running cascade of the preceding/previous step/stage - must lie/rest at the limits, which ensure the maximum use of kinetic input energy; in this case the expansion angle of diffuser must not exceed 8-10.

To evaluate the total losses of ζ in lattice with the optimum compression depending on the height/altitude of h_0 can serve the empirical formula of $\zeta = \zeta_{opt} + 0.75 \frac{h}{2} 10^{-2}$, which is valid for Mach numbers = 0.70-0.9 and Re numbers $\geq 4.0 \cdot 10^5$.

DOC = 76041693

PAGE ~~20~~
149

Profile losses of aaaa can be taken according to test data of
fcil lattices.

Fig. 27. The principal notations of grid/cascades with meridian shaping.

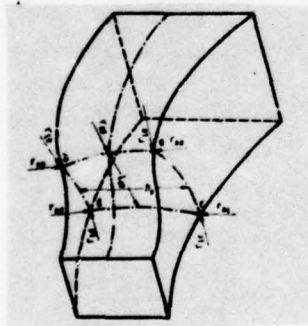
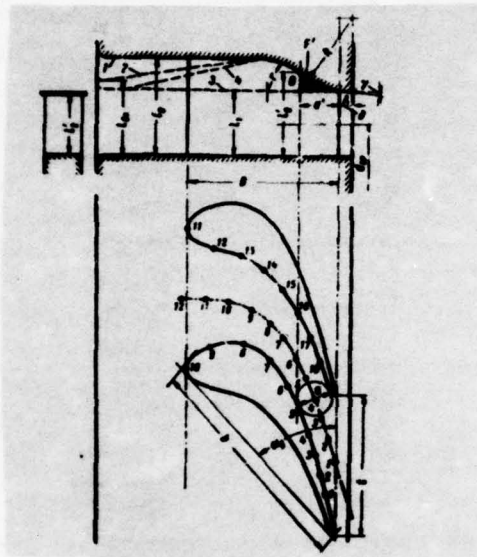


Fig. 28. Three-dimensional/space diagram of vane channel with meridian shaping.

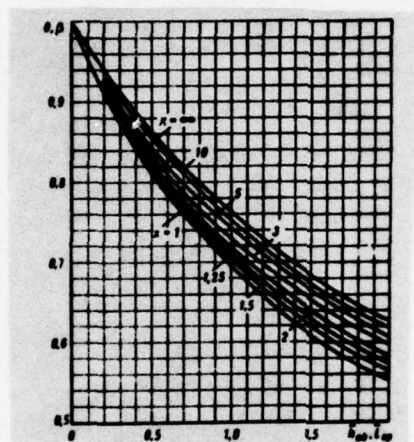


Fig. 29.

Fig. 29. On the calculation of meridian shaping. A decrease in the losses $\Delta \xi = 1 - \xi$ during the application/use of a compression in foil lattice composes $\Delta \xi = 0.7 \frac{\epsilon}{\lambda} 10^{-1}$.

The form of the curve of compression can be selected on the basis of the calculation of three-dimensional/space potential incompressible flow in channel. For this purpose, is utilized the method of calculation of curvilinear axisymmetric channels [34], in which the velocity distribution law along equipotential is determined by formula (see §8)

where

$$\frac{c}{c_0} = \frac{1}{1 + \bar{z} - \bar{z}_0}; \quad (29)$$

$$\bar{z}_1 = \frac{z_1 - 1}{z_0 - 1}; \quad \bar{z}_2 = \frac{z_2 - 1}{z_0 - 1};$$

$$\bar{z} = \frac{z}{z_0}; \quad \bar{z}_0 = \frac{z_0}{z_0}; \quad \bar{z}_\infty = \frac{z_\infty}{z_0}.$$

DOC = 76051693

EAGE ~~153~~

153

the principal notations are given in Fig. 28.

By acquiring the similar nature of velocity distribution by height of channel, we will obtain:

$$\frac{2}{3} - \frac{1}{1+\alpha}$$

for the channels of nozzle cascades it is possible to accept the curvature of streamlines by height along equipotential and the curvature of the lower wall of constant, i.e.,

$$r_{10} = r_{20}; \quad r_{10} = r_{20}; \quad r_1 = r_2$$

in addition to this it is assumed that the length of equipotential remains constant by height of channel. On the known geometry of channel, we construct equipotential plane and, bypassing it on edges, let us write the distribution of the velocities along equipotential taking into account the curvature of the upper enclosure in points a and b:

$$\frac{v}{v_0} = \frac{1 + \frac{r_{10}}{r_1} + \frac{r_{20}}{r_2}}{1 + \frac{r_{10}}{r_1} - \frac{r_{20}}{r_2}} \cdot \frac{1}{1 + \frac{r_{10}}{r_1} - \frac{r_{20}}{r_2}} \quad (27)$$

where

$$\begin{aligned} \bar{u}_w &= \frac{u_w}{l_w}; \quad l_w = \frac{L}{l_w}; \\ h_1 &= \frac{h_1 - l_w}{l_w}; \quad x_1 = \frac{x_1 - l_w}{l_w}; \quad i_w = \frac{i_w}{l_w}; \\ h_2 &= \frac{h_2 - l_w}{l_w}; \quad x_2 = \frac{x_2 - l_w}{l_w}; \quad i_w = \frac{i_w}{l_w}. \end{aligned}$$

The velocity in any cross section with the known flow rate of the incompressible fluid is determined from the equation of continuity.

Mean integral velocity on the upper enclosure is calculated from equation

$$u = \frac{1}{L} \int_0^L u \, dx$$

DOC = 76051693

PAGE

~~155~~
156

. The volumetric flow rate of the incompressible fluid through the channel in this case will be:

$$V = c_p \rho A v_{\text{avg}}$$

(29)

where

$$\alpha = \frac{1 + \bar{l}_{op}}{1 + \frac{k_2 \bar{l}_{op}^2}{k_3 \bar{l}_{op}}}; \quad (30)$$

$$\beta = \frac{1}{\bar{l}_{op}} \cdot \frac{1}{\sqrt{1 + 4k_4}} \times \\ \times \ln \frac{1 - 2k_2 \bar{l}_{op} / (1 + \sqrt{1 + 4k_4})}{1 - 2k_2 \bar{l}_{op} / (1 + \sqrt{1 + 4k_4})}; \quad (31)$$

$$\delta = \frac{1}{\bar{l}_{op}} \cdot \frac{1}{\sqrt{1 + 4k_4}} \times \\ \times \ln \frac{1 - 2k_2 \bar{l}_{op} / (1 + \sqrt{1 + 4k_4})}{1 - 2k_2 \bar{l}_{op} / (1 + \sqrt{1 + 4k_4})}; \quad (32)$$

$$k_4 = \frac{x_0 - 1}{2\bar{l}_{op} - \bar{l}_{op}}; \quad x_0 = \frac{\bar{l}_{op} - 1}{\bar{l}_{op}}; \quad \bar{l}_{op} = \frac{\bar{l}_{op}}{\bar{l}_{op}};$$

For the sake of simplicity in the calculations, are given the curve/graphs of the dependences of $\delta / (\bar{l}_{op}; x_0)$ and $\beta / (\bar{l}_{op}; x_0)$ (Fig. 29). If

lower band/shroud/tire is plane, then

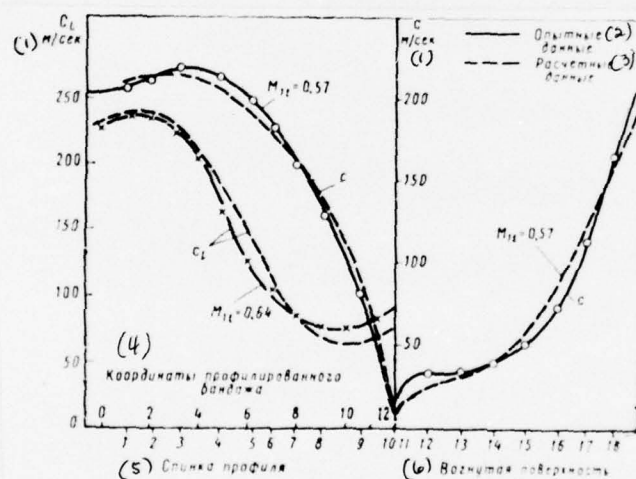
$$\beta = \frac{2}{l_{sp}} \ln(0.5l_{sp} + 1);$$

$$\alpha = \frac{1 + 0.5M_{sp}}{1 - 0.5M_{sp}}.$$

the account of compressibility effect is conducted by one-dimensional diagram, since velocity distribution according to equipotential plane it is possible to consider independent variable of compressibility effect [34]. From the parameters before the grid/cascade, they are determined λ_1 and q_1 ; further from the relationship/ratio of areas, is determined the $q_1 \frac{l_1}{l_2}$ for any cross section of channel.

Fig. 30. The comparison of the calculated and experimental distribution of the velocities in channel with meridian shaping (coordinates of drainages see Fig. 27).

Key: (1). m/s. (2). Experimental data. (3). Are calculated data. (4). Coordinates of the shaped band/shroud/tire. (5). Back of airfoil/profile. (6). Concave surface.



From q_1 and q_5 are determined the relations of $(\frac{\lambda^*}{\lambda})_1$ and $(\frac{\lambda^*}{\lambda})_5$, also, from them the dimensionless velocity in the arbitrary cross section s :

$$\lambda_s = \lambda_1 \frac{\partial_{s1}}{\partial_{s1}} \cdot \frac{(\lambda_{s1})_1}{(\lambda_{s1})_5} \quad (3)$$

the comparison of the experimental and calculated distribution of velocities along the enclosures of the channel of nozzle cascade presented in Fig. 30. Was calculated the divergent-convergent channel, formed by the airfoil/profiles of TS2A ($b = 51.5$ mm; $\bar{t} = 0.74$; $\bar{l}_1 = 0.35$; $\Delta \bar{l}_0 = 0.4$). Good agreement of experimental and calculated data gives grounds to apply this method for the calculation of spatial flow in the channels of the nozzle cascades of low altitude.

The solution of the reverse problem, i.e., the construction of channel in the specified distribution of velocities, presents no difficulties, since out of four three walls of channel are assigned/prescribed and it is required to determine only the upper enclosure of channel.

With known velocity along the upper enclosure of aaaa (for example along center line), the known flow rate of V and the assigned geometry of step/stage, disregarding in the first approximation, curvature along equipotential ab ($\alpha = 1$), according to formula (27) we determine the velocity in the point of a . Further in accordance with formula (29) we select the height/altitude of aaaa and radius of curvature in mean section. After this according to formula (27) we determine velocity taking into account the alternating/variable curvature ($\alpha \neq 1$) of a . During the considerable deviation of aaaa and aaaa, is conducted the repeated selection of a and a on the velocity of l_p and again is computed the value of the velocity of a . With the appropriate skill already the second approach/approximation turns out to be sufficient.

Central is the question concerning the selection rational the diagram/curve of pressures (velocities) concerning the enclosure of airfoil/profile, concerning the upper (shaped) and lower walls. On back it is necessary to ensure convergent flow with the maximum accelerating pressure gradients in output part. On the shaped and lower walls the distribution of pressures must be convergent with

being gradually decreased grad p to trailing edges, in order that would be provided for the uniform static-pressure field at output/yield from nozzle cascade.

For providing convergent flow on the upper shaped enclosure, it is necessary at output/yield from the channel where most probable diffuser section, to fulfill the taper of band/shroud/tire at an angle $\gamma = 2-4^\circ$ (see Fig. 27). The smaller values of angle γ pertain to welded diaphragms with relations $\theta < 20$, and large - to the milled setting (with large $\theta > 20$).

In connection with the difficulty of selection optimum the diagram/curves of velocities for each case it is possible to utilize the simplest method of the construction of meridian enclosure, based on experimental data.

1. Is selected the rake angle of the upper band/shroud/tire $\gamma = 2-4$ (see Fig. 27).

2. On curve/graphs (see Fig. 26) is selected the value of the

optimum compression depending on the relative height/altitude of nozzle cascade $\bar{\lambda}_1$.

For intermediate step/stages the value of $\Delta \bar{\lambda}_0$ is selected minimum in order that the expansion angle of diffuser would not exceed 8-10° (see Fig. 27).

3. Special attention with the shaping of the channels of nozzle cascades must turn to the relation of $\frac{l_0 - l'_0}{l_s - l'_s}$, which characterizes the compression of flow in skew shear of grid/cascade after throat (designation - cm. Fig. 27). The value of $\frac{l_0 - l'_0}{l_s - l'_s}$ is selected within limits from 0.30 to 0.44.

4. From point A, is reduced the perpendicular to the line of taper and by radius R through points A and E it is carried out circumference (radius R under these conditions is determined unambiguously).

5. By radius $r \sim R$ is mated the direct/straight and curved line of the upper enclosure.

After shaping it is necessary to determine reaction in the arbitrary cross section of step/stage, at known value in the root cross section of e . for formula

$$q = 1 - (1 - q_0) \left(\frac{r_0}{r_1} \right)^{2 \cos^2 \alpha_1} \exp \left[\sin^2 \alpha_1 \frac{r_1 - r_0}{kl_1} \right]. \quad (34)$$

. The difference in the reactions in root and peripheral cross sections is determined (with $e = 0$) on the following dependence:

$$\Delta q = q_0 - q_1 = 1 - \left(\frac{0 - 1}{0 - 1} \right)^{2 \cos^2 \alpha_1} \exp \left[\sin^2 \alpha_1 \frac{l_1}{R} \right]. \quad (35)$$

where

$$\theta = d_p / l_1$$

. The form of channels in meridian plane depends on the basic geometric parameters of step/stage, in particular, ratios θ (or $\bar{\ell}$) d/b , etc.

Depending on the indicated parameters, is changed not only the form upper, but also lower enclosures. Specifically, at some values θ and $\bar{\ell}$ it is necessary the internal lower enclosure of diaphragm to fulfill that which was shaped in order that the reaction in root cross section would not prove to be less than the reaction of apex/vertex.

The shaping of nozzle cascades in meridian plane leads to an increase in the throat area of channels, since shaping seizes oblique the section/shear of channels. Approximately the value of the output area of nozzle cascades can be determined by the following formula:

DOC = 76051693

PAGE

166

$$F_{s, n} = n \left(a l_1 + \frac{F'}{\cos \alpha_1 \sin \alpha_2} \right). \quad (36)$$

here:

n - the number of channels;

a - the value of the throat of channel;

F' - an increase in the area in meridian plane (see Fig. 27).

Experiments show that during the determination of area from formula (36) the coefficients of flow rate

$$\mu = \frac{G}{2 \pi F_{s, n} \sqrt{p_0} v_0}$$

prove to be somewhat less than for grid/cascades with direct/straight band/shroud/tires. This connected with the increased nonuniformity of the velocity fields in throat cross section and with the inaccurate determination of the area of $F_{..}$ is displaced in oblique section/shear and it will be than less calculated according to formula (36).

Taking into account the difficulty of the determination of the area of $F_{..}$ the calculation it can be carried out according to the usual formula $F = na_{l1}$, and the coefficients of flow rate μ are taken according to the experimental data given in Fig. 45 for the airfoil/profile of S-9015A with the optimum form of the upper enclosure (see §32). One should show that meridian shaping it is expedient to apply in sufficiently low relative height/altitudes $\bar{l} < 1.0$ and low fanning $\theta > 15$. In large fanning are applied other methods of a decrease in the tip losses in nozzle cascades (see 26).

§14. Rational forms of the channels of active running cascades with the low altitudes of blades.

As showed the experimental studies [51; 1], the losses from the secondary flows in curved channels and in the grid/cascades of low altitude, they do not reach the minimum during continuously convergent flow, if angle of rotation in channel is great, but static pressures at entrance and exit are close (impulse cascades).

The organization of divergent-convergent flow in the vane channels of impulse cascades with the wide angles of rotation of flow $\Delta\beta > (115-120^\circ)$ leads to sharp contraction in the tip losses

$$\Delta\beta = 180^\circ - (\beta_1 + \beta_2)$$

. It is possible to indicate the different methods of the construction of cascade profiles, which correspond the indicated requirement. The most economical method lies in the fact that, in order to adapt for low altitudes the existing airfoil/profiles of impulse cascades, by simple changes in their form. This way makes it possible to preserve widespread airfoil/profiles in production at turbine-constructing plants, introducing for the low altitudes of the modification of the initial airfoil/profiles.

The new airfoil/profiles, intended for low altitudes, were obtained by means of the trimming of concave surface so that vane channel would have expanded being constricted form, in this case the back of airfoil/profile was retained constant/invariable. Fig. 31, shows two airfoil/profile: initial (R-3021A) and with diffuser section at entry (P-3021A₀).

Page 25.

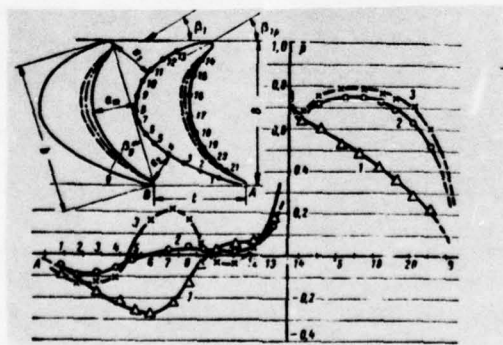


Fig. 31. Distribution of pressure according to the enclosure of airfoil/profile with different diffusivity at the entry:

1 - $\bar{\alpha}_m = 0.5^\circ$; 2 - $\bar{\alpha}_m = 1.0^\circ$; 3 - $\bar{\alpha}_m = 1.5^\circ$ ($\beta_1 = 25^\circ$; $M = 0.6$).

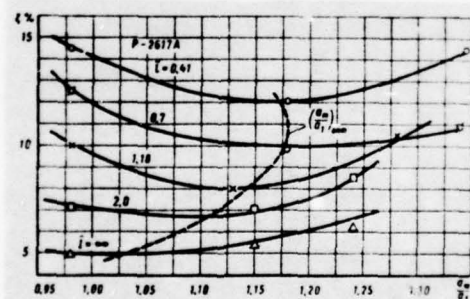


Fig. 32. Effect of the relation of aaaa and height/altitude on the loss factor in the grid/cascade of R-2617A ($\beta_1 = 23^\circ$; $M = 0.6$).

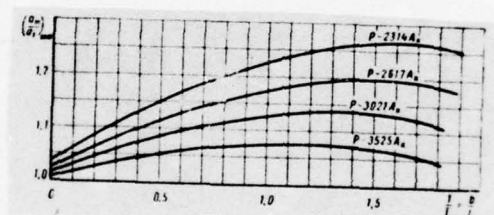


Fig. 33. Effect of angle of rotation in grid/cascade through the optimum diffusivity of aaaaaaaaaa.

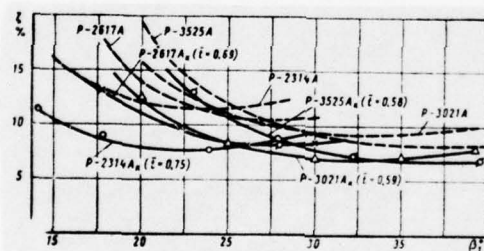


Fig. 34. Effect of reentrance angle to losses in the grid/cascades, designed for different angles of rotation ($M = 0.6-0.7$).

Here are given the most significant dimensions of the channel: width at entry a_1 , the width of the middle part of the channel of a_m and the width of throat cross section at output/yield a_2 .

The grid/cascades of the initial airfoil/profiles are characterized by the relations of $\bar{a}_m < 1$ and $\bar{a}_1 > 1$. Grid/cascades (group of A_1) they have diffuser channels at entry, i.e., are characterized by relations of $\bar{a}_m > 1$ and the $\bar{a}_1 > 1$.

It should be noted that a change in space and angle of setting leads to a change in the characteristic cross sections of channel and their relations of \bar{a}_m and \bar{a}_1 . During some values of t and β , the initial airfoil/profiles of group A also form divergent-convergent channels. However, in this case, as a rule, is not provided the optimum diffusivity at entry, and considerably change the flow exit angles, which leads to an essential increase in the losses in grid/cascades.

During the construction of the impulse cascades of low altitude, by solving inverse problem, it is necessary correctly to select the initial diagram/curve of pressures on airfoil/profile, which ensures

the minimum tip losses. It is possible to show that initial the diagram/curve of velocities depends on the basic geometric parameters of grid/cascade and, in essence, on its relative height/altitude. In connection with the complexity of the task, corrected with detailed calculation of tip losses and search optimum the diagram/curves of velocities, were utilized experimental data.

Fig. 31 gives the diagram/curves of pressure for the channels of the various forms of the grid/cascade of R-3021A at relative height/altitude $\bar{h} = 1.17$. One should note substantial change the diagram/curve of pressures in proportion to the increase in the diffusivity at the entry: in the continuously constriction flow along back convergent to points 6-5, and from point 5 to trailing edge - the flow region of diffuser flow. In all extent/elongation of concave surface, the motion is convergent. In channels with the being expanded entry flow along the intake of back (point 12-10) also convergent.

In the nozzle divergent section of channel for the relation of $\bar{a}_m = 1.08$ the pressure along back (point 10-7) falls up to points 3-2.

As a result sharply is reduced diffuser section in skew shear on the back of airfoil/profile (point of the minimum of pressure significantly is displaced along flow). For a span of the blade $\bar{\ell} = 1.17$ airfoil cascades R-3021A this diffusivity of ($\bar{a}_m = 1.08$) is close to optimum, the total losses in grid/cascade in this case are minimum.

A further increase in the diffuser section at the entry of $\bar{a}_m = 1.23$ leads to the appearance of a diffuser section on the back of airfoil/profile (point 9-7) with the subsequent sharp acceleration of flow. The losses in grid/cascade grow/rise.

Thus, the analysis of the diagram/curves of pressure makes it possible to indicate the reasons, which lead to a reduction/descent in the tip losses in grid/cascades with divergent-convergent channels.

By such reasons three:

the first - the rotation of flow in vane channel occurs at lower

average speed. Consequently, decrease the transverse gradient of pressure and the intensity of overflowing from the concave to convex surface in end walls;

the second - on the output section of the back where are intensified secondary currents, flow it becomes more convergent; downstream pressure gradients they grow/rise;

the third - it is reduced the extent of diffuser section on back in skew shear, since the point of the minimum of pressure is displaced along flow.

Data given in Fig. 32, testify to the presence of the optimum diffusivity for the grid/cascade, designed for the known working conditions (M , Re , $\Delta\beta$) and having specific geometric parameters. (Value of $\bar{\alpha}_{min}$ in essence depends on height of grid/cascade). With a decrease in the height/altitude, the optimum value of $\bar{\alpha}$ corresponding to the minimum losses, grow/rises and it reaches maximum with $\bar{\lambda} = 0.6$. In the grid/cascades of the lower altitude, the optimum diffusivity decreases and with very low altitudes ($\bar{\lambda} < 0.2$) is expedient, apparently, to make channels convergent.

The effect of the angle of rotation of flow in grid/cascade to the optimum value of α can be estimated on curves in Fig. 33. For the greatest angle of rotation, provided with the grid/cascade of P-231A, the optimum diffusivity is approximately $\alpha_{\text{opt}} \approx 1.22$, while for the grid/cascade of the P-3525A, of $\alpha_{\text{opt}} \approx 1.06$ at relative height/altitude $h = 1.18$. The grid/cascades of P-2617A and P-3021A occupy respectively intermediate position. The dependence of losses on space for all tested grid/cascades turns out to be sufficiently flat whereupon the optimum space noticeably it grow/rises with an increase in the camber (angle of rotation of flow).

Grid/cascade tests of the group of aaaa at the alternate angles of entry show that in the sufficiently broad band of a change of the $\Delta\beta$, $\sim (10-15)^\circ$ the loss in grid/cascades is changed insignificantly, just as in the grid/cascades of group A; the optimum reentrance angles for the grid/cascades of new group decrease in comparison with group A, which is explained by a decrease in the skeletal/skeleton reentrance angle of airfoil/profile due to the trimming of concave surface (see Fig. 34).

At the same time curve/graphs in Fig. 34 confirm that the maximum advantages of the grid/cascades of the group of A, at low

altitudes are exhibited for the most curved forms R-2314A - R-3021A. A difference in the loss factors descends with an increase of the reentrance angle of flow and for the grid/cascade of R-3525A at $\beta_1 > 35^\circ$ it turns out to be minimum. This result again confirms the advisability of applying such types of grid/cascades for the wide angles of rotation of flow.

Compressibility does not have a noticeable effect on losses in grid/cascades to $M \sim 1$. This experimental fact served as base/root for testing the possibility of the execution of the impulse cascades of group b - for transonic speeds ($0.9 < M < 1.3$) - with divergent-convergent channels. The comparison of two types of grid/cascades b and of b. shows that and at small supersonic inlet velocities the diffuser duct inlets favorably show up in losses.

Page 26.

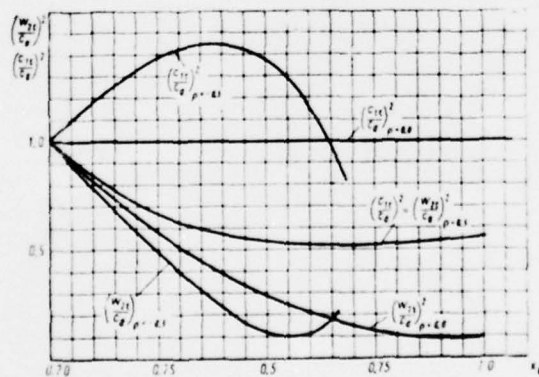


Fig. 35. Fraction of losses in nozzle and running cascades for three values of reaction ($\rho = 0$; $\rho = -0.5$; $\rho = +0.5$).

The characteristics of the grid/cascades of A_* and B_* are given on plates 25-30 and 34-35.

§15. Shaping of nozzle and running cascades for step/stages with low to the relations of u/c_a

By the most widely accepted method of a decrease in weight and dimensions of turbines is an increase wear/operated the step/stages of heat drops with the increased number of revolutions. In this case for step/stages, is retained the optimum relation of the velocities of u/c_a . the efficiency of turbine it remains high. However, if number of revolutions assigned/prescribed, then this way not always is optimum, since it requires the use of reducer.

Another method entails application/use in the step/stages of the reduced relations of u/c_a . This is reached either by a direct increase in the wear/operated heat drops at constant peripheral speed, or by a decrease in the peripheral speed (by decrease in the diameters) with constant heat drops, or by that and other methods. A decrease in the u/c_a leads to an increase in the energy losses in step/stages. In single step/stages this is connected, in essence, with an increase of leaving losses and losses in running cascades.

For intermediate step/stages the basic increase in the losses during a decrease in the α_a is caused by the low reentrance angles of flow to the nozzle cascades of diaphragms. An increase in the cost-effectiveness/efficiency of $\alpha_a < \alpha_{a\text{opt}}$ it is possible to attain variously.

From experiment it is known that the maximum stage efficiency, designed for subsonic speeds, is reached with the heat drops, which correspond to Mach numbers $\sim 0.75-0.85$. Many contemporary turbines of active type are designed for $\alpha_a \sim 0.5$ and above with $M < 0.5$. Thus, already because of the selection of the optimum heat drops is a possibility to reduce the number of step/stages, without increasing their diameters and retaining the previous cost-effectiveness/efficiency. To raise the efficiency of the single step/stages, which work with small relations α_a possible by applying vaned diffusers after running cascade. This method makes it possible to decrease the losses at outlet velocity.

In order substantially to decrease the α_a in step/stage, retaining high cost-effectiveness/efficiency, it is necessary to design flow area and the airfoil cascades, which ensure the minimum of losses at low reentrance angles and the wide angles of rotation of

flow. In addition to this, must be correctly produced the laying out of static heat drops to the first, intermediates and the last/latter step/stage of section for the target/purpose of the provision for the minimum losses to outlet velocity and identical

x_a

FOOTNOTE 1. The static heat drop is determined from the static parameters of the gas before and after step/stage. ENDFOOTNOTE.

Let us estimate the fraction of losses in nozzle and running cascades in the step/stage with variable x_a . The energy losses in nozzle and running cascades, referred to available energy in step/stage $h_a = \frac{c_a^2}{2}$, are record/written in the following form:

$$\xi_n \left(\frac{c_n}{c_a} \right)^2; \xi_r \left(\frac{w_r}{c_a} \right)^2$$

ξ_n and ξ_r - the coefficients of energy losses in nozzle and running cascades, referred to available energy in the appropriate grid/cascade:

$$\zeta_1 = 1 - \left(\frac{c_1}{c_0} \right)^2 = 1 - q^2; \quad \zeta_2 = 1 - \left(\frac{w_2}{w_1} \right)^2 = 1 - q^2$$

(coefficients of the losses of ζ_1 and ζ_2 are determined from the data of the static studies of grid/cascades).

Fig. 35, depicts the curve/graphs of the fractions of losses in nozzle and running cascades with $\alpha_1 = 15^\circ$ and of three values of reactions ($\rho = 0; 0.5$ and -0.5), from which it follows that with a decrease in the κ_0 the fraction of losses increases and only in the nozzle cascade of step/stage with negative reaction falls. Taking into account also that with a decrease in the κ_0 decrease the reentrance angles and increase the angles of rotation of flow in grid/cascades, which leads to an increase in the losses, we come to the conclusion about need especially it is thorough to shape grid/cascades to low κ_0 .

The given in atlas airfoil/profiles of nozzle cascades (plates

9-15) are designed for the different reentrance angles and output/yield. Structural/design reentrance angle was selected to 5-10° less than calculated. The curvature of the enclosures of airfoil/profiles was calculated from the conditions of the optimum distribution of velocities. The calculation of velocities was performed by the channel method and verified on installation EHDA. For a series of airfoil/profiles (plates 14-15) back and concave surface were constructed on lemniscates.

The selection of running cascades for the step/stages, designed for low aaaa is based on the thermal design of turbine. On velocity triangles at entrance and exit from rotor wheel, is located from atlas the corresponding airfoil/profile. The degree of reaction it is expedient to accept close to zero.

For providing a high cost-effectiveness/efficiency, besides the selection of airfoil/profiles, it is important correctly to break heat drops on step/stages. The ratio of the static heat drop of first stage to the heat drop of intermediate with equal diameters and under the condition of the axial entry of flow to first stage can be written:

$$\frac{h_1}{h_0} = \frac{\cos^2 \alpha_1}{1 + (\epsilon_0 \cos \alpha_1 - \epsilon_0^2)} \quad (37)$$

. With axial output/yield from the last/latter step/stage, the ratio of static heat drop to the last/latter step/stage to the static heat drop of intermediate step/stage will be written in the following form:

$$\frac{h_0^*}{h_1^*} = \frac{1 - \cos^2 \alpha_1^*}{1 - \cos^2 \alpha_1^* (\cos \alpha_1 - \cos \alpha_0)} + 1, \quad (38)$$

where the α_1^* - the flow exit angle from the nozzle cascade of the last/latter step/stage (it is determined from the condition of the evenness of flow area for the equation of continuity):

DCC = 76051693

PAGE ~~188~~

187

$\epsilon_a = \frac{u}{c_a}$ - the relation of velocities for an intermediate step/stage.

The heat drop to the average step/stage is determined from the following formula:

$$h_0 = \frac{H_0}{\left(z \frac{\cos^2 \alpha_1}{4(x_a \cos \alpha_1 - x_g^2)} + \frac{W_a^2 - \cos^2 \alpha_1}{4 \cos^2 \alpha_1 (x_a \cos \alpha_1 - x_g^2)} + 1 \right)}, \quad (39)$$

where H_0 is the available heat drop to entire section;

z - the number of step/stages in section.

The approximate estimate of the cost-effectiveness/efficiency of the section of turbine can be produced on the basis of the static investigations of airfoil/profiles in formula

AD-A039 286

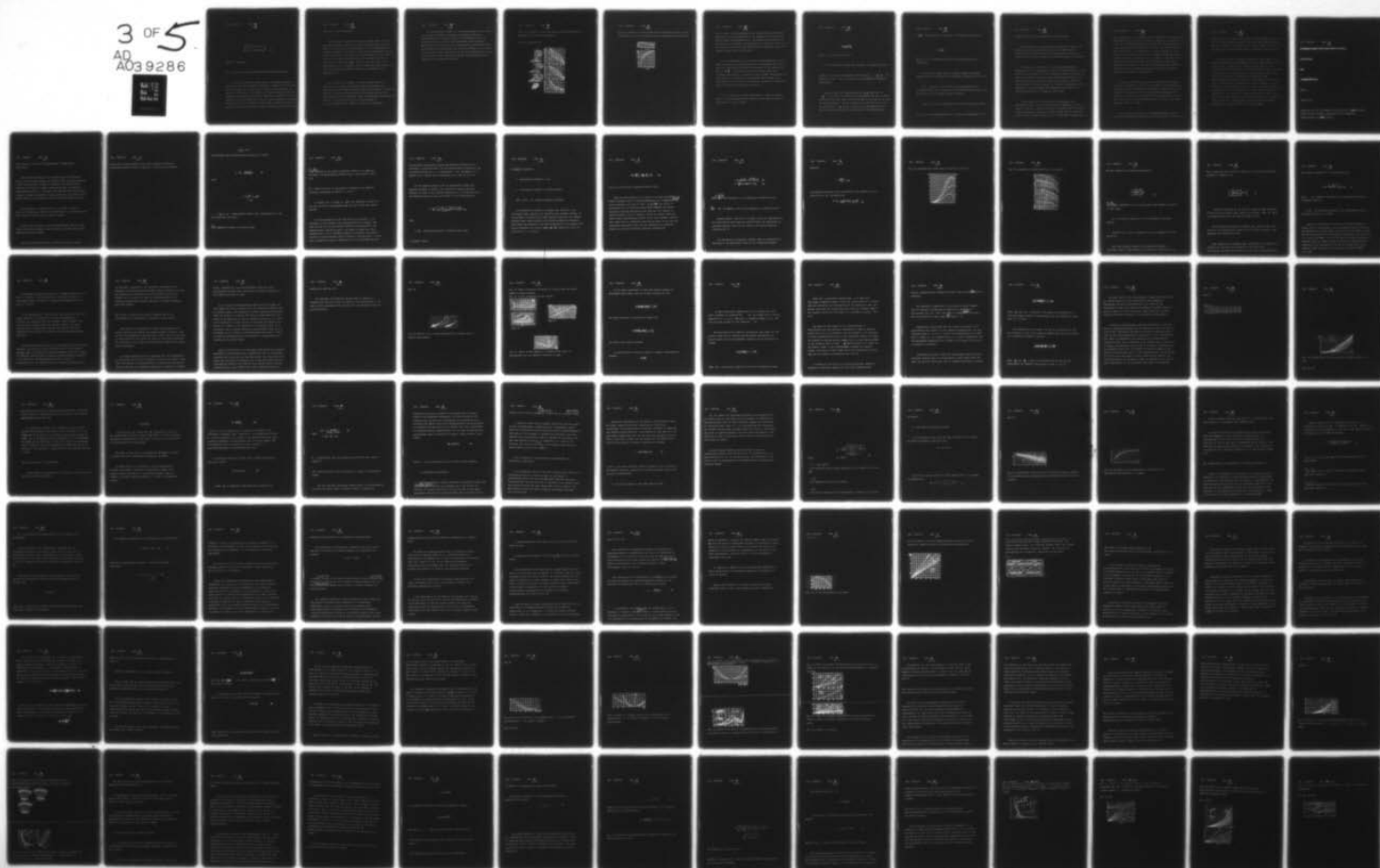
FOREIGN TECHNOLOGY DIV WRIGHT-PATTERSON AFB OHIO
ATLAS OF THE CASCADE PROFILES OF AXIAL-FLOWS TURBINE, (U)
DEC 76 M Y DEYCH, G A PHILIPP, L Y LAZAREV
FTD-ID(RS)T-1693-76

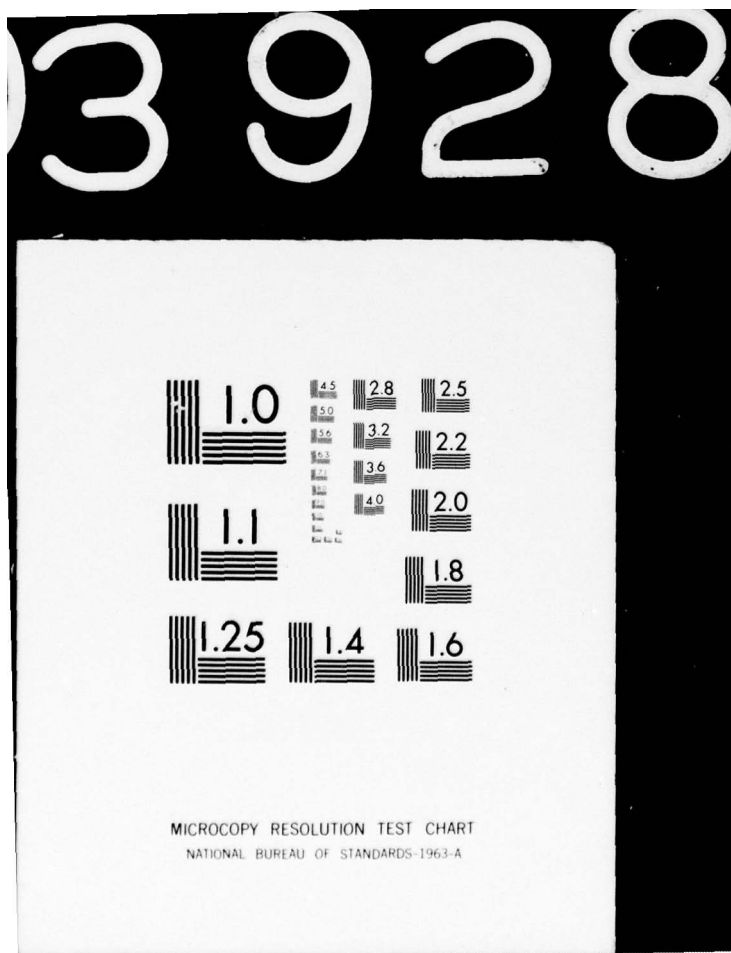
F/G 21/5

UNCLASSIFIED

NL

3 OF 5
AD
A039286





MICROCOPY RESOLUTION TEST CHART
NATIONAL BUREAU OF STANDARDS-1963-A

$$\eta_{\text{rot}} = 1 - \frac{h_0 + \frac{c_a^2}{2}}{H_0} \left\{ [z_c + k z_{cs}] + (z - 2) [z_c + k z_{cs}] + \frac{4x_a^2}{\cos^2 \alpha_1} \left[z_c + \left(1 - \frac{3}{4} \cos^2 \alpha_1 \right) z_{cs} + \sin^2 \alpha_1 \right] \right\}. \quad (40)$$

(here $k = 1 - 2x_a \cos \alpha_1 + x_a^2$).

§16. Shaping of nozzle cascades rotary controlling diaphragm

For the steam turbines, which have the adjustable selections pair, often are used revolving diaphragms. A change in the flow rate the pair through the turbine during varying loads is achieved by overlap at the entry of the channels of nozzle cascade. Are applied nozzle cascades with that which was divided and that which was not divided by throttle/chokes [13; 14]. The nozzle cascades of revolving diaphragms with the undivided throttle/choke, unlike the usual, for providing a total closing have a width of channel at entry less than

the width of airfoil/profile.

Widely common at present the nozzle cascades, which have the extended vane/blade channel of constant width with sharp rotation near exit section (Fig. 36, grid/cascade 1). The investigation of revolving diaphragms [13; 14] it showed that a considerable decrease in the losses over a wide range of mode/conditions it is possible to achieve by a decrease in the length of the straight portion of channel after rotary ring [$l_0 = (0.1-0.2) a_0$], and also by the application/use of an inclined, but not axial entry into rotary ring and of a respectively sloping channel ($\alpha_0 = 20-30^\circ$; Fig. 36, grid/cascade 2).

This change in the shaping of nozzle cascades leads to a decrease in the losses, since during full gate increase the longitudinal accelerating pressure gradients and decrease the loss of friction in channel. During partial discovery/openings in this grid/cascade, the flow expansion occurs simultaneously with rotation, whereas in grid/cascades with the extended intake is realize/accomplished the rotation of flow at a high speed.

The more effective method of a reduction/descent in the losses in the nozzle cascades of revolving diaphragms entails the application/use of sectional nozzle airfoil/profiles (Fig. 36, grid/cascade 3), and also of airfoil/profiles with deflectors [deflectors are shown in Fig. 36, grid/cascade 2 (cell/element A)]. The advantage of grid/cascades with sectional blades are the absence of sharp edges on the duct inlet, and also the favorable form of vane channel (Laval nozzle) during the partial discovery/openings when jump/drop in grid/cascade increases.

191

Fig. 36. Comparison of the loss factors in the grid/cascades of different type revolving diaphragms.

Key: (1). Grid/cascade.

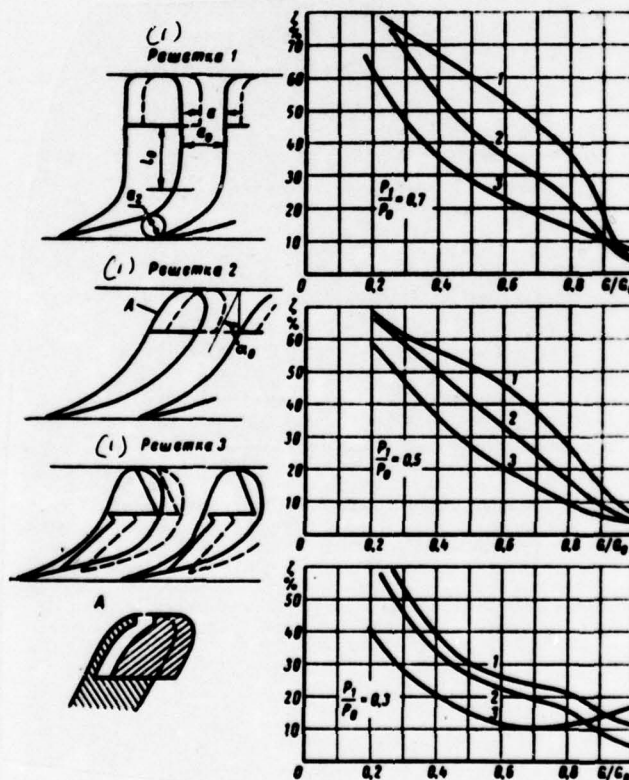
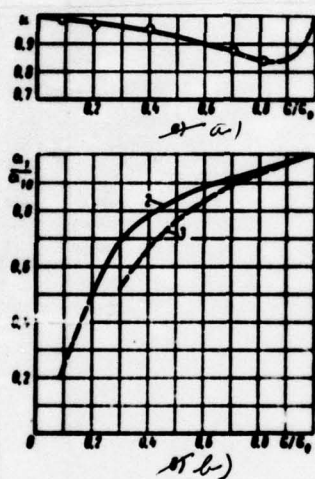


Fig. 37. Dependence of the coefficient of flow rate (a) and of angle of departure (b) on the relative flow rate through the grid/cascade.



To the number of deficiency/lacks, one should relate technological difficulties during manufacture and an increase in the edge losses during partial discovery/openings. Grid/cascade with deflectors is considerably less complex in manufacture, but solves the only part of the task: is removed one, most unfavorably the affecting sharp edge concave surface upon the duct inlet.

For the comparison of the cost-effectiveness/efficiency of the nozzle cascades of revolving diaphragms on curve/graph (Fig. 36) are given the experimental loss factors depending on the relative flow rate of $\bar{q} = \frac{q}{q_0}$ for different pressure differentials. Most economical turns out to be sectional nozzle cascade (grid/cascade 3). Substantially high losses has grid/cascade with inclined entry (grid/cascade 2). The quite high losses are obtained in grid/cascade with direct/straight entry (grid/cascade 1).

The real flow rate through grid/cascade G with the assigned degree of discovery/opening and during assigned mode/conditions is determined from usual formula

$$Q = \mu_0 B F \sqrt{\frac{h}{\rho_0}}$$

where q - the given flow rate 1;

B - the discharge coefficient, depending on adiabatic index k .

FOOTNOTE 1. Tabulated gas-dynamic function [6] of $\frac{q}{q_{cr}} = \frac{G}{G_{cr}}$ is ratio of the given gas flow through the grid/cascade to critical.
ENDFOOTNOTE.

When the degree of discovery/opening $\delta = \frac{A_1}{A_2}$ less than the $\frac{A_1}{A_2}$ the ratio of the output area of nozzle to the area of nozzle at entry during full gate,, which determines is the area of the slot of throttle/choke $F = A_1$. The coefficient of the flow rate of the throttle/choke of μ_0 can be selected on by experimental data of Fig. 37a, taken from [13]. of the degrees of discovery/opening

$\mu > \frac{h}{h_0}$ the coefficient of flow rate is determined from formula

$$\mu = \mu_{\text{ex}} \mu_0$$

where μ_0 - the coefficient of flow rate during full gate $\mu_0 =$
(0.97-0.98).

The flow exit angles from the nozzle cascade of revolving diaphragm can be determined to the pografiku, presented in Fig. 37b.

With a decrease in the degree of discovery/opening and, correspondingly, with a decrease in the relative flow rate G/G_0 angle of departure α_1 from nozzle cascade decreases;

(α_{10} ; G_0 - angle of departure and flow rate during full gate).

§17. Special feature/peculiarities of design and calculation of the

cross sections of the grid/cascades of large farming.

Airfoil/profiles in different cross sections by height of the nozzle and running cascades are selected in accordance with velocities and reentrance angles and output/yield, obtained as a result of the detailed thermal and aerodynamic design of step/stage.

If velocities by height of an entire grid/cascaderemain subsonic, then it is necessary to apply the airfoil/profiles of group A. For nozzle cascades with little differing angles of departure α_1 entry α_0 is applied one and the same airfoil/profile for all cross sections, which can differ by height only in terms of chord. The cross sections of running cascade are selected in accordance with the calculated reentrance angles and output/yield from atlas or are constructed according to lemniscate method (§9).

In the majority of the last/latter step/stages, which wear/operate great heat drops and having low relations θ , flow by height of cascade is mixed, velocities are changed from the subsonic to large supersonic values. In nozzle cascades flow of peripheral cross sections subsonic, while in root - supersonic. Consequently, in

such grid/cascades in peripheral cross sections must be utilized the airfoil/profiles of group A, on average - group b, in root: with $1.2 < M_1 < 1.4$ - airfoil/profiles with concave back, the generatrices the being constricted vane channel, and with $M_1 > 1.4$ airfoil/profiles with concave back, the generatrices the being expanded in output cross section channel (group c). For providing the optimum spaces in the cross sections of nozzle cascade by height in step/stages with low θ airfoil chord one should make that which is increasing to periphery. An increase in the chord in step/stages with uncovered flow area makes it possible also the more evenly to distribute convergence by height of grid/cascade.

During the function of large heat drops flow in the running cascades of step/stages with low θ also mixed: of the periphery of the velocity after grid/cascade supersonic, in root cross sections subsonic or transonic. In such grid/cascades peripheral cross sections are fulfilled in skew shear with reverse/inverse concavity [40; 41]. Channel being constricted (with $M_2 < 1.4$) or with small expansion (with $M_2 > 1.4$).

The shaping of skew shear is realize/accomplished per the common/general/total recommendations, presented into §§10 and 11. The

procedure for the shaping of root cross sections remains the same as for the impulse cascades of group A and of B, with that difference, that with shaping and selection of the form of channel the low level of losses must be provided for with low relative lattice spacings t .

The mean sections of running cascades are shaped just as the reactive transonic airfoil/profiles of group B with reentrance angles $\beta_1 = 40-120^\circ$. At subsonic and transonic speeds shaping can be realized/accomplished according to lemniscate method. With an increase of velocities, one should change the form of back in skew shear, transfer/converting to rectilinear or curvilinear (with reverse/inverse concavity) enclosures. For providing the necessary area of airfoil/profile correction one should produce, in essence, because of concave surface. With the shaping of running cascades with long blades, it is very important to ensure a smooth change in the curvature of the enclosures of airfoil/profile along span of the blade. This will ensure, in turn, a uniform change in the isobars and will decrease the radial pressure gradients and the streamline curvature in the vane channels of running cascades.

DOC = 76061693

PAGE ~~1~~

199

~~MICROFILM HEADER EDR 76061693 / CONT. / UNCLAS~~

~~HT/ST 76 1693~~

~~1693~~

~~SUBJECT CODE 4457D~~

Page 28.

Chapter III.

Calculation of the aerodynamic characteristics of ~~grid~~/cascades,
effect of some geometric parameters on the aerodynamic
characteristics of ~~grid~~/cascades.

§18. Losses for friction in grid/cascades. Boundary-layer calculation.

When the grid/cascades of the design/projected step/stages cannot be taken from standards or from the atlas of airfoil/profiles or when the available in atlas grid/cascades are utilized under conditions for which are absent experimental these, aerodynamic characteristics they are calculated from empirical and semi-rational formulas. Primary aerodynamic characteristics are the coefficients of energy losses in grid/cascades ζ and the flow exit angles α_1 (β_2).

Energy losses in grid/cascades it is accepted to class to profile (in flat/plane, infinite height/altitude to grid/cascade) and end, connected with the finite length of blades.

Profile losses include losses to boundary-layer friction, eddy losses with flow breakaway on airfoil/profile and eddy losses after trailing edge (edge losses).

The loss factor for friction is called the ratio of kinetic

DOC = 76061693

PAGE 8

201

energy loss in grid/cascade to the kinetic energy of flow after
grid/cascade during isentropic expansion. This value is calculated

Page 202

from boundary layer characteristics according to formula

$$\zeta_{mp} = \frac{\Delta E_{mp}}{E_1} = \frac{\sum k_1 k_2 N^{***} \delta^{**}}{1 + \sum k_1 - \sum k_2 N^{***} \delta^{**}} \quad (41)$$

where

$$k_1 = \left(\frac{1 - \xi_1}{1 - \xi_{1t}} \right)^{\frac{1}{n-1}}; \quad k_2 = \left(\frac{\xi_1}{\xi_{1t}} \right)^n;$$

$$k_3 = \frac{\xi_1}{\xi_{1t}};$$

$\xi_1 = \frac{c_1}{c_{1max}}; \xi_{1t} = \frac{c_{1t}}{c_{1max}}$ - dimensionless speeds after grid/cascade for real and theoretical processes;

δ^{**} - the momentum thickness of boundary layer;

$$H^{***} = \frac{\delta^{***}}{\delta^{**}}$$

the relation of the energy thicknesses (δ^{***}) to the momentum thickness, the approximately constant value, taken equal to $H^{***} = 1.8$;

$H^* = \delta^*/\delta^{**}$ are ratio of displacement thickness to the momentum thickness, approximately equal $H^* = 1.3-1.4$.

In formula (41) the sign Σ means the summation of values in the exit section of grid/cascade from the side of back and concave surface.

For the calculation of the loss factor for friction, it is necessary to know boundary layer characteristics on trailing edge from the side of back and concave surface of airfoil/profile. The boundary-layer calculation most it is simple to carry out, after assuming that a layer completely laminar or turbulent on an entire surface of airfoil/profile from the intake to trailing edges. In this case, preliminarily must be designed by one of the methods (see §6)

or determined experimentally speed distribution according to the enclosure of airfoil/profile. For the boundary-layer calculation, can be selected methods of L. G. Loytsyanskiy, I. Ye. Kalikhmana, N. M. Markov, M. Ye. Deutsch and A.E.Zaryankin, etc. [28; 29; 25; 31].

For the laminar boundary layer of compressible liquid when pressure gradient is present, the solution to integral momentum equation it leads to the following expression for the distribution of the momentum thickness along the surface of the airfoil/profile:

$$\delta^{**} = \sqrt{\frac{0.45 \alpha_1}{\lambda_1^{1.25} \left(1 - \frac{k-1}{k+1} \lambda_1^2\right)^{1.25}} \int_{\alpha_0}^{\lambda_1^{1.25} \left(1 - \frac{k-1}{k+1} \lambda_1^2\right)^{1.25} d\lambda_1} \lambda_1^{1.25} \left(1 - \frac{k-1}{k+1} \lambda_1^2\right)^{1.25} d\lambda_1} \quad (42)$$

here:

$\lambda_1(\bar{x})$ - dimensionless speed on boundary layer edge;

α_0 - critical speed;

ν - kinematic viscosity;

x - the moving coordinate: $= x/L$;

L - the length of convex or concave surface;

$\bar{\delta}^{**} = \delta^{**}/L$ - the relative momentum thickness.

The calculation according to formula (42) turns out to be relatively simple. However, for obtaining more reliable results, it is necessary to consider that under specific conditions the laminar boundary layer loses stability and transfer/converts to turbulent. Tentatively the boundary of the loss of stability of the laminar flow can be determined by critical number $Re_{cr}^{**} = \frac{\delta^{**}_{cr}}{\nu}$, formula for which is proposed to A. P. Melnikov.

$$Re_{cr}^{**} = \frac{0.085}{E_0^{1/2}} \left(1 + \frac{0.005 \cdot u_1}{0.005 \cdot u_1} \cdot \frac{dA_1}{dx} \right) + 225; \quad (43)$$

here E_0 is the initial turbulence level of flow.

Then the determination of the point of the loss of stability of laminar boundary layer is realized/accomplished by a comparison of $Re_{cr}^{**} = \varphi(\bar{x})$ curves [equation (43)] and to $Re^{**} = \varphi_1(\bar{x}) = \frac{1.6 \cdot u_1}{v_1}$, the point of intersection of the indicated curves will represent the unknown coordinate. Numerous experiments show that the transfer of laminar boundary layer to turbulent occurs in certain transition region whose size/dimensions depend on the local pressure gradient, Mach number and Re , turbulence level and so forth. On the basis of processing experimental data for the calculation of transition region, are obtained following empirical formulas [6]:

$$\bar{s} = \frac{s}{L} \approx \left(\frac{100}{Re} \right)^{0.15} \left(3.7 + 5.5 \frac{\left| \delta^{**} \frac{dc}{ds} \right|_{s=s_{sp}}}{v_1} \right); \quad (44)$$

$$r^{**} = \frac{Re_{sp}^{**}}{Re_n^{**}} \approx (7 + 100/\delta)^{0.15 + 1/\delta} + 0.12 M_1. \quad (45)$$

$$f_0 = \frac{\delta^{**} a_2}{v_1} \frac{dh_1}{ds}$$

where f_0 a form-parameter in the beginning of transition zone;

$\frac{Re_{sp}^{**}}{Re_n^{**}}$ and Re_n^{**} — Re number at the end and beginning of transition zone.

Knowing values s and r^{**} , it is easy to find the coordinates of the cross section from which one should conduct the calculation of turbulent boundary layer and the value of the initial momentum thickness for it.

The calculation of turbulent boundary layer is constructed on the basis of the experimental data for low downstream pressure

DOC = 76061693

PAGE 208

gradients

$$r = \frac{u_0 \frac{d\delta^*}{dx}}{v_0} > -0.02$$

the momentum thickness can be calculated on the formula of M. Ye.

Deutsch and A. Ye. Zaryankin [6]:

$$\delta^* = \frac{\delta^{**}}{L} = \frac{1}{f_1 \text{Re}_x^{0.5}} \left[\delta^{**0.5} \text{Re}_x^{0.5} f_0 + \int_0^x f_1 dx \right]^{0.5} \quad (46)$$

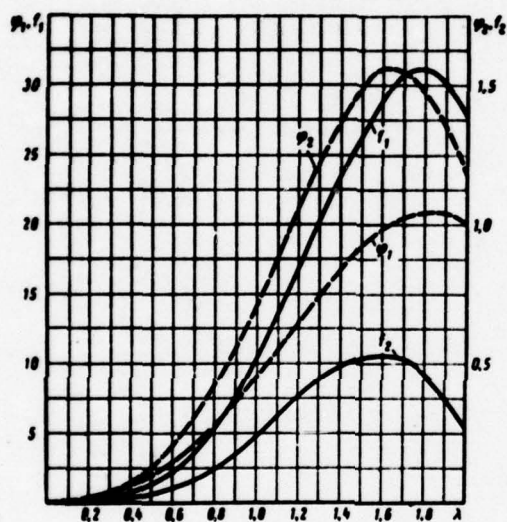
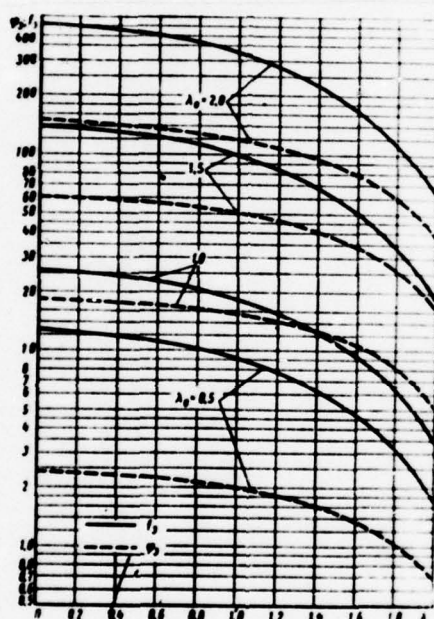
Fig. 38. Dependence of coefficients ϕ_1 ; ϕ_2 and f_1 ; f_2 on λ .

Fig. 39. Dependence of coefficients ϕ_3 , f_3 on λ_0 and λ .

Are here accepted the following designations:

$$\begin{aligned} f_1 &= \lambda_1^{2.38} (6 - \lambda_1^2)^{1.45}; \\ f_2 &= 0.0026 \lambda_1^{2.38} (6 - \lambda_1^2)^{2.41}; \\ f_3 &= \lambda_0^{4.17} (6 - \lambda_1^2)^{1.41}; \end{aligned} \quad (47)$$

$Re_c = \frac{a \cdot L}{\nu_c}$ —
 Re number, determined on the critical speed and kinematic viscosity
 on wall ν_c ; \bar{x}_c ; \bar{x}_0 .

λ_0 - the value of quantities in the beginning of turbulent section.

Functions f_1 , f_2 and f_3 depending on λ_1 are represented in Fig. 38 and 39.

With high pressure gradients, the momentum thickness is calculated from the same formula; only instead of functions f_1 , f_2

and f_3 substitute with respect to function φ_1 , φ_2 and φ_3 , determined according to formulas [6]

$$\left. \begin{aligned} \varphi_1 &= \lambda_1^{2.35} (6 - \lambda_1^2)^{1.3} e^{0.105 \lambda_1^2}; \\ \varphi_2 &= 0.0078 \lambda_1^{2.69} (6 - \lambda_1^2)^{2.62} e^{0.31 \lambda_1^2}; \\ \varphi_3 &= \lambda_0^{2.94} (6 - \lambda_1^2)^{1.62} e^{0.131 \lambda_1^2}. \end{aligned} \right\} \quad (48)$$

Values of functions φ_1 , φ_2 and φ_3 are given in Fig. 38 and 39. If upon entry to boundary-layer profile is turbulent, then $\bar{\alpha}''$ and $\bar{\alpha}_0$ in formulas (44-48) they are accepted equal to zero.

The calculation according to formulas (46), (47) and (48) with the use of the design charts turns out to be simple and gives a good agreement with experimental data.

When conducting the boundary-layer calculation it is possible to consider the increased flow turbulence at the entry into grid/cascade. The momentum thickness in this case is determined from

the formula, proposed to V. A. Vrublevskoy [2]:

$$\delta_{E_0}^{**} = \delta_0^{**} e^{k(E_0 - 0.005)} \\ (k = 2.31 - 1.095 \cdot 10^{-6} Re_0 + 0.855 \cdot 10^{-12} Re_0^2), \quad (49)$$

where $\delta_{E_0}^{**}$ - a momentum thickness in the instantaneous value of turbulence level E_0 ;

δ_0^{**} - the momentum thickness in the instantaneous value of turbulence level in $E_0 = 0.005$.

During the calculation of losses for friction according to formula (41) it is necessary to use experimental data for values of the parameters of boundary layer H^* and H^{***} . For subsonic speeds during the execution of the approximate computations, are accepted $H^* = 1.3-1.4$, and $H^{***} = 1.8$. In the case of increased turbulence of external flow, one should consider a decrease in parameter H^{***} . According to the experiments of the MPI on increase E_0 to 100/o parameter H^{***} decreases by 12-15/o and it composes $H^{***} = 1.53-1.60$.

At supersonic speeds the parameter H^* somewhat grow/rises and with $M = 1.6-1.7$, it reaches values of $1.5-1.6$ (in the case of nonseparable flow), and values of parameter H^{***} decrease (to 1.6 with $M = 1.6-1.7$).

On the measurements of many authors, the turbulence level under actual conditions in turbine reaches great significance (to $20-30\%$). In connection with this already at small distance from entering edges boundary-layer flow becomes turbulent. If nozzle cascade works at supercritical speeds, then form of turbulence undergoes on vane channel the action of high accelerating pressure gradients.

Some investigations, carried out in our country [16] and outside boundary, they showed that with prolonged action on the turbulent boundary layer of accelerating pressure gradients occurs the transfer of turbulent boundary layer to laminar ("reverse/inverse" transfer). On the section of "reverse/inverse" transfer, occurs the laminarization of the velocity profile of velocity and decrease in

its thickness. Knowledge of the conditions, necessary for the emergence of "reverse/inverse" transfer, makes it possible to refine the procedure for calculation δ^{**} and for losses for friction. However, up to now there is exist no reliable methods of the calculated determination during transition of turbulent boundary layer into laminar.

§19. Effect of thickness and form of trailing edge on the effectiveness of grid/cascades. Calculation of edge losses.

Edge losses in grid/cascade are called the expenditures of kinetic energy on maintaining vortex/eddy movement for outlet edge and for the dissipation of eddy/vortices in main flow (for the mixing of vortex wake with flow core). The value of edge losses depends on the thickness of edge, form of airfoil/profile, geometric and regime lattice parameters.

One should emphasize that in accordance with the determination of edge losses with the zero thickness of edge are not equal to zero, since with descent from airfoil/profile (from back and from concave surface) flow has the nonuniform distribution of speeds (in boundary

layer). Consequently, even with absolutely sharp edge after grid/cascade is formed eddy, and part of the kinetic energy it is lost during flattening of flux.

In the atlas of airfoil/profiles (part II) it is brought the test results of airfoil cascades with the determined thickness ratio of trailing edges. Upon transition to another thickness of trailing edges for initial, is selected well waste of airfoil/profile, and a change in the thickness of edge is conducted by means of the strain of its enclosures on output section. In practice are applied three methods of a change in the thickness of the trailing edges: 1) by variations only in concave surface of airfoil/profile (Fig. 40); 2) by changes in the enclosure of airfoil/profile only from the side of the back of airfoil/profile; 3) by decrease or respectively by an increase in the airfoil chord.

Each of the methods by the determined form affects the geometric parameters of grid/cascades and, consequently, also its aerodynamic characteristics (loss and the flow exit angle). Work [24] shows that during the thickening of trailing edges in the first method and the corresponding change in the relative space profile losses increase insignificantly. Other methods give a more essential increase in

DOC = 76061693

PAGE ~~28~~
217

losses [15] (see Fig. 41).

The available semi-empirical methods make it possible to estimate edge losses and angle of departure from grid/cascade on the basis of the experimental data, obtained for the determined types of airfoil/profiles.

DOC = 76061693

PAGE ~~24~~
218

Page 30.

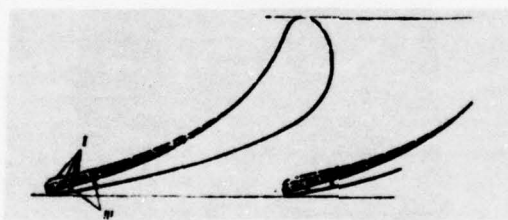


Fig. 40. Methods of the formation/education of trailing edges in turbine grid/cascades.

Fig. 41. Effect of form and thickness of trailing edges on profile losses in nozzle cascades.

Fig. 42. On the calculation of edge losses.

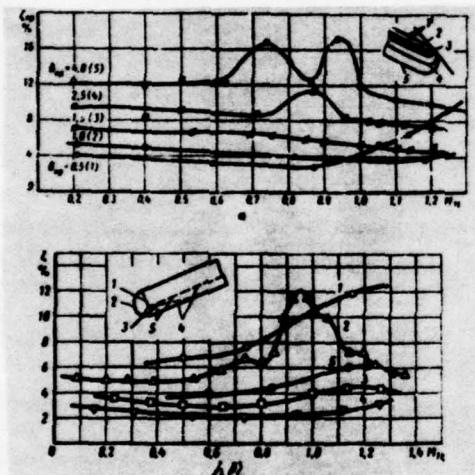


Fig. 41

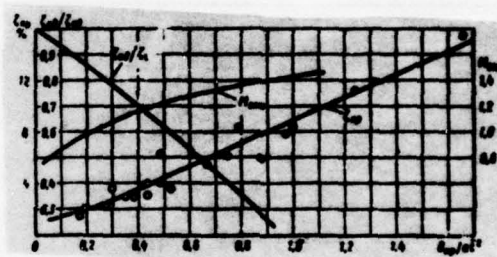


Fig. 42

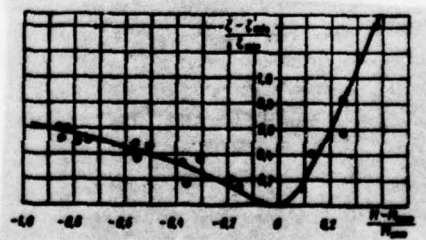


Fig. 43. Effect of Mach number on a change of the losses in grid/cascade with the different thickness of edge.

At the small thicknesses of edges and subsonic speeds for determining edge losses, they can be used formula [17, 24]:

$$\zeta_{\text{e}} = 0,003 \frac{h}{r_{\text{min}}} = 0,003 \frac{h}{\delta} \quad (50)$$

for nozzle cascades or jet/reactive workers and

$$\zeta_{\text{e}} = 0,005 \frac{h}{r_{\text{min}}} = 0,005 \frac{h}{\delta} \quad (51)$$

for active type running cascades.

In some literature sources is given G. Fluegel's approximation formula:

$$\zeta_{\text{e}} = K \frac{h}{\delta}$$

. As show experiments, coefficient K it is changed over wide limits depending on geometric ζ , etc. and regime (Re, M) lattice parameters ($K = 0.1-0.3$). Therefore G. Fluegel's formula can be used only for rough estimate of the magnitude L .

The generalization of numerous experimental data shows that the factor of edge loss of subsonic speeds depends substantially on relative space and for grid/cascades (group A) can be determined by formula

$$L = L_0 + 0.008 \frac{L_0}{\sigma^2}, \quad (22)$$

where L_0 - the factor of edge loss of the zero thickness of edge.

Value L is determined analytically, if is known flow conditions in boundary layers on back and concave surface of trailing edge and, therefore, the diagram/curve of the speeds in a layer with descent from edge. The calculations show that for a laminar layer a for turbulent ~ 0.012 . On the average it is possible to accept $L \sim 0.01$.

The effect of Mach number on the characteristics of grid/cascades with the different thicknesses of edges at subsonic speeds turns out to be different. With an increase in the thickness of edges, grow/rises the value of the optimum Mach number with which are reached the minimum profile losses. Fig. 42, gives dependence L on the thickness ratio of edge δ . The evaluation of a change of the profile losses in the grid/cascades, designed for subsonic speeds, with change in Mach number and in the thickness of trailing edge can be produced on curve/graph (see Fig. 43).

It should be noted that for the airfoil/profiles, specially profiled on supersonic speeds (with the being expanded output

section, reverse/inverse concavity on back) effect M and δ_{KP} will be different.

The approximate computation of tip losses in nozzle cascades with the different thicknesses of edges can be conducted on curve/graphs (Fig. 42), where are given to dependence $\frac{L_{t, \delta}}{L_{t, 0}}$ tip losses with the thickness of edge, equal to δ (with $\delta = 0$).

Experimental studies show that the losses of friction in the grid/cascades with change of δ are changed insignificantly. So, upon transition from $\delta = 0$ to $\delta = 4$ mm for the airfoil/profile of S-9012A with $t = \text{const}$ are changed from 1.5 to 2.5c/o. Consequently, for the approximate computations by a change in the losses of friction it is possible to disregard.

Calculation of profile losses for grid/cascades from the with a thickness trailing edge of airfoil/profile, which differs from that which was given in atlas (part II), is conducted according to formula

$$\delta_1 = \delta_0 + 0.005 \frac{\delta_0 - \delta_1}{\delta_0} \quad (22)$$

where δ_0 and δ_1 - thickness of the edge of airfoil/profile in atlas and profile losses in grid/cascade with this thickness of edge (with $M = 0.5-0.8$).

The calculation of tip losses δ for an airfoil/profile with the thickness of edge δ with known tip losses from atlas by thickness δ_1 is conducted according to formula

$$\delta = \delta_1 \left(1 + \frac{\delta_1}{\delta_0} - \frac{\delta_1}{\delta_0} \right) \quad (23)$$

where $\frac{\delta_1}{\delta_0}$ and $\frac{\delta_1}{\delta_0}$ - they are determined from the generalized curve/graphs for subsonic grid/cascades, given in Fig. 42.

For other types of the grid/cascades of experimental data thus far insufficiently for the construction of the generalized dependences. During the determination of the effect of the thicknesses of edges, one should by calculation determine losses on friction (§18), tip (§21) and profile (§20) losses and to conduct further calculation according to the procedure outlined above.

To losses in grid/cascades, substantially affect not only the method of formation/education and the thickness of edge, but also the form of edge. Previously experiments [50] and [5 conducted] showed that the most advantageous form of edge with $M > 1.0$ is rounded off. This effect is explained by the structure of the flow about the rounded off edge. With an increase in the velocity and an increase in Re number, the separation points flow on the edge of airfoil/profile are displaced along flow. The rounded off section of edge and the back of airfoil/profile form the short expanding duct, the conditions of flow in which correspond to flow in Laval nozzle. Therefore in such grid/cascades the minimum of losses is displaced to the side of great significance M , and by subsonic loss rates, they grow/rise.

DOC = 76061693

PAGE ~~33~~

226

Page 31.

Table 6.

7	1.0	1.05	1.10	1.15	1.20	1.25	1.30
K'	2.4	2.44	2.48	2.515	2.55	2.59	2.62

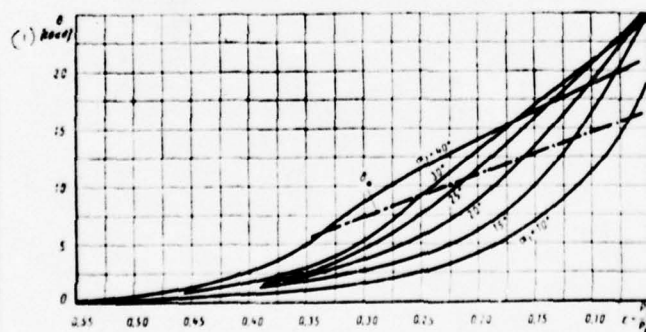


Fig. 44. Airflow angle δ in skew shear and beyond its limits ($k = 1.3$).

Key: (1) deg.

With forms of the edges (is square and obliquely cut), separation point on which are fixed, losses prove to be more in all range of mode/conditions (see Fig. 41).

The study of the effect of the thickness of edge in nozzle cascades with expanding ducts showed that an increase in the edge losses with an increase in the thickness ratio of edge depends on number M_u at output/yield from grid/cascade. With an increase M_u the effect of the thickening of edge on the loss factor decreases, which is connected with the displacement of separation points and decrease in the edge wake in comparison with the geometric thickness of edge.

§20. Profile losses in grid/cascades.

Profile losses in grid/cascades are defined as sum of losses for the friction and edge losses:

$$\zeta_{sp} = \zeta_{mp} + \zeta_{ep}$$

. By definition, the coefficient ζ characterizes losses in the grid/cascade of infinite length. This value is the most important aerodynamic characteristic, which shows the degree of the perfection of airfoil/profile and grid/cascade.

The factor of edge loss is determined by calculation according to formula (52) after preliminary calculation ζ (§18).

In certain cases it is possible to use the approximation formulas, which make it possible to tentatively estimate value without detailed calculation of constituting losses. Thus, for instance, for small subsonic speeds by G. A. Zal'f is recommended formula

$$\zeta_{sp} = \frac{\xi}{Re^m \sin \alpha_{1sp}} \quad (55)$$

. Here $m = 0.5$ for laminar and $m = 0.25-0.3$ for turbulent flow conditions in boundary layer. Coefficient ξ is changed within limits $\xi = 0.25-0.6$ depending on the shape of the airfoil/profile and basic geometric parameters of grid/cascade. With the use by formula (55) the conversion from one thickness of edge to another is realized/accomplished on relationship/ratio (53).

At supersonic speeds the profile losses include additionally wave shock losses:

$$\zeta_{sp} = \zeta_{sp} + \zeta_{sp} + \zeta_{wsm} \quad (56)$$

. Value ζ_{wsm} is determined from theoretical formulas [10]

$$\zeta_{\text{geom}} = 1 - \frac{(K' - \bar{p})^2}{\frac{k+1}{k-1} \cdot \frac{1}{k^2} \left(1 - \varepsilon \frac{k-1}{k}\right) \cos^2 \theta}, \quad (57)$$

where

$$\bar{p} = \frac{p_2}{p_{np}}; \quad \varepsilon = \frac{p_2}{p_0}; \quad \bar{l} = \frac{a_1}{a_{np}};$$

K' - characterizes flow in divergent section of the vane channel (Table 6).

§21. Flow exit angles from grid/cascade at subsonic and supersonic speeds.

The most important aerodynamic characteristic of grid/cascade is the flow exit angle; angle of departure makes it possible to

construct the velocity triangles of step/stage and to calculate losses in the subsequent grid/cascade. At short distances after trailing edge, the flow has periodically the nonuniform field of velocities and angles, which with removal/distance from grid/cascade is equalized. The mean angle of the flushed flow after grid/cascade is determined usually experimentally. For the newly design/projected grid/cascades angle of departure at subsonic speeds calculate from formula

$$\alpha_1(\beta_1) = \arcsin\left(m \frac{a}{l}\right), \quad (58)$$

where a - the size/dimension of exit section of vane channel;

m - experimental coefficient;

correction factor in formula (58) makes it possible to pass from $\beta_{100} \approx \beta_1 (\beta_{100} = \arcsin \frac{a}{l})$ to Coefficient m depends on Re numbers and M , and also on the thickness of trailing edge and on the form of back in skew shear. Experiments show that for airfoil/profiles with rectilinear back in

$$p_1 = p_{\infty} \quad (m \approx 1).$$

$$p_{\infty} \quad (m \approx 0.97 + 1).$$

oblique cut and small losses. For a convex back β_2 , somewhat less.

It should be noted that at subsonic speeds the flow exit angle β_2 and, correspondingly, coefficient m to a considerable degree depend on distribution pressures along the back of airfoil/profile in skew shear. If the pressure in minimum cross section is less than pressure after grid/cascade, angle of departure β_2 can prove to be more than effective angle $\beta_{2\phi}$, a coefficient $m > 1$ and, on the contrary, with increased pressure in the minimum cross section of channel angle β_2 can be less. $p_{\infty} \quad (m < 1).$

With an increase of energy losses in grid/cascade, the coefficient m grow/rises.

At the supersonic speeds in the zone of narrow cross section, is establish/installed the critical speed. In skew shear of grid/cascade, occurs the wave spectrum whose structure depends on flow conditions. The wave spectrum it includes (in the simplest case) two rarefaction waves and three shock waves (for one channel) [6]. This system of waves and jumps determines the average flow angle after grid/cascade.

During the intersection of the system of the rarefaction waves and jumps, separate flow lines repeatedly and differently transformed. The averaged angle of departure increases in comparison with subsonic mode/conditions - flow deviates in skew shear. For the approximate computations with not the very high expansion ratios of flow in skew shear, widely they use formula for the airflow angle, obtained from equation continuity (Baire/Beer's formula):

$$\delta = \arcsin \left(\frac{1}{q} \sin \beta_{2\alpha\delta} \right) - \beta_{2\alpha\delta}. \quad (59)$$

. Here q - the given flow rate, which is defined in on the tables of gas-dynamic functions depending on a relative pressure differential of aaaa on grid/cascade;

δ - the airflow angle in skew shear (see Fig. 44).

Fig. 44, depicts the calculated dependence (see formula 59) of the airflow angle in skew shear from the relation of pressures and skeletal/skeleton angle of nozzle and rotor blades, the constructed for overheated water vapor ($k = 1.3$). The dash-line line determines the greatest airflow angle, possible within the limits of skew shear, and, thus, it separate/liberates the zone, which corresponds to the deflection of flow in skew shear from the zone of the deflection of flow beyond its limits.

The more precise formulas, which consider a series of supplementary factors, were obtained by G. Yu. Stepanov [39], A. S. Natalevichem [32] et al. In the MPI [10] for the calculation of the airflow angle in grid/cascades with expanding ducts is obtained the following formula

$$\operatorname{tg} \delta = \frac{\sqrt{\left(\frac{k}{k-1}\right)^2 \bar{p} \left\{ \operatorname{ctg} a_{1sp} - (f^2 - 1) \right\} + \frac{k+1}{k-1} \left[k^2 - \frac{(k-1)(K' - pf)^2}{k+1} - \frac{2pfk(K' - pf)}{k+1} \right]}}{\frac{\frac{pk}{k-1} \sqrt{\operatorname{ctg} a_{1sp} - (f^2 - 1)}}{(K' - pf)}}, \quad (60)$$

where

$$a_{1sp} = \arcsin \frac{a_{sp}}{l};$$

$$K' = k + 1 + \frac{1}{2} \left(1 + \frac{p_1}{p_{sp}} \right) (f - 1)$$

- the coefficient whose change depending on \bar{f} is presented in Table 6 §20;

$$f = \frac{a_1}{a_{sp}}$$

- the expansion ratio of vane channel;

$$\bar{p} = \frac{p_2}{p_{sp}}$$

- the ratio of pressure after grid/cascade to pressure in the throat

DOC = 76061693

PAGE ~~47~~

237

of channel;

k - the index of isentropic process.

It is necessary to note that the angle of deflection is counted off from the geometric flow exit angle

$$\alpha_{1\phi} = \arcsin(\sin \alpha_{1,p}).$$

For the low airflow angles ($\delta < 10^\circ$) formula (60) it is possible to simplify [6]

$$\operatorname{tg} \delta \approx \frac{k+1}{2k} \cdot \frac{\left[k^2 - \frac{(k-1)(K'-p)^2}{k-1} - \frac{2p[k(K'-p)]}{k+1} \right]}{p(K'-p) \sqrt{1 - \operatorname{tg}^2 \alpha_{1,p}} (j^2 + 1)}. \quad (61)$$

Page 32.

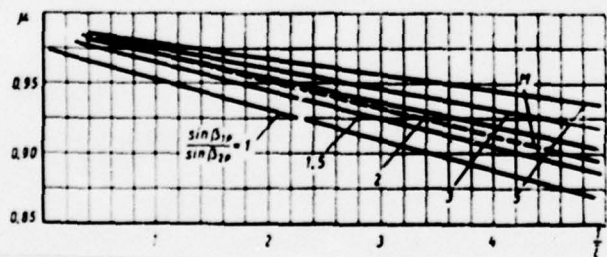


Fig. 45. Coefficients of the flow rate in nozzle and running cascades of the optimum lattice spacings and the reentrance angles of flow ($Re > 8 \cdot 10^5$).

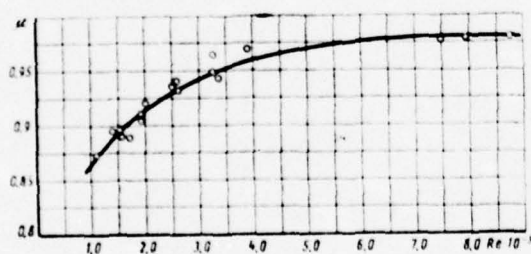


Fig. 46. Dependence of the coefficients of the flow rate in jet/reactive grid/cascades on Re number.

If we in equations (60) and (61) place $\bar{f} = 1$ (constriction) that they convert G. S. Stepanov's known formulas [39].

It should be noted that all formulas given above are obtained under the assumption of the infinitely fine/thin sterns. In grid/cascades with the final thickness of trailing edges, the deflection of flow in skew shear at supersonic speeds turns out to be different. The approximate account of the effect of the thickness of trailing edge can be produced according to A. S. Natalevich's formula [32].

§22. Coefficients of the expenditure of turbine grid/cascades.

During the calculation of the flow areas of nozzle and running cascades, it is necessary to know real flow pattern in grid/cascade. The presence of wall boundary layer of channel, the nonuniformity of velocity fields and the presence of the secondary flows lead to the fact that the real expenditure differs from the theoretical. This difference is considered by the coefficient of expenditure μ , equal to the ratio of the real expenditure G to theoretical G_t .

Values μ depend on how is formulated the concept of the theoretical flow rate of G_t . In accordance with the equations of continuity the real consumption of the mass of gas nozzle cascade can be calculated by the different methods:

$$G = \mu G_t = \frac{\mu_1 \pi d_1 l_1 Q_1 c_{1t} \sin \alpha_{1,\phi}}{\mu_1 \pi d_1 l_1 Q_1 c_{1t} \sin \alpha_1} = \frac{\mu^* \pi d_1 l_1 Q_m c_{mt} \sin \alpha_{1,\phi}}{\pi d_1 l_1 Q_1 c_{1t} \sin \alpha_1} \quad (62)$$

. Here d_1 ; l_1 is the mean diameter and the height/altitude of grid/cascade;

ρ_{1t} ; c_{1t}

- the density and the speed of flow after grid/cascade during isentropic expansion;

ρ_{mt} ; c_{mt}

- averaged density and the speed in throat cross section with isentropic expansion;

α_1 - the averaged real (expenditure) angle of departure from grid/cascade.

The coefficients of the consumption in equation (62) are respectively related: to the area of throat cross sections and the theoretical parameters after grid/cascade μ_1 ; to the area of throat cross sections and the theoretical parameters in these cross sections μ^* ; to the discharge area and the theoretical parameters in this of μ'_1 .

Are possible other methods of the expression of the gas flow through the grid/cascade. Thus, for instance, formula (62) can be written thus:

$$G = \mu_1 \pi d_1 l_1 \rho_1 c_1 \sin \alpha_{1,\varphi}.$$

where $\rho_1 c_1$ - averaged real (taking into account losses) density and the speed in throat cross sections.

The enumerated coefficients of consumption are interconnected:

$$\mu_1 = \mu^* \frac{Q_{int}^{int}}{Q_{int}^{ext}} = \mu_1 \frac{\sin \alpha_1}{\sin \alpha_1 \sin \alpha_2} = \mu_1^* \frac{Q_{int}^{int}}{Q_{int}^{ext}} \quad (63)$$

they can be approximately expressed ¹ through the velocity coefficient

$$\eta = \mu_1 \frac{Q_{int}}{Q_1} = \frac{\sin \alpha_1 \sin \alpha_2}{\sin \alpha_1} = \mu_1 \frac{Q_{int}}{Q_1} = \mu^* \frac{Q_{int}}{Q_{int}} = \frac{c_{int}}{c_{ext}} = \frac{\sin \alpha_1 \sin \alpha_2}{\sin \alpha_1} = \mu_1 \frac{c_1}{c_{int}} = \frac{\sin \alpha_1 \sin \alpha_2}{\sin \alpha_1} \quad (64)$$

FOCTNOTE 1. During the determination of velocity coefficient the averaging of the parameters is done in the equation of the momentum, and coefficient of consumption - in the equation of continuity.

ENDFOCTNOTE.

The selection of the discharge characteristic of grid/cascade is determined first of all by the reliability of those experimental data, on which it is calculated.

During the experimental determination of the coefficients of consumption μ^* , of μ^*_1 , μ'_1 , and also during the thermal design of step/stage according to these coefficients it is necessary to accurately know the distribution of the parameters in throat cross section and of the angles after grid/cascade α_1 . In many instances these data are absent, even the insignificant error in the evaluation of angles of departure can lead to essential error during the calculation of the flow passage cross-sectional area of grid/cascade. Therefore in the practice of the thermal designs at plants, they use in essence the coefficients of the consumption μ_1 , which can be

obtained from experiments on the maximum accuracy/precision.

The coefficients of consumption, referred to the throat cross sections of the nozzle and running cascades, are calculated from formulas

$$\mu_1 = \frac{G}{F_{1M} Q_{1M} w_{1M}}; \mu_2 = \frac{G}{F_{2M} Q_{2M} w_{2M}} \quad (6.5)$$

. Here: $F_{1M} = \pi d l_1 \sin \alpha_{1M}$ is an area of the throat cross sections of nozzle cascade and $F_{2M} = \pi d l_2 \sin \beta_{2M}$ is an area of the throat cross sections of running cascade, $\sin \alpha_{1M} = a_1 / l_1$ and $\sin \beta_{2M} = a_2 / l_2$; Q_{1M}, w_{1M} and Q_{2M}, w_{2M} - theoretical density and the speed in relative movement for running cascade.

All geometric parameters, which determine the areas of F_{1M} and F_{2M} , easily are measured when conducting the corresponding experiments. During the thermal design these parameters are establish/install on drawings. The coefficients of consumption, obtained experimentally, depend on the numerous geometric and regime parameters and first of all on the form of airfoil/profile, relative

height/altitude and reentrance angles and output/yield, Re numbers and M.

For nozzle and running cascades with the optimum reentrance angles and the optimum spaces of $Re > 8 \cdot 10^4$ and $M \approx 0.4-0.9$, coefficients of consumption can be taken on experimental curve/graphs (Fig. 45). Values μ in Fig. 45 are obtained by processing experimental data on formulas (65). The velocity fields in the minimum cross sections of channels were considered uniform.

In practical calculations of discharge characteristics when using curve/graphs (Fig. 45) it is necessary to consider the following supplementary factors:

1. The distribution of the speeds in the minimum cross section of channel, which depends on the form of airfoil/profiles (curvature of the enclosures of back and concave surface, the geometric reentrance angles and output/yield, etc.) and of the performance characteristics: Mach numbers and Re, the reentrance angles of flow α_0 (β_1).

2. Regime parameters: Mach number and Re , and also reentrance angles α_0 (β_1).

3. Deviations of parameters \bar{t} and of $\alpha_y(\beta_y)$ from the optimum values.

The distribution of the speeds in the minimum cross section of channel is determined from experimental or calculated (§§8, 9) static pressures on back and concave surface. For nozzle cascades with low angles of departure ($\alpha_1 < 13^\circ$) pressure in throat cross section (as a rule) it proves to be above than static pressure after grid/cascade. At wide angles of departure $\alpha_1 > 16^\circ$, picture is changed (characteristic diagram/curves of pressures for different airfoil/profiles are given in Fig. 13).

From the number of regime parameters, most strongly affects the coefficient of consumption Reynolds number. To evaluate the coefficients of the consumption μ in nozzle and running cascades during a change in Re numbers it is possible to use the curve/graph,

given in Fig. 46.

The calculation of consumption through the grid/cascade by supersonic speeds is conducted with the aid of the coefficient of consumption μ^* . In this case the density and the speed in throat cross sections in theoretical process are equal to critical values $(\rho_{mf} = \rho_0; c_{mf} = c_0)$. Values of coefficients μ are accepted according to those curve/graphs, given in Fig. 45.

The calculation of the coefficients of consumption of subsonic and supersonic speeds is realized/accomplished according to the thickness of displacement δ^* in the throat cross section:

$$\mu^* = 1 - \frac{\sum (\rho_{mf} c_{mf} \delta^*)_i}{l_i \rho_{mf} c_{mf} \sin \alpha_{i,sp}} \quad (66)$$

. In accordance with formula (66) for determining μ^* it is necessary to calculate value $\sqrt{(\rho_{mf} c_{mf} \delta^*)}$ for a back, a concave surface and the end walls of channel and to find their sum. One should emphasize that the calculation of the coefficients of consumption in formula (66)

makes it possible to consider the Reynolds number effect and M on μ^* , since the value of displacement thickness is determined on known values of M and Re . Formula (66) can be utilized for setting the character of the dependence of coefficient μ_1 on Re and M . In the first approximation, effect Re with $M > 1$ can be estimated on curve/graph (Fig. 46).

Re numbers are computed in this case from flow parameters in throat cross section to significant dimension it is accepted the throat of channel.

During small changes in the space, angle of setting and reentrance angle of flow, these changes can not be considered.

DOC = 76071693

PAGE 2

Page 33.

250

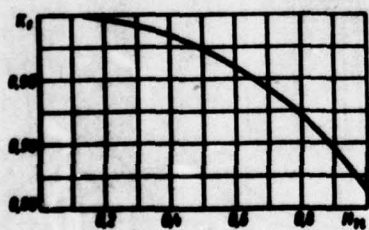
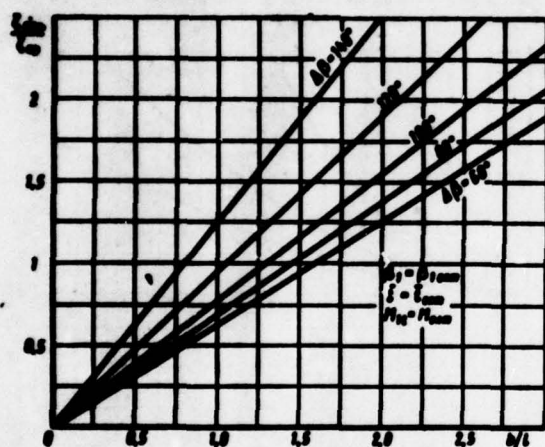


Fig. 47. on the calculation of tip losses.

Fig. 48. Effect of relative height/altitude and angle of rotation through tip losses in active and jet/reactive grid/cascades.



DCC = 76071693

PAGE

252

Key: (1) Impulse cascades without diffuser section at entry. (2) Jet/reactive grid/cascades without compression by height. (3).

Laminar boundary layer. (4). Turbulent boundary layer. (5). Impulse cascades with divergent-convergent channels. (6). Jet/reactive grid/cascades with unsymmetric compression in skew shear.

Table 7.

(1) Активные решетки без диффузорного участка на входе				(2) Реактивные решетки без поджатия по высоте			
(3) Ламинарный пограничный слой		(4) Турбулентный пограничный слой		(3) Ламинарный пограничный слой		(4) Турбулентный пограничный слой	
A	B	A	B	A	B	A	B
m=0.5		m=0.25		m=0.5		m=0.25	
0.45	5.5	0.13	1.50	0.45	2.0	0.13	0.7
(5) Активные решетки с диффузорно-конфузорным каналом				(6) Реактивные решетки с несимметричным поджатием в поном срезе			
-	-	0.13	1.00	-	-	0.13	0.30

§23. Effect of relative height/altitude on the cost-effectiveness/efficiency of grid/cascades. Calculation of tip losses.

In the nozzle and running cascades of low relative height/altitude the basic fraction of losses they compose tip losses. The formation/education of tip losses is connected with the curvature of vane channels, the presence of the transverse gradients of the pressures in channel, which cause the secondary eddy of gas in boundary layers from concave surface on flat/plane walls to back. The energy, spent on maintaining the secondary (vortex/eddy) motion and for the overcoming of supplementary friction on flat/plane walls, composes tip losses.

The value of tip losses depends on the geometric and regime parameters, namely: from relative span of the blade, angle of rotation of flow in grid/cascade, convergence of channel, space, overlap/ceiling, reentrance angle β_1 , of Mach numbers and Re , of the nonuniformity of flow at entry, turbulence, etc.

The absolute value of tip losses to known limits does not depend on the height/altitude of grid/cascade. Consequently, the factors of tip loss linearly change depending on b/z . At certain minimum height/altitude occurs the joining of the secondary flows and flow pattern in grid/cascade is changed: the range of the increased losses occupies entire middle part of the channel.

Experiments show that any changes in the geometric parameters, which produce an increase in the transverse gradient of pressure in channel in the cross sections, where the curvature is maximum, it leads to an increase in the tip losses. This first of all is related to the angle of rotation of the flow, with an increase of which the intensity of tip losses increases. An increase in the space of nozzle cascades leads at first to decrease ($\text{to } \bar{t}_{onm}$), and then to an increase in the tip losses. With the optimum space an increase in the angles of setting airfoil/profile produces a reduction/descent in the losses, while with low pitches, on the contrary, with an increase of $\alpha_y(\beta_y)$ tip losses they grow/rise.

An increase in the overlap/ceiling leads to an increase in thickness and eddying of boundary layer on end walls, the intensity of the secondary flows increases.

The studies of grid/cascades with nonuniform field of inlet velocities show that the maximum tip losses are observed with that elongated in the middle part the diagram/curve of the velocities, minimum - at increasing speeds of blade tips.

An increase in Mach numbers and Re and, correspondingly, the refinement of wall boundary layer of channel leads to a decrease in the tip losses.

Decreases in the tip losses in the grid/cascades of low altitude it is possible to achieve by means of the correct selection of the cross sections of channel and curvature of the enclosures of both of the airfoil/profile itself and the end walls of channel (the impulse cascades of the group of A_K and jet/reactive grid/cascades from meridian by shaping, see §§13 and 14).

Strict solution of the problem of tip losses in grid/cascades must be based on the three-dimensional equations of motion of the viscous compressible liquid. However, by taking into account the difficulty of this solution, it is possible, being based on the dimensional theory and on the basis of considerations of the physical nature of the secondary flows, to construct structural formula with the numerical coefficients, obtained from experiment. This formula is proposed in the MPI [12]:

$$\zeta_{\text{sum}} = \frac{AK_1}{Re^2} \left\{ 1 + B \left[1 + \varphi(\lambda) \frac{d\varphi(\lambda)}{d\lambda} \right]^2 r^2 \cos^2 \beta_1 \right\}. \quad (67)$$

. Here: K_1 is the coefficient, which considers compressibility effect (Fig. 47). Function $\varphi(\lambda) = \rho_2/\rho_1$ (ρ_1 and ρ_2 - density before and after grid/cascade). The density ratio easily is replaced by the relation of the dimensionless velocities in this form:

$$\varphi(\lambda) = \left(\frac{1 - \lambda^2}{1 - \lambda_1^2} \right)^{\frac{1}{\gamma-1}}.$$

where ξ_1 and ξ_2 are dimensionless velocities to grid/cascade and after it.

Values of coefficients of η , A and B are given in Table 7.

Table 7 shows that for nozzle cascades with meridian shaping and active working grid/cascades with divergent-convergent channels coefficient of η in formula (67) substantially decreases.

For the approximate estimate of tip losses in subsonic active and jet/reactive grid/cascades depending on the angle of rotation of flow with optimum β_1 , β_2 , \bar{t} and M it is possible to use the generalized curve/graphs (Fig. 48). For reentrance angles, different from the optimum, tip losses can be estimated on curve/graphs in Fig. 65 (§27).

For the same purpose serve some approximate dependences and, in particular, the formula of TsKTI:

DCC = 76071693

PAGE ~~22~~
258

$$\zeta_{\text{tip}} = (0.02 + 0.03) \lambda \frac{1}{T},$$

where the $\lambda_p = 1 - \left(\frac{\sin \alpha}{\sin \beta}\right)^2$ - for nozzle cascades and an $\lambda_p = 1 - \left(\frac{\sin \beta}{\sin \alpha}\right)^2$ for running cascades.

In conclusion recall that the total losses in grid/cascade are equal to the sum of the profile and tip losses:

$$\zeta = \zeta_p + \zeta_{\text{tip}} \quad (66)$$

§24. Selection of the optimum lattice spacing and angle of setting airfoil/profiles.

One of the most important dimensional characteristics of grid/cascade is the relative space $\bar{t} = t/b$. During a change in the space, is changed velocity distribution according to airfoil/profile and respectively the structure of boundary layers and loss by friction, change edge losses. Thus, for instance, increase in the space leads to a decrease in the fractions of edge losses, but from another side produces the bias of the point of the minimum of pressures on the back of airfoil/profile against flow, which increases losses for friction.

The value of the optimum space strongly depends on the different regime parameters and, in the first place, on the reentrance angles and flow discharge, Mach numbers and Re. For the working and nozzle cascades, designed for subsonic speeds at the calculated reentrance angles, the optimum value of the relative space depending on angle of departure can be selected on curves in Fig. 49, which are constructed on the basis of processing numerous experimental data.

During difference in pitch from the optimum to evaluate increase

in the profile losses, one should utilize the generalized experimental dependence, presented in Fig. 50. Curves in Fig. 49 and 50 are valid only for subsonic speeds. For supersonic pitch-change rates leads to a change in the calculated parameter \bar{f} - ratio of the exit section to minimum (see §§11, 12) whose effect on losses is more substantially than change in the space.

The important dimensional characteristics of grid/cascade is the angle of setting the airfoil/profile of $\alpha_y(\beta_y)$. A change in the angle of setting leads to a change in pressure distribution according to the enclosures of airfoil/profile. In accordance with this, change the pressure gradients on convergent and diffuser sections and the structure of boundary layer. As a result the profile losses with an increase in the $\alpha_y(\beta_y)$ decrease at first, and then they grow/rise.

Page 34.

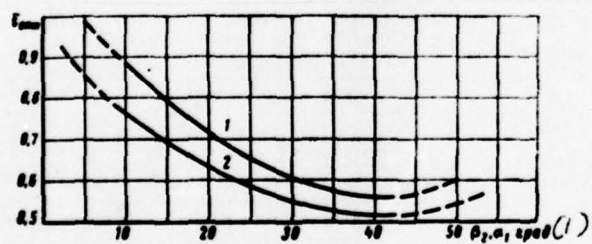


Fig. 49. To the selection of the optimum space: 1 - for jet/reactive grid/cascades; 2 - for impulse cascades.

Key: (1) deg.

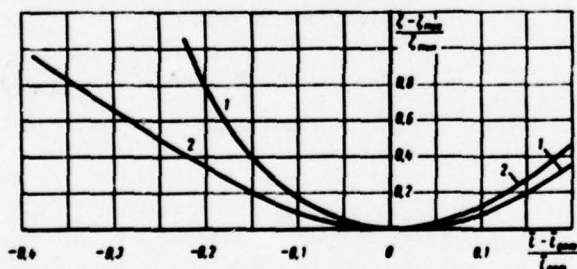


Fig. 50. Effect of relative space on the effectiveness of the grid/cascades: 1 - in impulse cascades; 2 - in jet/reactive grid/cascades.

Fig. 51. Effect of the angle of setting airfoil/profile on losses in grid/cascades at the subsonic speeds: 1 - in impulse cascades; 2 - in jet/reactive grid/cascades.

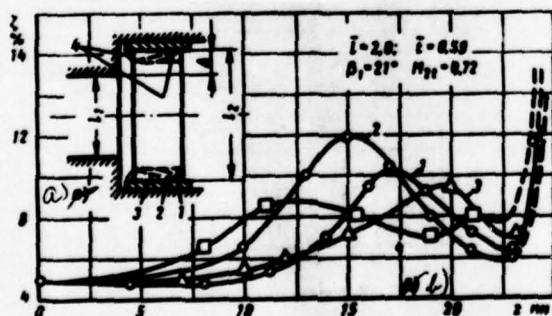
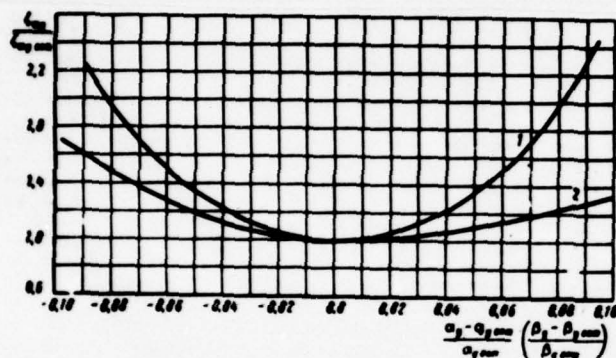


Fig. 52. Effect of the form of band/shroud/tire on the distribution of losses by height of grid/cascade during constant overlap/ceiling.

Fig. 53. Effect of relative overlap/ceiling and reentrance angle to a change in the losses: a) in jet/reactive grid/cascades; b) in impulse cascades.

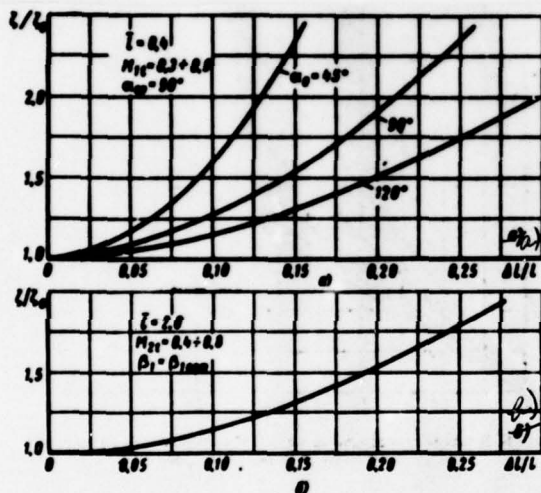


Fig. 54. Effect of relative height/altitude and overlap/ceiling on losses in nozzle and running cascades at the optimum reentrance angles.

Key: (1). Nozzle. (2). Worker.

Consequently, for each grid/cascade is a specific range of the optimum angles of setting. It is necessary to note that this range depends on lattice spacing. Effect a change in the α_y and β_y to effectiveness of grids can be approximately estimated in curves in Fig. 51.

§25. Account of the effect of overlap/ceiling on tip losses in nozzle and running cascades with variable reentrance angles.

The given in atlas aerodynamic characteristics of airfoil cascades were obtained at the determined constant values of overlap/ceiling. For the nozzle (reactive) grid/cascades of investigation, are carried out with zero overlap/ceiling, while for active workers was accepted positive overlap/ceiling $\Delta = 1.5$ mm (Fig. 52). Under actual conditions depending on the specific conditions of the design/projected step/stage, the overlap/ceiling can be changed within some limits.

The analysis of the air-load distributions according to the enclosures of airfoil/profile and the end walls of channels shows that with an increase of overlap/ceiling in connection with sudden

flow expansion at the entry into grid/cascade and the respectively increased nonuniformity of the velocity profile of velocities by height grow/rise the boundary layer thickness and the transverse gradients of pressure. For this reason are amplified the secondary overflowing and it is observed an essential increase in the tip losses. The negative effect of overlap/ceiling especially strongly pronounces at low relative height/altitude and at the low reentrance angles of flow. The effect of overlap/ceiling turns out to be more noticeable at supersonic speeds.

To evaluate the effect of relative overlap/ceiling at different reentrance angles to the effectiveness of the nozzle cascades, designed for subsonic speeds, it is possible to use curve/graphs (Fig. 53a). The effect of overlap/ceiling on losses at active running cascades is estimated according to curve/graphs (Fig. 53b). Curve/graphs on Fig. 53 are constructed for the determined relative height/altitudes. With a change in altitude, the fraction of losses of overlap/ceiling will be changed. The corresponding corrections are introduced on the curves of Fig. 54.

Taking into account that the overlap/ceiling is unavoidable, one should approach a decrease in its negative effect.

For the jet/reactive and impulse cascades of this it is possible to attain with use of conical band/shroud/tires, which make it possible to decrease the intake overlap/ceiling down to the minimum value. In impulse cascades it is possible to apply the curvilinear band/shroud/tires, rounded off at entry. Fig. 52, depicts the test results of the impulse cascade of R-2617A with the various forms of band/shroud/tire. As can be seen from curve/graphs (see Fig. 52), the presence of oblique band/shroud/tire and especially band/shroud/tire with the smooth rounded off entry it leads to a considerable decrease in the tip losses.

§26. Effect of fanning on the distribution of losses according to the height/altitude of circular grid/cascades. Account of slope/inclination and curvature of blades in radial plane.

The total losses in circular grid/cascades are not equal to losses in the lattices of the same relative height/altitude. This is connected first of all with change relative space by height of blades (with constant chord). However, even with retention of the

constant/invariable relative space of losses in the peripheral cross sections of circular grid/cascades somewhat decrease in comparison with direct/straight grid/cascades, and in root cross sections sharply they grow/rise. A decrease in the losses in peripheral cross sections is connected with the compression of flow to band/shroud/tire by centrifugal forces. This leads to the fact that the flow along the length of channel, including in skew shear, occurs with accelerating pressure gradients. Boundary layer on band/shroud/tire and on the enclosures of channel fine/thin. The intensity of the secondary overflowing, connected with the transverse gradients of pressures, is low.

Page 35.

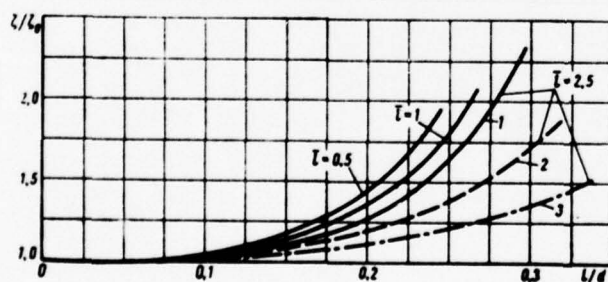


Fig. 55. Effect of fanning and height/altitude on losses in the circular nozzle cascades: 1 - $k = \text{const.}$; 2 - $\bar{t} = \text{const.}$; 3 - inclined blade.

Fig. 56. Diagrams of the circular grid/cascades: a) the radial-established/installed blades; b) inclined blades; c) curvilinear blades.

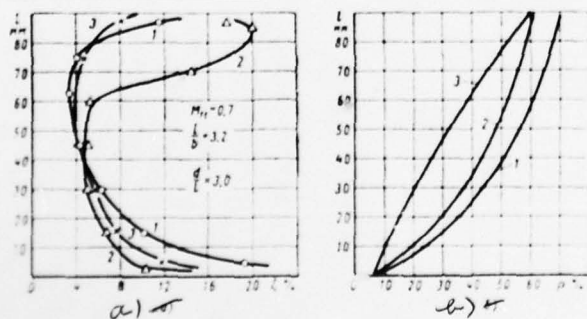
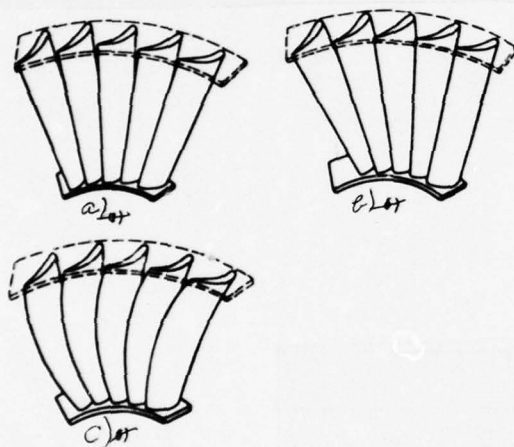


Fig. 57. Change in the coefficient of losses (a) and of reaction (b) by height of the circular grid/cascades: 1 - radial blades; 2 - inclined blades; 3 - curvilinear blades.

The basic reasons the formation/education of the increased losses in root cross sections is:

- 1) accumulation of the lower band/shroud/tire of the stagnation liquid, which flows in boundary layer and in edge wake under the effect of radial pressure gradient;
- 2) the solid angle, formed by the back of airfoil/profile and by the cylindrical band/shroud/tire whose flow about leads to the overexpansion of flow with the subsequent braking, or at supersonic speeds to the emergence of the system of jumps;
- 3) the fluid friction against end walls;
- 4) the secondary flows along band/shroud/tire and the back of airfoil/profile, caused by the transverse gradients of pressure in vane channel.

In the very low relations of $\theta = d_{cp}/l$ in diffuser range under

the action of centrifugal forces, the flow can be detached away from sleeve.

On the basis of the theoretical calculations and experimental results of the studies of circular and direct/straight nozzle cascades with angles $\alpha_1 = 12-18^\circ$, is constructed the curve/graph (Fig. 55), which makes it possible to approximately estimate a change of the losses in grid/cascades with change l/d and l/b . With an increase l/d , occurs a considerable increase in the losses in circular grid/cascade in comparison with straight line. An especially intense increase in the losses is observed at low relative height/altitudes.

Grid/cascade tests with alternating/variable chord ($\bar{t} = \text{const}$) show that an increase in the losses in this case is less intense (twisting 2). To a lesser degree of loss, grow/rise in circular grid/cascades during the application/use of a special shaping (inclined and curvilinear blade) [43]. The presence of rotor wheel can change the character of the distribution of losses, since occurs the acceleration of flow and the parameters by height after rotor wheel they are equalized, breakaway is localized. Furthermore, the streamline curvature after nozzle cascade and respectively the

distribution of losses depends on the relationship/ratio of the areas of working ΔF_n and nozzle ΔF_c of grid/cascades over cross sections.

For a decrease in the losses in root cross sections, it is expedient to apply the sloped nozzle blade, which adjust flow to root cross section (Fig. 56b). The angle of the slope of γ_{cp} one should select not more than 10° . With decrease θ , the slope angle decreases. For $\theta \approx 3$, $\gamma_{cp} = 3-4^\circ$. When the expansion/disclosure of flow area is present,) conical band/shroud/tire) and the respectively increased losses in peripheral cross sections it is necessary to perform blades curvilinear (Fig. 56c), that ensure the compression of flow both to the root enclosure and to peripheral. As an example in Fig. 57a is presented the distribution of losses by height for the radial-established/installed (1), inclined (2) and curvilinear (3) blades.

For curvilinear blades the slope angle in root cross sections one should select according to formula

$$\gamma_k > \gamma_{k, \min} \approx \arctg \frac{l_k}{r_k}.$$

. In peripheral sections the angle is computed on equation

$$\gamma_s > \gamma_{s, \min} \approx \arctg \frac{a_s \lg v_s}{l_s}.$$

where the l_k, l_s - space in root and upper cross sections;

a_s

- the value of exit section of vane channel in the upper cross section;

v_s

is an expansion angle of flow area of the grid/cascade;

r_1, r_2

- a radius of grid/cascade of sleeve and periphery.

The radii of curvature of the generatrices of blade are determined from formula

$$R = \frac{r_1^2 + r_2^2}{2(r_1 \sin \gamma_1 + r_2 \sin \gamma_2)} \quad (69)$$

. The application/use of inclined and curvilinear blades leads to a substantial change in parameter distribution by height of blades in comparison with radial-established/installed. If one assumes that the losses by height of blades and angle α_1 are constant, then speed distribution along a radius it is possible to calculate according to formula [43]

DOC = 76071693

PAGE ~~37~~
276

$$\frac{r_1}{r_{1\infty}} = \left(\frac{r_\infty}{r}\right)^{\eta_1 \cos^2 \alpha_1} K_1 K_2, \quad (71)$$

where K_1 is the correction factor, which considers the streamline curvature in the meridian plane:

$$K_1 = \exp \left[\frac{2\eta_1 \sin^2 \alpha_1}{\pi(0-1)R_{1p}} \left(1 - \cos \frac{\pi}{2} (r-1)(0-1) \right) \right]; \quad (71)^0$$

K_2 - the correction coefficient, which considers the forces of the effect of blades on flow

$$K_2 = \frac{5\eta_r \sin^2 \alpha_c \left[\frac{(0+1)^2}{40} \left(\sin \gamma_s \frac{0+1}{0-1} \sin \gamma_s \right) + \frac{0+1}{0-1} \sin \gamma_s \right]}{\exp \frac{5\eta_r \sin 2\alpha_c (0-1)^2 \sin \gamma_s}{160} \cdot \frac{0+1}{0-1} \sin \gamma_s \cdot \frac{r^2-1}{2}}; \quad (72)$$

$$r = \frac{r}{r_s}; B = \frac{B}{r_s}; \theta = \frac{d_{cp}}{l}; R_{cp} = \frac{R_{cp}}{r_s};$$

$$1/R_{cp} = \pi^2 \frac{r_s}{2B^2} \cos \pi \left(\frac{r}{B} \right);$$

$\eta_r = (1 - \frac{\eta_r}{\eta_r})$

the efficiency of nozzle cascade.

FOOTNOTE 1. Formulas (71) - (74) are obtained together with engineer
Van Chzhun-tsi. ENDFOOTNOTE

For inclined blades ($R = \infty$)

$$K_2 = r \frac{5 \sin 2\alpha_1 r_x \sin \gamma_x \eta_1}{4B} \quad (73)$$

. The reaction in arbitrary cross section is determined from formula

$$q = 1 - (1 - q_k) \left(\frac{r_k}{r} \right)^{2\eta_1 \cos^2 \alpha_1} K_1^2 K_2^2 \quad (74)$$

where the ρ_K - degree of the reaction in of rcot section.

The slope/inclination of blades due to flow leads to a decrease in the radial pressure gradients and, corresponding, the reaction. The application/use of curvilinear blades makes it possible to obtain the virtually arbitrary character of the distribution of reaction by

height of grid/cascades. Fig. 57b, gives the approximate character of a change in the reaction for three grid/cascades; with radial-established/installed 1, with inclined 2 and with curvilinear 3 blades.

§27. Effect of the slope/inclination of band/shroud/tires (expansion/disclosure of flow area) to the effectiveness of nozzle and running cascades.

In the practice of the design of turbines, unavoidably it is necessary to apply inclined band/shroud/tires both in the last/latter step/stages of steam and gas turbines and in step/stages with the low altitudes of blades. In the nozzle circular grid/cascades, which have the wide expansion angle of flow area and diffuser at entry before the grid/cascade (Fig. 58), losses turn out to be those which were increased.

Fig. 58. Distribution of losses by height of circular grid/cascade with the expansion/disclosure of flow area: 1 - the radial blades of ($\nu = 0$); 2 - the radial blades of $\nu = 40^\circ$; 3 curvilinear blades of $\nu = 40^\circ$.

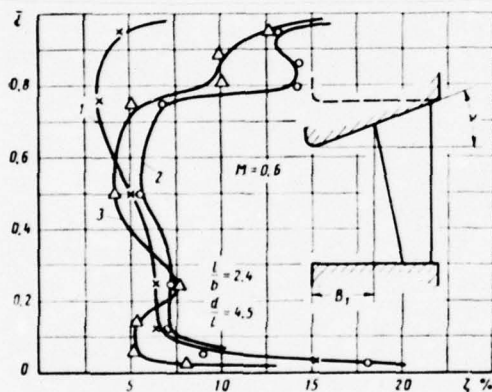


Fig. 59. Effect of the expansion angle (a) and of relative height/altitude (b) on losses in the nozzle circular grid/cascades: 1 - radial blades; 2 - curvilinear blades.

Key: (1) deg.

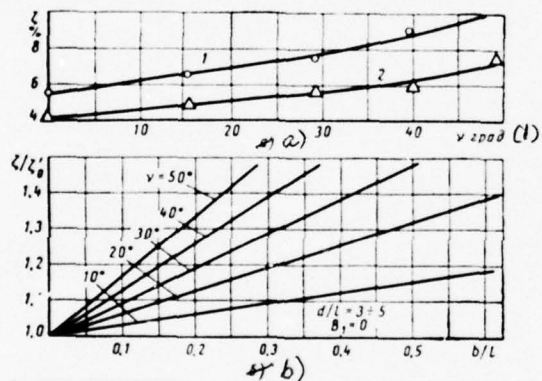


Fig. 60. Effect of the expansion angle (a) and of relative height/altitude (b) on losses in active circular grid/cascades at different reentrance angles.

Key: (1) deg.

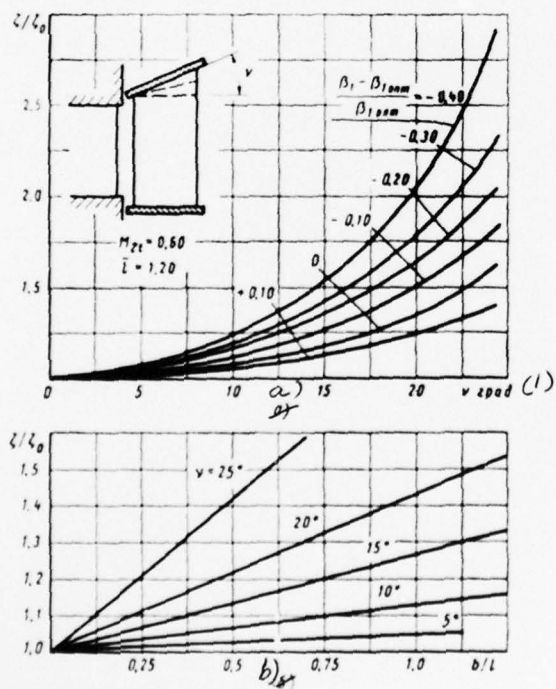
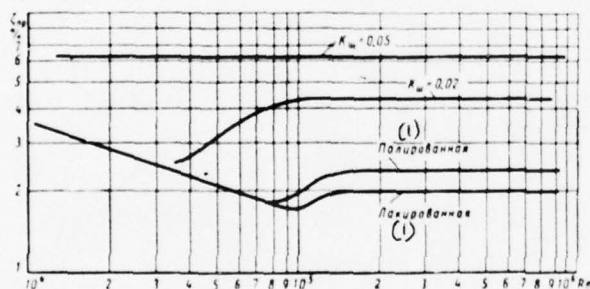


Fig. 61. Effect of roughness and Re number on losses in jet/reactive grid/cascade.

Key: (1). Polished.



AD-A039 286

FOREIGN TECHNOLOGY DIV WRIGHT-PATTERSON AFB OHIO
ATLAS OF THE CASCADE PROFILES OF AXIAL-FLOWS TURBINE, (U)
DEC 76 M Y DEYCH, G A PHILIPP, L Y LAZAREV
FTD-ID(RS)T-1693-76

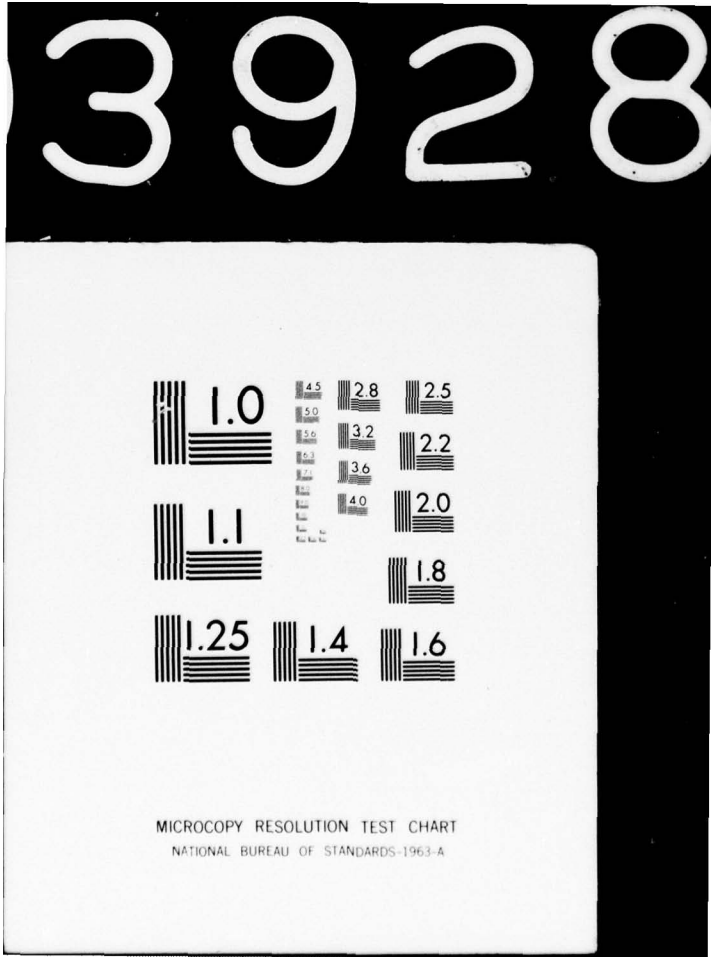
F/G 21/5

UNCLASSIFIED

NL

4 OF 5
AD
A039286





This is explained by diffuser flow in space down to grid/cascade, by a decrease in the convergence of vane channels in skew shear and after grid/cascade. The basic shape factors, which affect losses in peripheral cross sections, are: the expansion angle of flow area (angle of taper) of aaaa and the length of the diffuser before grid/cascade B_1 . To the losses they affect and other parameters: the allanite of blades B , the form of vane channel, reentrance angles α_0 (β_1) and output/yield α_1 (β_2) of flow, the height/altitude and the chord of blades.

Fig. 58, gives the distribution of losses by height of circular grid/cascades with the expansion angles of the upper band/shroud/tire of $\nu = 0^\circ$ and $\nu = 40^\circ$ ($\bar{L} = 2.42$; $\theta = 4.5$); the losses in grid/cascade with the conical band/shroud/tire of ($\nu = 40^\circ$) grow/rise not only of periphery, but also on an entire span of the blade. The total losses increase from 5.5 to 8.30/c.

For the target/purpose of a decrease in the losses, produced by the concavity of the upper enclosure, are applied the increased axial size/dimensions of diaphragms (increased width of blades), special curvilinear blades, the torsion of flow on entry, etc. Curvilinear blades adjust flow not only to root, but also the apex/vertex of

blades, which decreases the tip losses (is curve 3 in Fig. 58). With an increase of the angle of the slope of the band/shroud/tire of ν , the effect from the application/use of curvilinear blades increases (Fig. 59a).

For the approximate estimate of losses in circular grid/cascades with opening of the flow area with $\theta \approx 3-5$ without inlet diffuser ($B_1 = 0$) it is possible to use the curve/graphs, presented in Fig. 59b.

The effect of the conicity of band/shroud/tire on losses in active type running cascades, designed at angles of rotation $\Delta\beta = 150-120^\circ$, can be estimated on the curve/graphs, presented in Fig. 60a. With a decrease in the reentrance angle of flow, the fractional losses of ζ/ζ_0 (where ζ_0 is loss factor in the grid/cascade of of $\nu = 0$) grow/rise especially intensely, which is connected with an increase in the diffusivity of channel. The dependence of losses on the angle of taper of band/shroud/tire (Fig. 60a) is given for a relative height/altitude $\bar{t} = 1.2$. The effect of relative height/altitude and angle of aaaa at the optimum reentrance angle β_1 is estimated according to curve, given in Fig. 60b. Data given in Fig. 60, are related to lattices. For circular running cascades the

effect of inclined band/shroud/tire will be somewhat different, since because of the compression of flow to periphery (with small reentrance angles) will occur the redistribution of energy losses by height: of band/shroud/tire the losses somewhat decrease, and in root section they grow/rise; the total losses decrease.

§28. Effect of roughness and technological defects on the cost-effectiveness/efficiency of grid/cascades.

Procedure for the performance calculation of grid/cascades presented and experimental data given in atlas, are related to the aerodynamic smooth surfaces of blades. Investigations show that in operation the surface roughness substantially increases as a result of corrosion and erosion of blades, and also as a result of the deposit of salts.

Tentative values of the absolute surface roughness of blades are given in Table 8.

For the characteristics of state of the surfaces of blades, is

introduced the relative roughness of $k_{rel} = \frac{k_m}{b}$.

The profile and total losses in grid/cascades grow/rise with an increase in the relative roughness. Of the flow about the aerodynamic smooth surfaces the coefficient of profile losses decreases with an increase of Reynolds number and in logarithmic coordinate this dependence approximately is depicted as inclined straight line [20] (Fig. 61). The position of straight line $\lg \zeta_{np} = f(\lg Re)$ depends on the type of grid/cascade, reentrance angle of flow, turbulence level and other parameters of those affecting ζ_{np} .

For a grid/cascade it is possible to note three characteristic mode/conditions of flow. With low Re , when the thickness of the internal part of boundary layer with the high velocity gradients of velocity considerably exceeds medium size of the projections of roughness, the latter does not affect losses in the grid/cascades: the surfaces of blade can be considered as aerodynamically smooth. With increase in Re , part of boundary layer near the wall and entire layer, is thinned, and the prominence/protrusions of roughness gradually emerge in the exterior of the layer where their flow occurs at high speeds and is accompanied by flow separations and by vortex formations.

Page 37.

Table 8.

(1) Состояние поверхности лопатки	(2) Полнрованные и шлифованные лопатки	(3) Фрезерованные и тиснутые лопатки	(4) Корродированные поверхности лопатки	(5) Лопатки точного литья
(8) Средняя высота выступов шероховатости $k_{ш}$ в мм	0,001—0,002	0,015—0,025	0,01—0,03	0,015—0,030

(6) Лопатки грубого литья	(7) Лопатки, загрязненные солями
0,06—0,25	0,10—0,40

Key: (1). State of surface of blades. (2). Polished and ground blades. (3) the milled and pulled blades. (4). Corroded surfaces of blades. (5). Blades of precision casting. (6). Blades of rough casting. (7). Blades, carried by salts. (8). The medium altitude of the projections of the roughness of aaaa in mm.

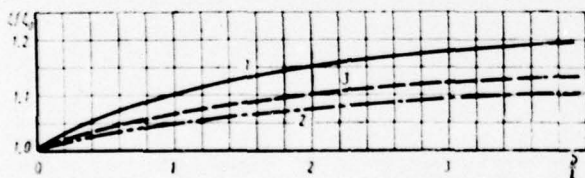


Fig. 62. Effect of the method of the manufacture of diaphragms and shrouded rotor wheels on losses in the grid/cascades: 1 - welded diaphragm; 2 - setting fully-milled; 3 - shrouded rotor wheel.

In this case, sharply grow/rises the intensity of turbulence and loss to boundary-layer friction, profile losses with increase in Re they grow/rise. Such mode/conditions one should consider as the transfer to mode/conditions flows with the developed roughness, which are characterized by the independence of λ_{sp} from Re - mode/conditions automodel according to Re number.

The comparison of lines in Fig. 61 shows that the beginning of transfer to the zone of self-similarity depends substantially on the downstream pressure gradient, initial turbulence level of flow, reentrance angle etc. These parameters affect also the extent of transient condition.

The available experimental data are insufficient for the development of the reliable method of calculation of λ_{sp} taking into account roughness. The approximate estimate of the effect of roughness can be obtained by the calculation of the momentum thickness of trailing edges with different roughness.

Another procedure, developed by G. A. Zal'f, entails the use of an empirical formula

$$\lambda_{sp} = \frac{\xi}{A^{2m} \sin \alpha_{1,sp}} \left(\frac{k_{sp}}{b} \right)^m, \quad (75)$$

where A - the coefficient, determined according to test data with one roughness. On by the datum of MPI $A = 200 + 70 (E_0 - 1)$ for $E_0 < 1-80/c$;

E_0 - turbulence level in percentages; $m = 0.25-0.30$; $\xi = 0.68$.

A great effect on losses in grid/cascades has technology of the manufacture of step/stages. It is logical, to consider all the possible technological deviations and the effect of the different methods of manufacture impossibly. Therefore here are given data, that evaluate the effect only of the most important and most frequently being encountered methods of the manufacture of diaphragms (welded and setting entire-milled).

At the low relative height/altitudes of nozzle blades, form of band/shroud/tire and technology of manufacture especially strongly affect losses in grid/cascades (Fig. 62). During the application/use of welded diaphragms an increase in the losses in comparison with the circular grid/cascade of similar geometry (band/shroud/tire is fulfilled just as in lattices) it is possible to estimate in curve 1, and dependence of an increase in the losses in diaphragms with setting blades - in curve 2. For active type rotor wheels with band/shroud/tires, the evaluation of an increase in the losses in comparison with lattices can be produced on curve 3 (Fig. 62).

DOC = 76081693

PAGE 8

293

~~REF ID: A66748~~ / ~~CONFIDENTIAL~~ / UNCLAS

~~REF ID: A66748~~

~~CONFIDENTIAL~~

~~REF ID: A66748~~

Page 38.

Chapter IV.

EFFECT OF THE REGIME PARAMETERS ON THE EFFECTIVENESS OF
~~CONFIDENTIAL~~/CASCADES.

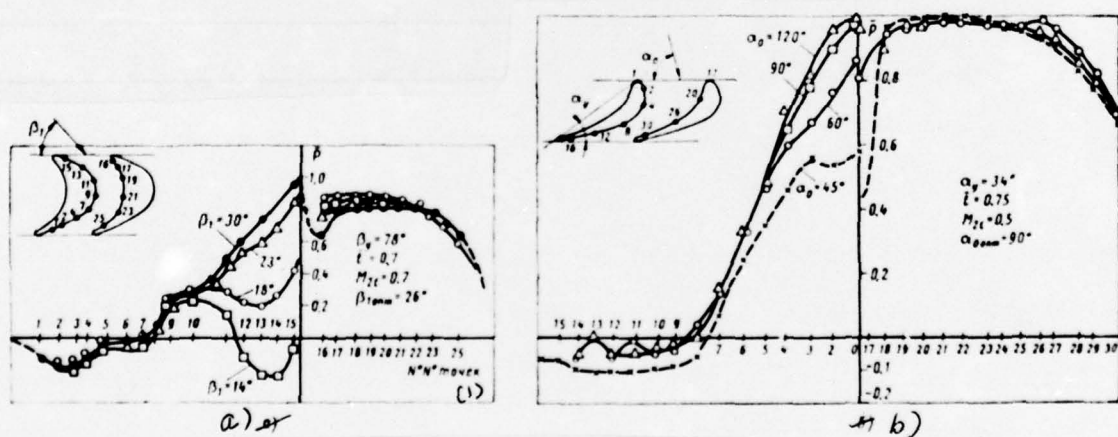


Fig. 63. Effect of reentrance angle to pressure distribution of the enclosures of the airfoil/profile: a) impulse cascade; b) jet/reactive grid/cascade.

Key: (1) points.

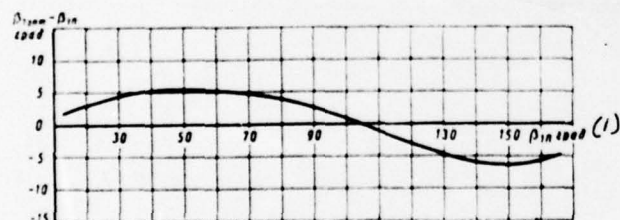


Fig. 64. Difference between the optimum and geometric reentrance angles in different type grid/cascades (designed for different reentrance angles).

Key: (1) deg.

§29. Reentrance angle of flow into nozzle and running cascades.
Calculation of losses at off-design reentrance angles.

For the calculation of the varying load of the step/stages of steam and gas turbines, it is necessary to know the effect of the reentrance angle of flow into nozzle and running cascades to losses in them. For the airfoil/profiles, designed for $\beta_{1p} < 90^\circ$ especially adverse are the mode/conditions with low reentrance angles ($\beta_1 < 45^\circ$), when at the intake section of back appears noticeable diffuser section. For airfoil/profiles from $\beta_{1p} > 120^\circ$ more adverse turn out to be the mode/conditions with wide reentrance angles ($\beta_1 > 140^\circ$). During the deviation of the reentrance angle of flow from the calculated, change the air-load distributions, according to airfoil/profile, appear the diffuser sections, in extent/elongation of which intensely increases the boundary layer thickness, and in certain cases appears flow breakaway. As an example Fig. 63, gives the curve/graphs of profile pressure distribution of jet/reactive and impulse cascades during the optimum spaces, the angles of setting and Mach numbers.

The theoretical calculation of profile losses at the alternate angles of entry is hindered/hampered, since the flow pattern in the grid/cascade with variable α_0 (β_1) affects the large number of geometric and regime parameters; the relative space \bar{t} , the form and the thickness of entering edge, the degree of the convergence of channel, the geometric reentrance angles of β_{1n} and output/yield of the β_{2n} of Mach number and Re, etc. For the approximate estimate of losses at off-design angles α_0 (β_1) it is possible to use formula [46]

$$\zeta = \zeta_{\min} + 0.22 \left(\frac{\sin \Delta\beta \sin \beta_2}{\sin \beta_1 \sin \beta_{1 \min}} \right), \quad (75)$$

where of the ζ_{\min} - the factor of minimum loss in the grid/cascade of $\beta_{1 \min}$ and $\beta_{2 \min}$.

Taking into account that the minimum losses in the grid/cascades of ζ_{\min} correspond to the optimum reentrance angles of $\beta_{1 \min}$, differing from the geometric, on Fig. 64 is given the curve/graph,

which shows the deviation of the optimum reentrance angle of β_{1opt} from geometric β_{1n} . For grid/cascades from $\beta_{1n} < 110^\circ$, the minimum losses prove to be with $\beta_1 > \beta_{1n}$, while for the $\beta_{1n} > 110^\circ$ with of $\beta_1 < \beta_{1n}$.

It should be noted that at supersonic speeds the dependence of losses on reentrance angle can considerably differ from that which was indicated.

For the calculation of losses it is possible to use also by other formulas [27; 38], from which most precise is formula [38]

$$\zeta = A + B \left(\frac{\sin \beta_2}{\sin \beta_1} \right)^2 + C \left(\frac{\sin \Delta \beta \sin \beta_2}{\sin \beta_1 \sin \beta_{1n}} \right), \quad (77)$$

where $A = (0.4-0.6)$; B ; $C = 0.265$; $B = 0.058$.

The basic disadvantages of formulas (76) and (77) lies in the fact that they do not consider the effect of space and Mach number.

From experiment it is known that with decrease with a decrease in the relative space the effect of off-design reentrance angle decreases. With a decrease in the reentrance angle, the optimum value of Mach number increases.

For the approximate estimate of profile losses at the alternate angles of entry it is possible to use also curve/graphs (Fig. 65a). Curve 1 is constructed according to experimental data for impulse cascades to the wide angles of rotation of flow $\Delta\beta = 150-120^\circ$. Curve 2 characterizes a change of the profile losses in jet/reactive grid/cascades with large radii of the rounding of entering edge. Curve 3 - for the peripheral cross sections of the rotor blades of large fanning, designed at angles of entry $\beta_1 = 140-160^\circ$.

Especially strongly affects reentrance angle to tip losses in grid/cascades, which is connected in essence with a change of the transverse gradients of pressure in channels and, correspondingly, by the intensity of secondary currents. On the basis of experimental data for jet/reactive and impulse cascades in Fig. 65b, have been constructed growth curves in the tip losses of the ζ_K in comparison with tip losses at the calculated reentrance angle of α for the different angles of rotation of flow in grid/cascade $\Delta\beta = 180^\circ -$

DOC = 76081693

PAGE

300

$\Delta\beta = 180^\circ - (\beta_{1, \text{min}} + \beta_2)$. Curves 1, 2 ($\Delta\beta = 120-150^\circ$) are related to working impulse cascades, 3, 4 - to nozzle cascades with low reentrance angles even 5 to nozzle jet/reactive grid/cascades with a large radius the roundings of entering edge and $\Delta\beta = 70^\circ$.

Fig. 65. Effect of the reentrance angle of flow to losses in the grid/cascades: a) profile; 1 - working impulse cascades; 2 - nozzle jet/reactive grid/cascades; 3 - peripheral and to the middle of the cross section of long blades; b) end: 1 - the angle of rotation of flow $\Delta\beta = 180^\circ - (\beta_{1onm} + \beta_2) = 150^\circ$; 2 - $\Delta\beta = 120^\circ$; 3 - $\Delta\beta = 110^\circ$; 4 - $\Delta\beta = 100^\circ$; 5 - $\Delta\beta = 75^\circ$.

Key: (1) deg.

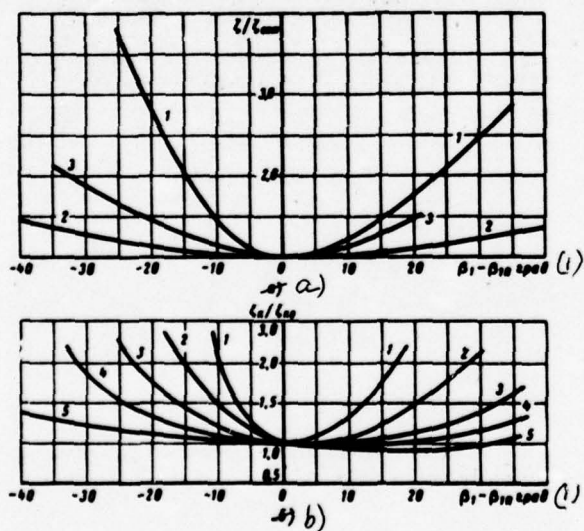


Fig. 66. Effect of Re number on the profile losses: 1 - in impulse cascades; 2 - in jet/reactive grid/cascades.

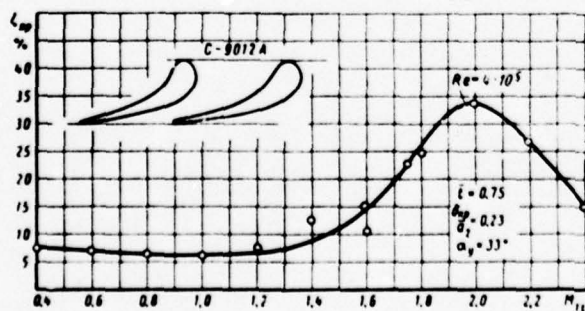
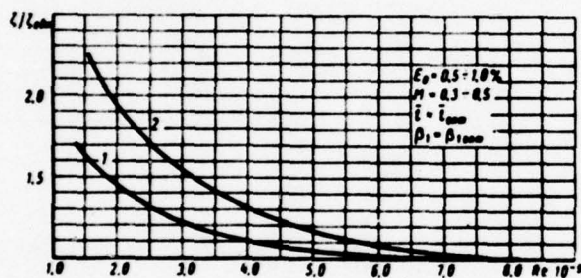


Fig. 67. Dependence of profile losses in the grid/cascade of S-9012A on Mach number and Re .

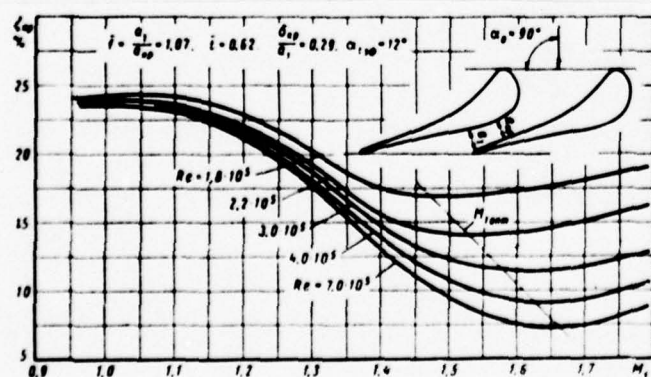


Fig. 68. Dependence of profile losses in grid/cascade with expanding duct on Mach numbers and Re .

§30. Reynolds number effect and compressibility (Mach numbers) to the characteristics of turbine grid/cascades.

The given in atlas characteristics of grid/cascades, as a rule, are obtained during a simultaneous change in Mach numbers and Re , which, it is natural, it impedes the evaluation of losses in grid/cascades at other values of the most important regime parameters. In connection with this for practical calculations, it is necessary to have characteristics which would make it possible to consider the separate effect of Re numbers and M .

The character of a change of the losses in grid/cascades and of the flow exit angles from Re number to a considerable degree depends on geometric dimensions (convergence and curvature of the enclosures of channels, the thickness of trailing edge, the form of airfoil/profile, roughness) and the regime parameters (reentrance angle, turbulence level, Mach number) ¹.

FOOTNOTE 1. The effect of Re number is partially examined in §28.
ENDFOOTNOTE.

Consequently, the effect of Re number on aerodynamic characteristics of grid/cascades is necessary to examine is separate for the determined intervals of values of Mach numbers, of turbulence level E_0 , and also for the different groups of grid/cascades (A, B and C).

At the present time the greatest number of experimental data is obtained for subsonic speeds ($M \leq 0.4$) with low turbulence levels ($E_0 \leq 1-20/0$), when effect of compressibility can be disregarded.

During subsonic ($M \leq 0.4$) nonseparated flow with an increase of Re, profile and tip losses in grid/cascade continuously decrease, particularly intensely in zone low Re (for airfoil/profiles with relatively fine/thin trailing edge). With increase in Re, is thinned a boundary layer, a range of the transfer of a laminar layer to turbulent is displaced against flow it increases the filling of the velocity profile of velocity in the turbulent section of a layer. The shift of the range of transfer decreases the intensity of a

reduction/descent in the losses with an increase of Re ; however, the beginning of zone of virtual self-similarity for such grid/cascades is shift/sheared to the side large $Re_{som} > (6+10) \cdot 10^4$. Angle of departure from grid/cascade continuously decreases with an increase of $Re < Re_{som}$.

Is especially great the effect of Re number on losses and the flow exit angle during the detached flow of back and for airfoil/profiles with the relatively thick trailing edge when breakaway on back or on edge occurs to the transition point of a laminar layer to turbulent. In this case with increase in Re , occurs the agitation of a layer in breakaway zone and breakaway is displaced along the flow: losses sharply decrease. The beginning of the zone of practical self-similarity according to Re number depends on many geometric and regime parameters. Specifically, with growth of initial flow turbulence and by a decrease in the reentrance angle of $\beta_1 < \beta_{1n}$ the value of Re_{som} decreases.

For the aerodynamically ideal nozzle and running cascades with low initial turbulence level $E_0 = 0.5-1.50/c$ and subsonic speeds of flow ($M = 0.3-0.5$) the approximate estimate of the effect of Re number can be produced on the curve/graphs, given in Fig. 66 (where

the η_{loss} - the ratio of the coefficient of energy losses of alternating/variable Re to the coefficient of the losses of of Re_{nom} .

The effect of the form of airfoil/profiles on the behavior of the coefficients of energy losses and the beginning of the zone of self-similarity of variable values of Mach numbers and Re is given in Fig. 67, 68 and 69. The detailed study of the jet/reactive airfoil/profile of group A (S-9012A) with the different thicknesses of trailing edges (Fig. 67) they showed that at subsonic speeds the zone of practical self-similarity according to Re number begins with $Re_{\text{nom}} \approx (6+9) \cdot 10^4$. With growth of M number in supersonic range ($M > 1$) the value of Re_{nom} grow/rises. For the nozzle cascade of group B, that has the geometric parameters: $\bar{t} = 0.62$, $\alpha_{1 \text{ to } 4} = 12^\circ$, $\bar{f} = 1.07$, a change in the coefficients of profile losses from Mach number of the different Re numbers is shown in Fig. 68. As for the airfoil/profile of group A, with an increase of Mach number, the value of Re_{nom} grow/rises. Importantly to note also other feature in the behavior of the curves of ζ_{np} during testing this grid/cascade: with a decrease in Re number, decreases the value of the optimum number of $M_{1 \text{ on } m}$. Thus, for instance, with $Re = 7 \cdot 10^4$, $M_{1 \text{ on } m} = 1.7$ and with $Re = 2.8 \cdot 10^5$, $M_{1 \text{ on } m} = 1.45$. This is connected with the fact that during decrease in Re increases the boundary layer thickness in the exit section of

channel and with respect decreases the real relation of $\bar{t} = a_i/a_{i,p}$.

For the airfoil cascade, which corresponds to the upper cross sections of long blades, the dependence of ζ_{np} on Re and M has similar character. This grid/cascade is carried out with constrictions and with the large relative space $\bar{t} = 0.895$. Calculated reentrance angle of the flow of $\beta_{1p} = 135^\circ$ the angle of departure of $\beta_{2\phi} = 14^\circ$. The loss factors in this grid/cascade depending on Re and M are given in Fig. 69.

With constant Re the compressibility effect (Mach number) for $M \leq 0.8$, turns out to be insignificant (for grid/cascades of group A). However, with increase in M, profile losses somewhat descend. Tip losses in nozzle and running cascades in subsonic range with an increase of M also descend. A noticeable increase in the losses is noted in transonic zone ($M > 0.9$). The further rise in M brings to a certain increase in the profile losses.

Fig. 69. Dependence of profile losses in the grid/cascade of the upper cross section of long blade.

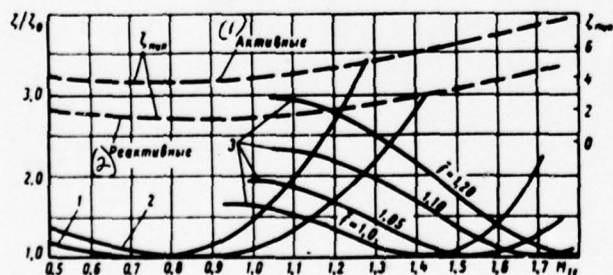
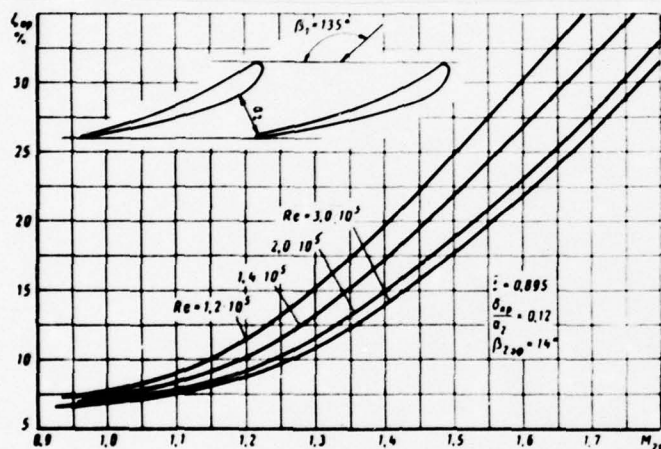


Fig. 70. Effect of Mach number on profile losses in the active and jet/reactive grid/cascades: 1 - the grid/cascade of group A; 2 - the grid/cascade of group B; 3 - the grid/cascade of group C.

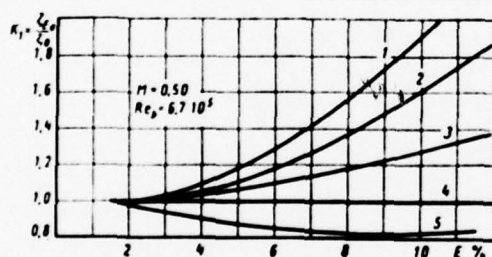


Fig. 71. Effect of turbulence level on profile 1, 2 and end 3, 4, 5 loss for jet/reactive 2, 5 and active 1, 3, 4 grid/cascades.

DOC = 76081693

PAGE ~~22~~
311

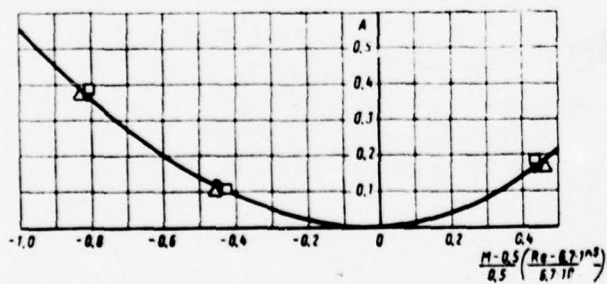


Fig. 72. On the calculation of eddy effect in the different Mach numbers.

For a group *B* (back with reverse/inverse concavity, the being expanded vane channels) the effect of Mach number, it turns out to be different. The minimum losses are observed in narrow calculated, supersonic zone, and maximum - at transonic speeds.

For the approximate estimate of effect, Mach numbers on profile losses in active and jet/reactive grid/cascades are given to the graph (Fig. 70) of the minimum losses in the grid/cascades, specially profiled to the different optimum Mach numbers. In this same Fig. 70, are given curved changes in the losses during deviation from M_{onm} for grid/cascades with different geometric parameters.

§31. Effect of flow turbulence on profile and total losses in nozzle and running cascades.

The given in atlas aerodynamic characteristics of airfoil cascades were obtained in wind tunnels with the low turbulence levels of the incident flow ($E_0 = 0.01-0.02$). The flow in the step/stage of turbine is characterized by high turbulence. The measurements, manufactured in different step/stages, they showed that in intermediate step/stages the turbulence level reaches values $E_0 =$

DCC = 76081693

PAGE ~~28~~

3/3

18-35o/o. Under turbulence level E_0 in this case, is understood the ratio of the average quadratic pulsating speed $\Delta \bar{c}$ to the average rate of flow \bar{c} (see §2):

$$E_0 = \frac{\Delta \bar{c}}{\bar{c}} = \frac{1}{\bar{c}} \sqrt{\frac{1}{\Delta t} \int_0^{\Delta t} c'^2 dt}.$$

. Taking into account that the pulsations are observed in all three directions, for a turbulence characteristics, they find arithmetic mean from the mean effective values of constituting pulsations.

Numerous experimental data show that a change in the turbulence level leads to the shift of the zone of the transfer of laminar boundary layer to turbulent on fairing and thereby affects the resistance of airfoil/profile.

It should be noted that an increase in the turbulence level differently affects the characteristics of the badly/poorly and streamline profiles [2; 30; 4].

Is at present a limited amount of the experimental data, which show the effect of turbulence level on the effectiveness of turbine grid/cascades. The available data are related, in essence, to nozzle and working impulse cascades, designed for subsonic speeds.

For the calculation of profile and total losses in turbine grid/cascades at different values E_0 Fig. 71, gives curve/graphs, construction on the basis of processing experimental these different organizations [2; 30; 4]. The evaluation of eddy effect on profile losses for working impulse cascades is conducted on curve 1, and for jet/reactive - on curve 2. The change of the tip losses depending on turbulence is determined for running cascades with wide angles of rotation ($\Delta\beta \approx 150^\circ$) according to curve 3, and for $\Delta\beta \approx 120^\circ$ - on curve 4. For jet/reactive grid/cascades tip losses with an increase in turbulence somewhat decrease (is curve 5).

Given in Fig. 71 correction curves are constructed for the

constant values of Mach number = 0.5 and $Re = 6.7 \cdot 10^5$. In other values of Re and M , the eddy effect turns out to be quantitatively different. With a decrease and increase Re and M , is observed an increase in the losses; in Fig. 72 is given the corresponding correction curve for profile and tip losses during a change in the mode/conditions. It should be noted that the curve in Fig. 72 is constructed on the basis of the experimental data, obtained with $M < 0.9$. With an increase of $M > 0.9$, eddy effect, apparently, will again decrease.

The calculation of losses with increased turbulence of ζ_{E_0} is performed as follows: on known profile and tip losses in grid/cascade ζ_0 with low degree of turbulence ($E_0 = 1-2\%$) and Mach number = 0.5, taken from atlas, and to correction factor K_1 (see Fig. 71) find the losses of the ζ_{E_0} :

$$\zeta_{E_0} = K_1 \zeta_0$$

. During a change in Mach number in value $M=0.5/0.5$, is determined the correction A :

$$A = \frac{\left(\frac{C_{R_2}}{C_0}\right)_M - \left(\frac{C_{R_2}}{C_0}\right)_{M=0.5}}{\left(\frac{C_{R_2}}{C_0}\right)_{M=0.5}} = \frac{(C_{R_2}/C_0)_M - K_1}{K_1}$$

(Fig. 72) and the loss in the assigned mode/conditions they are designed from formula

$$(C_{R_2})_M = (AK_1 + K_1) (C_0)_M. \quad (78)$$

§32. Nonuniformity of velocity fields in turbine grid/cascades.

Account of the effect of nonuniformity on losses in grid/cascades.

It is known that the flow at the entry into working and nozzle cascades possesses the considerable nonuniformity of speeds, angles and pressures on space and by height, caused by vortex/eddy movement for edge and the secondary flows of the blade tips of the preceding/previous series, overlap/ceilings, but also inflows or leakages of root and band/shroud/tire. It is logical, that nonuniformity of velocity fields it leads to a substantial change in the characteristics of grid/cascade in comparison with the characteristics, obtained under the idealized conditions. Depending on velocity diagram at entry, the total losses can both decrease and increase.

Effect of step nonuniformity of velocity fields on losses according to the results of static tests [26], when the nozzles located within the limits of one space were fixed in the different positions of the relatively investigated channel of running cascade, appeared insignificant. The average losses in such experiments turned out to be the close to the losses obtained during tests in steady flow.

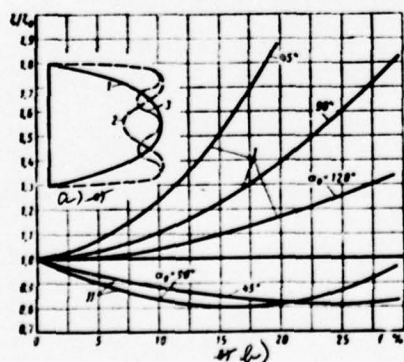


Fig. 73. Effect of degree of nonuniformity and reentrance angle to profile I and the total II ($\bar{\beta} = 0.4$) losses in nozzle cascades.

Some the test results, carried out on turned models, they showed that the losses in running cascades somewhat grow/rise.

The nonuniformity velocity field, caused by the presence of boundary layer on faces (of type I, Fig. 73a), it leads to an increase in total losses [4]. The approximate estimate of a change in the total losses for a parabolic velocity diagram at entry can be produced on curve/graph, given on Fig. 73b, where along the axis of abscissas is deposited/postponed the degree of irregularity of $1 - (1 - \frac{c}{c_{max}}) 100\% \alpha_{av}$ and α_{max} - average by height and maximum velocity of incident flow), but along the axis of ordinates - the ratio of the total losses ξ in the nonuniform velocity field to the total losses of ξ_0 during the even distribution of velocities by height of grid/cascade at entry ($f = 0$).

In turbine grid/cascades frequently is encountered the nonuniformity of type 2 (Fig. 73a) with failures of velocities at certain distance from shrouds of type 3 (Fig. 73a) with failure of the velocities in the mean sections of grid/cascade (failures of velocities are caused by the secondary motion in grid/cascades). The diagram/curve of velocities of type 3 it is encountered with low reentrance angles to the grid/cascade when the maximum losses occur

in mean sections.

The evaluation of the effect of the nonuniformity of types 2 and 3 on the cost-effectiveness/efficiency of grid/cascades turns out to be more complex than in the case diagram/curves of type 1. This is connected with the fact that the nonuniformity affects differently profile and tip losses. For each relative height/altitude of grid/cascade, is an optimum value of the nonuniformity by which the total losses turn out to be minimum.

On Fig. 73b, is given the dependence of the ratio of the total losses ξ during the nonuniform distribution of velocities of type 3 to ξ_0 with $f = 0$. From curve/graph it is evident, that minimum total losses in jet/reactive grid/cascade ($\bar{L} = 0.40$, $L = 25$ mm) at reentrance angle $\alpha_0 = 90^\circ$ occur with $f \approx 150/o$. For a reentrance angle $\alpha_0 = 45^\circ$, when tip losses turn out to be those which were increased, the optimum nonuniformity increases to $f \approx 300/o$ (Fig. 73b). The given characteristics are constructed for Mach numbers ≈ 0.7 . With a change in Mach number, the effect of nonuniformity quantitatively turns out to be different. For approximate estimates by curve/graphs, given in Fig. 73, it is possible to use in the range of Mach numbers = 0.5-0.9.

DOC = 76081693

PAGE ~~42~~

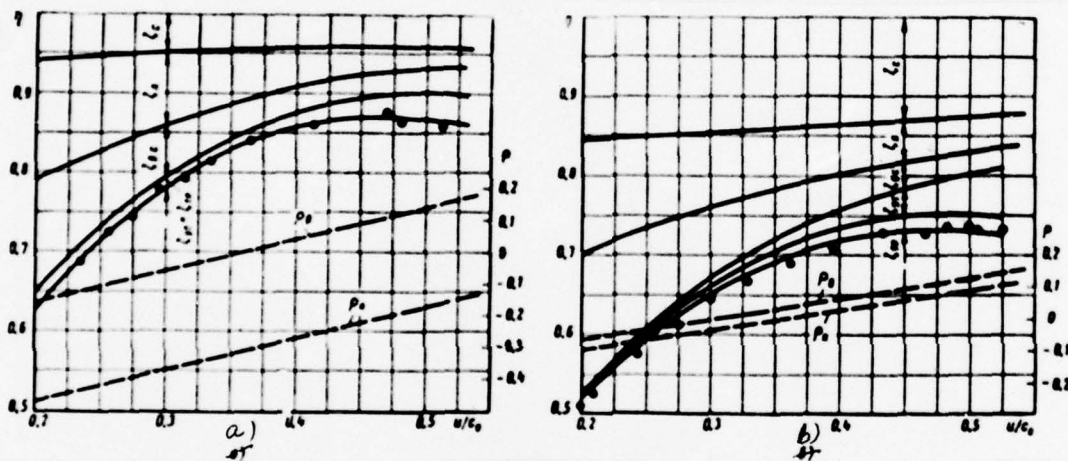
321

Page 42.

Chapter V.

CALCULATION OF THE ~~STAGES~~/STAGES OF STEAM AND GAS TURBINES ACCORDING TO
THE DATA OF STATIC STUDIES.

Fig. 74. Comparison of experimental and computed values stage efficiency: $\alpha) \beta = 0.3; \bar{\tau}_1 = 0.94; \beta) \beta = 0.0; \bar{\tau}_1 = 0.90$



§33. Procedure for the thermal design of step/stages with the use of aerodynamic characteristics of atlas.

In the practice of turbine-constructing plants, are most common two method of calculation of flow areas of the turbines.

The first method is based on the use of the generalized characteristics, obtained during investigation of the determined type of model step/stages in experimental turbines (method of calculation according to test data of model step/stages). This method has a series of the essential advantages which ensured to it wide application. The key advantages of methodology are: the simplicity of the calculation and the reliability of results for this type of step/stages.

Second method [47] is based on the use of coefficients of the energy losses and coefficients of the flow rates in the nozzle and running cascades, obtained experimental (under the static conditions)

and by calculation. The calculation is conducted according to velocity triangles. This method thus far is still less reliable, than the first; however, it is more demonstrative and makes it possible to determine the effect of energy losses in the separate cell/elements of flow area of the turbine. In different regime and geometric parameters appears the possibility to determine the ranges of the maximum losses and to mark the ways of an increase in the cost-effectiveness/efficiency of step/stages.

During application/use of a new type of blading in turbines, and also during calculations of intermediate step/stages for varying load (if are absent the experimental data, obtained in experimental turbines) the method, based on the calculation according to by velocity triangles, it is only, that ensures acceptable accuracy/precision. During the calculation of step/stages with long blades (large fanning $d/z < 7-10$) the only possible is at present the method, based on velocity triangles.

The accumulated experimental material, which characterizes the step/stages of large fanning, is insufficient for the construction of the generalized dependences; therefore the calculation is conducted according to cross sections. Furthermore, because of clarity this

method is most advisable in presenting the material in academic process ¹.

FOOTNOTE ¹. The detailed presentation of the method of calculation of the step/stages of turbines according to velocity triangles can be found in manuals from steam and gas turbines. Specifically, it is possible to be utilized by A. V. Shchetlyaeva's book "steam turbines" [48]. ENDFOOTNOTE.

For determining the cost-effectiveness/efficiency of step/stage with $d/l > 10$ calculation is conducted according to mean section taking into account tip losses in grid/cascades. The relative internal efficiency:

$$\eta_{int} = 1 - \frac{\Delta h_{n1} + \Delta h_{n2} + \Delta h_{c1} + \Delta h_{c2}}{\Delta h_{n1} + \Delta h_{n2} + \Delta h_{c1} + \Delta h_{c2} + \Delta h_{r1} + \Delta h_{r2}} \quad (79)$$

where the loss in nozzle and running cascades

DCC = 76081693

PAGE ~~43~~
324

$$\xi_s = \left(\frac{c_{11}}{c_{10}} \right)^2 \xi_{s1}; \quad \xi_s = \left(\frac{c_{21}}{c_{20}} \right)^2 \xi_{s2} \quad (80)$$

at outlet velocity

$$\xi_s = \left(\frac{c_{11}}{c_{10}} \right)^2; \quad (81)$$

for the friction of disk

$$\xi_{\text{fric}} = 10^{-2} \frac{dV_0^2}{c_{11} \sin \alpha_{11} \phi}; \quad (82)$$

from leakages

$$\xi_{\text{sum}} = \frac{\mu_2}{\mu_1} \cdot \frac{F_2}{F_1} \cdot \frac{1}{V_2} \sqrt{\frac{Q_2}{1 - Q_2}} \quad (83)$$

here: c_a is the fictitious velocity, calculated on the available heat drop; μ_y, μ_1 - the coefficients of flow rate for the radial shroud clearances of rotor wheel and for the nozzle cascade of ($\mu_y \approx 0.7$; $\mu_1 = 0.98$); z - the number of crest/peaks of the shroud packing/seals of rotor wheel; α, α_s - the reaction of step/stage in peripheral mean sections; ξ, ξ_s - the loss factors, obtained during the static studies of grid/cascades; e is a degree of admission; F_y - clearance area.

The coefficients of ξ and ξ_s are taken on experimental curve, given in atlas. If in atlas are absent the empirical curves, which correspond to the necessary geometric and regime parameters of the calculated step/stage, one should use the generalized dependences.

From the number of dimensional characteristics, it is necessary to consider the effect: the technological defects, the surface finishes, thickness of trailing edges, space, angle of setting, fanning, slope/inclination of blades, meridian enclosures, overlap/ceiling, etc. At low relative height/altitudes special attention must be given to technology of the manufacture of step/stages, also, first of all the diaphragms: milled, setting, welded or cast. From the number of regime parameters, must be considered the effect: the reentrance angle, turbulence, nonuniformity of flow, Mach numbers and Re , of humidity, dust content, etc.

The data on the effect of the geometric and regime parameters on losses and angles of departure are brought in §§19-32. The procedure for the account of corrections is given in these paragraphs. The velocity triangles are constructed on experimental or calculated angles of departure ($\alpha_1; \beta_2$), expenditure stage characteristics are determined from the minimum cross sections of grid/cascades and the effective angles of ($\alpha_{1,eff}; \beta_{2,eff}$).

§34. Examples of the calculation of turbine stages.

The account of the enumerated in the preceding/previous paragraph geometric and regime parameters on the generalized curve/graphs of atlas makes it possible with sufficient high accuracy/precision to calculate cost-effectiveness/efficiency and expenditure stage characteristics. The highest accuracy/precision is obtained for the step/stages of the average fanning ($d/l \approx 10$) with large relative spans of the blade ($l/b > 1.0$). An error in the calculation composes $\Delta \eta_{0i} \approx \pm 1.5\%$.

With a decrease in the relative height/altitude, the accuracy/precision of the calculation falls due to stronger effect of technology of the manufacture of band/shroud/tires, and also of leakages, overlap/ceilings, nonuniformity of flow, etc. The large deviations of calculation data from the experimental in turbines are obtained for step/stages with the low $d/l < 4$, which is connected in essence with flow breakaway in root cross sections, the streamline curvature, the deviation of reaction from the calculated.

For an example on curve/graphs (Fig. 74) are given experimental and calculated (according to the characteristics of atlas) curves for

step/stages with the following geometric and regime parameters:

$$a) \theta = 8.3; l_1 = 0.94; M_0 = 0.7; Re_{eff} = 5 \cdot 10^5;$$

$$b) \theta = 40; l_1 = 0.2; M_0 = 0.8; Re_{eff} = 7 \cdot 10^5.$$

on curve/graphs is given also the balance of losses in these step/stages.

Calculations of the sections of the turbines, which consist of several step/stages, also gave a good agreement with the experimental data, obtained in experimental turbines.

Less precise results are obtained during the calculation of the step/stages, which work at supersonic speeds. This is explained in essence by considerable building to the characteristics of the supersonic step/stages of the geometric parameters of grid/cascades, which not always accurately succeeds in considering in the calculations.

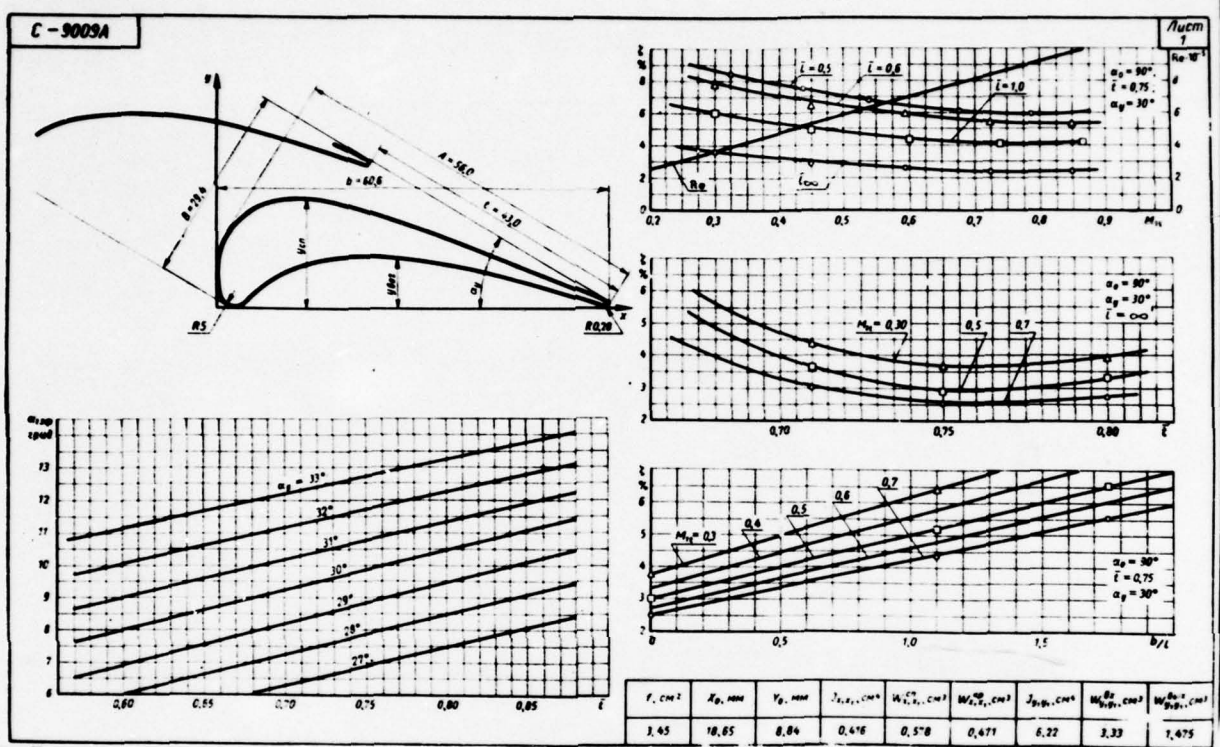
DOC = 76081693

PAGE ~~54~~

331

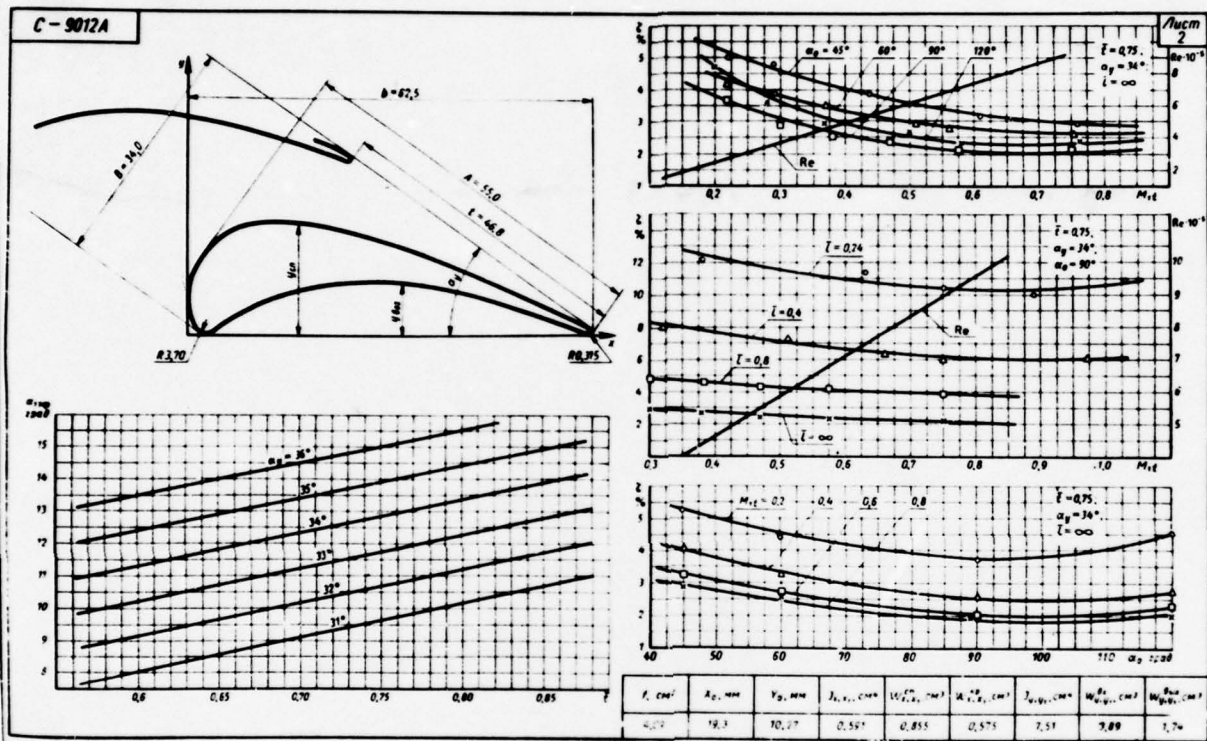
Page 43.

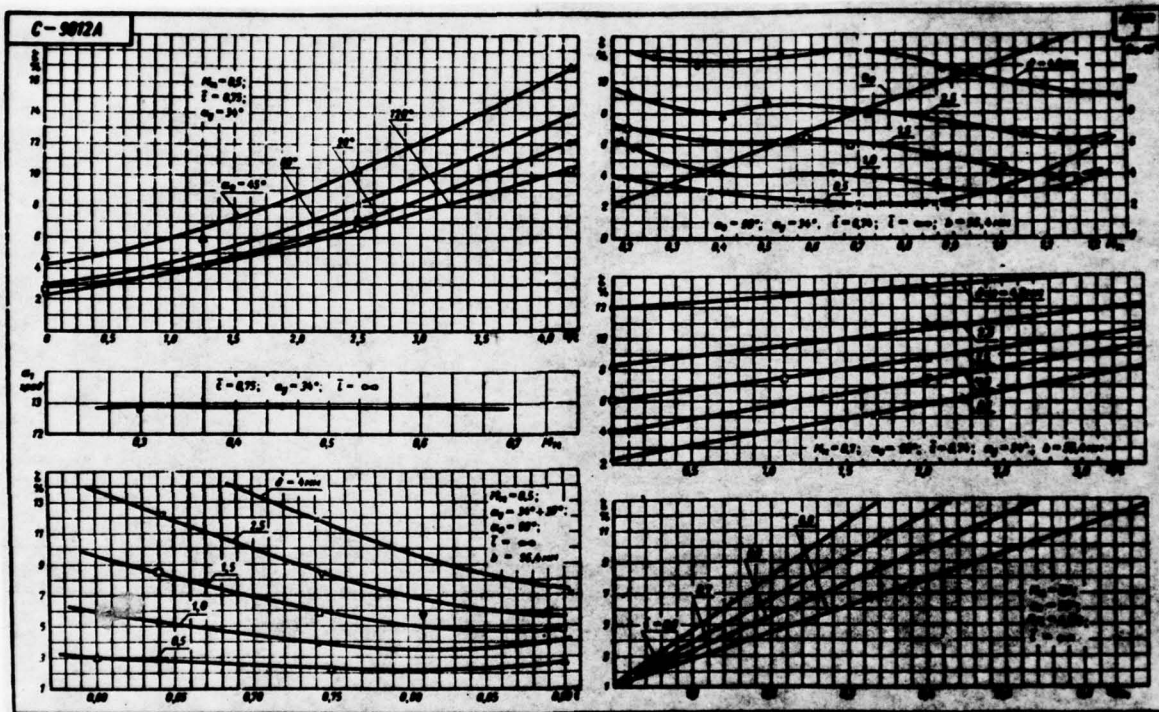
Part Two. Airfoil~~s~~~~profiles~~, the aerodynamic and strength characteristics of ~~grid~~/cascades.

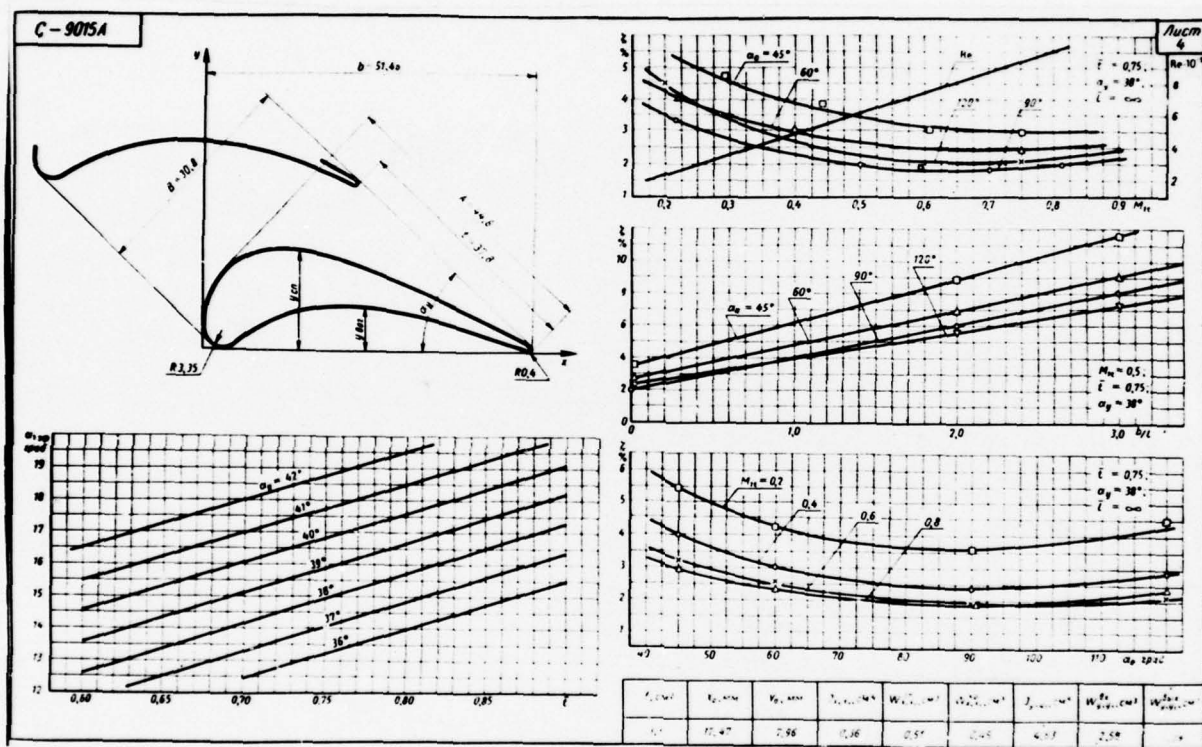


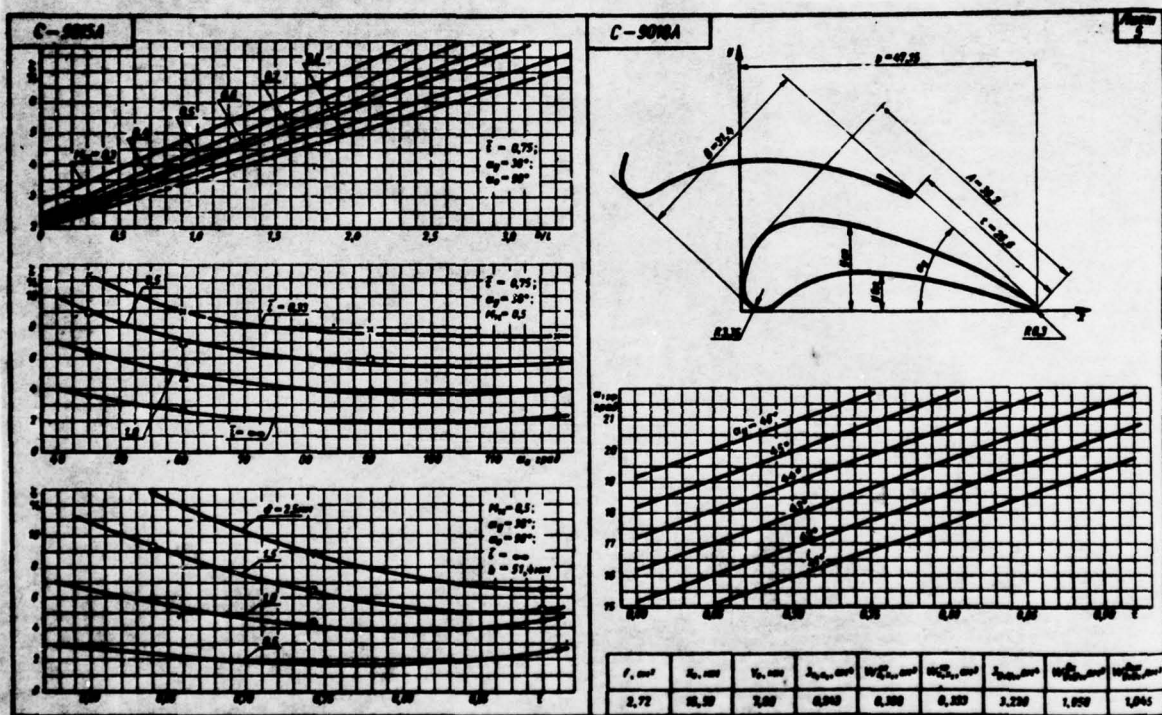
Лист = sheet

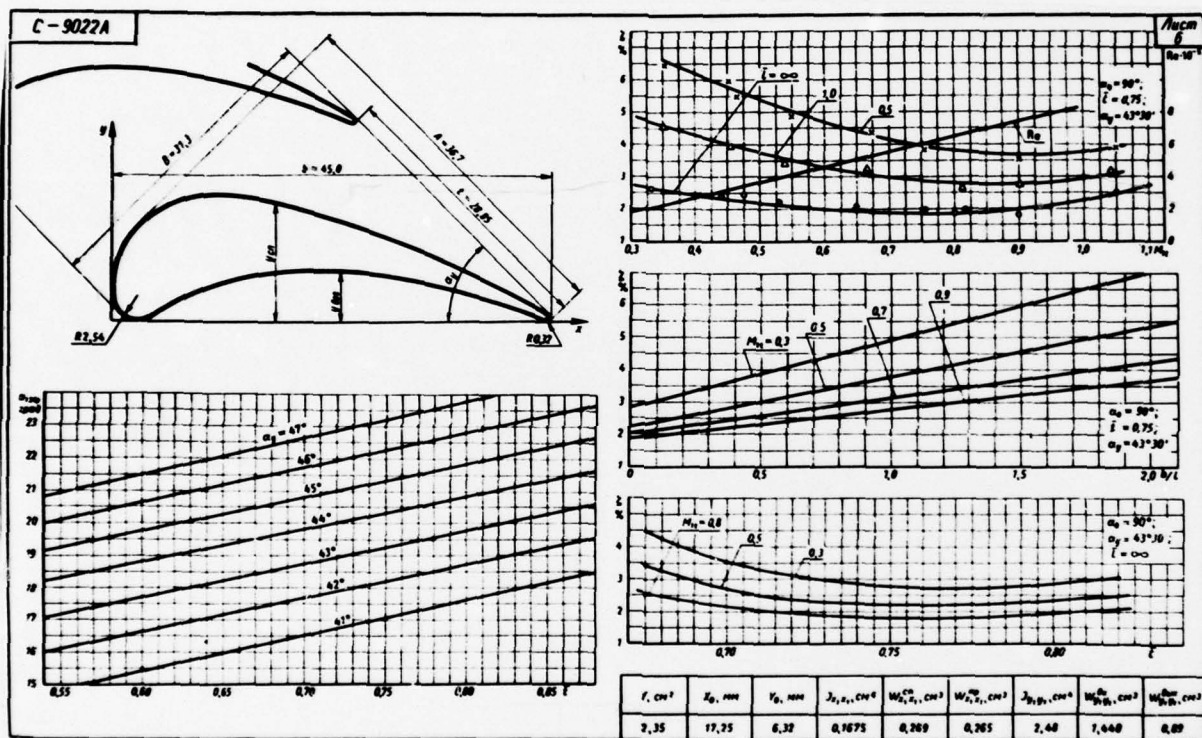
град = degree

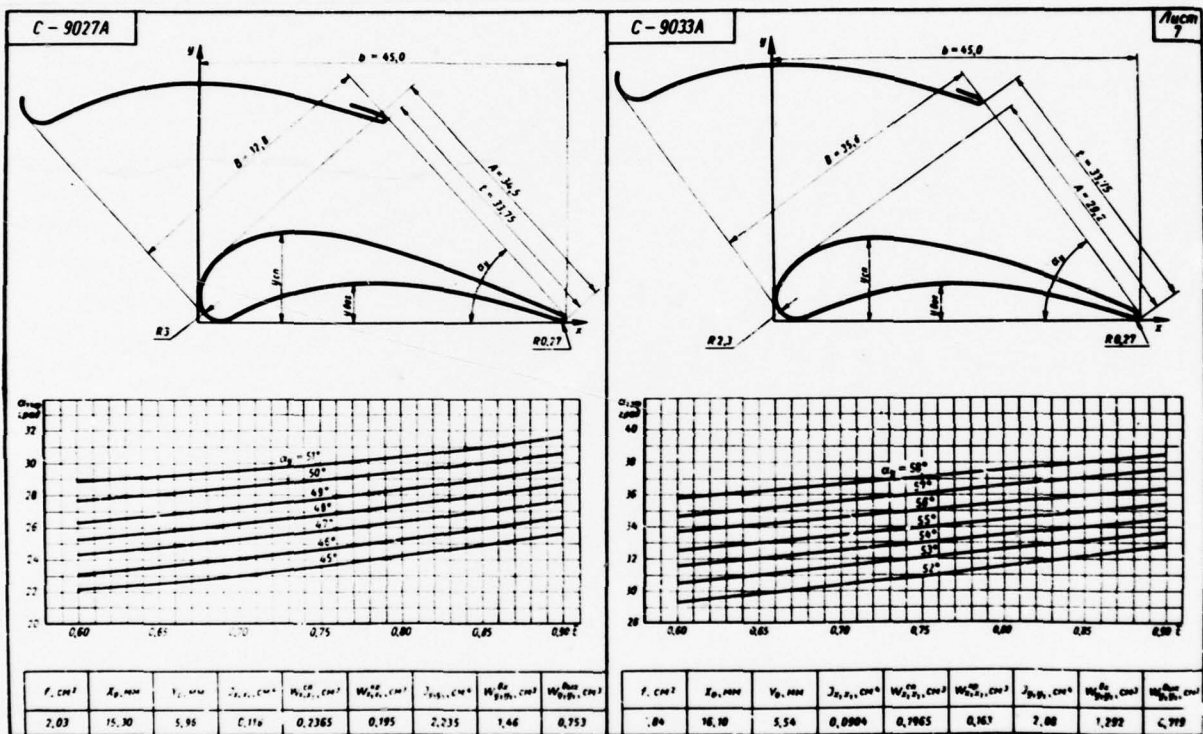


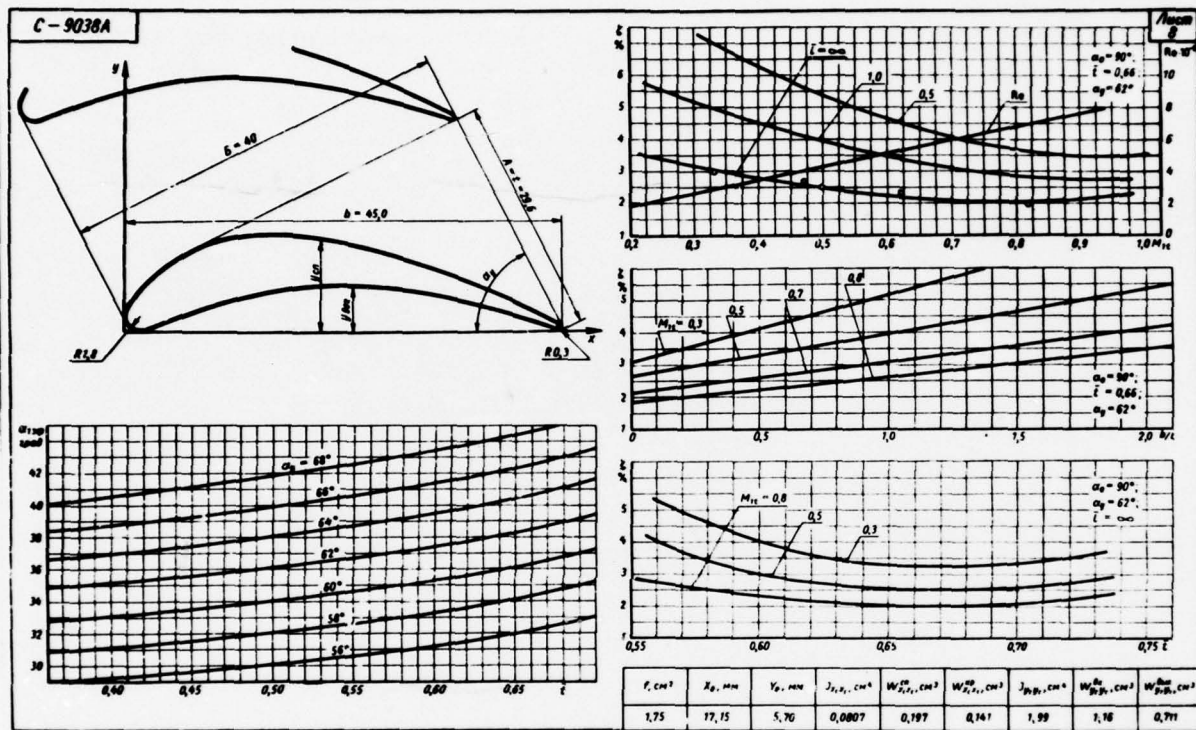




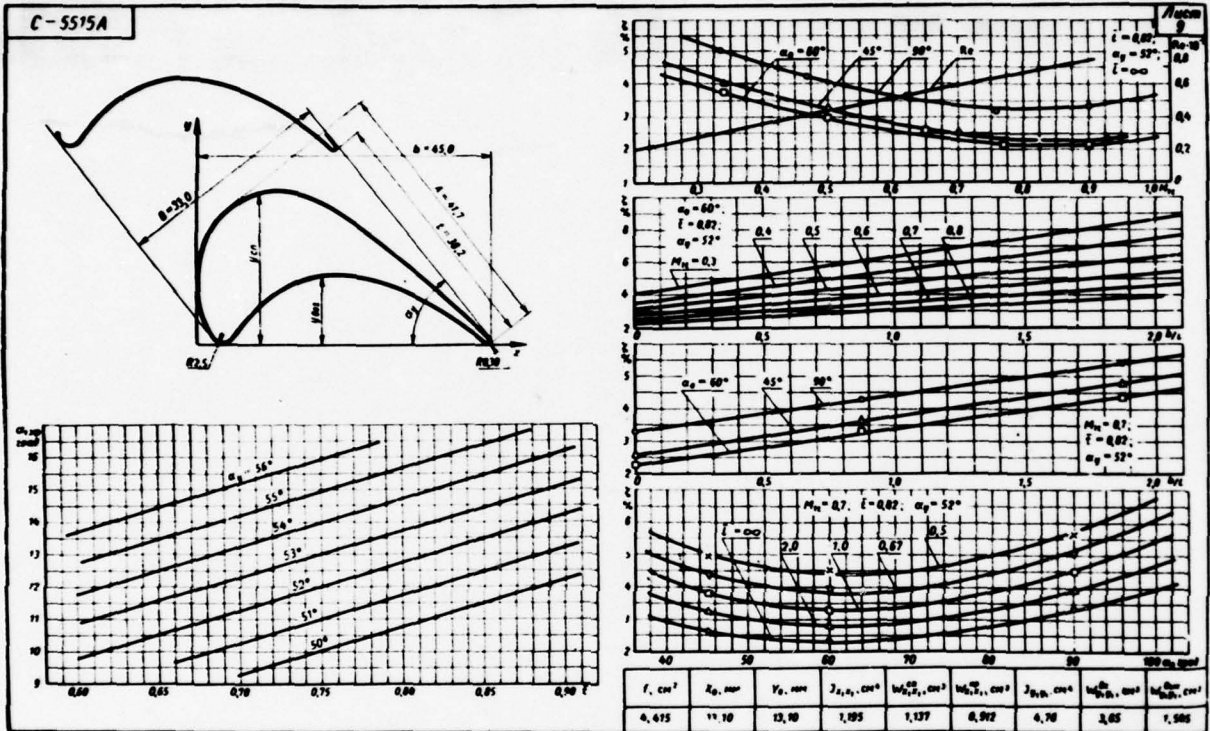




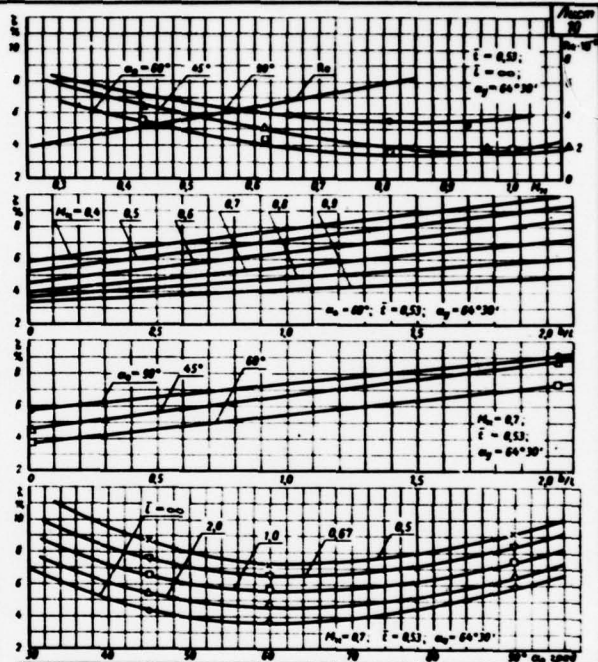
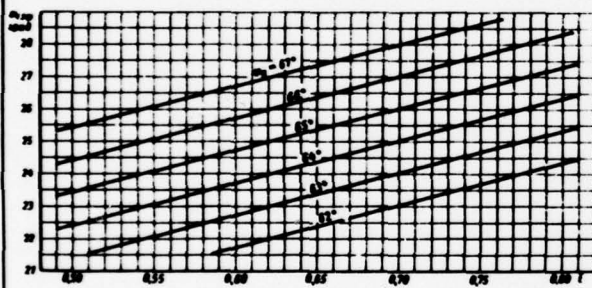
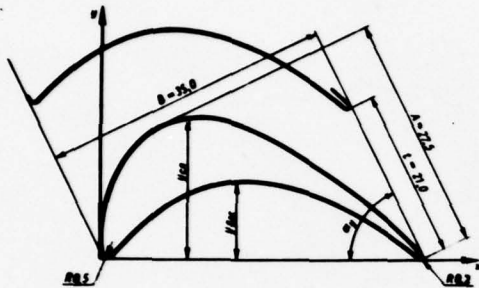




Page 340

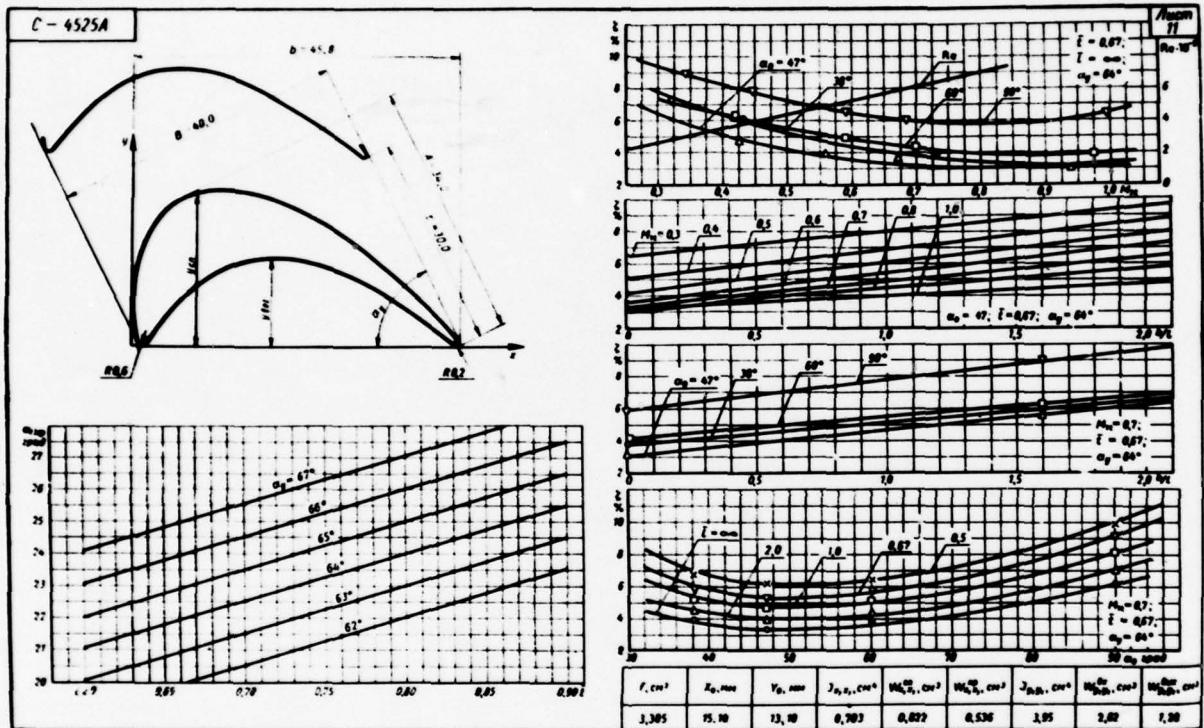


C-5520A

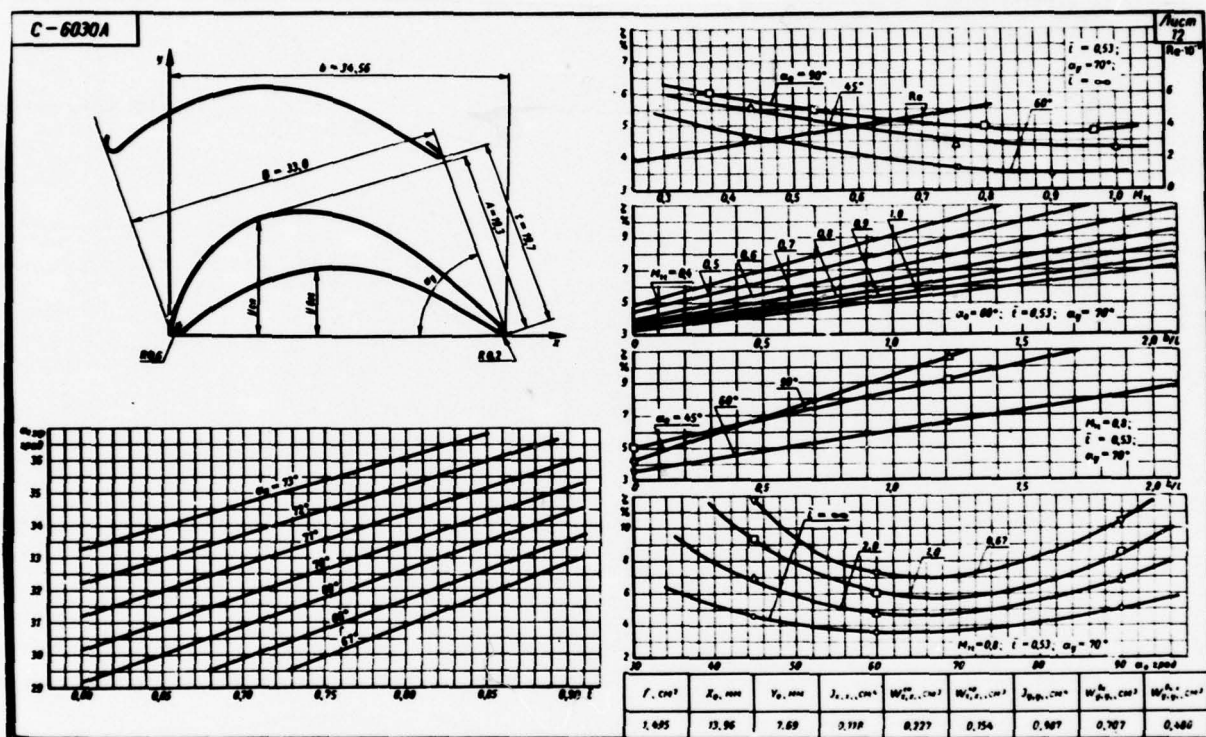


f, cm^2	X_0, mm	Y_0, mm	$J_{x_0, x_0}, \text{cm}^4$	$W_{x_0, x_0}, \text{cm}^3$	$W_{y_0, y_0}, \text{cm}^3$	$J_{y_0, y_0}, \text{cm}^4$	$W_{y_0, x_0}, \text{cm}^3$	$W_{x_0, y_0}, \text{cm}^3$
2.15	15.19	9.92	0.273	0.416	0.275	1.30	0.04	0.523

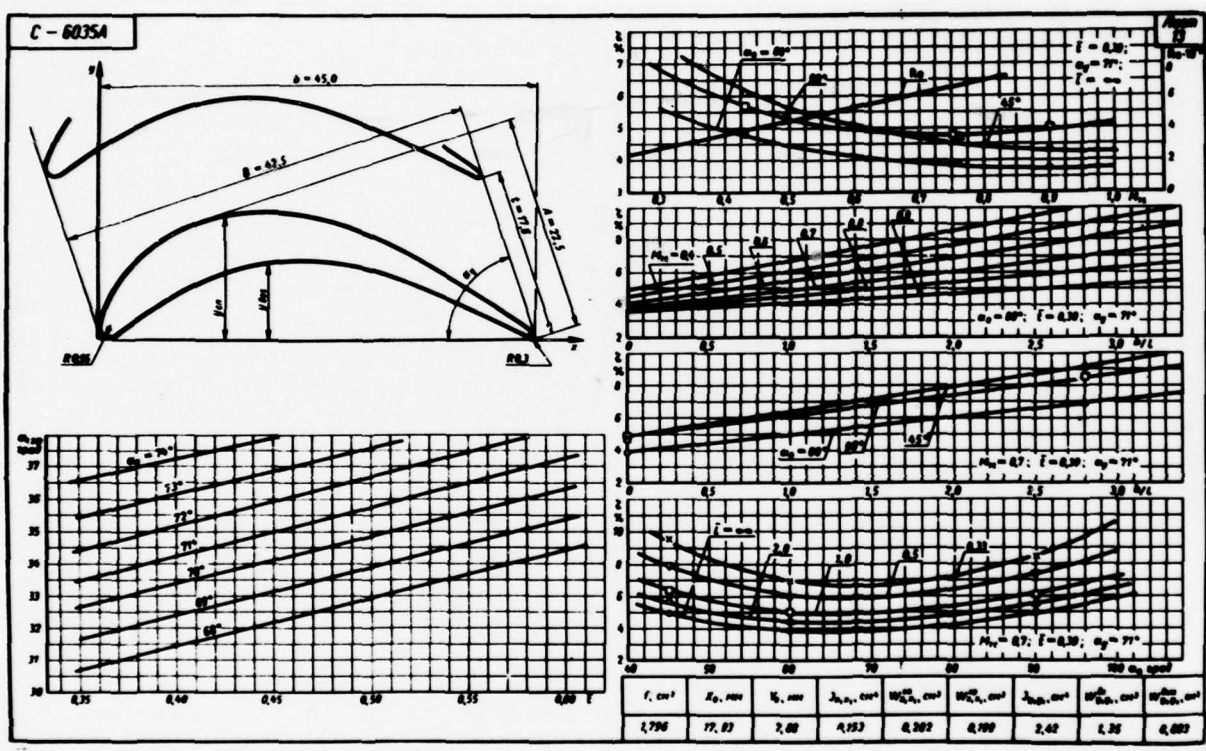
Page 342



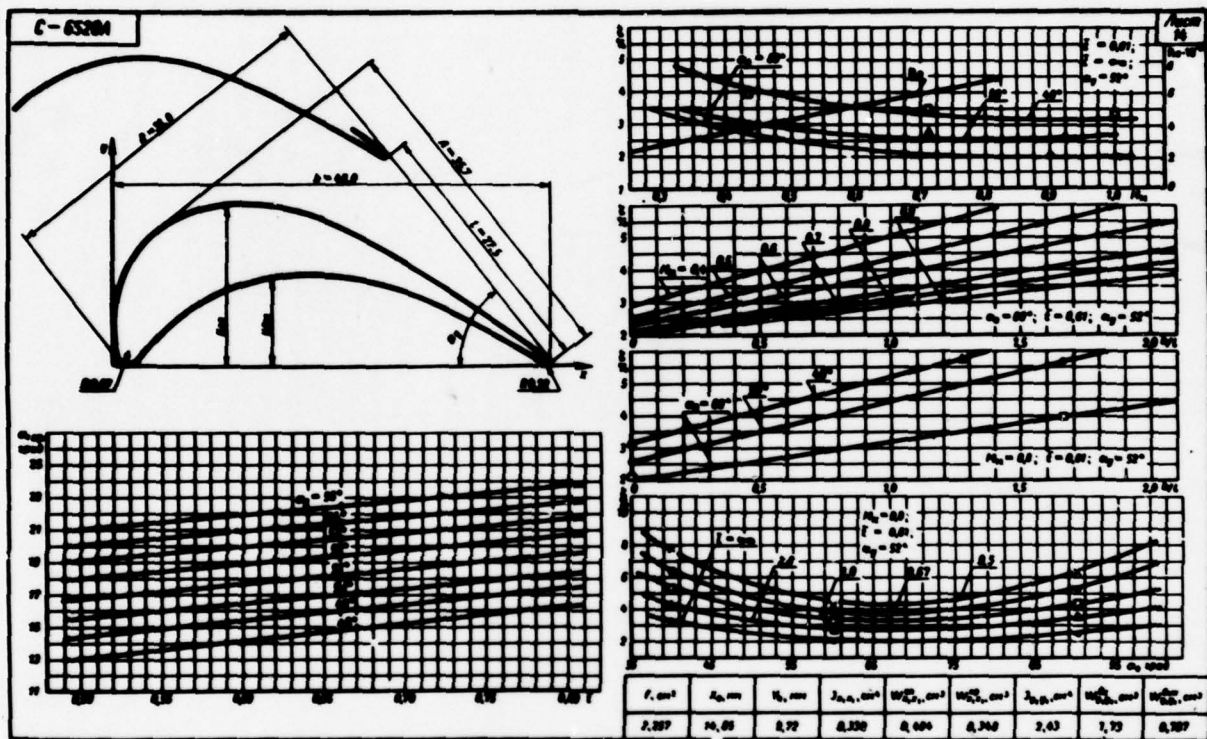
page 343



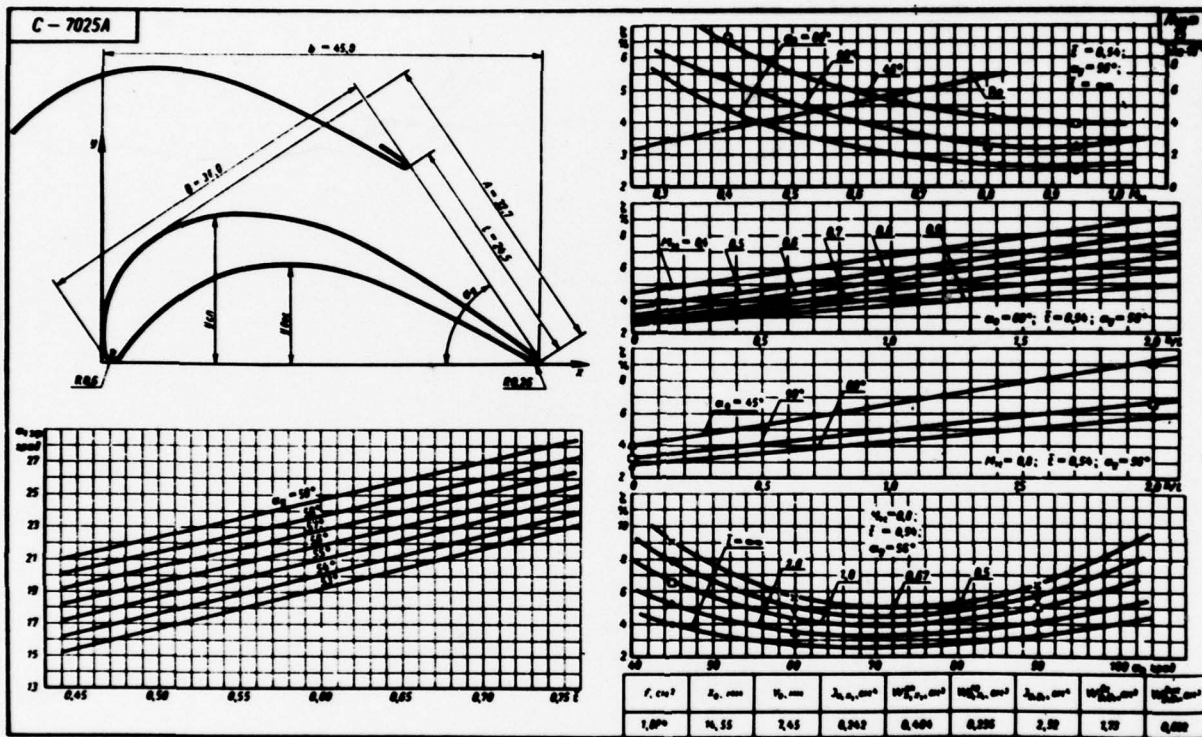
page 344



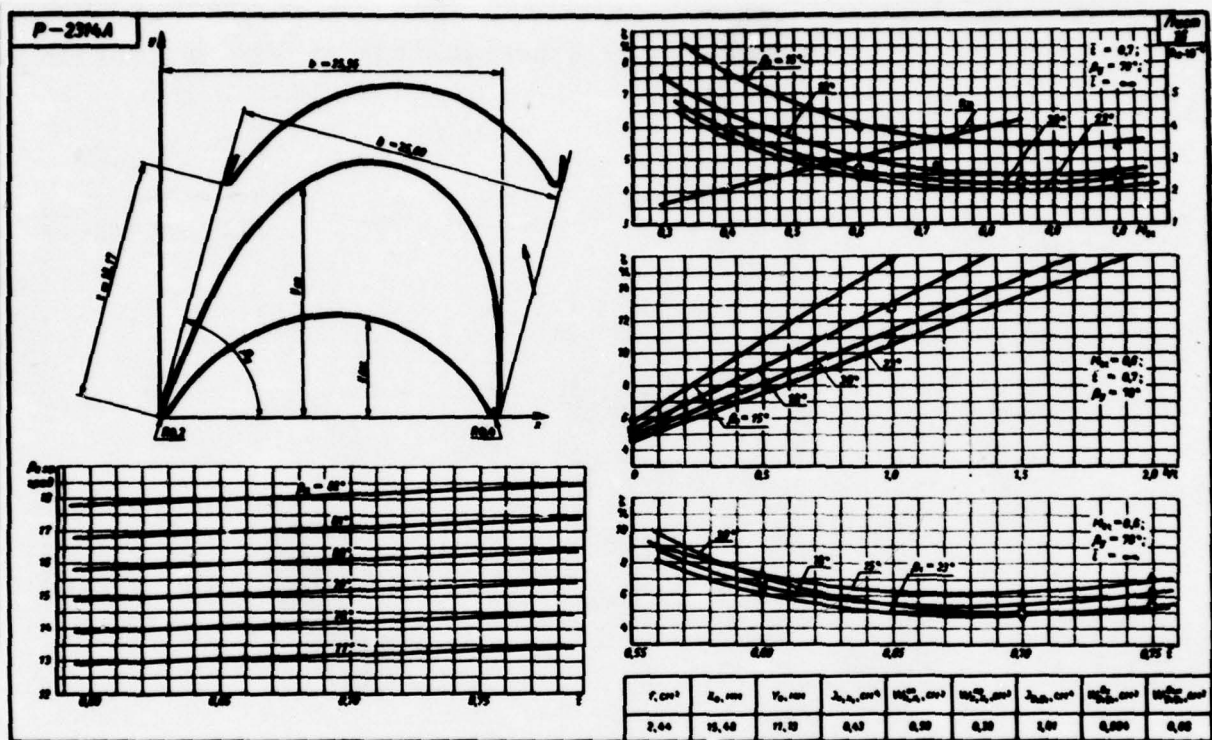
Page 345

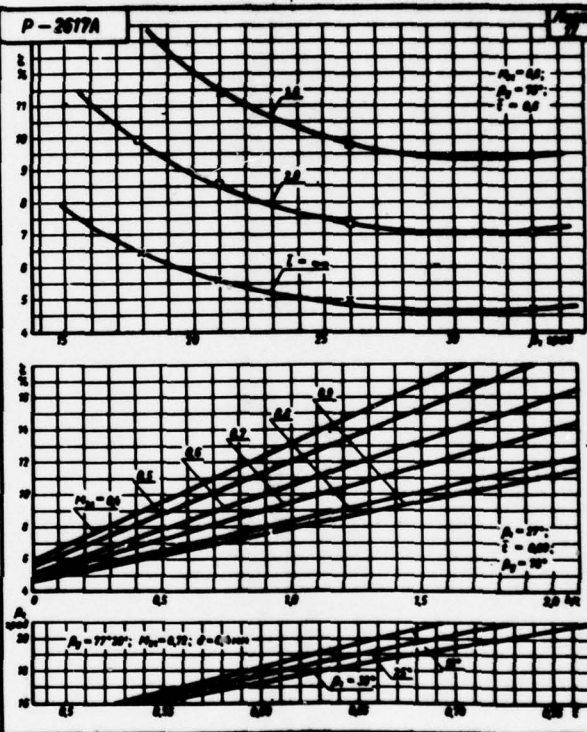
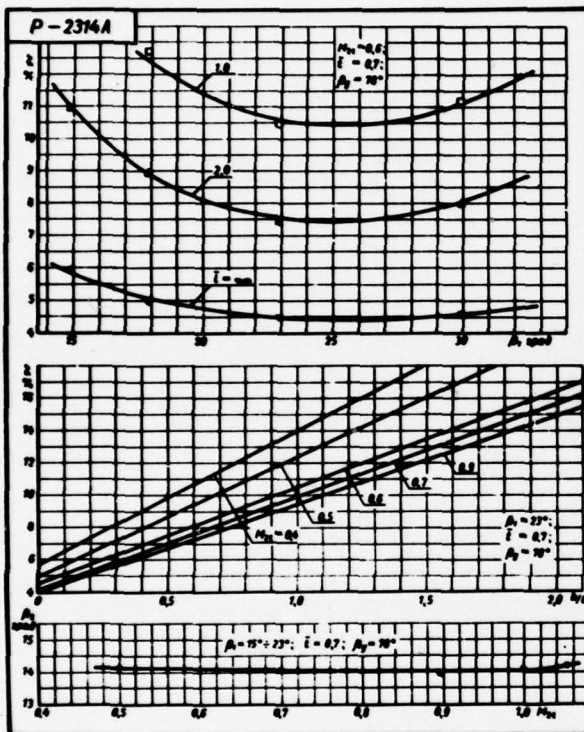


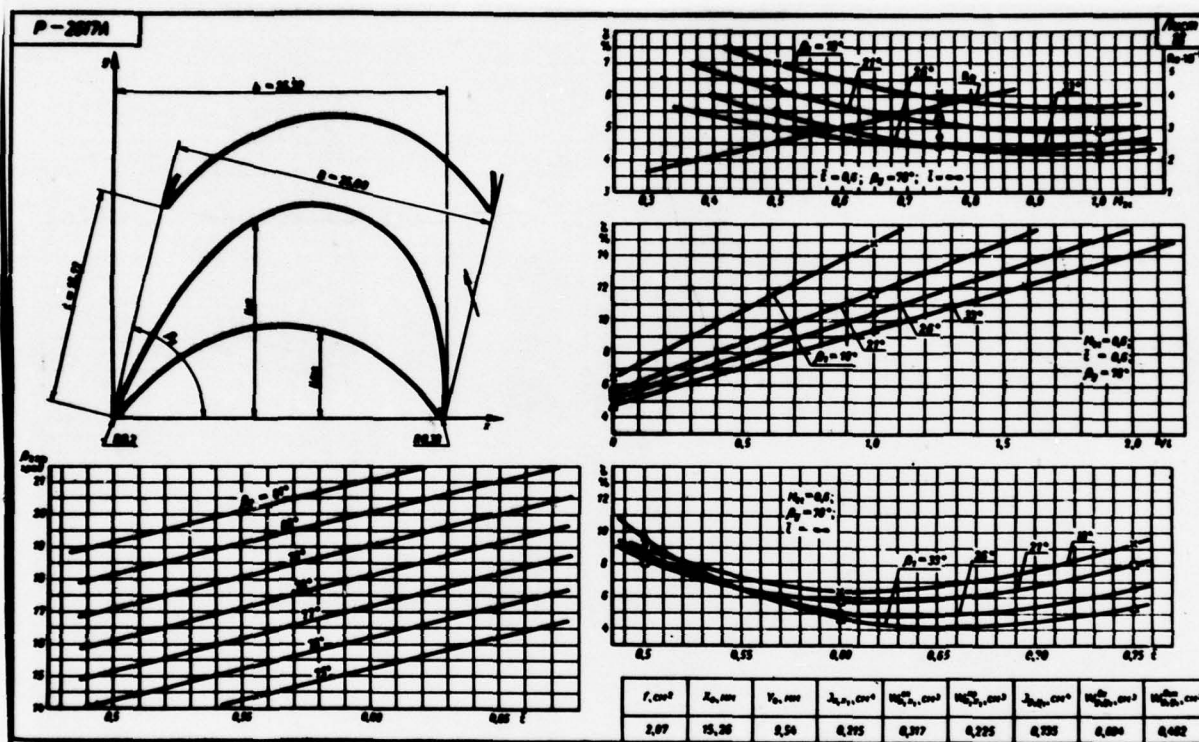
Page 346

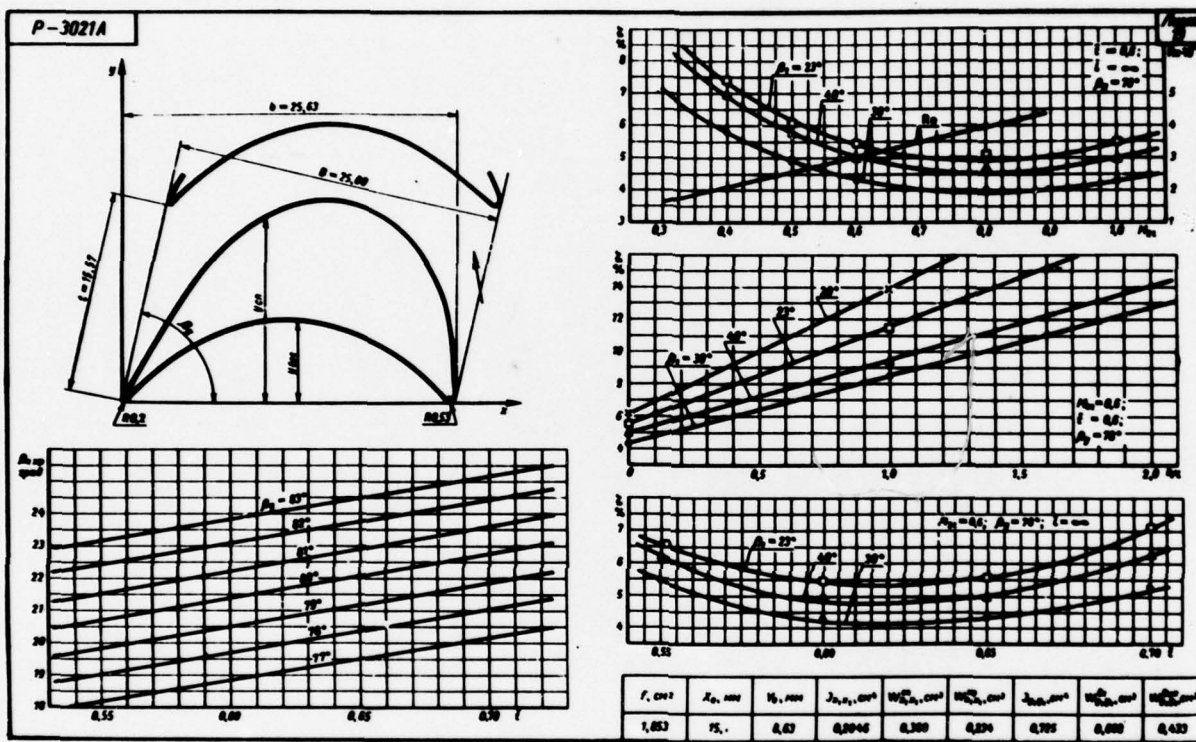


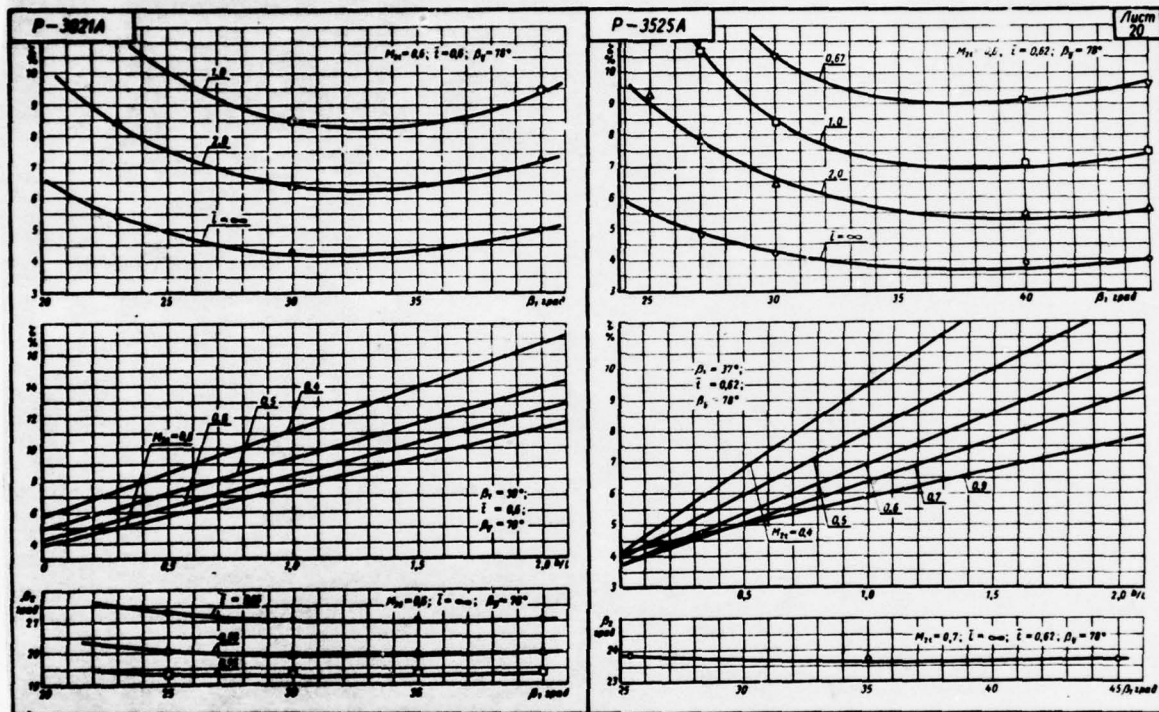
Page 347



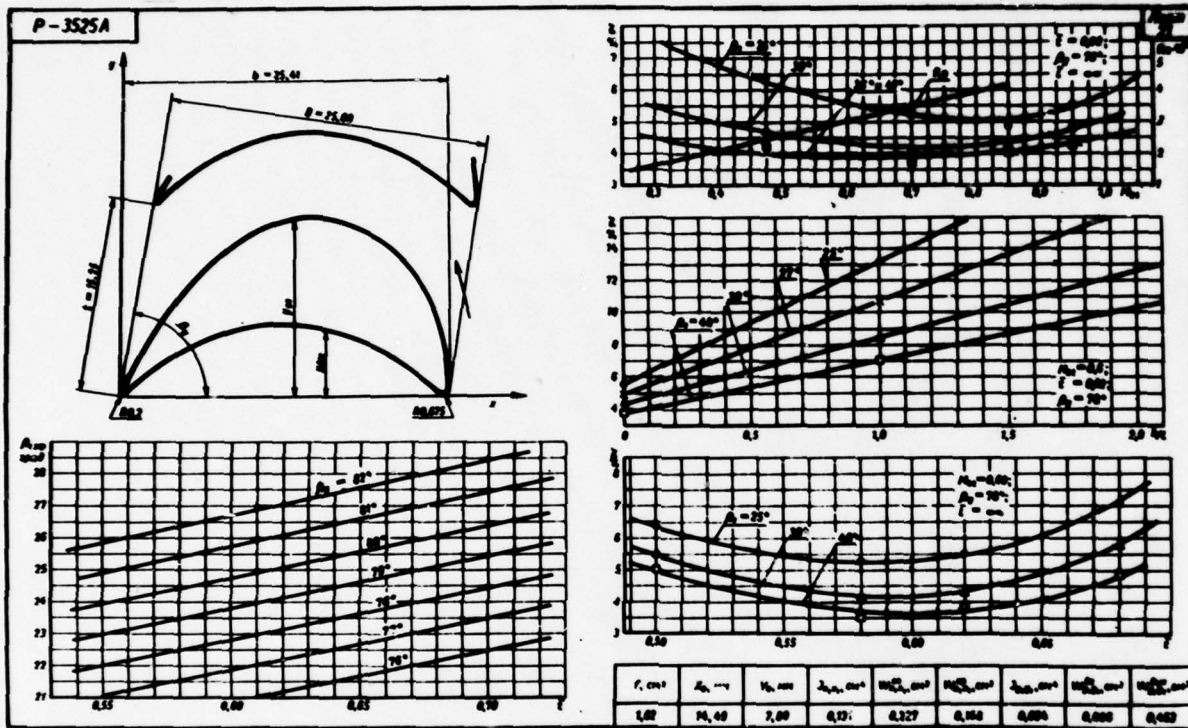




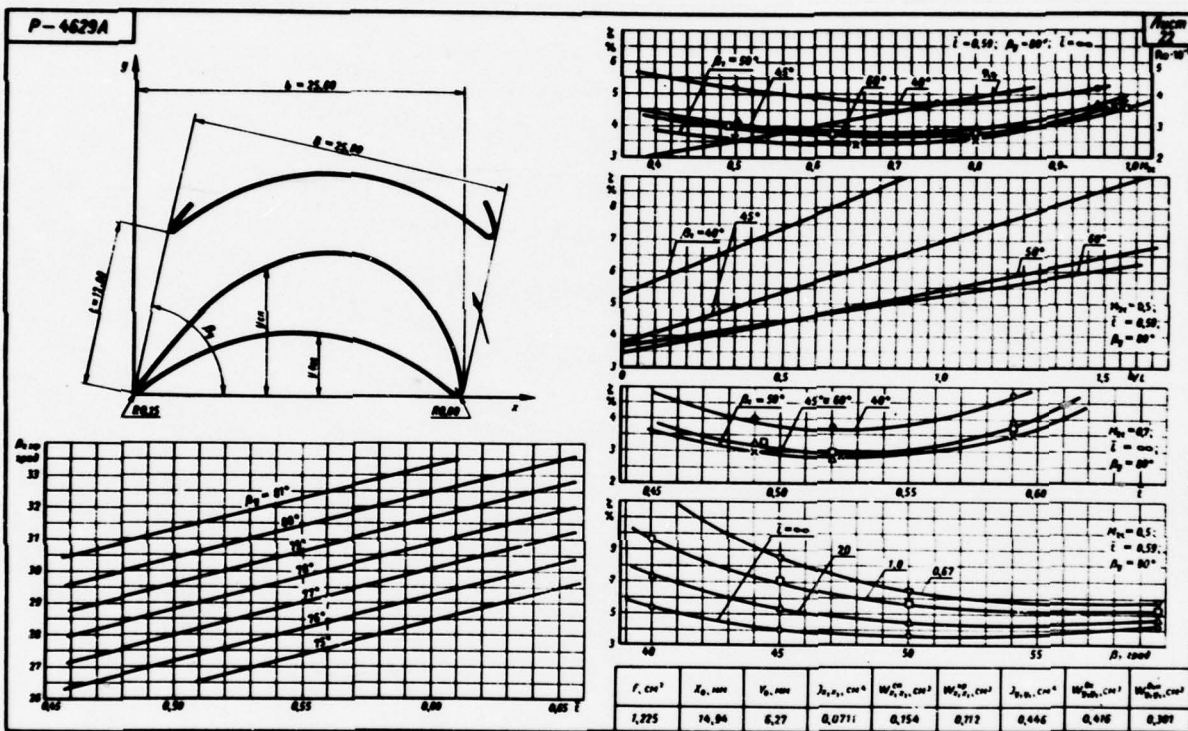


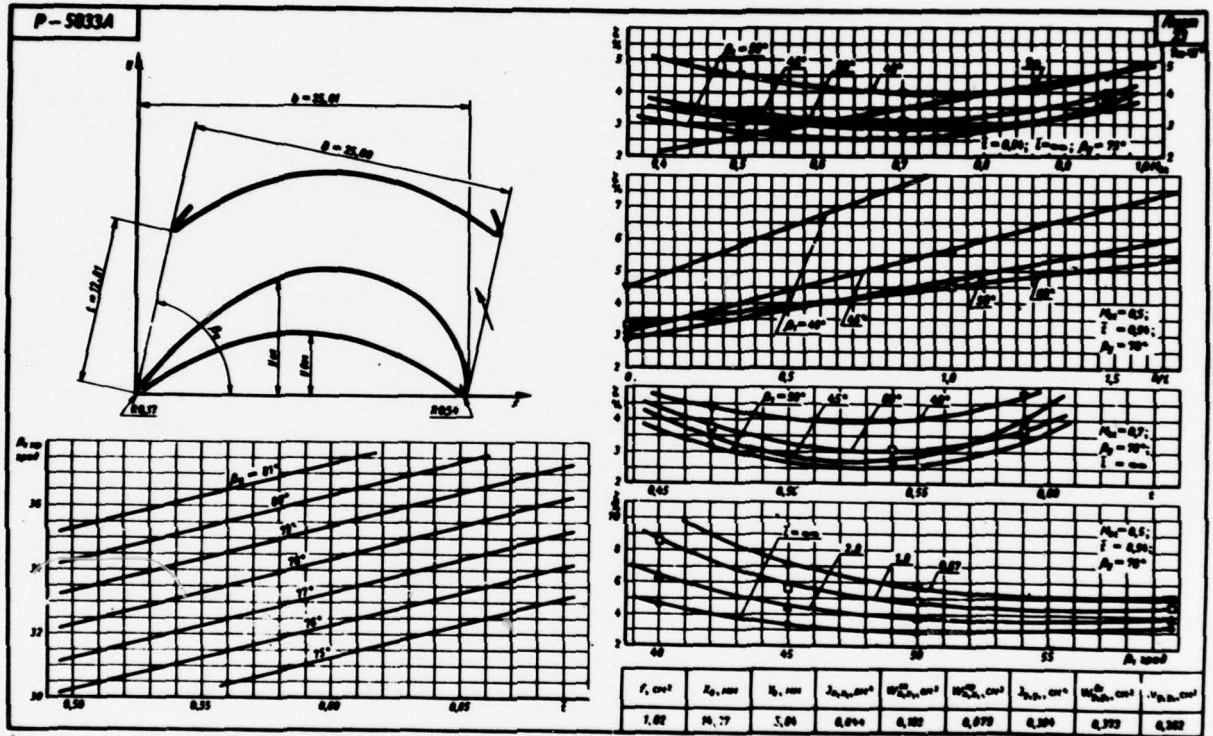


Page 352

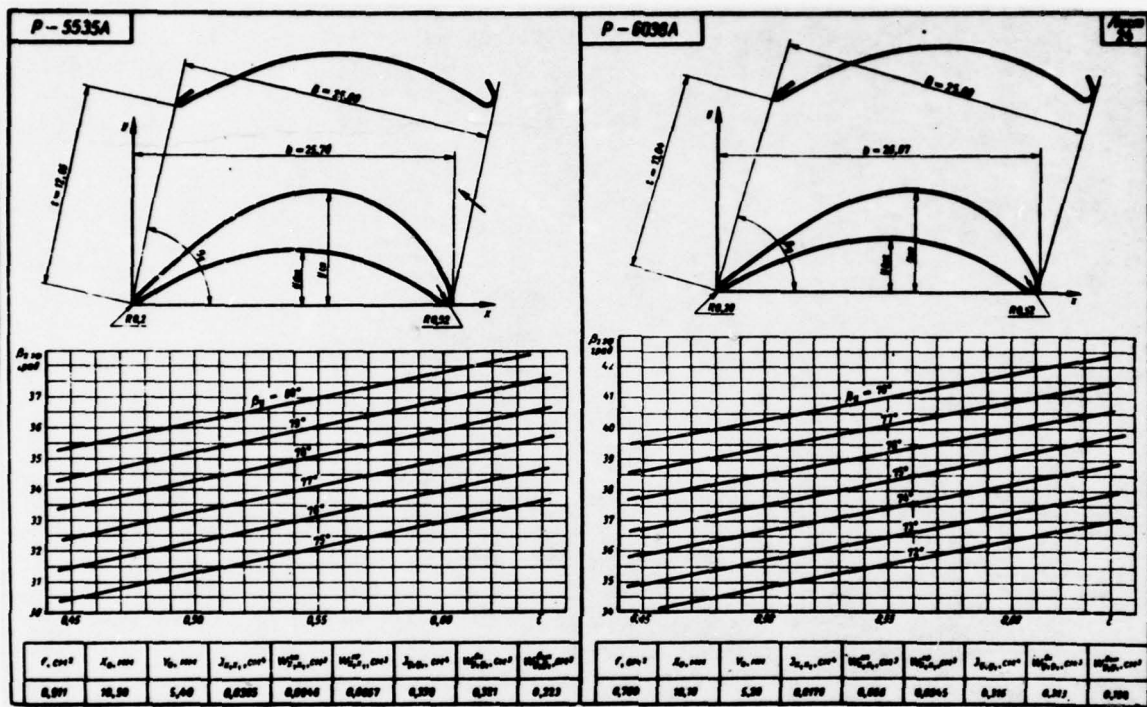


page 353

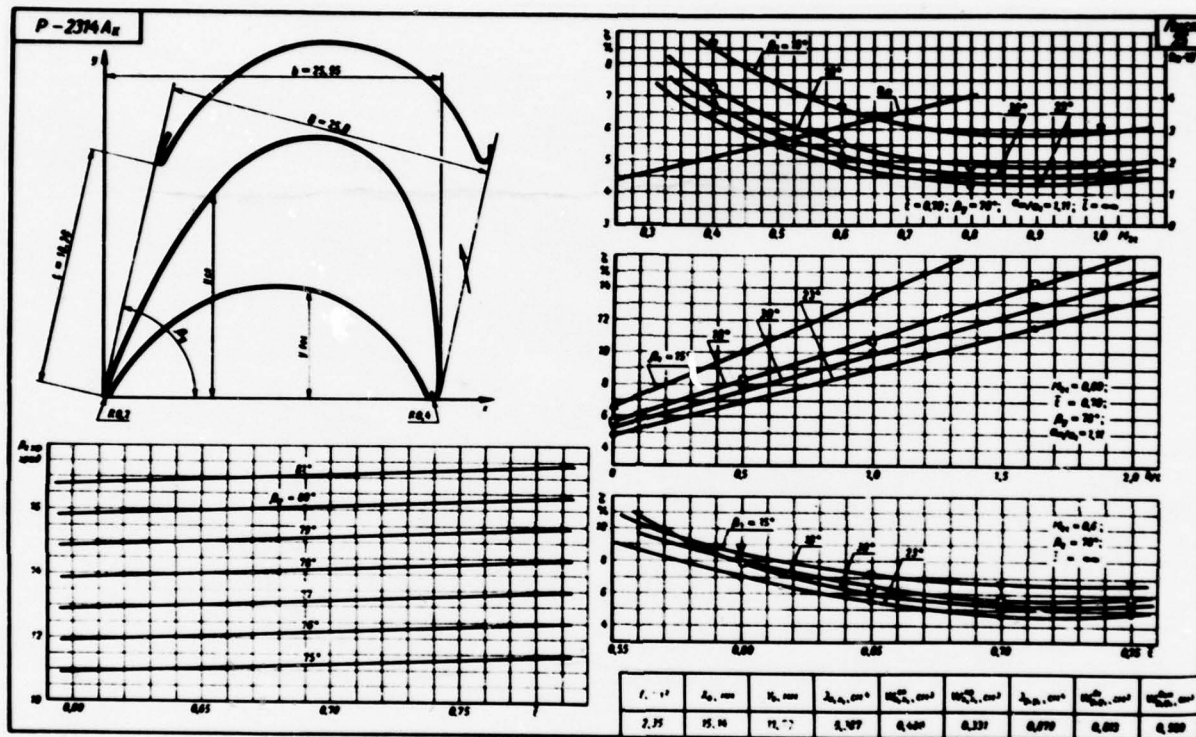




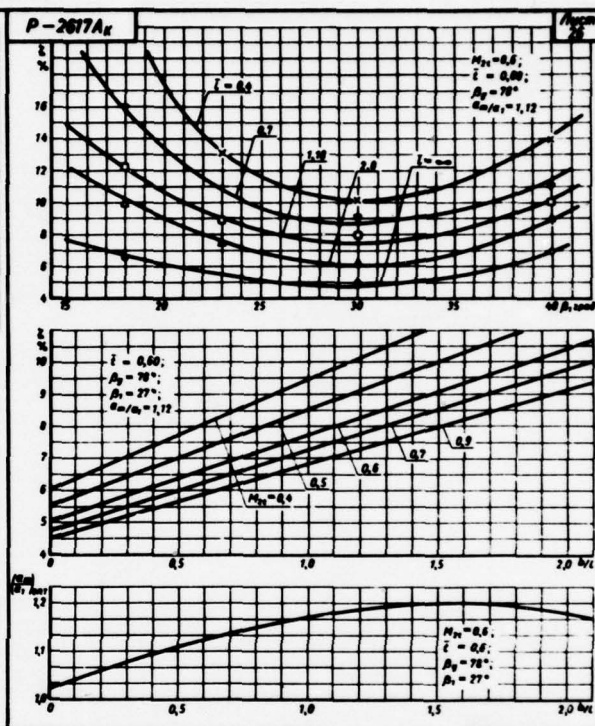
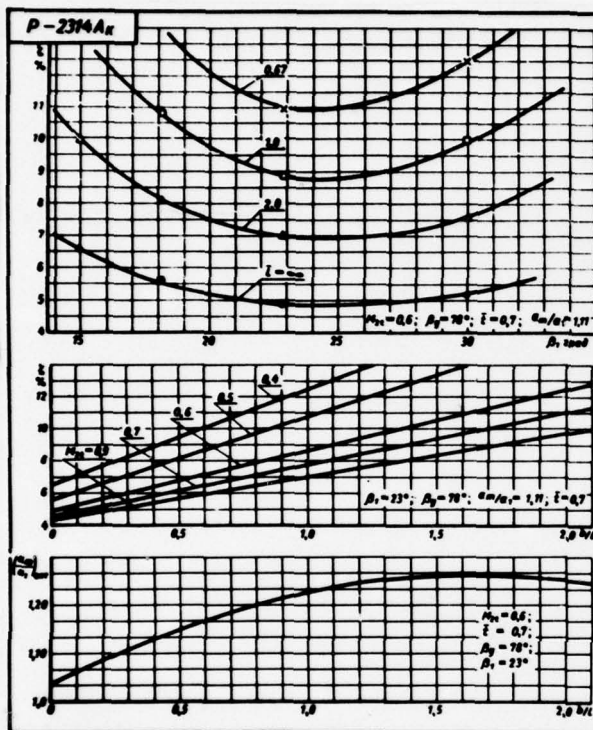
page 355



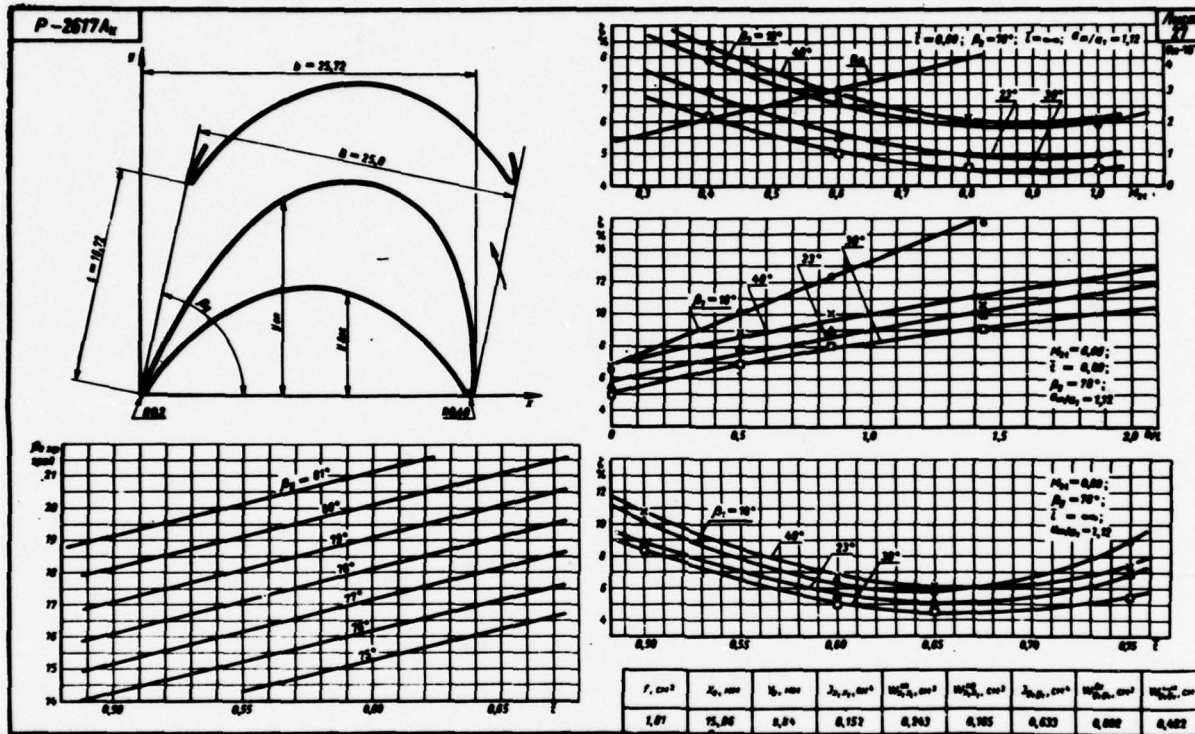
page 256



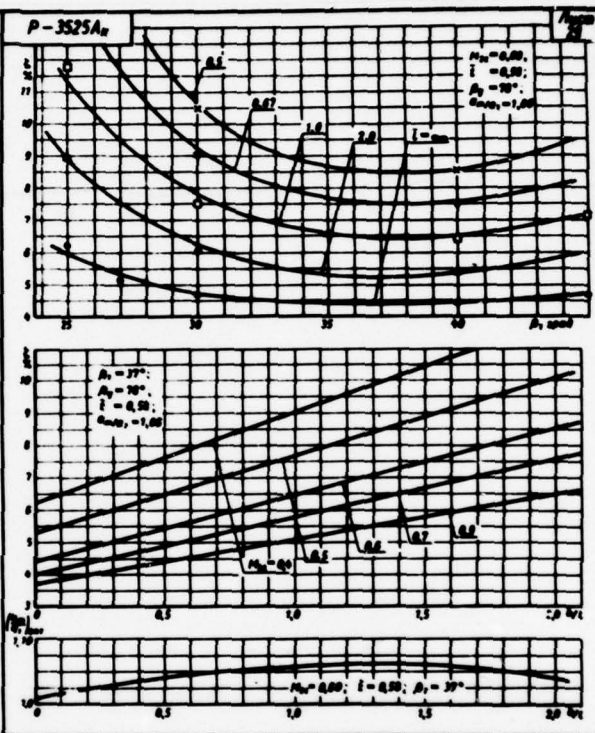
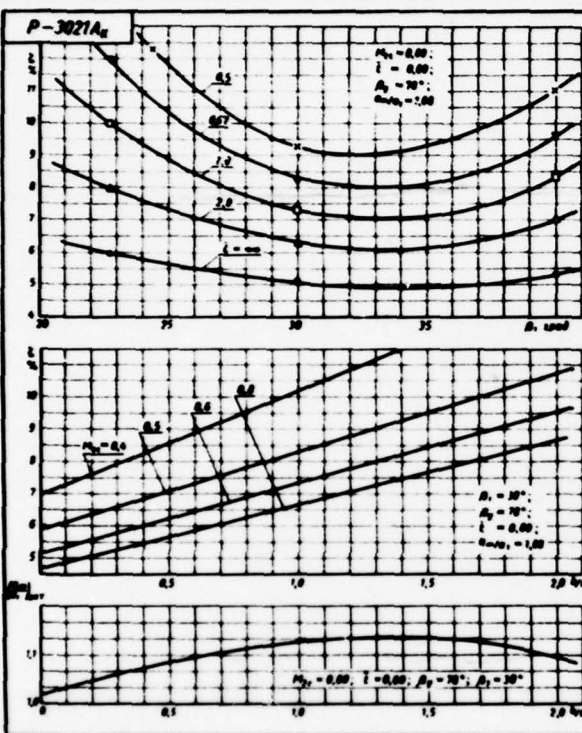
Page 357



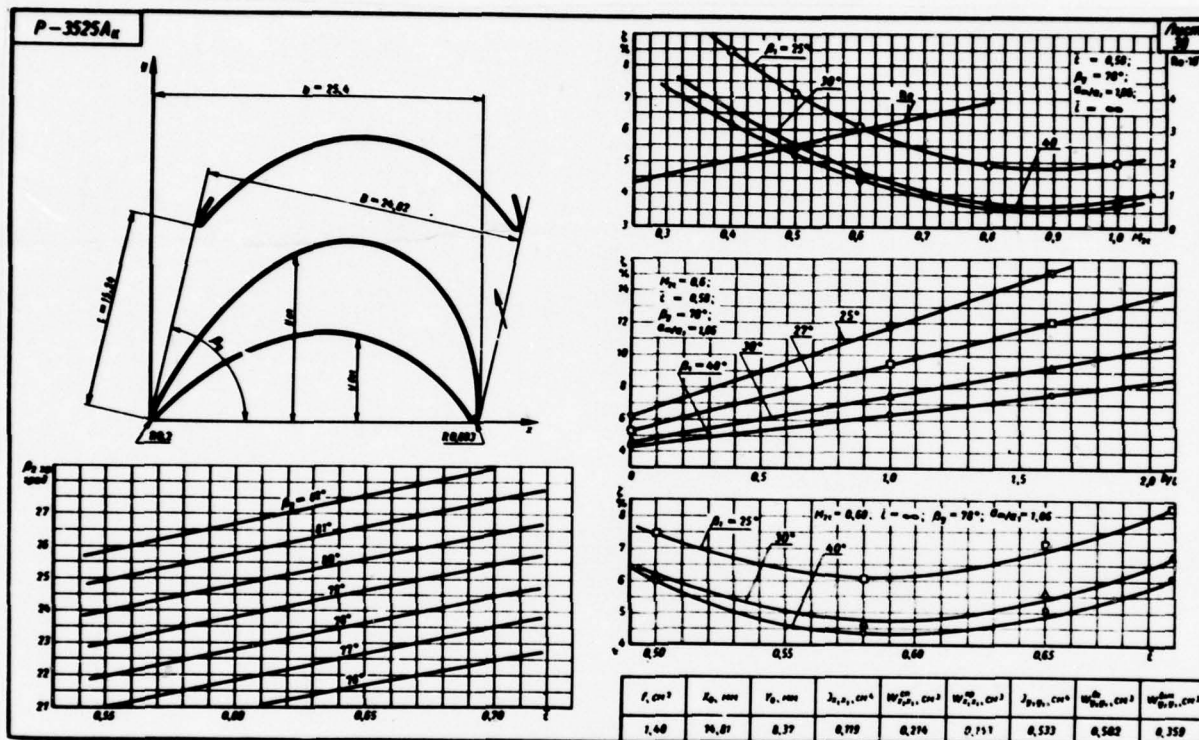
page 358



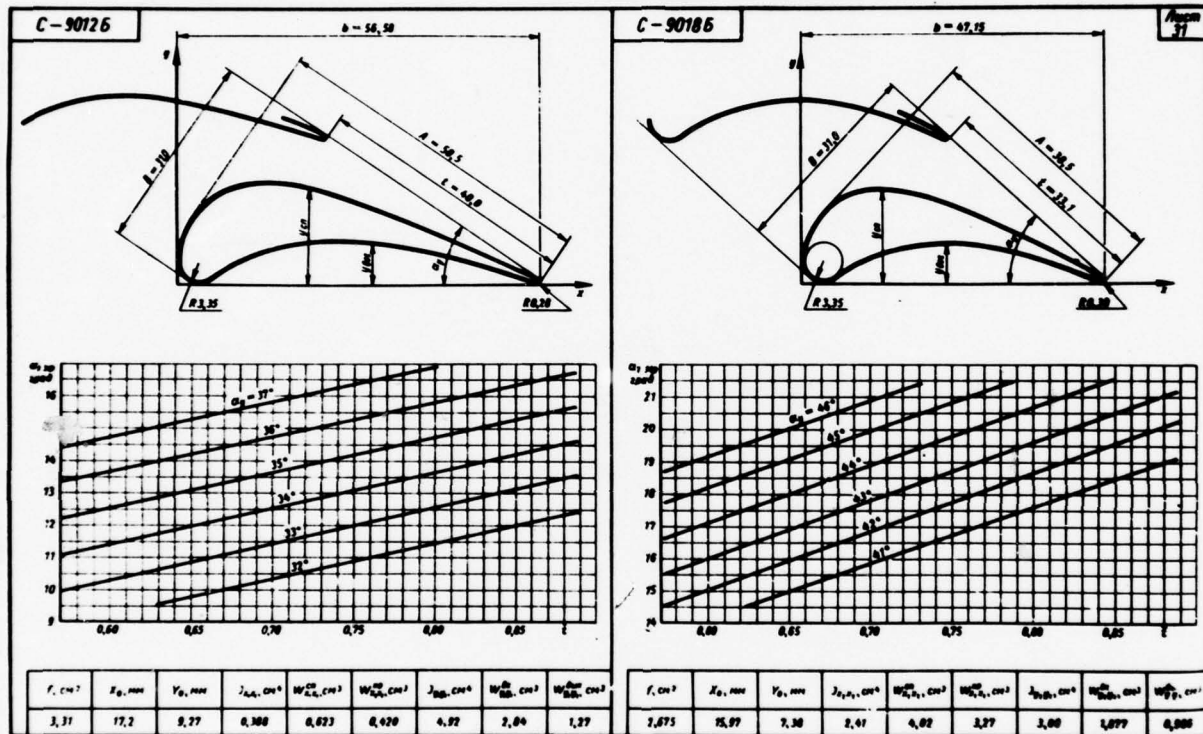
Page 360



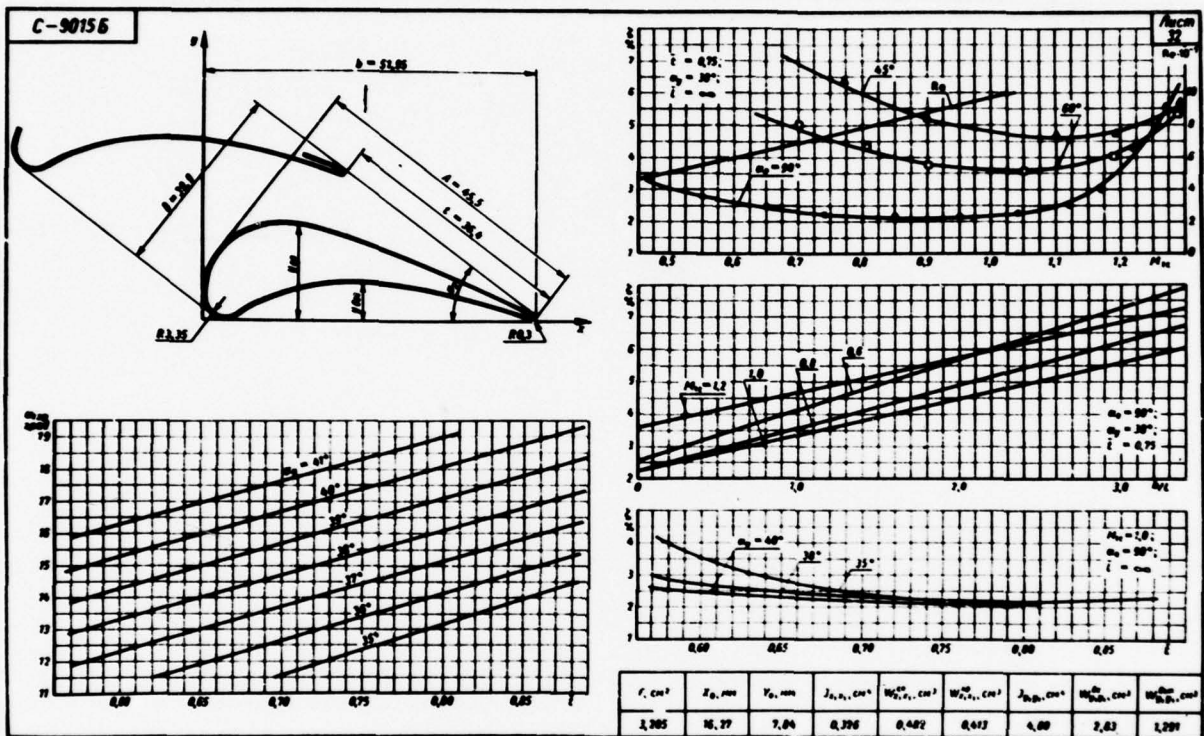
Page 361

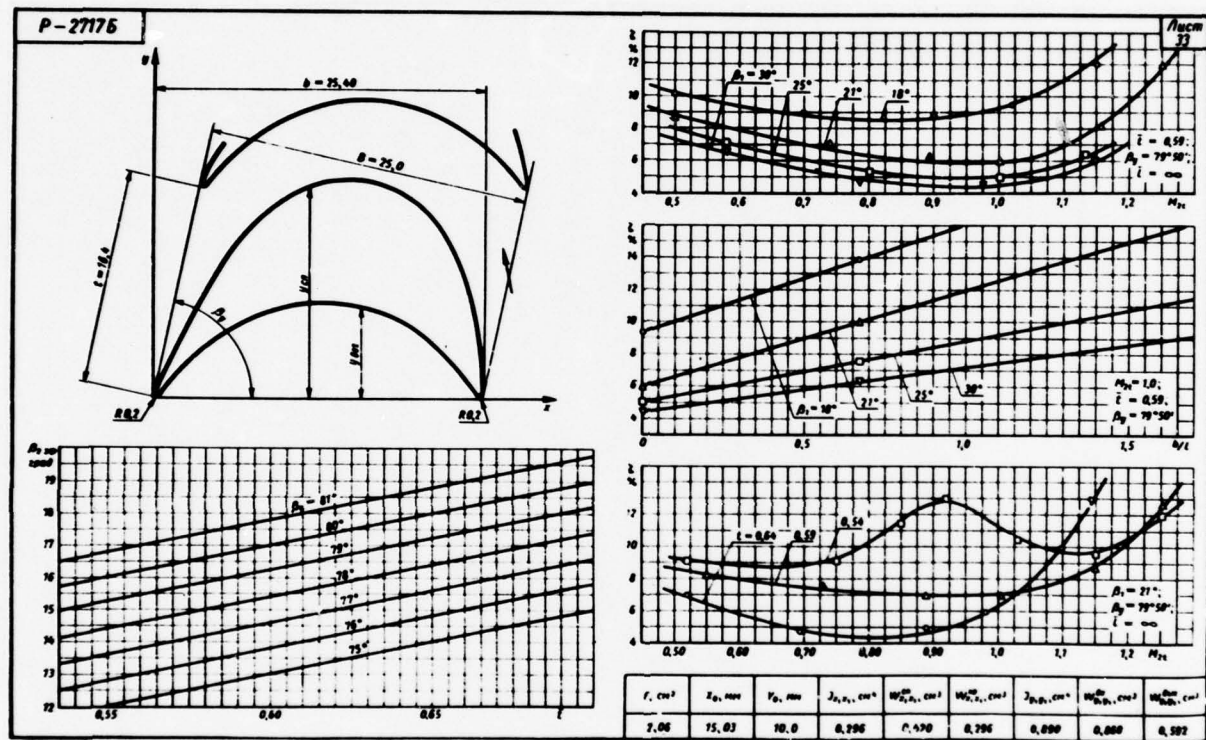


Page 362

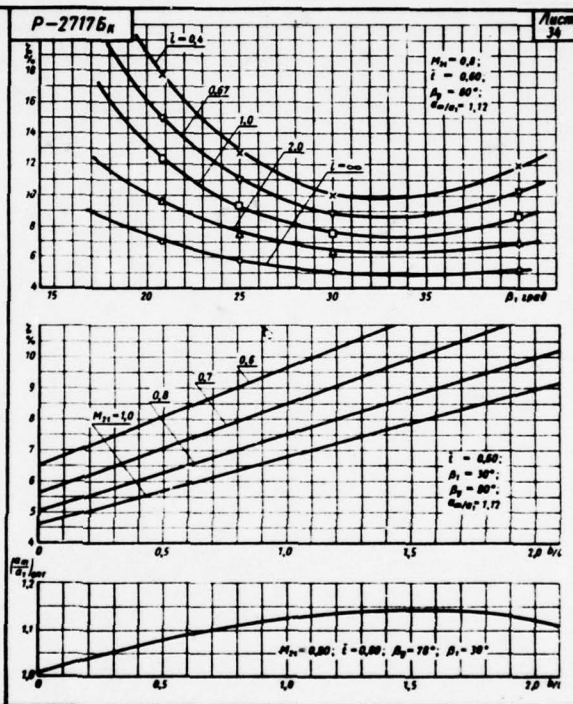
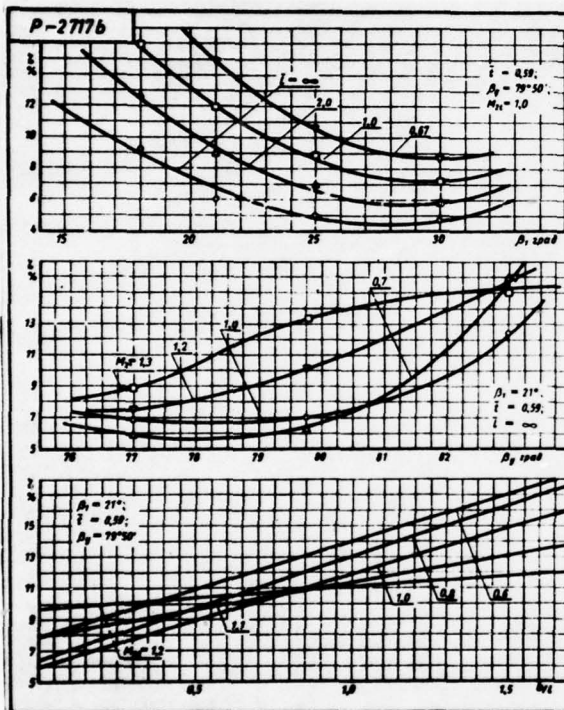


Page 363

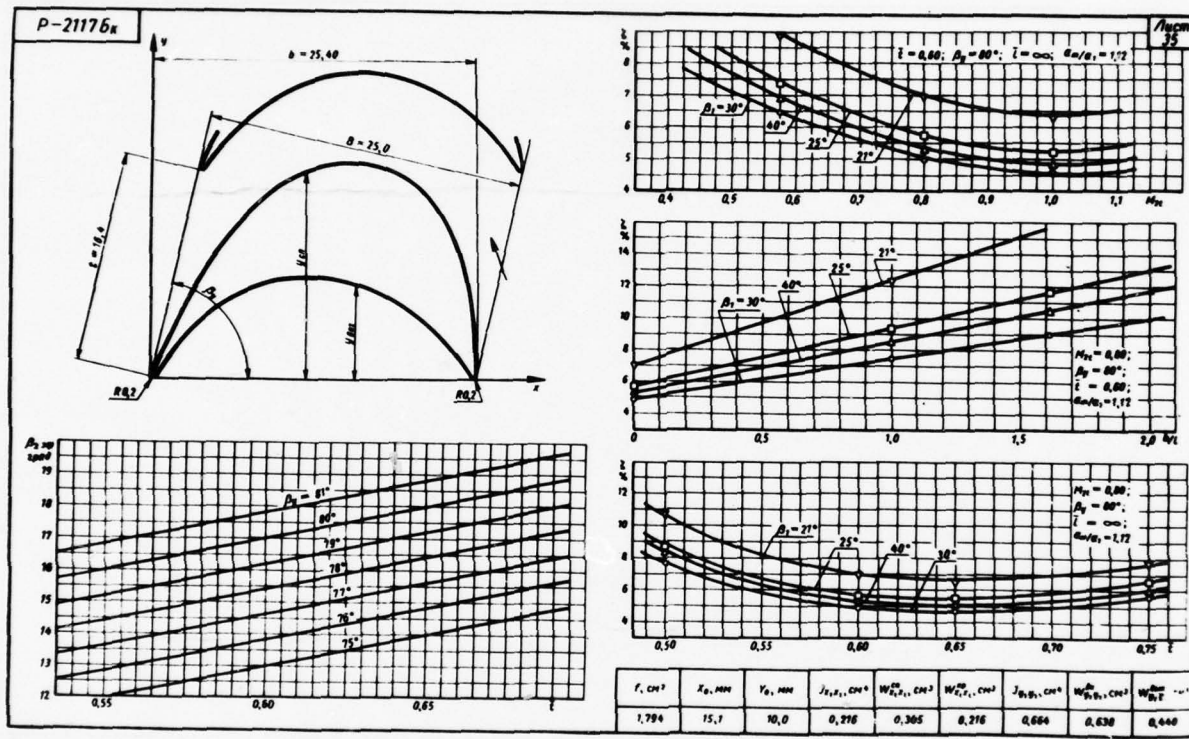




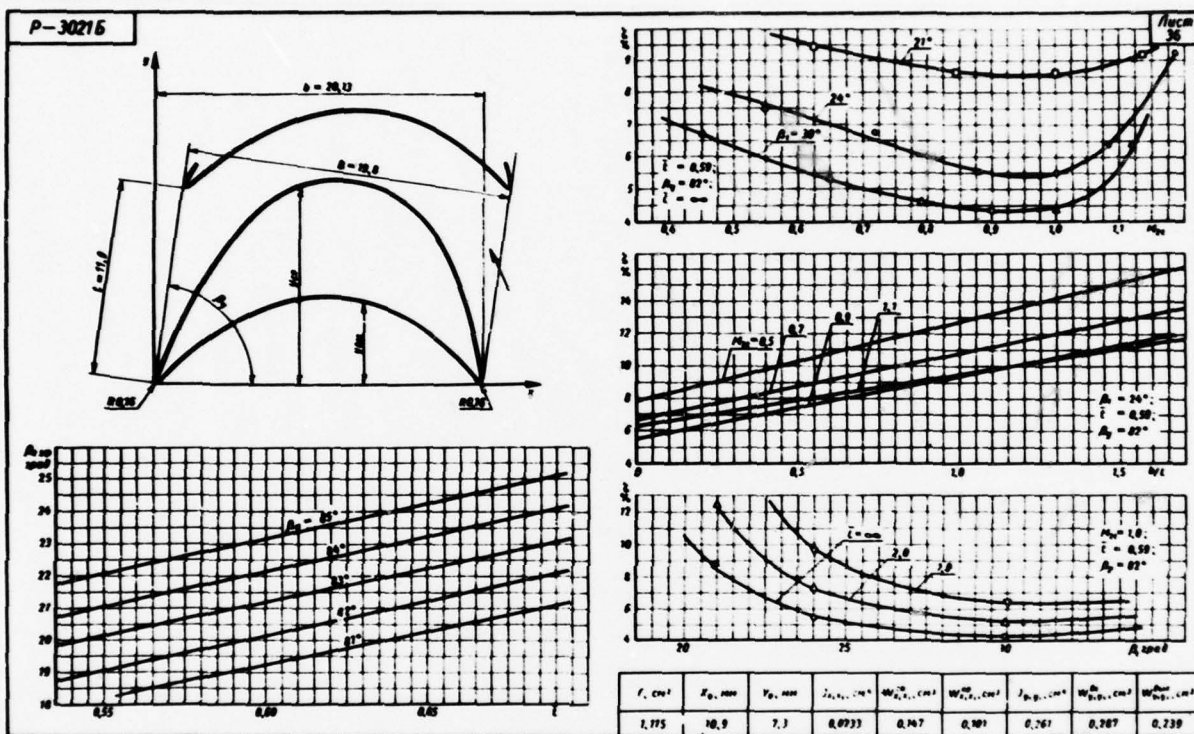
page 365



page 366

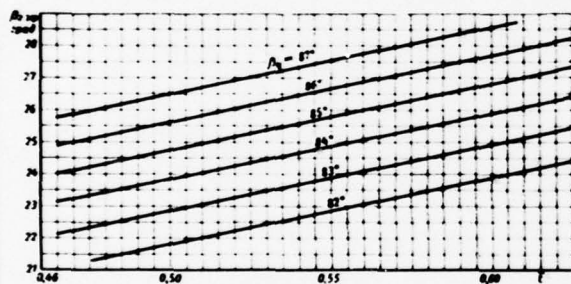
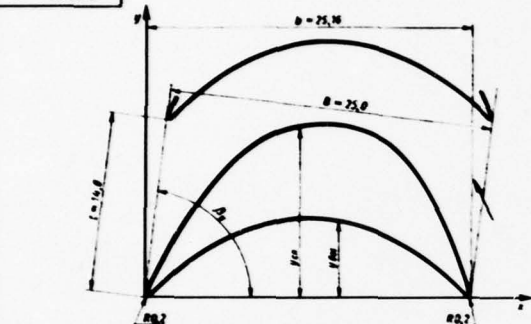


Page 367



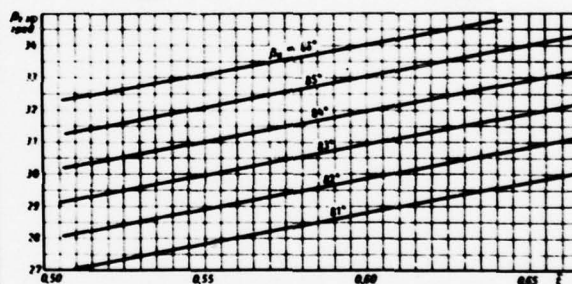
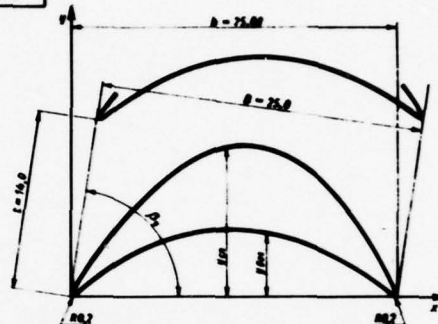
page 368

P-35256



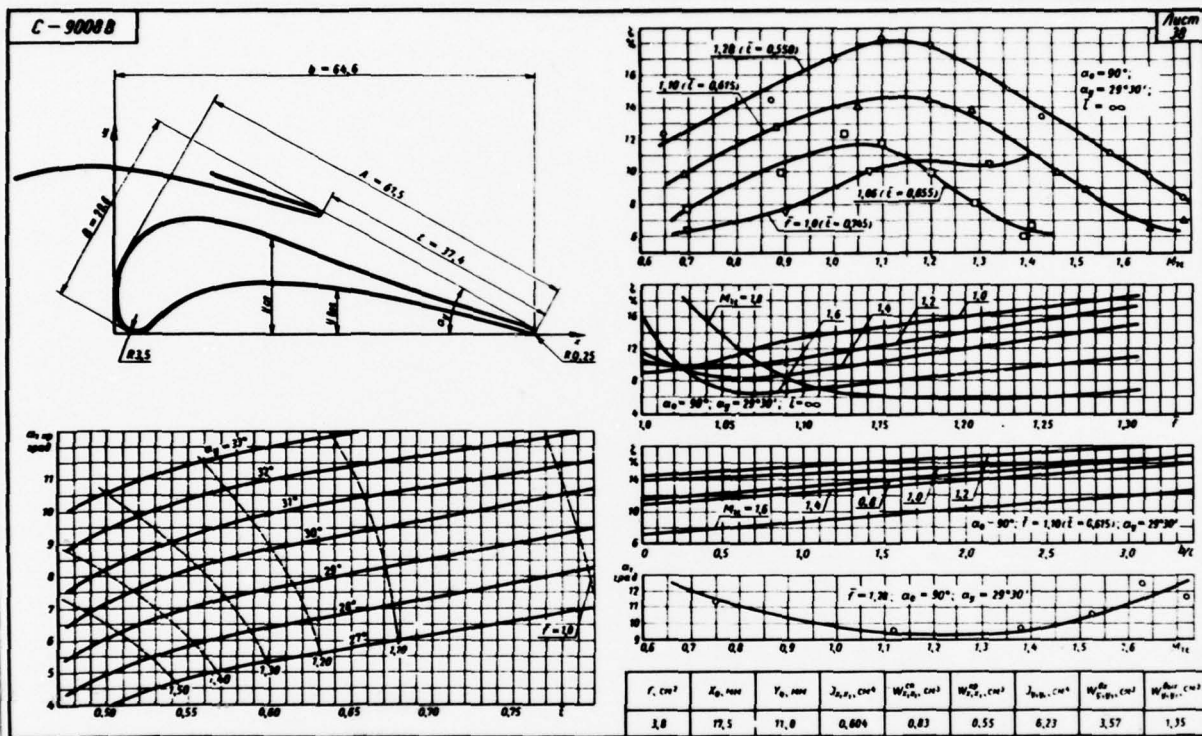
$F, \text{ cm}^2$	$Z_0, \text{ mm}$	$V_0, \text{ mm}$	$J_{x_0}, \text{ cm}^4$	$W_{x_0}^{\text{top}}, \text{ cm}^3$	$W_{x_0}^{\text{bot}}, \text{ cm}^3$	$J_{y_0}, \text{ cm}^4$	$W_{y_0}^{\text{top}}, \text{ cm}^3$	$W_{y_0}^{\text{bot}}, \text{ cm}^3$
1.513	13.70	7.95	0.126	0.279	0.159	0.495	0.629	0.367

P-46296



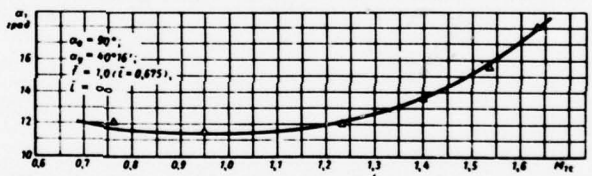
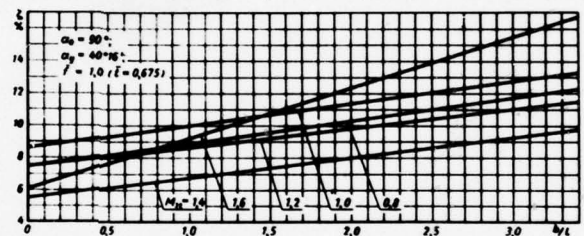
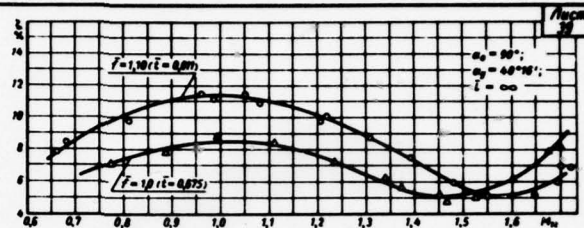
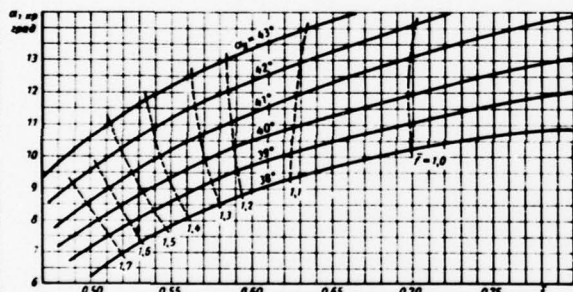
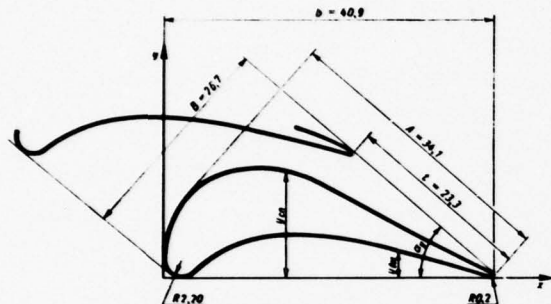
$F, \text{ cm}^2$	$Z_0, \text{ mm}$	$V_0, \text{ mm}$	$J_{x_0}, \text{ cm}^4$	$W_{x_0}^{\text{top}}, \text{ cm}^3$	$W_{x_0}^{\text{bot}}, \text{ cm}^3$	$J_{y_0}, \text{ cm}^4$	$W_{y_0}^{\text{top}}, \text{ cm}^3$	$W_{y_0}^{\text{bot}}, \text{ cm}^3$
1.06	13.34	6.84	0.0823	0.1405	0.091	0.223	0.242	0.276

page 369



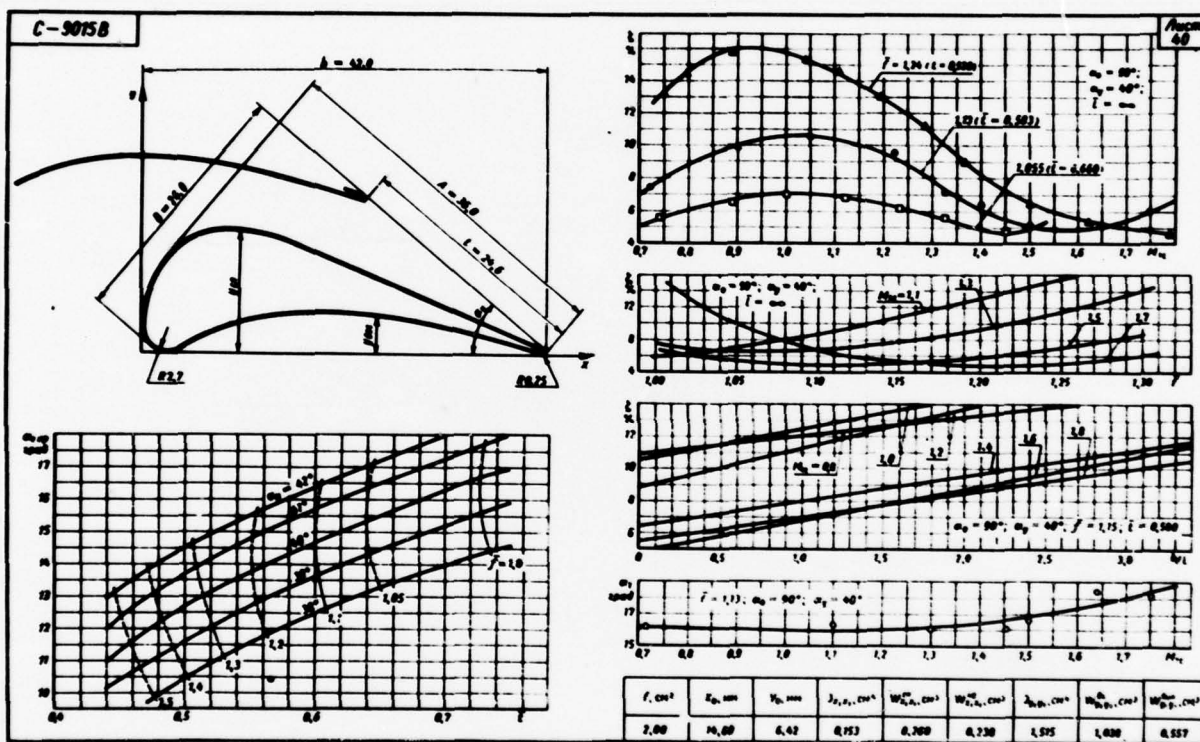
page 370

C-9012B

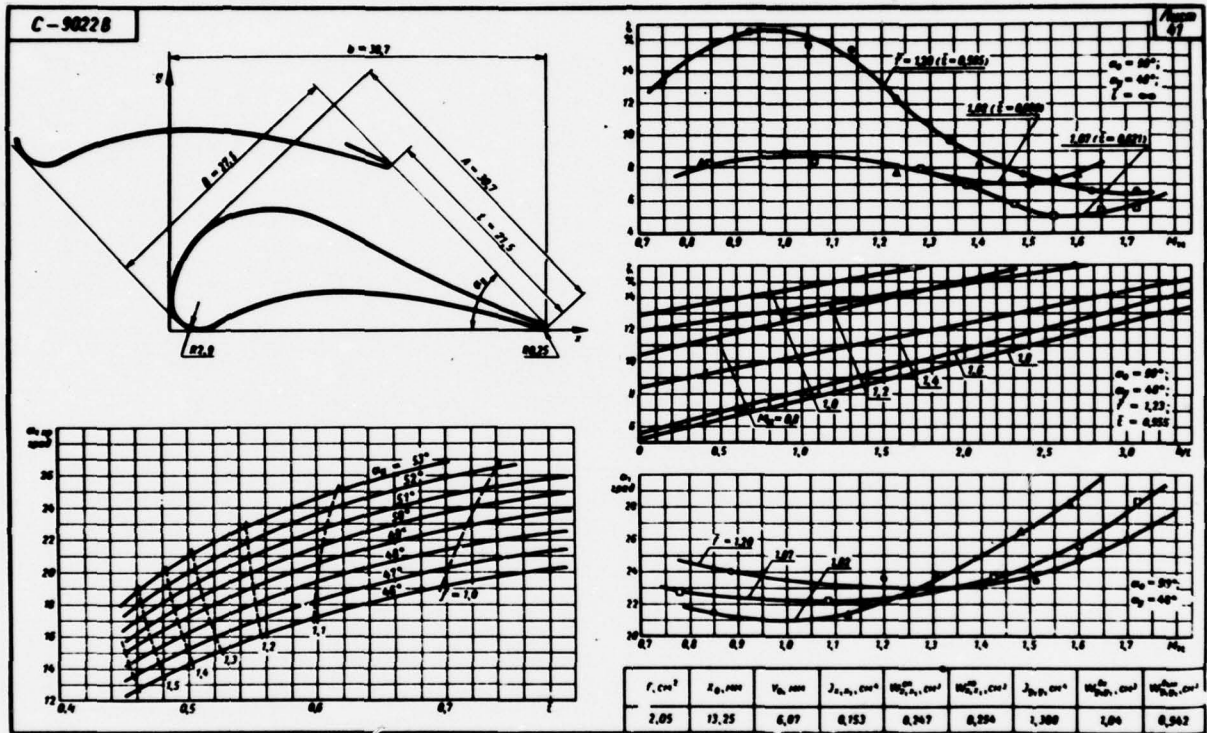


f, cm^2	x_0, mm	y_0, mm	z_0, cm^2	w_0, cm^2	w_0^2, cm^2	z_0^2, cm^2	w_0^2, cm^2	w_0^2, cm^2
2.305	13.70	2.32	0.237	0.375	0.324	1.807	1.302	0.701

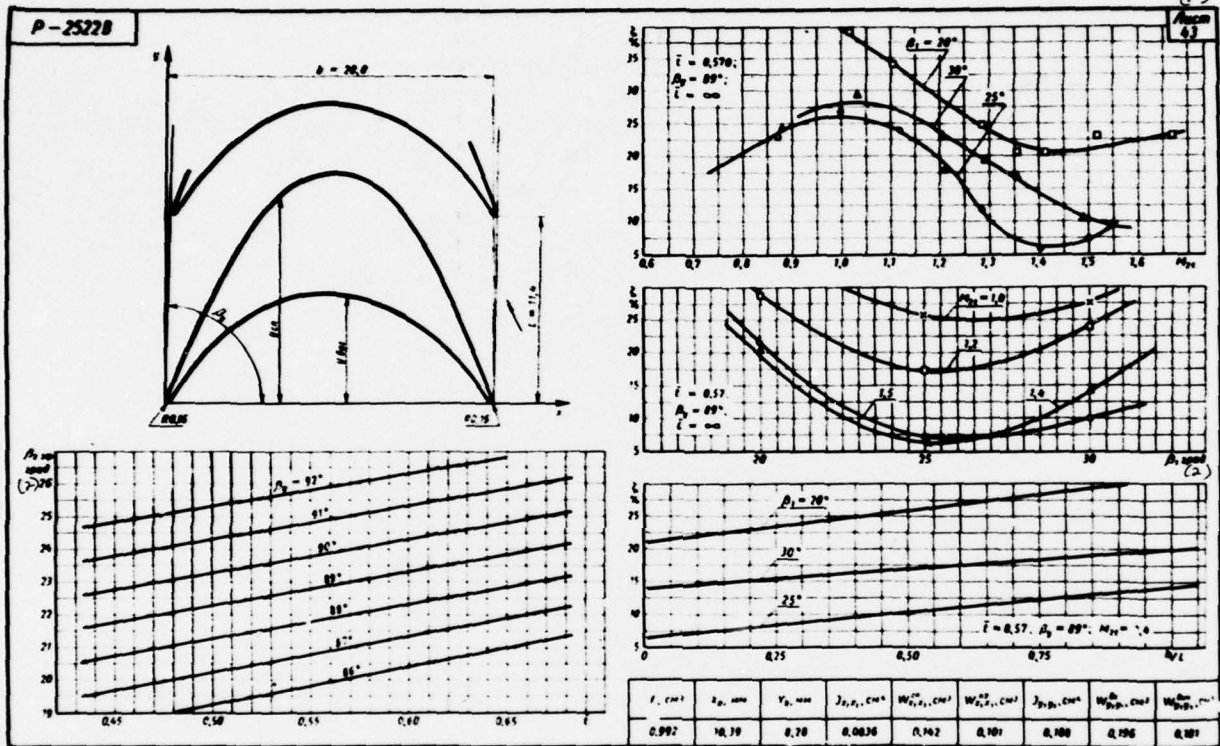
Page 371



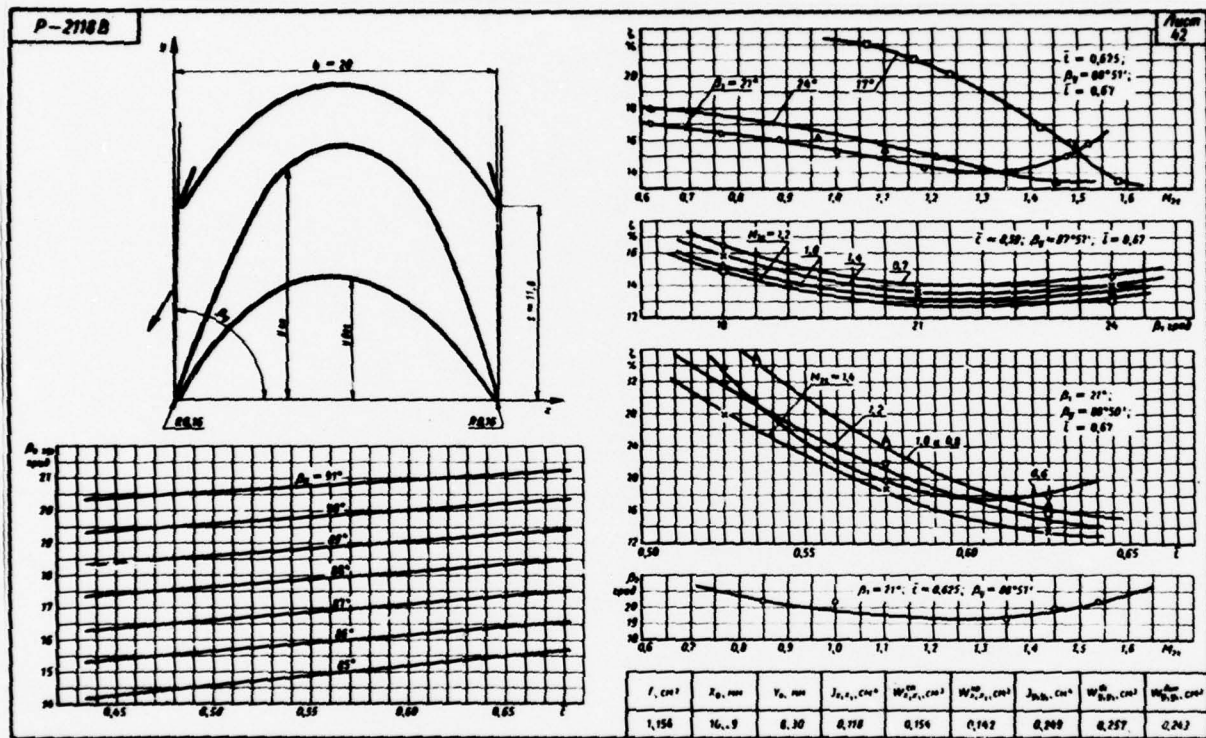
page 372



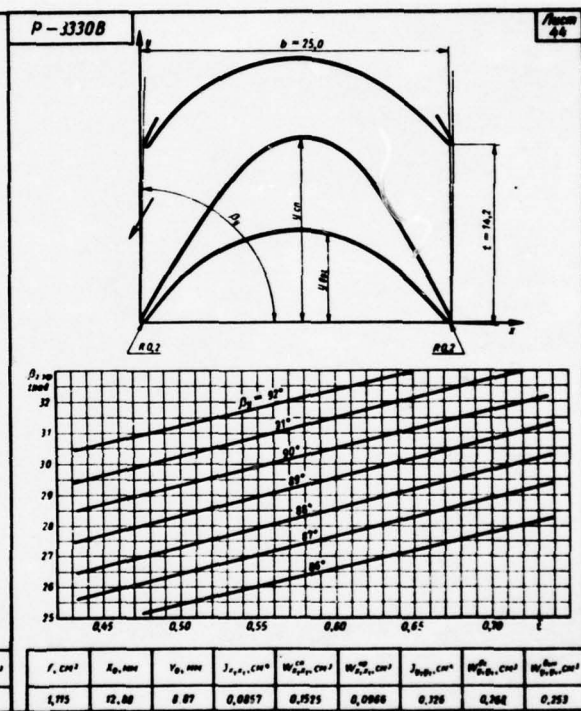
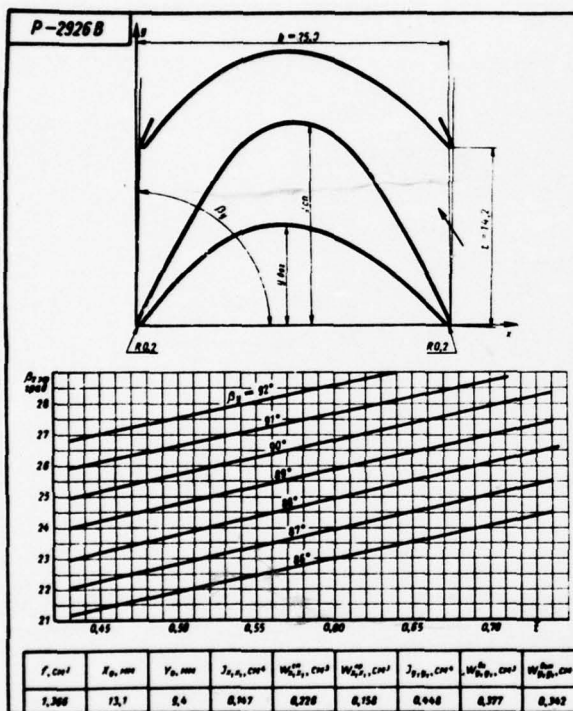
Page 373



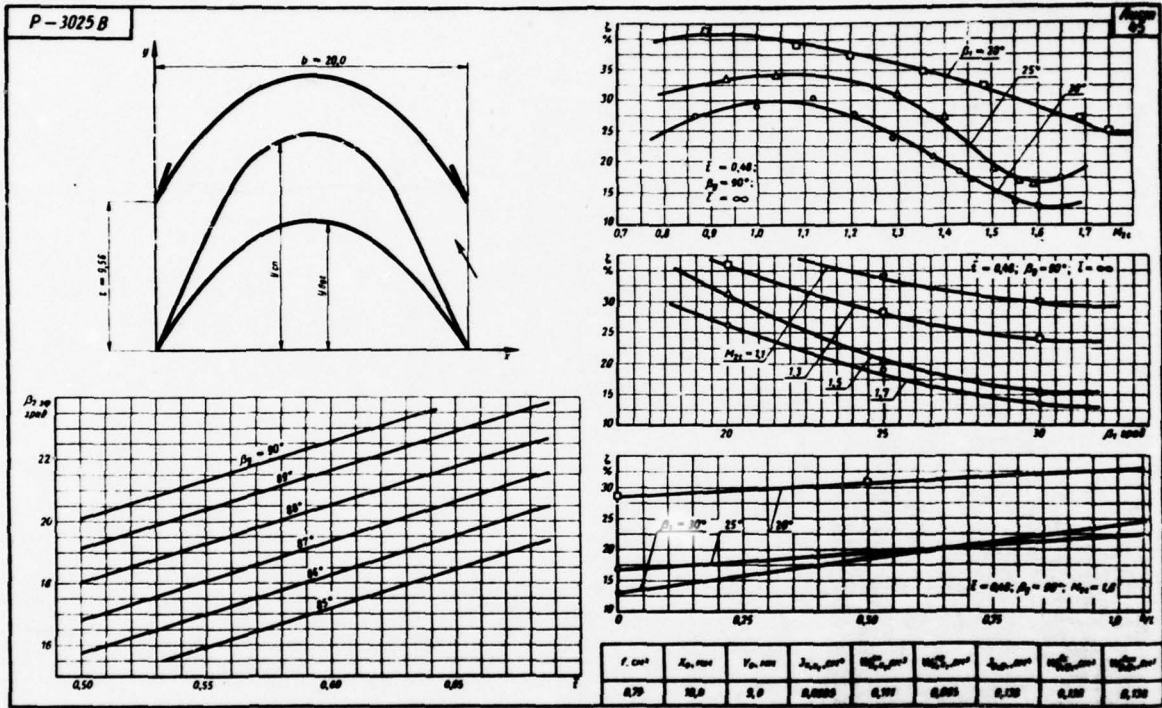
Page 374

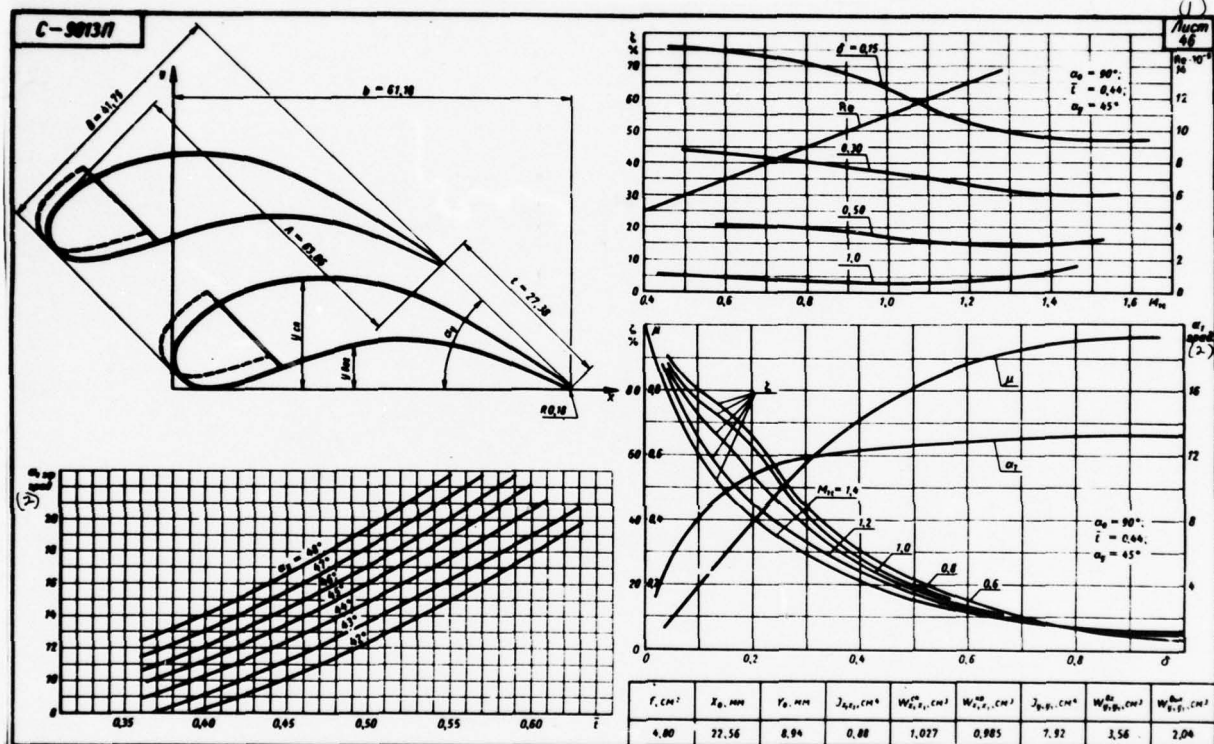


page 375

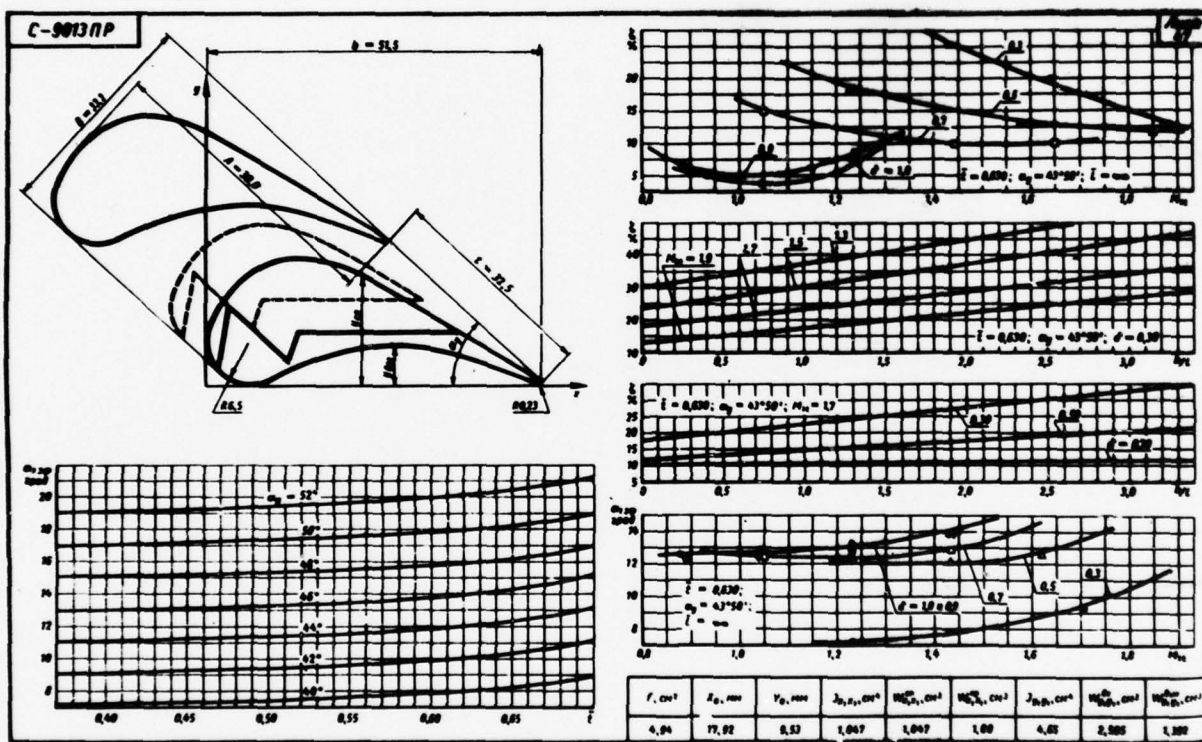


Page 376

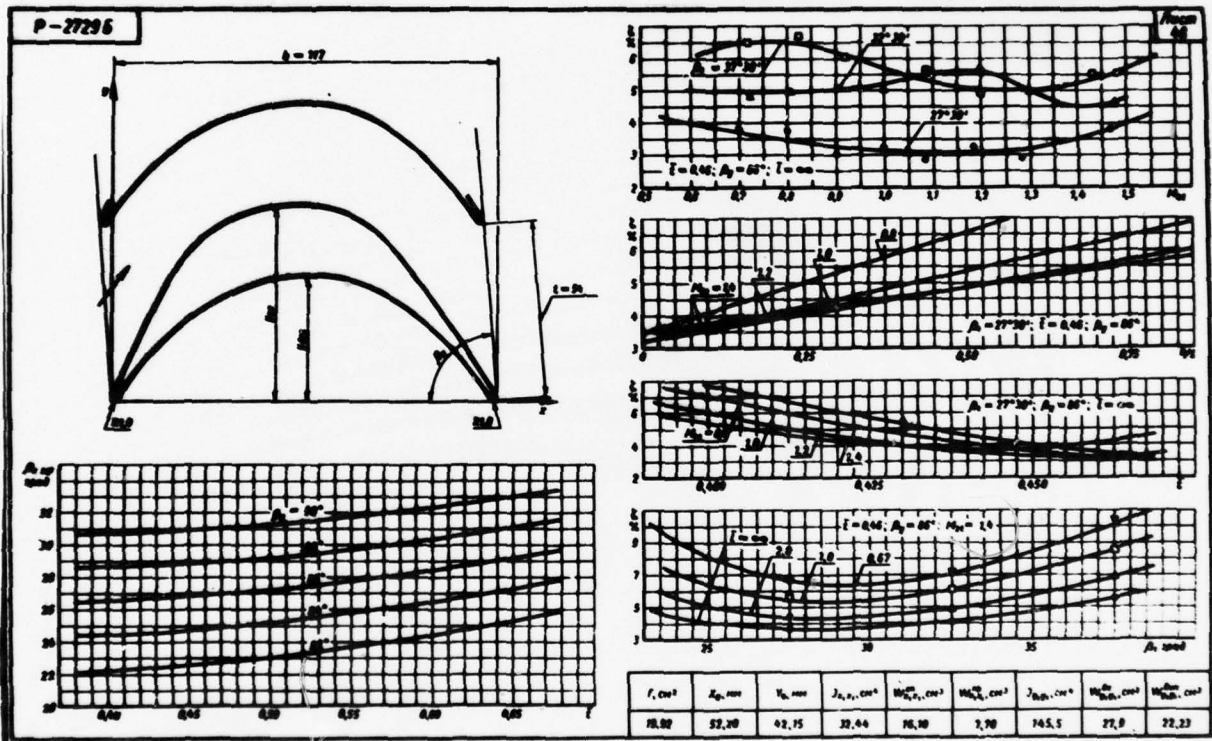




page 378



Page 379



AD-A039 286

FOREIGN TECHNOLOGY DIV WRIGHT-PATTERSON AFB OHIO
ATLAS OF THE CASCADE PROFILES OF AXIAL-FLOWS TURBINE, (U)
DEC 76 M Y DEYCH, G A PHILIPP, L Y LAZAREV
FTD-ID(RS)T-1693-76

F/G 21/5

UNCLASSIFIED

NL

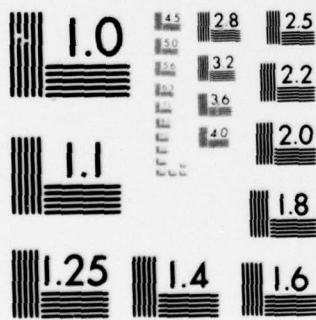
5 OF 5
AQ
A039286



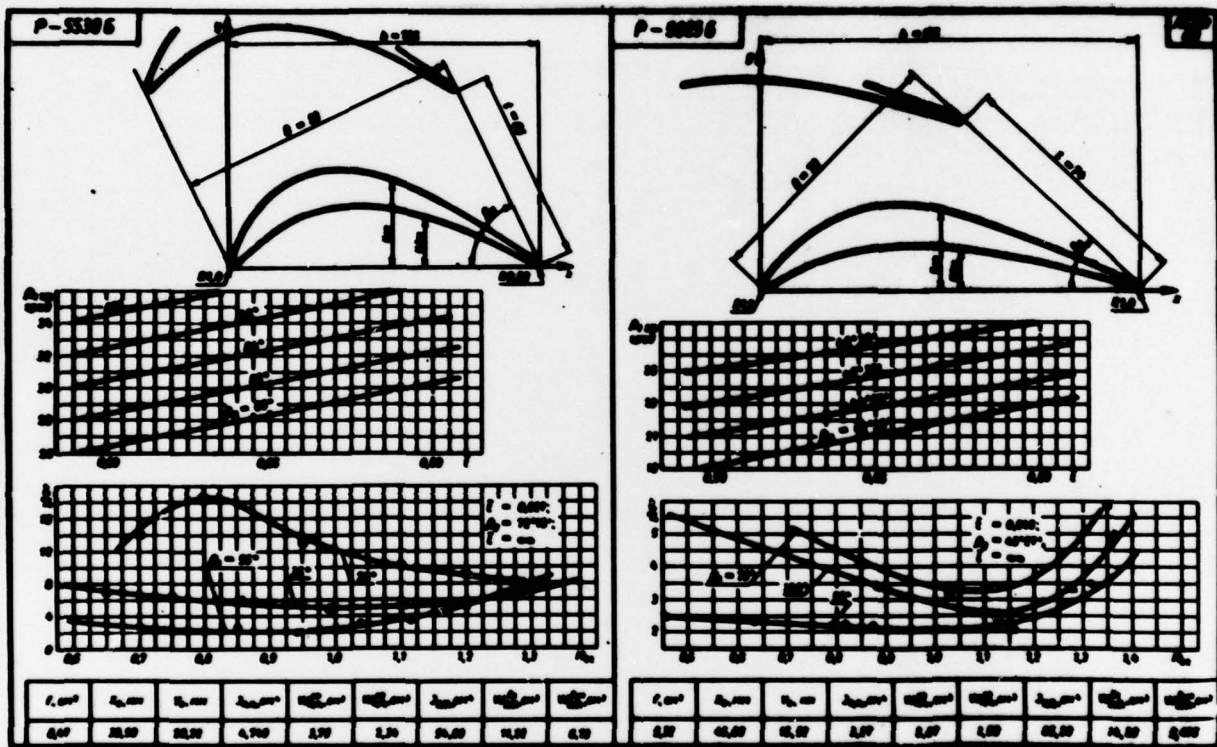
END

DATE
FILMED
5-77

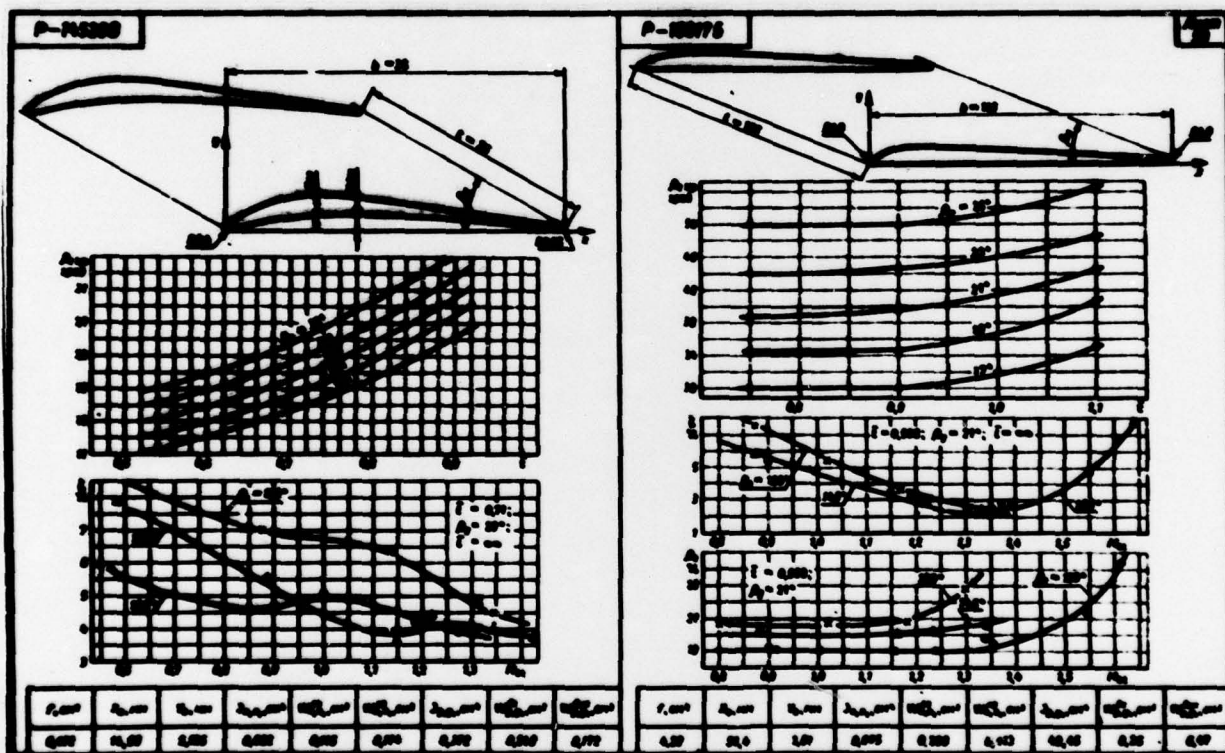
3928



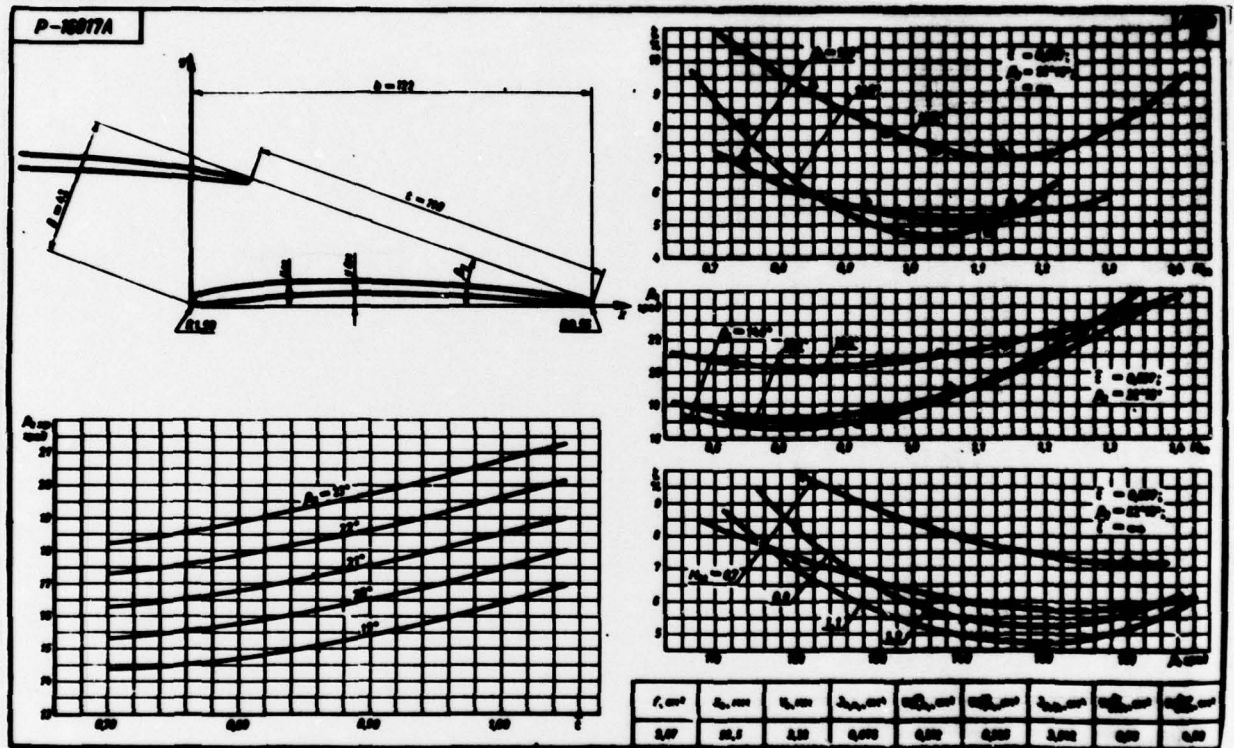
MICROCOPY RESOLUTION TEST CHART
NATIONAL BUREAU OF STANDARDS-1963-A



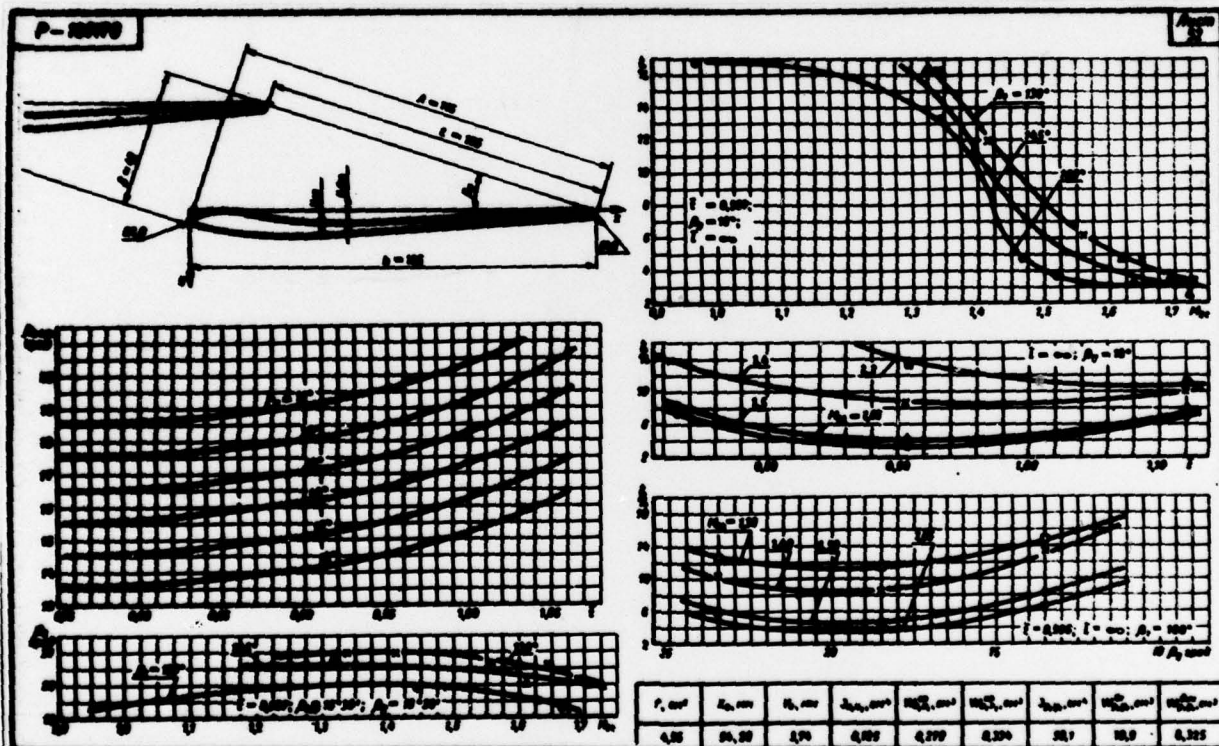
page 381



page 382



page 383



1. Алексеев Р. Н., Лазовский И. Д. и Рязанцев Ю. В. Методы исследования гидродинамических турбинных лопаток и их профилирование. — «Теплоэнергетика», 1955, № 6.
2. Врублевская В. А. Основы начальной стадии турбулентности потока на характеристике направляющих в рабочих решетках турбин. — «Теплоэнергетика», 1955, № 2.
3. Гурьев А. В. Исследования обтекания решеток турбин при сверхзвуковых скоростях. Известия вузов. — «Авиационная техника», 1952, № 2.
4. Губарев А. В., Ли Цай Сю. Основы неравномерности потока на характеристике решеток. — «Теплоэнергетика», 1953, № 6.
5. Гурьев А. В., Сив И. И. и Лазарев Л. Я. Влияние толщины выходящих слоев на характеристики направляющих решеток турбин. — «Теплоэнергетика», 1953, № 8.
6. Девя М. Е. Техническая гидродинамика. Гостехиздат, 1953, 1961.
7. Девя М. Е. и Самойлович Г. С. Основы аэродинамики осевых турбомашин. Машгиз, 1959.
8. Девя М. Е. и Лазарев Л. Я. Новые сверхзвуковые сопловые решетки МЭИ. Труды МЭИ. — «Сверхоаэродинамическое», 1953, № 47.
9. Девя М. Е. и Зарянкин А. Е. Исследования и улучшение сопловых решеток регулируемых ступеней. — «Теплоэнергетика», 1955, № 10.
10. Девя М. Е., Губарев А. В., Лазарев Л. Я. и др. Исследование новых сопловых решеток МЭИ для сверхзвуковых скоростей. — «Теплоэнергетика», 1952, № 10.
11. Девя М. Е. и Губарев А. В. Исследование активных рабочих решеток при больших скоростях. — «Теплоэнергетика», 1955, № 12.
12. Девя М. Е. и Зарянкин А. Е. Приближенный метод расчета конических потерь в турбинных решетках. — «Теплоэнергетика», 1955, № 9.
13. Девя М. Е. и Шейкин А. Г. Исследование регулирующих вторичных диффузоров отопительного отбора турбин (25—100). МВТ. — «Теплоэнергетика», 1953, № 1.
14. Девя М. Е., Троицкий В. М. Исследования и расчеты ступеней осевых турбин. Машгиз, 1954.
15. Девя М. Е., Баранов В. А. и Розанов К. А. Исследование решеток турбинных профилей методом эквивалентности реактивной силы. Научные доклады высшей школы. — «Энергетика», 1955, № 3.
16. Девя М. Е. и Лазарев Л. Я. Исследование перехода турбулентного пограничного слоя в ламинарный. — «Инженерно-физический журнал», 1954, № 4.
17. Лазарев В. С. Расчеты профилейных потерь решеток профилей судовых турбин с выходящими слоями конечной толщины. — «Судостроение», 1957, № 8.
18. Жиринский Г. С. Конструкция и расчет на прочность деталей паровых турбин. Гостехиздат, 1950.
19. Жиринский Г. С., Локат В. И., Мансурова М. К. и др. Газовые турбины авиационных двигателей. Оборонгиз, 1953.
20. Жиринский Г. С. Авиационные газовые турбины. Оборонгиз, 1955.
21. Жуковский М. И. Расчет обтекания решеток профилей турбомашин. Машгиз, 1950.
22. Жуковский М. И. Метод профилирования турбинных решеток. — «Сверхоаэродинамическое», 1950, № 7.
23. Жуковский М. И., Дураков Н. И. и Новикова О. И. Расчет потенциального обтекания неплотной лопаткой профилейных решеток лопаточных профилей на вихревой выходящей линии. — «Теплоэнергетика», 1953, № 6.
24. Жуковский М. И. и Сиварь Н. А. К вопросу о применении усеченной линии обтекания решеток. — «Сверхоаэродинамическое», 1957, № 2.
25. Кавказов Л. Е. Гидродинамическая теория теплопередачи. — «Промышленная химия и металлургия», Т. 10, 1955.
26. Кромов В. Г. Влияние периодичности нестационарности потока в турбинной ступени на потерю активной мощности. — «Известия ВТИ», 1955, № 5.
27. Локат В. И. Зависимость профилейных потерь в решетках от угла атаки. — «Известия АН СССР. ОТН», 1954, № 6.
28. Лойманский Л. Г. Аэродинамический анализ. Гостехиздат, 1951.
29. Лойманский Л. Г. Ламинарный обтекательный слой. ГИИИИЛ, 1952.
30. Локат В. И. Д. Турбулентность потока в турбинной ступени и профилейных потерях активной мощности. — «Известия ВТИ», 1950, № 5.
31. Марков Н. М. Расчет аэродинамических характеристик плоской решетки профилей осевых турбомашин. Машгиз, 1952.
32. Натальев А. С. Течение газа в щели между лопатками и в соплах авиационных турбин. Труды МАИ. Вып. 35, 1955.
33. Саламатов Н. Е. Профилирование лопаток турбин, обтекаемых ламинарным потоком. — «Известия вузов. Авиационная техника», 1959, № 1.
34. Самойлович Г. С. и Шерстюк А. Н. Расчет аэродинамических характеристик лопаток. — «Известия АН СССР. ОТН», 1955, № 4.
35. Самойлович Г. С. Расчет потенциального потока в аэродинамическом канале. — «Теплоэнергетика», 1954, № 7.
36. Сунцов Н. Н. Методы анализа в аэродинамике. ГИИИИЛ, 1955.
37. Степанов Г. Ю. Гидродинамика решеток турбомашин. ГИИИИЛ, 1952.
38. Степанов Г. Ю. и Шерстюк А. Н. К вопросу об определении потерь в соплах турбинных решетках при пересечении углов атаки. — «Известия АН СССР», 1953, № 6.
39. Степанов Г. Ю. Гидродинамические методы расчета установившихся обтеканий решеток турбомашин. — «Вестник АН СССР», 1955, № 1.
40. Троицкий В. М. и Майорский Е. В. Исследование решеток рабочих лопаток последних ступеней паровых турбин. Известия вузов. — «Энергетика», 1952, № 5.
41. Троицкий В. М. и Майорский Е. В. Профилирование и исследование влияния сечений рабочих лопаток последних ступеней мощных паровых турбин. — «Теплоэнергетика», 1952, № 7.
42. Фадеев А. Аэродинамическая сверхзвуковая теория. ГИИИИЛ, 1953.
43. Фадеев А. А. и Ван Чу-Шя. Расчеты осесимметричного течения в ступенях турбомашин большой скорости. — «Труды МЭИ», 1953, № 47.
44. Швей К. И. Метод построения лопаточного профиля паровых турбин по условиям срединной линии. — «Труды института теплоэнергетики АН СССР», 1952, № 6.
45. Шерстюк А. Н. Приближенный метод расчета аэродинамических потерь. — «Теплоэнергетика», 1955, № 8.
46. Шерстюк А. Н. К определению потерь в турбинных решетках при пересечении углов атаки. «Известия АН СССР. ОТН». — «Энергетика и автоматизация», 1955, № 2.
47. Щеглаев А. В., Девя М. Е. и Фадеев А. А. Расчет ступеней турбин по результатам статических продувок решеток. — «Теплоэнергетика», 1955, № 3.
48. Щеглаев А. В. Паровые турбины. Гостехиздат, 1948.
49. Boser E., Stetter I. R., Wiedershi L. Application of supersonic vortex flow theory to the design of supersonic impulse compressors or turbine blade sections. NACA, RML 55B. 04, April, 1952.
50. Lanch et Quirk. Bulletin de L'association technique maritime et aeronautique, N 52, 1953.
51. Nipper X. Ober den Strömungsverlauf in gekrümmten Kanälen. — «Forschungsarbeiten auf dem Gebiete des Ingenieurwesens» N 350, 1955.
52. Oswalitsch K. Allgemeine Wärmetechnik, I, 1955.
53. Oswalitsch K. Potentialtheorie — Gitter für Umströmung geschlossener Zylinder. Zeitschrift für Flugwissenschaften, 4, N 1—2, 1955.

UNCLASSIFIED

SECURITY CLASSIFICATION OF THIS PAGE (When Data Entered)

REPORT DOCUMENTATION PAGE		READ INSTRUCTIONS BEFORE COMPLETING FORM
1. REPORT NUMBER FTD-ID(RS)T-1693-76 ✓	2. GOVT ACCESSION NO.	3. RECIPIENT'S CATALOG NUMBER
4. TITLE (and Subtitle) ATLAS OF THE CASCADE PROFILES OF AXIAL- FLOWS TURBINE		5. TYPE OF REPORT & PERIOD COVERED Translation
7. AUTHOR(s) M. Ye. Deych, G. A. Philipp, L. Ya. Lazerev		6. PERFORMING ORG. REPORT NUMBER
9. PERFORMING ORGANIZATION NAME AND ADDRESS Foreign Technology Division Air Force Systems Command U. S. Air Force		8. CONTRACT OR GRANT NUMBER(s)
11. CONTROLLING OFFICE NAME AND ADDRESS		10. PROGRAM ELEMENT, PROJECT, TASK AREA & WORK UNIT NUMBERS
14. MONITORING AGENCY NAME & ADDRESS (if different from Controlling Office)		12. REPORT DATE 1965
		13. NUMBER OF PAGES 384
		15. SECURITY CLASS. (of this report) UNCLASSIFIED
		15a. DECLASSIFICATION/DOWNGRADING SCHEDULE
16. DISTRIBUTION STATEMENT (of this Report) Approved for public release; distribution unlimited.		
17. DISTRIBUTION STATEMENT (of the abstract entered in Block 20, if different from Report)		
18. SUPPLEMENTARY NOTES		
19. KEY WORDS (Continue on reverse side if necessary and identify by block number)		
20. ABSTRACT (Continue on reverse side if necessary and identify by block number) 10; 13		

DISTRIBUTION LIST

DISTRIBUTION DIRECT TO RECIPIENT

ORGANIZATION	MICROFICHE	ORGANIZATION	MICROFICHE
A205 DMATC	1	E053 AF/INAKA	1
A210 DMAAC	2	E017 AF/RDQLR-W	1
B344 DIA/DS-4C	8	E404 AEDC	1
C043 USAMIA	1	E408 AFWL	1
C509 BALLISTIC RES LABS	1	E410 ADTC	1
C510 AIR MOBILITY R&D	1	E413 ESD	2
LAB/FIO		FTD	
C513 PICATINNY ARSENAL	1	CCN	1
C535 AVIATION SYS COMD	1	ETID	3
C557 USAIIC	1	NIA/PHS	1
C591 FSTC	5	NICD	5
C619 MIA REDSTONE	1		
D008 NISC	1		
H300 USAICE (USAREUR)	1		
P005 ERDA	2		
P055 CIA/CRS/ADD/SD	1		
NAVORDSTA (50L)	1		
NAVWPNSCEN (Code 121)	1		
NASA/KSI	1		
544 IES/RDPO	1		
AFIT/LD	1		